Nanostructured Hybrid Electrodes for Organic Photovoltaic Devices

Aiko Kira

2010

Contents

General Introduction

1. Present Situation of Energy Issue

Major source of energy supply has depended on fossil fuels such as petroleum, coal, and natural gas during the 20th century. In 2001, global annual energy consumption was 13.2 terawatts (TW), of which 79% was generated from fossil fuels.[1] Different scenarios have been proposed for future global annual energy needs with values of 30 TW–60 TW by 2050 since the world's population will rise to 10 billion.[2] There is increased concern regarding the exhaustion of the fossil fuels by massive energy consumption, considering that the global reserves-to-production ratios of petroleum, coal, and natural gas are 42 years, 120 years, and 60.4 years, respectively, in 2008.[3] In addition, the fossil fuels release exhaust gas such as NO_x, SO_x, and CO_2, which contributes to the air pollution and the global warming leading to a serious environmental problem. Therefore, it is quite important to develop new and clean energy-producing technology for the sustainable improvement in the standard of living in this century. Nuclear, wind, and geothermal energy have already been used as some of the alternative energy resources. Although nuclear power provides 16% of the total power generation in the world in 2005,[4] nuclear power generation possesses issues concerning the safety and the disposal of nuclear wastes. Wind and geothermal energy limit the power plant site to generate a certain amount of electricity.

Solar energy is an inexhaustible energy source. The sun provides about 120 000 TW to the earth's surface, which is about 4 orders of magnitude larger than the present rate of the world's energy consumption. The challenge today is to capture and utilize solar energy for sustainable development on a grand scale. There are different manifestations of solar energy conversion, of which the most potential technique is the conversion to electrical energy, namely solar cells. They have attracted particular attention as next generation technology because they yield no pollutant such as NO_x, SO_x, and even CO_2 in addition to the inexhaustible supply of energy. Silicon-based inorganic solar cells have been put to practical use. They exhibit the high power conversion efficiencies (η) of 10–20%,[5] but the high price and enormous energy waste in the production processes have limited their further spread.

In contrast, organic solar cells are defined as photovoltaic devices in which the active layer is made of organic material. Some scientists and engineers believe that organic solar cells will provide a low-cost alternative to conventional inorganic solar cells, because the production cost is expected to go down in comparison to the current costs for the inorganic materials and manufacturing processes of the inorganic ones. Furthermore, the merits of

organic solar cells might be color and shape flexibility and lightweight. Organic solar cells are divided into three categories: dye-sensitized solar cells (DSSCs)[6], artificial photosynthetic solar cells,[7] and bulk heterojunction solar cells.[8] In this context, the author describes studies on development of novel photosensitizers for DSSCs and construction of artificial photosynthetic photoelectrochemical devices.

2. Dye-sensitized Solar Cells

The basic photocurrent generation mechanism of DSSC is as follows (Figure 1). The dye molecule immobilized on mesoporous TiO_2 particles collects the incident light, and injects electrons into a conduction band (CB) of the TiO_2 after the photoexcitation. The resulting dye cation is regenerated by the iodide anion, and the following triiodide anion is reduced at the counter electrode, with circuit being completed via electron movement through the external load. DSSC with mesoporous TiO_2 has been regarded as one of the most promising candidates for the regenerative energy sources because the highest η for the organic solar cells has so far reached 11.5% obtained from the DSSC using Ru polypyridine complexes as dyes.[9] As well as Ru complexes, organic dyes have recently, been stimulating intensive research efforts because of their advantages as photosensitizers for DSSC: there are no concerns about resource limitations.[10] High performance dyes are requested to display broad light absorption capability along with fast injection of electrons from the photo-excited states to the CB of the TiO_2 electrodes, and slow charge recombination from the injected electrons to resulting dye radical cations and/or I^-/I_3^- redox couples. *Considering that an organic sensitizer is composed of an anchoring group for immobilization of the dye on a TiO_2 surface and a π-conjugated moiety for light-harvesting, the rationale molecular design of the both units is crucial to improve the cell performance.*

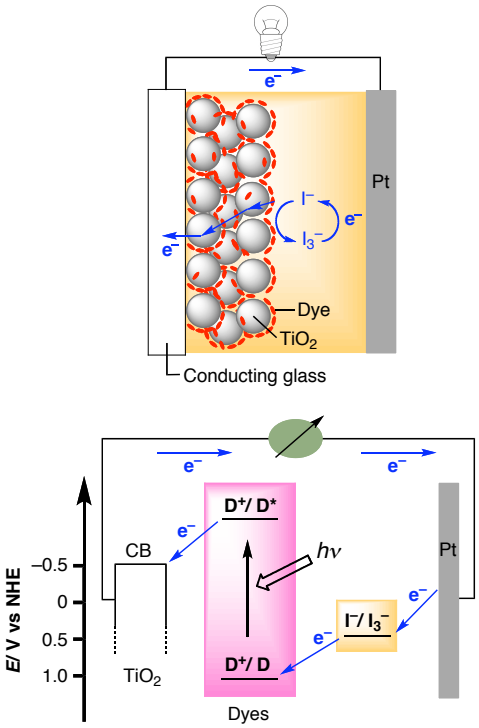

Figure 1. Fundamental processes in DSSC and the energy-level diagram.

The first objective of this thesis is the development of novel organic photosensitizers for DSSC focusing on optimization of anchoring groups and π-conjugative systems for light-harvesting. Binding ability between a dye and a TiO_2

electrode as well as electron transfer properties significantly depend on an anchoring group.[11] Nevertheless, the variations of the anchoring groups are limited to carboxylic acid,[12] a cyanoacrylic acid,[13] carboxylic acid anhydride,[14] acetylacetonate,[15] sulfonic acid,[16] phosphonic acid,[17] catechol,[18] and siloxane.[19] In Chapter 1, the author describes an oligothiophene bearing 1-oxo-1-hydroxydithieno[2,3-*b*:3',2'-*d*]phosphole as a novel anchoring group for DSSC (Figure 2).

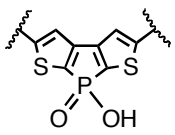

Figure 2. The novel anchoring group.

Next, the author focused on the molecular design of π-conjugative moieties for light-harvesting. Porphyrins have been frequently employed as sensitizers for DSSCs due to their strong Soret (400–450 nm) and moderate Q bands (550–600 nm).[20] Nevertheless, porphyrins typically showed inferior performances to ruthenium polypyridyl complexes as sensitizers because of the insufficient light-harvesting ability in the visible and near-infrared (NIR) regions. Broadening and red-shift of Soret and Q bands by elongation of the π-conjugation and loss of the symmetry in porphyrins are promising strategy to tackle the above problem.[10c] For instance, quinoxalino[2,3-β]porphyrin acid (ZnQMA) showed broadened, red-shifted, and amplified light absorption properties, leading to the relatively high power conversion efficiency.[21] In Chapter 2, benzoquinoxalino[2,3-β] porphyrin acid (ZnBQA) and quinoxalino[6,7-β]porphyrin acid (ZnQCA) (Figure 3) have been synthesized to evaluate the effects of the unsymmetrical π-elongation and the fused position of quinoxaline-fused porphyrins on the optical, electrochemical, and photovoltaic properties of the porphyrins.

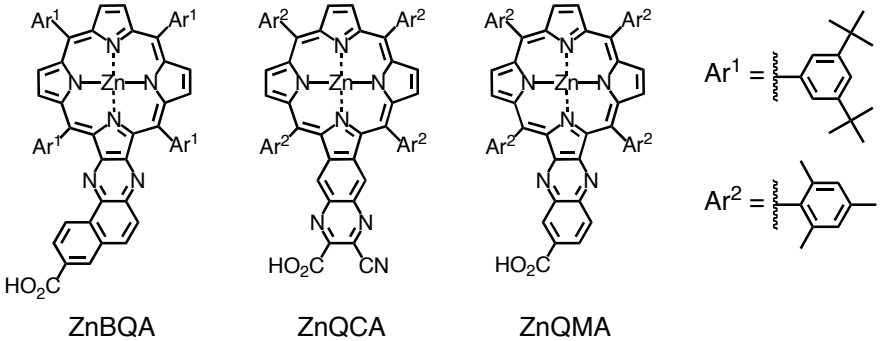

Figure 3. Quinoxaline-fused porphyrins.

3. Artificial Photosynthetic Solar Cells

Another important strategy in solar energy conversion is known as natural photosynthesis on the earth, and we can be inspired by the elaborate constructions of light-harvesting assemblies and photosynthetic reaction centers coupled with the multistep

sequences that eventually lead to the conversion of solar energy into chemical energy. The natural photosynthesis process begins by storing the energy of sunlight in the form of separated charges. For instance, in purple photosynthetic bacteria, the antenna complexes, including chlorophylls and carotenoid polyenes, harvest light in the blue and the red part of the sunlight. The antenna features strong absorption by multiple chromophores and extremely rapid singlet-singlet energy transfer among chromophores. The collected energy is funneled into the chlorophyll dimer (special pair) in the reaction center, whose role is to initiate the directional transfer of electrons by charge separation to give oxidized special pair and pheophytin anion. The subsequent multistep electron transfer takes place unidirectionally along the well-arranged chromophores that are embedded in a lipid bilayer membrane protein in the sequence of dimer, pheophytin, and quinone, leading to the generation of an electrochemical potential gradient across the biological membrane. Both the primary energy transfer and the electron transfer are ultrafast (occurring in 0.1–1 ps), leading to the trapping of the excitation energy at the reaction center on a 100 ps timescale and subsequent electron transfer in about 3 ps with almost 100% quantum yield.[22] Namely, in natural photosynthesis, the organized assemblies of photofunctional chromophores and catalysts within proteins allow to attain the highly efficient solar energy conversion by following three processes: (i) extensive light-harvesting in the visible and near infrared regions, (ii) efficient energy transfer in the chromophore complexes and subsequent charge separation, and (iii) efficient vectorial electron transport, minimizing undesirable charge recombination. Since the 1970s, many approaches to molecule-based artificial photosynthesis have been reported.[23] Covalent bonds of functional building blocks with well-defined molecular geometries and donor-acceptor distances allow precise control over energy and electron transfer. This is required for the first steps of solar energy conversion because the excited states and initially formed charge-separated states are thermodynamically and kinetically prone to reactions that convert the stored solar energy to useless heat. Imahori and Sakata et al. prepared and studied different porphyrin-linked C_{60} dyads and disclosed that the dyads generate long-lived charge-separated state with a high quantum yield due to the small reorganization energies of electron transfer.[24] Achieving an artificial photosynthesis for efficient photovoltaic devices requires hierarchical organization of these molecules on electrodes at the nanometer and/or sub-micrometer scales. Self-assembled monolayer,[24,25] Langmuir-Blodgett,[26] and lipid bilayer membrane methods[27] provided assemblies of large numbers of molecules into films. However, these attempts did not give fruitful results (the overall quantum yield = 1–25%) due to the poor light-harvesting performance and the instability of the film on electrodes. Furthermore, covalent syntheses of

large molecular arrays are highly inefficient and expensive. On the other hand, self-assembly and supramolecular organization lead to ordered molecular architectures in unique three-dimensional structures that can bridge length scales from nanometers to macroscopic dimensions. Intermolecular interactions such as hydrophobic/ hydrophilic, π-π, hydrogen bonding, and metal-ligand interactions are used to direct the formation of supramolecular structures having enhanced energy capture and charge transport properties.[28–30] Therefore, *these non-covalent interactions are potential approaches for controlling assembly of donor-acceptor molecules on an electrode, which can behave as an efficient artificial photosynthetic solar cell.*

The second objective of this thesis is the construction of donor-acceptor architectures on semiconducting electrodes using noncovalent interactions aiming at efficient solar energy conversion. In previous studies, composite molecular nanoclusters of porphyrins and C_{60} have been successfully prepared in a mixture of polar and nonpolar solvents due to π-π and lyophobic interactions and then assembled on a SnO_2 electrode using an electrophoretic deposition technique.[31] In such devices, high light-harvesting efficiency in the visible region due to multilayer of the chromophores and nanostructured electron-hole highway as a result of segregated nanoarrays of porphyrin-fullerene molecules contributed to efficient photocurrent generation. However, the light absorption ability of porphyrins in the long-wavelength region is insufficient as organic photovoltaic materials. Additionally, relationship between the molecular structures, the film structures, and the photoelectrochemical properties at molecular level remains elusive due to difficulty in achieving precise arrangement of bicontinuous donor-acceptor arrays on electrodes. Thus, the author have focused on the improvement of the light-harvesting performance and control donor-acceptor nanostructures on electrodes using hydrogen bonding and coordination bonding interaction which are strong interactions relative to π-π and lyophobic interactions.

In Chapter 3, clusters of phthalocyanine as donor with acceptors have been prepared and electrophoretically deposited on nanostructured SnO_2 electrodes toward the improvement of the photocurrent generation efficiency in the near infrared region.

Supramolecular assembly of donor and acceptor using hydrogen bonds ensures the formation of stable and well-ordered donor-acceptor dyads.[28] In Chapter 4 and Chapter 5, the author fabricated porphyrin and fullerene composites with hydrogen bonding on semiconducting electrodes (SnO_2 and TiO_2) and examined hydrogen bonding effects on surface structure, photophysical, and photoelectrochemistry.

If these bicontinuous donor-acceptor arrays can be arranged vertically on electrodes, electron and hole will be allowed to transport to their respective electrodes; a cathode and an

anode.[32] In Chapter 6, a novel strategy has been developed to construct the vertical arrangement of bicontinuous donor-acceptor arrays on a SnO_2 electrode. The relationship between the film structure and photoelectrochemical properties has been elucidated as a function of the number of donor layer for the first time.

References

(1) (a) Goldemberg, J.; Johansson, T. B. *World Energy Assessment Overview: 2004 Update*, UNDP, UN-DESA and the World Energy Council, 2005. (b) Eisenberg, R.; Nocera, D. G. *Inorg. Chem.* **2005**, *44*, 6799.

(2) Service, R. F. *Science* **2005**, *309*, 548.

(3) *BP Statistical Review of World Energy June 2009*.

(4) Agency for Natural Resources and Energy (http://www.enecho.meti.go.jp/genshi-az/atom/world_generate/method.html)

(5) (a) Butler, D. *Nature* **2008**, *453*, 558. (b) Service, R. F. *Science* **2008**, *319*, 718.

(6) (a) O'Regan, B.; Grätzel, M. *Nature* **1991**, *353*, 737. (b) Nazeeruddin, M. K.; Kay, A.; Rodicio, I.; Humphry-Baker, R.; Müller, E.; Liska, P.; Vlachopoulos, N.; Grätzel, M. *J. Am. Chem. Soc.* **1993**, *115*, 6382. (c) Grätzel, M. *Acc. Chem. Res.* **2009**, *42*, 1788.

(7) Imahori, H. *J. Mater. Chem.* **2007**, *17*, 31.

(8) (a) Tang, C. W. *Appl. Phys. Lett.* **1986**, *48*, 183. (b) Yu, G.; Gao, J.; Hummelen, J. C.; Wudl, F.; Heeger, A. J. *Science* **1995**, *270*, 1789. (c) Mayer, A. C.; Scully, S. R.; Hardin, B. E.; Rowell, M. W.; McGehee, M. D. *Mater. Today* **2007**, *10*, 28. (d) Heremans, P.; Cheyns, D.; Rand, B. P. *Acc. Chem. Res.* **2009**, *42*, 1740. (e) Liang, Y.; Xu, Z.; Xia, J.; Tsai, S.-T.; Wu, Y.; Li, Gang.; Ray, C.; Yu, L. *Adv. Mater.* DOI: 10.1002/adma.200903528.

(9) (a) Nazeeruddin, M. K.; Angelis, F. D.; Fantacci, S.; Selloni, A.; Viscardi, G.; Liska, P.; Ito, S.; Takeru, B.; Grätzel, M. *J. Am. Chem. Soc.* **2005**, *127*, 16835. (b) Gao, F.; Wang, Y.; Shi, D.; Zhang, J.; Wang, M.; Jing, X.; Humphry-Baker, R.; Wang, P.; Zakeeruddin, S. M.; Grätzel, M. *J. Am. Chem. Soc.* **2008**, *130*, 10720. (c) Chen, C.-Y.; Wang, M.; Li, J.-Y.; Pootrakulchote, N.; Alibabaei, L.; Ngoc-le, C.; Decoppet, J.-D.; Tsai, J.-H.; Grätzel, C.; Wu, C.-G.; Zakeeruddin, S. M.; Grätzel, M. *ACS Nano* **2009**, *3*, 3103.

(10) (a) Mishra, A.; Fischer, M. K. R.; Bäuerle, P. *Angew. Chem., Int. Ed.* **2009**, *48*, 2474. (b) Ooyama, Y.; Harima, Y. *Eur. J. Org. Chem.* **2009**, 2903. (c) Imahori, H.; Umeyama, T.; Ito, S. *Acc. Chem. Res.* **2009**, *42*, 1809.

(11) (a) Campbell, W. M.; Burrell, A. K.; Officer, D. L.; Jolley, K. W. *Coord. Chem. Rev.*

2004, *248*, 1363. (b) Ernstorfer, R.; Gundlach, L.; Felber, S.; Storck, W.; Eichberger, R.; Willig, F. *J. Phys. Chem. B* **2006**, *110*, 25383. (c) Chen, R.; Yang, X.; Tian, H.; Wang, X.; Hagfeldt, A.; Sun, L. *Chem. Mater.* **2007**, *19*, 4007. (d) Wiberg, J.; Marinado, T.; Hagberg, D. P.; Sun, L.; Hagfeldt, A.; Albinsson, B. *J. Phys. Chem. C* **2009**, *113*, 3881.

(12) (a) Hara, K.; Sayama, K.; Ohga, Y.; Shinpo, A.; Suga, S.; Arakawa, H. *Chem. Commun.* **2001**, 569. (b) Horiuchi, T.; Miura, H.; Sumioka, K.; Uchida, S. *J. Am. Chem. Soc.* **2004**, *126*, 12218. (c) Liu, W.-H.; Wu, I-C.; Lai, C.-H.; Lai, C.-H.; Chou, P.-T.; Li, Y.-T.; Chen, C.-L.; Hsu, Y.-Y.; Chi, Y. *Chem. Commun.* **2008**, 5152.

(13) (a) Wang, Z.-S.; Cui, Y.; Dan-oh, Y.; Kasada, C.; Shinpo, A.; Hara, K. *J. Phys. Chem. C* **2008**, *112*, 17011. (b) Choi, H.; Baik, C.; Kang, S. O.; Ko, J.; Kang, M.-S.; Nazeeruddin, M. K.; Grätzel, M. *Angew. Chem., Int. Ed.* **2008**, *47*, 327. (c) Zhang, G.; Bala, H.; Cheng, Y.; Shi, D.; Lv, X.; Yu, Q.; Wang, P. *Chem. Commun.* **2009**, 2198.

(14) (a) Shibano, Y.; Umeyama, T.; Matano, Y.; Imahori, H. *Org. Lett.* **2007**, *9*, 1971. (b) Li, C.; Yum, J.-H.; Moon, S.-J.; Herrmann, A.; Eickemeyer, F.; Pschirer, N. G.; Erk, P.; Schöneboom, J.; Müllen, K.; Grätzel, M.; Nazeeruddin, M. K. *ChemSusChem.* **2008**, *1*, 615.

(15) Heimer, T. A.; D'Arcangelis, S. T.; Farzad, F.; Stipkala, J. M.; Meyer, G. J. *Inorg. Chem.* **1996**, *35*, 5319.

(16) (a) Ma, T.; Inoue, K.; Noma, H.; Yao, K.; Abe, E. *J. Photochem. Photobiol. A* **2002**, *152*, 207. (b) Chen, Y.-S.; Li, C.; Zeng, Z.-H.; Wang, W.-B.; Wang, X.-S.; Zhang, B.-W. *J. Mater. Chem.* **2005**, *15*, 1654.

(17) (a) Odobel, F.; Blart, E.; Lagrée, M.; Villieras, M.; Boujtita, H.; Murri, N. E.; Caramori, S.; Bignozzi, C. A. *J. Mater. Chem.* **2003**, *13*, 502. (b) Nazeeruddin, M. K.; Humphry-Baker, R.; Officer, D. L.; Campbell, W. M.; Burrell, A. K.; Grätzel, M. *Langmuir* **2004**, *20*, 6514.

(18) (a) Dai, Q.; Rabani, J. *Chem. Commun.* **2001**, 2142. (b) Mosurkal, R.; He, J.-A.; Yang, K.; Samuelson, L. A.; Kumar, J. *J. Photochem. Photobiol. A* **2004**, *168*, 191. (c) Tae, E. L.; Lee, S. H.; Lee, J. K.; Yoo, S. S.; Kang, E. J.; Yoon, K, B. *J. Phys. Chem. B* **2005**, *109*, 22513.

(19) Baik, C.; Kim, D.; Kang, M-S.; Kang, S. O.; Ko, J.; Nazeeruddin, M. K.; Grätzel, M. *J. Photochem. Photobiol. A* **2009**, *201*, 168.

(20) (a) Kay, A.; Grätzel, M. *J. Phys. Chem.* **1993**, *97*, 6272. (b) Campbell, W. M.; Jolley, K. W.; Wagner, P.; Wagner, K.; Walsh, P. J.; Gordon, K. C.; Schmidt-Mende, L.; Nazeeruddin, Md. K.; Wang, Q.; Grätzel, M.; Officer, D. L. *J. Phys. Chem. C* **2007**, *111*,

11760. (c) Park, J. K.; Lee, H. R.; Chen, J.; Shinokubo, H.; Osuka, A.; Kim, D. *J. Phys. Chem. C* **2008**, *112*, 16691. (d) Mozer, A. J.; Griffith, M. J.; Tsekouras, G.; Wagner, P.; Wallace, G. G.; Mori, S.; Sunahara, K.; Miyashita, M.; Earles, J. C.; Gordon, K. C.; Du, L.; Katoh, R.; Furube, A.; Officer, D. L. *J. Am. Chem. Soc.* **2009**, *131*, 15621. (e) Wang, X.-F.; Kitao, O.; Zhou, H.; Tamiaki, H.; Sasaki, S. *J. Phys. Chem. C* **2009**, *113*, 7954. (f) Imahori, H.; Hayashi, S.; Hayashi, H.; Oguro, A.; Eu, S.; Umeyama, T.; Matano, Y. *J. Phys. Chem. C* **2009**, *113*, 18406. (g) Lu, H.-P.; Mai, C.-L.; Tsia, C.-Y.; Hsu, S.-J.; Hsieh, C.-P.; Chiu, C.-L.; Yeh, C.-Y.; Diau, E. W.-G. *Phys. Chem. Chem. Phys.* **2009**, *11*, 10270.

(21) Eu, S.; Hayashi, S.; Umeyama, T.; Matano, Y.; Araki, Y.; Imahori, H. *J. Phys. Chem. C* **2008**, *112*, 4396.

(22) (a) Fleming, G. R.; van Grondelle, R. *Physics Today* **1994**, *47*, 48. (b) McDermott, G.; Prince, S. M.; Freer, A. A.; Hawthornthwaite-Lawless, A. M.; Papiz, M. Z.; Cogdell, R. J.; Isaacs, N. W. *Nature* **1995**, *374*, 517. (c) *The Photosynthetic Reaction Center*; Deisenhofer, J., Norris, J. R., Ed.; Academic Press: San Diego, 1993. (d) *Anoxygenic Photosynthetic Bacteria*; Blankenship, R. E., Madigan, M. T., Bauer, C. E., Ed.; Kluwer Academic Publishing: Dordrecht, 1995.

(23) (a) Moore, T. A.; Gust, D.; Mathis, P.; Mialocq, J.-C.; Chachaty, C.; Bensasson, R. V.; Land, E. J.; Doizi, D.; Liddell, P. A.; Lehman, W. R.; Nemeth, G. A.; Moore, A. L. *Nature* **1984**, *307*, 630. (b) Meyer, T. J. *Acc. Chem. Res.* **1989**, *22*, 163. (c) Wasielewski, M. R. *Chem. Rev.* **1992**, *92*, 435. (d) Flamigni, L.; Armaroli, N.; Barigelletti, F.; Balzani, V.; Collin, J.-P.; Dalbavie, J.-O.; Heitz, V.; Sauvage, J.-P. *J. Phys. Chem. B* **1997**, *101*, 5936. (e) Gust, D.; Moore, T. A.; Moore, A. L. *Acc. Chem. Res.* **2001**, *34*, 40. (f) Redmore, N. P.; Rubtsov, I. V.; Therien, M. J. *J. Am. Chem. Soc.* **2003**, *125*, 8769. (g) Falkenstrom, M.; Johansson, O.; Hammarstrom, L. *Inorg. Chim. Acta.* **2007**, *360*, 741.

(24) (a) Imahori, H.; Sakata, Y. *Adv. Mater.* **1997**, *9*, 537. (b) Imahori, H.; Sakata, Y. *Eur. J. Org. Chem.* **1999**, 2445.

(25) (a) Imahori, H.; Yamada, H.; Nishimura, Y.; Yamazaki, I.; Sakata, Y. *J. Phys. Chem. B* **2000**, *104*, 2099. (b) Imahori, H.; Norieda, H.; Yamada, H.; Nishimura, Y.; Yamazaki, I.; Sakata, Y.; Fukuzumi, S. *J. Am. Chem. Soc.* **2001**, *123*, 100. (c) Yasutomi S.; Morita, T.; Imanishi, Y.; Kimura, S. *Science* **2004**, *304*, 1944. (d) Cho, Y.-J.; Ahn, T. K.; Song, H.; Kim, K. S.; Lee, C. Y.; Seo, W. S.; Lee, K.; Kim, S. K.; Kim, D.; Park, J. T. *J. Am. Chem. Soc.* **2005**, *127*, 2380. (e) Ludlow, M. K.; Soudackov, A. V.; Hammes-Schiffer, S. *J. Am. Chem. Soc.* DOI: 10.1021/ja910277p.

(26) (a) Tkachenko, N. V.; Vuorimaa, E.; Kesti, T.; Alekseev, A. S.; Tauber, A. Y.;

Hynninen, P. H.; Lemmetyinen, H. *J. Phys. Chem. B* **2000**, *104*, 6371. (b) Tkachenko, N. V.; Vehmanen, V.; Nikkanen, J.-P.; Yamada, H.; Imahori, H.; Fukuzumi, S.; Lemmetyinen, H. *Chem. Phys. Lett.* **2002**, *366*, 245. (c) Vuorinen, T.; Kaunisto, K.; Tkachenko, N. V.; Efimov, A.; Lemmetyinen, H. *Langmuir* **2005**, *21*, 5383. (d) Kotiaho, A.; Lahtinen, R. M.; Tkachenko, N. V.; Efimov, A.; Kira, A.; Imahori, H.; Lemmetyinen, H. *Langmuir* **2007**, *23*, 13117.

(27) (a) Seta, P.; Bienvenue, E.; Moore, A. L.; Mathis, P.; Bensasson R. V.; Liddell, P.; Pessiki, P. J.; Joy, A.; Moore, T. A.; Gust, D. *Nature* **1985**, *316*, 653. (b) Steinberg-Yfrach, G.; Liddel, P. A.; Huang, S.-C.; Moore, A. L.; Gust, D.; Moore, T. A. *Nature* **1997**, *385*, 239. (c) Steinberg-Yfrach, G.; Rigaud, J.-L.; Durantini, E. N.; Moore, A. L.; Gust, D.; Moore, T. A. *Nature* **1998**, *392*, 479. (d) Drain, C. M. *Proc. Natl. Acad. Sci. USA* **2002**, *99*, 5178. (e) Bhosale, S.; Sisson, A. L.; Talukdar, P.; Fürstenberg, A.; Banerji, N.; Vauthey, E.; Bollot, G.; Mareda, J.; Röger, C.; Würthner, F.; Sakai, N.; Matile, S. *Science* **2008**, *313*, 84.

(28) (a) van der Boom, T.; Hayes, R. T.; Zhao, Y.; Bushard, P. J.; Weiss, E. A.; Wasielewski, M. R. *J. Am. Chem. Soc.* **2002**, *124*, 9582. (b) Beckers, E. H. A.; Meskers, S. C. J.; Schenning, A. P. H. J.; Chen, Z.; Würthner, F.; Marsai, P.; Beljonne, D.; Cornil, J.; Janssen, R. A. J. *J. Am. Chem. Soc.* **2006**, *128*, 649. (c) Zhou, Z.; Chen, X.; Holdcroft, S. *J. Am. Chem. Soc.* **2008**, *130*, 11711. (d) Roncali, J. *Acc. Chem. Res.* **2009**, *42*, 1719.

(29) (a) Schenning, A. P. H. J.; Herrikhuyzen, J.; Jonkheijm, P.; Chen, Z.; Würthner, F.; Meijer, E. W. *J. Am. Chem. Soc.* **2002**, *124*, 10252. (b) Segura, M.; Sánchez, L.; de Mendoza, J.; Martín, N.; Guldi, D. M. *J. Am. Chem. Soc.* **2003**, *125*, 15093. (c) Jonkheijm, P.; Stutzmann, N.; Chen, Z.; de Leeuw, D. M.; Meijer, E. W.; Schenning, A. P. H. J.; Würthner, F. *J. Am. Chem. Soc.* **2006**, *128*, 9535. (d) Wasielewski, M. R. *Acc. Chem. Res.* **2009**, *42*, 1910.

(30) (a) Morisue, M.; Yamatsu, S.; Haruta, N.; Kobuke, Y. *Chem.-Eur. J.* **2005**, *11*, 5563. (b) Kobuke, Y. *Eur. J. Inorg. Chem.* **2006**, 2333. (c) Rodríguez-Morgade, M. S.; Torres, T.; Atienza-Castellanos, C.; Guldi, D. M. *J. Am. Chem. Soc.* **2006**, *128*, 15145. (d) Kuramochi, Y.; Sandanayaka, A. S. D.; Satake, A.; Araki, Y.; Ogawa, K.; Ito, O.; Kobuke, Y. *Chem.-Eur. J.* **2009**, *15*, 2317.

(31) (a) Kang, S.; Umeyama, T.; Ueda, M.; Matano, Y.; Hotta, H.; Yoshida, K.; Isoda, S.; Shiro, M.; Imahori, H. *Adv. Mater.* **2006**, *18*, 2549. (b) Imahori, H.; Ueda, M.; Kang, S.; Hayashi, H.; Hayashi, S.; Kaji, H.; Seki, S.; Saeki, A.; Tagawa, S.; Umeyama, T.; Matano, Y.; Yoshida, K.; Isoda, S.; Shiro, M.; Tkachenko, N. V.; Lemmetyinen, H. *Chem.-Eur. J.* **2007**, *13*, 10182.

(32) (a) Snaith, H. J.; Whiting, G. L.; Sun, B.; Greenham, N. C.; Huck, W. T. S.; Friend, R. H. *Nano Lett*. **2005**, *5*, 1653. (b) Tang, T.; Herrmann, A.; Peneva, K.; Müllen, K.; Webber, S. E. *Langmuir* **2007**, *23*, 4623. (c) Sisson, A. L.; Sakai, N.; Banerji, N.; Fürstenberg, A.; Vauthey, E.; Matile, S. *Angew. Chem., Int. Ed*. **2008**, *47*, 3727. (d) Bullock, J. E.; Carmieli, R.; Mickley, S. M.; Vura-Weis, J.; Wasielewski, M. R. *J. Am. Chem. Soc*. **2009**, *131*, 11919.

Chapter 1

Oligothiophene Bearing 1-Hydroxy-1-oxodithieno[2,3-*b*:3',2'-*d*] phosphole as a Novel Anchoring Group for Dye-sensitized Solar Cells

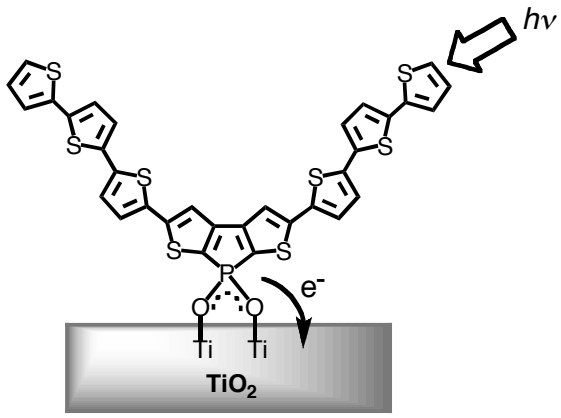

Abstract

An oligothiophene bearing 1-hydroxy-1-oxodithieno[2,3-*b*:3',2'-*d*]phosphole (**TP**) as a novel anchoring group has been synthesized for dye-sensitized solar cells (DSSC). **TP** was adsorbed on the TiO_2 surface through the 1-hydroxy-1-oxodithienophosphole. Attenuated total reflectance-Fourier transform infrared and X-ray photoelectron spectroscopy measurements disclosed the bidentate binding of the phosphinic acid unit to the TiO_2 surface. TiO_2 cell sensitized with **TP** yielded a maximum incident photon-to-current efficiency of 66% and a power conversion efficiency of 1.8%, implying that 1-hydroxy-1-oxodithienophosphole is a potential unit as a new type of anchoring groups for DSSC.

Introduction

In terms of the source limitation of fossil fuels and the environment pollution problem with their combustion, it is essential to develop alternative energy resources.[1] Generation of electrical energy from solar light is a long-term research interest, and various kinds of photovoltaic and/or photoelectrochemical devices have been explored.[2,3] Among them, dye-sensitized solar cells (DSSC) with mesoporous TiO_2 has been regarded as one of the most promising candidates for these regenerative energy sources because of the potential of low-cost production and high efficiency.[4] Although Ru complexes have proven to be excellent TiO_2 photosensitizers that have achieved a power conversion efficiency (η) up to 11%,[5] their extensive application would be hampered because of the limited availability and high cost of Ru metal. In this context, studies on metal-free or inexpensive metal-based organic chromophores for DSSC have grown rapidly.[6] Considering that an organic sensitizer is composed of a π-conjugated moiety for light-harvesting and an anchoring group for immobilization of the dye on a TiO_2 surface, the rationale molecular design of the both units is important to improve the cell performance. In this regard many π-conjugative molecules possessing light-harvesting capabilities have been developed using coumarin,[7] indoline,[8] thiophene,[9] cyanine,[10] porphyrin,[11] and/or others.[12] It is also crucial to optimize the binding ability of anchoring groups to a TiO_2 electrode as well as electron transfer properties through them for highly efficient DSSC.[13] Nevertheless, the variations of the anchoring groups are rather limited to carboxylic acid,[7a,8,9a,b,10,11a–d,12c–e,g] a cyanoacrylic acid,[7,9b–e,11d,12a,b] carboxylic acid anhydride,[12d,f] acetylacetonate group,[14] sulfonic acid,[15] phosphonic acid,[13a,16] catechol,[17] and siloxane.[18] Herein, the author reports an oligothiophene bearing 1-hydroxy-1-oxodithieno[2,3-*b*:3',2'-*d*]phosphole (**TP**) as a novel anchoring group for DSSC (Figure 1).

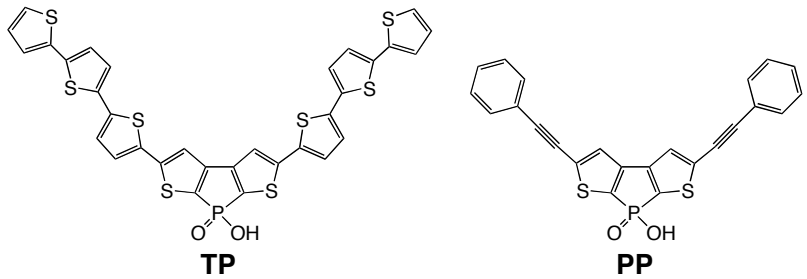

Figure 1. Molecular structures of the **TP** and **PP** sensitizers.

Phosphole changes its electronic structure by the introduction of π-conjugative substituents at the P-connected *cis*-1,3-diene function and possesses a capability of changing its optical and electrochemical properties by chemical functionalizations at the phosphorus center.[19,20] These prominent optical and electrochemical features allow phosphole-containing π-conjugated systems to be subject to considerable research toward applications in organic light-emitting diodes, field-effect transistors, and nonlinear optical devices,[19,20] while there has been no report of phosphole-based

sensitizers for DSSC. In the molecular design, 1-hydroxy-1-oxodithienophosphole is chosen as an anchoring group. The electron density of the LUMO of 1-hydroxy-1-oxodithienophosphole is extended to the phosphinic acid group due to the effective σ^*-π^* orbital interaction in the phosphole moiety,[19,20] as predicted by DFT calculations (Figure 2). Meanwhile, the conjugation between thiophene moieties and phosphinic acid group in the HOMO is broken at the P atom.[21]

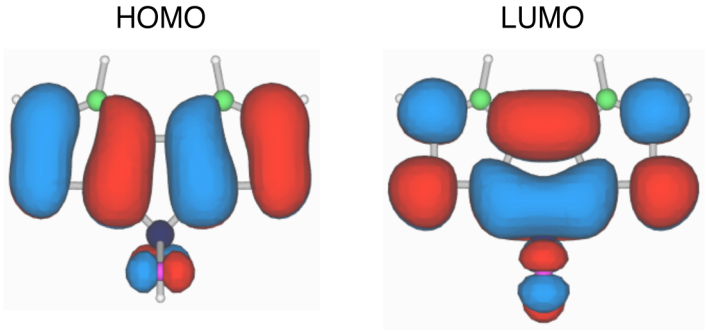

Figure 2. Molecular orbitals for 1-hydroxy-1-oxodithienophosphole determined by DFT calculations at B3LYP/3-21G* level (green sphere: C atom, white sphere: H atom, orange sphere: S atom, pink sphere: O atom, black sphere: P atom).

By introducing electron-donating π-conjugative chromophores (i.e., oligothiophene) as a light-harvesting moiety into the dithienophosphole core, the author expected the occurrence of fast electron injection from the dye excited state to a conduction band (CB) of the TiO_2 and slow charge recombination from the electron in the CB to the dye radical cation through the anchoring group, resulting in the improvement of cell performance. Furthermore, the possible bidentate binding to the TiO_2 surface together with the high electron density of the phosphinic acid group in the LUMO would ensure the formation of a stable, tight monolayer of **TP**.

Results and Discussion

Synthesis. The synthetic route to **TP** is shown in Scheme 1. Dithienophosphole **1** was synthesized according to the methods previously reported by Cristau et al.[22] Then, dithienophosphole **1** was treated with *N*-bromosuccinimide (NBS) to yield dibromodithienophosphole **2**. Terthiophene-linked dithienophosphole **3** was prepared by Stille coupling reaction of **2** with 5-tri(*n*-butyl)stannyl-2,2':5',2''-terthiophene. Finally, hydrolysis of **3** afforded **TP**. Phenylethynyl-linked 1-hydroxy-1-oxodithieno-phosphole (**PP**) was also prepared by Sonogashira coupling to compare the light-harvesting, optical, and photovoltaic properties with those of **TP**.

Scheme 1. Synthesis of **TP** and **PP**.

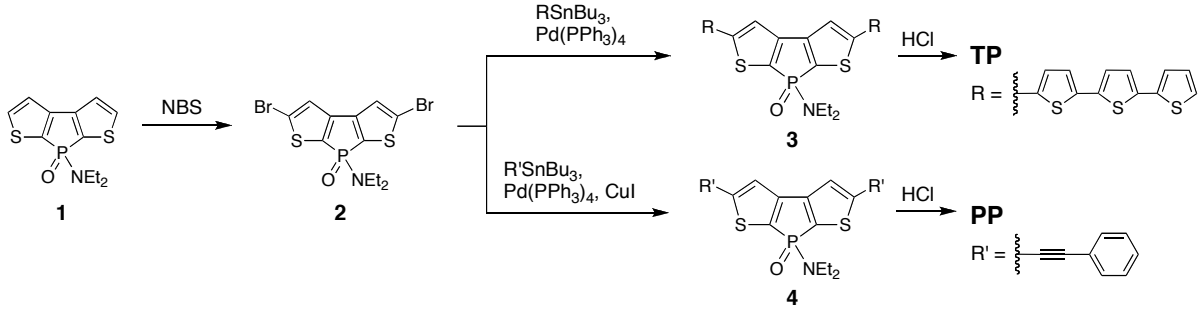

Optical and Electrochemical Properties. Figure 3a displays the UV-vis absorption and fluorescence spectra of **TP** and **PP** in THF. The absorption band of **TP** appears at 403 nm with a molar extinction coefficient (ε) of 4.80×10^4 M^{-1} cm^{-1}, whereas the fluorescence of **TP** is centered at 522 nm. The absorption maximum of **TP** is red-shifted by 32 nm compared with that of **PP**. The fluorescence quantum yield (Φ_f) of **TP** (10%) is larger than that of **PP** (3%). These results imply that the introduction of the electron-donating π-extended chromophores (i.e., terthiophene) into the dithienophosphole core improves the light-harvesting and fluorescence properties in the visible region considerably. In addition, the absorption and fluorescence maxima of **TP** are significantly red-shifted relative to those of **1** (λ_{abs} = 345 nm; λ_{em} = 422 nm) and terthiophene (λ_{abs} = 352 nm; λ_{em} = 428 nm), supporting the effective π-extension in **TP** (Figure 3b). The excitation energy ($E_{0\text{-}0}$) was estimated to

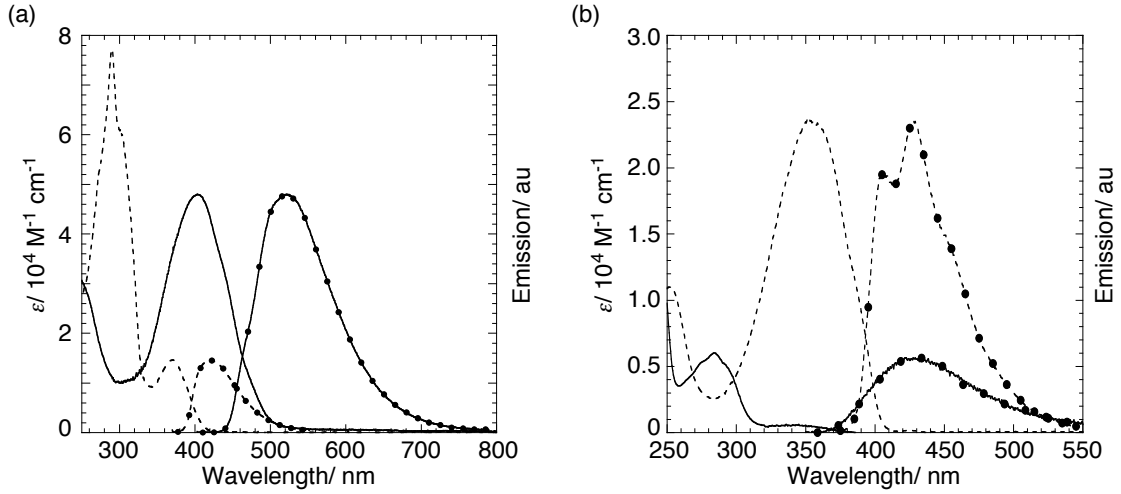

Figure 3. (a) Absorption spectra of **TP** (black solid line) and **PP** (black dashed line) and normalized emission spectra of **TP** (red solid line) and **PP** (red dashed line) in THF. Excitation wavelength: 403 nm for **TP**, 370 nm for **PP**. (b) Absorption spectra of **1** (black solid line) and terthiophene (black dashed line) and fluorescence spectra of **1** (red solid line) and terthiophene (red dashed line) in THF. The fluorescence spectra were normalized at the maxima of the corresponding absorption spectra for comparison. The excitation wavelength: 345 nm for **1** and 352 nm for terthiophene.

Table 1. Optical and Electrochemical Properties of **TP** and **PP**

	λ_{abs}/ nm [a] (e/ M^{-1} cm^{-1})	λ_{em}/ nm	Φ_f / % [d]	$E_{0\text{-}0}$/ eV [e]	E_{ox}/ V [f]	E_{ox}*/ V [g]
TP	403 (48 000)	522[b]	10	2.73	1.25	–1.48
PP	371 (14 500)	423[c]	3	3.14	1.52	–1.62

[a] Wavelength for the absorption maxima in THF. [b] Wavelength for the emission maxima in THF by exciting at 403 nm. [c] Wavelength for the emission maxima in THF by exciting at 370 nm. [d] Measured in THF using 9,10-diphenylanthracene as standard (Φ_f = 90% in cyclohexane). [e] Excitation transition energy determined from the intercept of the absorption and emission spectra. [f] Oxidation potential (vs NHE). [g] Excited-state oxidation potential (vs NHE).

be 2.73 eV (Table 1). The first one-electron oxidation potentials (E_{OX}) of **TP** (1.25 V vs NHE) and **PP** (1.52 V vs NHE) were determined by differential pulse voltammetry in THF containing Bu_4NPF_6 as a supporting electrolyte (Table 1). From the E_{OX} and $E_{0\text{-}0}$ values, the excited-state oxidation potentials (E_{OX}*) of **TP** and **PP** were estimated to be –1.48 V and –1.62 V vs NHE. Taking into account the energy levels of the CB of TiO_2 (–0.5 V vs NHE)[11c] and I^-/I_3^- couple (0.5 V vs NHE),[11c] electron injection from the dye excited singlet state to the CB of TiO_2 and charge shift from I^- to the resulting dye radical cation (1.25 V vs NHE) are thermodynamically feasible both in the **TP** and **PP** cells (Figure 4).

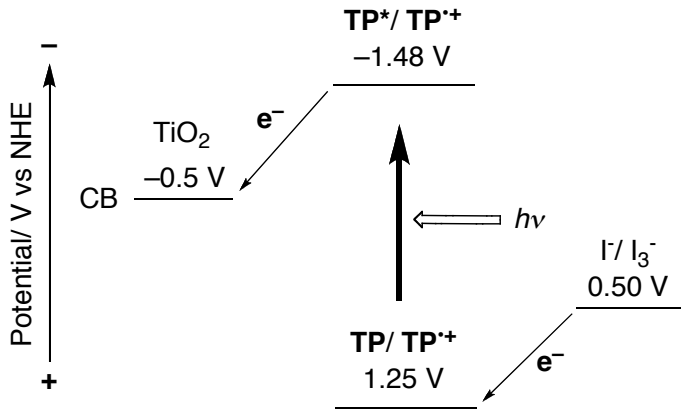

Figure 4. Energy diagram for the TiO_2/**TP** cell.

DFT Calculations. DFT calculations were employed to gain insight into the equilibrium geometry and electronic structures for the HOMO and LUMO of **TP** and the SOMO of **TP** radical cation (Figure 5). The optimized geometry has no negative frequencies. The LUMO is localized mainly over the dithienophosphole including the anchoring group, whereas the HOMO of **TP** and the SOMO of **TP** radical cation are delocalized except for the anchoring group. For **TP**, 70% of the electron density in the HOMO is located on the two terthiophene units, and 10% of the electron density in the LUMO is distributed on the phosphinic acid group. For **PP**, 37% of the HOMO is localized on

the two phenylacetylene units, and 14% of the LUMO lies on the phosphinic acid group. These results indicate that the HOMO-LUMO excitation of **TP** shifts the electron distribution from the chromophores to phosphinic acid group more obviously than **PP**. In organic dyes for DSSC, it was found that the delocalization of HOMOs of dyes over the π-conjugated systems and the delocalization of LUMOs over the anchoring part allow the not only ultrafast photoinduced electron injection from the dyes to TiO_2 electrodes by intramolecular charge transfer with respect to HOMO-LUMO transition but also slow recombination of the injected electron with the oxidized dyes due to their remoteness.[6,21] Therefore, one can expect an efficient photoinduced electron transfer from **TP** to the TiO_2 electrode and slow charge recombination from the electron in the CB to the dye radical cation.

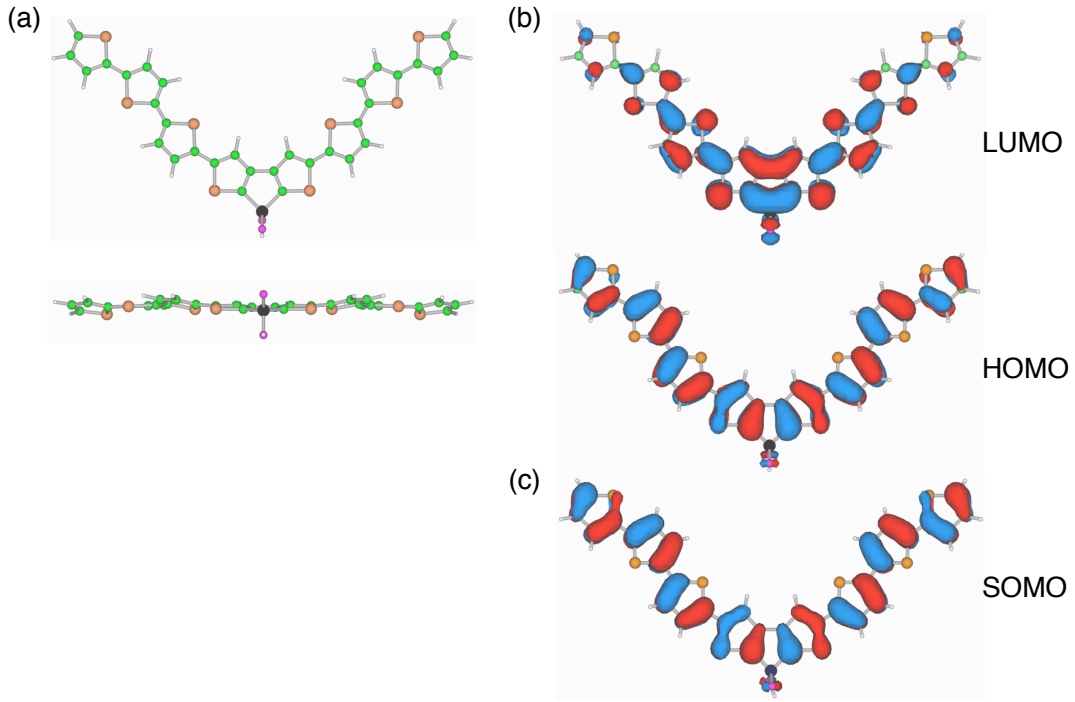

Figure 5. (a) Optimized geometries with different viewing angles, (b) the LUMO and HOMO of **TP**, and (c) the SOMO of **TP** radical cation determined by DFT calculations at B3LYP/3-21G* level.

Dye Adsorption on TiO_2. Mesoporous TiO_2 films (10-mm-thick) were prepared from colloidal suspension of TiO_2 nanoparticles (P-25) (see Experimental Section). **TP** and **PP** were sensitized onto TiO_2 electrodes as a working electrode in DSSC by the following method (denoted as TiO_2/**TP** and TiO_2/**PP**, respectively). The mesoporous P-25 based TiO_2 electrodes with a thickness of 10 μm were immersed into a THF solution of 0.5 mM **TP** or **PP** containing 2.5 mM chenodeoxycholic acid (CDCA) at room temperature for 12 h. Little shift and broadening of the absorption peak of **TP** on the TiO_2 are noted in comparison with that in THF (Figure 6), showing no considerable aggregation of **TP**

on the TiO_2 electrode. On the other hand, **3** did not bind to a bare TiO_2 electrode (Figure 7). Therefore, 1-hydroxy-1-oxodithenophosphole acts as an anchoring group to the TiO_2 surface through its phosphinic acid unit.

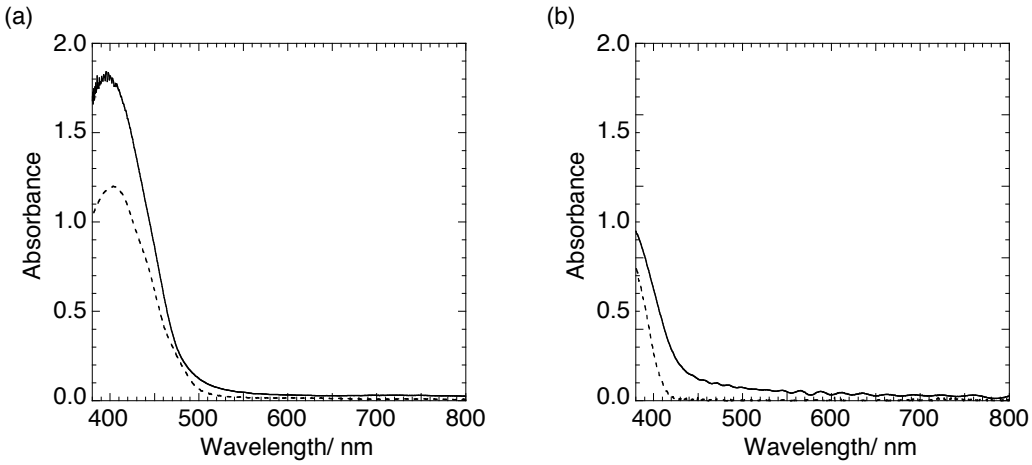

Figure 6. UV-vis absorption spectra of (a) TiO_2/**TP** electrode (solid line) and **TP** in THF (dashed line) and of (b) TiO_2/**PP** electrode (solid line) and **PP** in THF (dashed line). Thickness of the TiO_2 layer was adjusted to be 2 μm to evaluate the shape of the absorption. The absorption arising from the corresponding bare TiO_2 electrode was subtracted from the spectra.

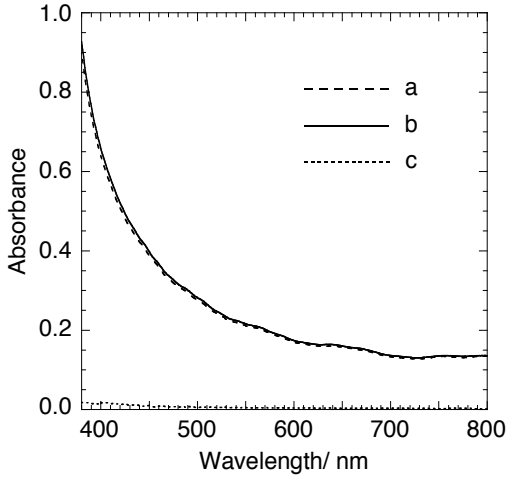

Figure 7. UV-vis absorption spectra of (a) a bare TiO_2 electrode (dashed line), (b) a TiO_2 electrode after treatment with a THF solution containing **3** (solid line), and (c) a difference between (a) and (b) (dotted line).

To get information on the binding mode of the molecules adsorbed on the TiO_2 electrode, attenuated total reflectance-Fourier transform infrared (ATR-FTIR) spectra were measured for powders of **TP** and **PP** as well as TiO_2/**TP** and TiO_2/**PP** (Figure 8). ATR-FTIR spectra of **TP** and **PP** reveal the characteristic bands of ν(P=O) and ν(P–OH) of the phosphinic acid group at around 1200 cm^{-1} and 960 cm^{-1}, respectively.[23] However, these bands disappear and a peak corresponding to ν(O–P–O) at

around 1040–1060 cm^{-1} emerges for the spectra of TiO_2/**TP** and TiO_2/**PP**.[23] These results demonstrate that the two equivalent P–O bonds are formed through a bidentate coordination of the phosphinate to the TiO_2 surface.[29]

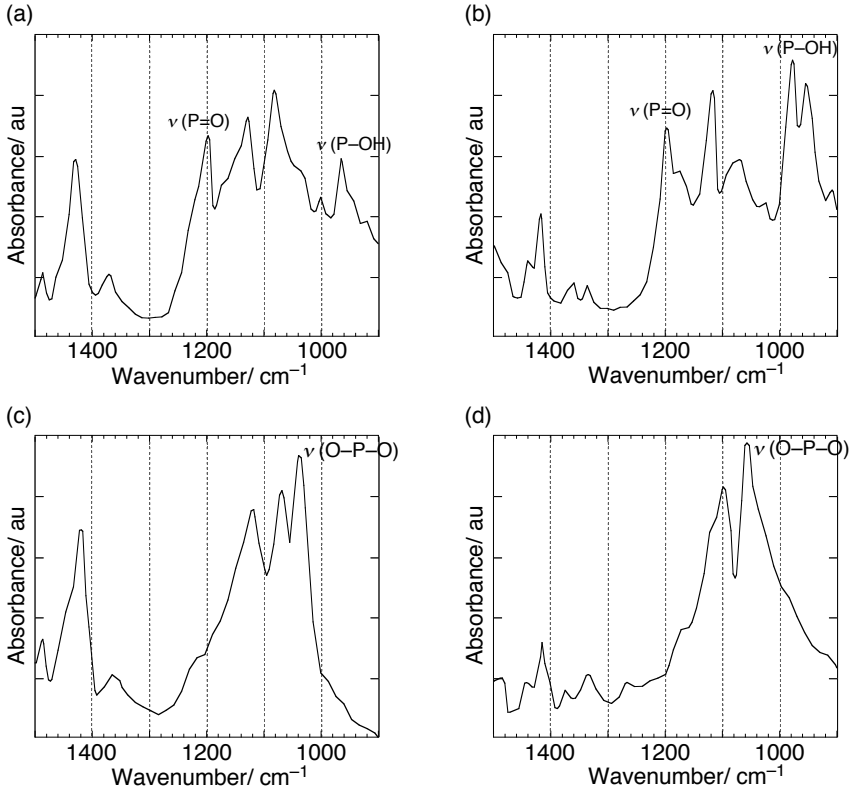

Figure 8. ATR-FTIR spectra of (a) **TP** and (b) **PP**, and (c) TiO_2/**TP** and (d) TiO_2/**PP** electrodes. The absorption arising from the corresponding bare TiO_2 electrode was subtracted from the spectra of TiO_2/**TP** and TiO_2/**PP** to obtain those of (c) and (d).

To further shed light on adsorption state of the dyes on the TiO_2 surface, X-ray photoelectron spectroscopy (XPS) measurements were performed for TiO_2/**TP** and TiO_2/**PP** together with **TP** and **PP**. Figure 9 depicts the O1s XPS spectra. The spectra of **TP** and **PP** were curve-fitted into two chemically different O1s subpeaks (Figure 9a,b and Table 2). The peaks arising at around 531 eV and 533 eV can be assigned to the oxygen atoms of P=O and of P–OH in the phosphinic acid, respectively.[23f,24] The spectra of TiO_2/**TP** and TiO_2/**PP** also exhibit two different peaks, respectively (Figure 9c,d and Table 2). The peaks at 530.2 eV stem from the oxygen atoms in TiO_2.[11c,24,25] The peaks at 531.2–531.6 eV can be attributed to the oxygen atoms of P–O–Ti bonds.[24] It is noteworthy that the peaks derived from the O atoms of P–OH at around 533 eV disappear in the spectra of TiO_2/**TP** and TiO_2/**PP**. Thus, one can conclude that the two oxygens in the phosphinate bind to the TiO_2 surface with the same binding energy through a bidentate coordination, which is in good agreement with the results on the ATR-FTIR measurements (vide supra).

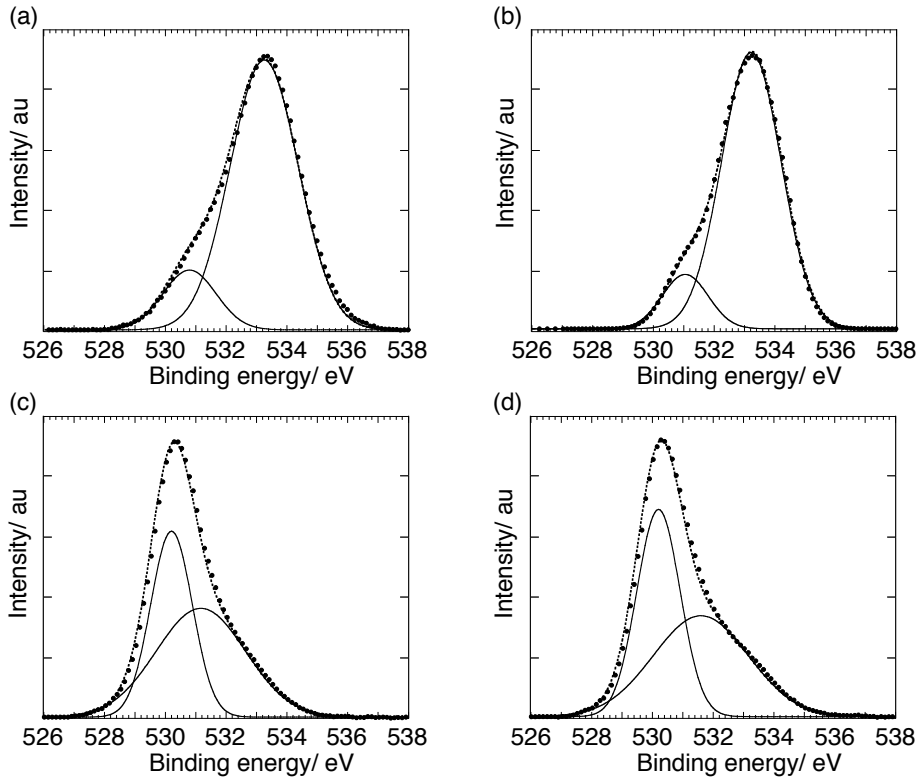

Figure 9. X-ray photoelectron O1s spectra of (a) **TP**, (b) **PP**, (c) TiO_2/**TP**, and (d) TiO_2/**PP**. The spectra are normalized for comparison.

Table 2. O1s Binding Energies for **TP**, **PP**, TiO_2/**TP**, and TiO_2/**PP**

	binding energy/ eV	assignment
TP	530.8	P=O
	533.3	P–OH
PP	531.0	P=O
	533.2	P–OH
TiO_2/TP	530.2	TiO_2
	531.2	P–O–Ti
TiO_2/PP	530.2	TiO_2
	531.6	P–O–Ti

Given the surface area of P-25 (54 $m^2 g^{-1}$),[11c] the packing densities (Γ) of **TP** and **PP** on the actual TiO_2 surface area are determined to be 1.9×10^{-10} mol cm^{-2} and 2.0×10^{-10} mol cm^{-2}. Assuming that **TP** and **PP** molecules are densely packed onto the TiO_2 surface yielding a full monolayer without CDCA, the calculated Γ values are 2.4×10^{-10} mol cm^{-2} and 3.2×10^{-10} mol cm^{-2}. The experimental Γ values are considerably lower than the calculated Γ values, implying that the dye molecules are isolated each other by the intercalation of CDCA molecules, thereby reducing the dye aggregation.

Photovoltaic Properties. Current-voltage characteristics of the TiO_2/**TP** and TiO_2/**PP** electrodes were evaluated under standard AM 1.5 conditions (100 mW cm^{-2}), using CH_3CN electrolyte solution containing 0.5 M LiI and 0.01 M I_2 (Figure 10a). An $\eta = 1.8\%$ value of the **TP** cell was obtained with a J_{SC} of 7.4 mA cm^{-2}, a V_{OC} of 0.46 V, and a *ff* of 0.54, whereas an $\eta = 0.56\%$ value of the **PP** cell was obtained with a J_{SC} of 2.3 mA cm^{-2}, a V_{OC} of 0.44 V, and a *ff* of 0.54. The remarkably large η value of the **TP** cell relative to the **PP** cell is consistent with the difference in the light-harvesting properties of **TP** and **PP** (vide infra). The photocurrent action spectra of the TiO_2/**TP** and TiO_2/**PP** electrodes are illustrated in Figure 10b. The action spectra and the absorption spectra are virtually similar for the electrodes, implying the involvement of the dyes for the photocurrent generation. The TiO_2/**TP** electrode exhibits a maximum IPCE (incident photon-to-current efficiency) value of 66% at 400 nm. This IPCE value for **TP** cell is comparable to that of N719-sensitized TiO_2 cell (72%) under our experimental conditions,[26] implying the occurrence of efficient electron injectionfrom the **TP** excited singlet state to the CB of TiO_2 due to sufficient strong electronic coupling between 1-oxo-1-hydroxydithienophosphole and 3d orbital of TiO_2. In contrast, the TiO_2/**PP** electrode reveals much lower IPCE values in the visible region (43% at 400 nm). Similar difference is noted for APCE (adsorbed photon-to-current efficiency) values of the TiO_2/**TP** (66%) and TiO_2/**PP** (44%) electrodes. The APCE values are lower limits because the author does not take into account the collection losses (e.g. reflection) in the TiO_2 films. To address the effect of the charge recombination, the author measured the current-voltage characteristics under dark conditions (Figure 10a). The onset of the dark current for **TP** cell appears at a higher potential than that for **PP** cell, indicating that the degree of the

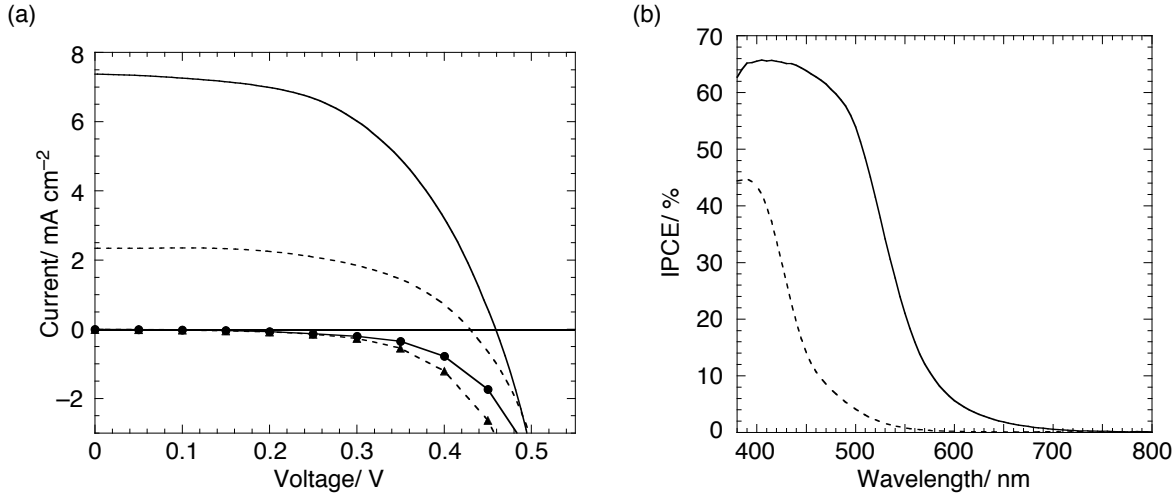

Figure 10. (a) Current-voltage characteristic of the TiO_2/**TP** (solid line) and TiO_2/**PP** (dashed line) electrodes under an irradiation of 100 mW cm^{-2} AM 1.5G sunlight and TiO_2/**TP** (solid line with circles) and TiO_2/**PP** (dashed line with triangles) electrodes in the dark. (b) Photocurrent action spectra of the TiO_2/**TP** (solid line) and TiO_2/**PP** (dashed line) electrodes. Electrolyte: 0.5 M LiI and 0.01 M I_2 in CH_3CN.

charge recombination for the **PP** cell is higher than that for **TP** cell. The differences in the APCE and IPCE values between **TP** and **PP** may be attributed to those in the fluorescence quantum yields as well as in the HOMO-LUMO distribution (vide supra).

Conclusion

The author has successfully synthesized oligothiophene bearing 1-hydroxy-1-oxodithenophosphole as a novel anchoring group for DSSC for the first time. The introduction of the oligothiophene moieties into 1-hydroxy-1-oxodithienophosphole was found to improve the light-harvesting property in the visible region, leading to enhancement in the cell performance relative to the reference device with the weak light-harvesting unit. The author has also disclosed the binding mode of the novel anchoring group to the TiO_2 surface by ATR-FTIR and XPS measurements. These results corroborate the potential utility of 1-hydroxy-1-oxodithienophosphole as a novel anchoring group for DSSC. Although the cell performance is moderate, the further improvement may be possible by introducing excellent light-harvesting and electron-donating chromophores into the 1-hydroxy-1-oxodithienophosphole as well as improving the device structure.

Experimental Section

Materials and General Procedures. Toluene and diisopropylamine were distilled from CaH_2 and NaOH, respectively. Other solvents and chemicals were of reagent grade quality, purchased commercially and used without further purification unless otherwise noted. Thin-layer chromatography and flash column chromatography were performed with Alt. 5554 DC-Alufolien Kieselgel 60 F_{254} (Merck) and Silica-gel 60N (SiliCycle), respectively. Melting points were recorded on a Yanagimoto micro-melting point apparatus and not corrected. ^{1}H NMR, ^{13}C NMR, and ^{31}P NMR spectra were measured on a JEOL EX-400 or an ECX-400P spectrometer. Chemical shifts are reported as the relative values vs tetramethylsilane (^{1}H, ^{13}C) or H_3PO_4 (^{31}P). High-resolution mass spectra (HRMS) were recorded on a JEOL JMS-MS700 spectrometer or a JEOL JMS-HX110A spectrometer. Syntheses of compounds **1** and 5-tri(*n*-butyl)stannyl-2,2':5',2"-terthiophene were carried out according to the previously reported method.[22,27]

Synthesis and Characterization. *Compound* ***2***. *N*-Bromosuccinimide (1.89 g, 10.6 mmol) was added to a solution of **1** (1.00 g, 3.53 mmol) in $CHCl_3$ (17 mL) and AcOH (17 mL). The reaction mixture was stirred for 2.5 h at room temperature, and then 20% KOH aqueous solution (34 mL) was added to neutralize AcOH. The organic layer was washed with brine, dried over Na_2SO_4, and concentrated in vacuum. Column chromatography on silica gel with CH_2Cl_2 and AcOEt afforded **2** as

a white solid (635 mg, 1.44 mmol, 41%): mp 143–144 °C; ^{1}H NMR ($CDCl_3$, 400 MHz) δ 7.07 (d, J_{HP} = 2.0 Hz, 2H), 3.08 (qd, J_{HH} = 6.8 Hz, J_{HP} = 12.7 Hz, 4H), 1.09 (t, J = 6.8 Hz, 6H); ^{13}C{^{1}H} NMR ($CDCl_3$, 100 MHz) δ 146.4 (J_{PC} = 20.6 Hz), 131.7, 130.4, 123.4 (J_{PC} = 10.7 Hz), 38.3 (J_{PC} = 5.8 Hz), 13.8 (J_{PC} = 2.5 Hz); ^{31}P{^{1}H} NMR ($CDCl_3$, 162 MHz) δ 18.82; HRMS (FAB, positive mode) found 439.8549 ($M+H^+$), $C_{12}H_{12}Br_2NOPS_2$ requires 438.8465.

*Compound **3***. A solution of **2** (75.8 mg, 0.172 mmol), $Pd(PPh_3)_4$ (9.96 mg, 0.00862 mmol), and 5-tri(*n*-butyl)stannyl-2,2':5',2"-terthiophene (205 mg, 0.381 mmol) in dry toluene (1.3 mL) was heated at reflux for 18 h under argon atmosphere. The reaction mixture was concentrated in vacuo and chromatographed on silica gel with CH_2Cl_2 and AcOEt to give **3** as an orange solid (80 mg, 0.103 mmol, 60%): mp 236–237 °C; ^{1}H NMR ($CDCl_3$, 400 MHz) δ 7.24 (d, J_{HP} = 1.0 Hz, 2H), 7.20–7.18 (m, 6H), 7.13–7.10 (m, 6H), 7.05–7.03 (m, 2H), 3.16 (qd, J_{HH} = 7.3 Hz, J_{HP} = 12.7 Hz, 4H), 1.13 (t, J = 7.3 Hz, 6H); ^{13}C{^{1}H} NMR ($CDCl_3$, 100 MHz) δ 148.7 (J_{PC} = 5.8 Hz), 137.6, 137.0, 136.9, 135.3, 134.8, 128.0, 125.6, 124.8, 124.5, 124.4, 124.0, 121.0, 120.7, 116.7, 116.6, 38.5 (J_{PC} = 4.9 Hz), 14.0 (J_{PC} = 2.5 Hz); ^{31}P{^{1}H} NMR ($CDCl_3$, 162 MHz) δ 19.69; λ_{abs} (CH_2Cl_2) nm (ε/ M^{-1} cm^{-1}) 403 (5.0×10^4); HRMS (FAB, positive mode) found 774.9528 (M^+), $C_{36}H_{26}NOPS_8$ requires 774.9518.

*Compound **TP***. Hydrochloric acid (12 N; 18 mL, 0.22 mol) was added to a solution of **3** (30.0 mg, 0.0387 mmol) in THF (50 mL) at 0ºC. The reaction mixture was stirred for 5 h at room temperature, and extracted with CH_2Cl_2. The organic layer was washed with brine and dried over $MgSO_4$. The solvent was removed, and precipitation from CH_2Cl_2/hexane gave **TP** as an orange solid (21 mg, 0.029 mmol, 75%): mp 227–228 °C; ^{1}H NMR (DMSO-d_6, 400 MHz) δ 7.58–7.56 (m, 2H), 7.39–7.29 (m, 12H), 7.15–7.12 (m, 2H); ^{31}P{^{1}H} NMR (DMSO-d_6, 162 MHz) δ –0.75; λ_{abs} (THF) nm (ε/ M^{-1} cm^{-1}) 403 (4.8×10^4); HRMS (FAB, positive mode) found 719.8712 (M^+), $C_{32}H_{17}O_2PS_8$ requires 719.8732. ^{13}C NMR spectrum could not be obtained because of the low solubility.

*Compound **4***. In a flask held under argon pressure was placed **2** (50.0 mg, 0.113 mmol), dry diisopropylamine (0.72 mL), dry toluene (0.50 mL), and $Pd(PPh_3)_4$ (7.94 mg, 0.00687 mmol). The reaction mixture was heated to 60°C, and phenylacetylene (37 mL, 0.33 mmol) and CuI (1.0 mg, 0.0053mmol) were added. The reaction was stirred under argon at 60°C for 10 h. The flask was allowed to cool to room temperature, and diethyl ether was added. The mixture was washed with 10% HCl, water, and brine and dried over Na_2SO_4. The solvent was evaporated, and the residue was chromatographed over silica gel using CH_2Cl_2 and AcOEt. The combined pure fractions yielded upon removal of the solvent gave **4** as a pale yellow solid (27.9 mg, 0.0577 mmol, 51%): mp 196–197 °C; ^{1}H NMR (CD_2Cl_2, 400 MHz) δ 7.56–7.53 (m, 4H), 7.41–7.38 (m, 6H), 7.29 (d, J_{HP} = 2.0 Hz, 2H), 3.10 (qd, J_{HH} = 7.3 Hz, J_{HP} = 12.7 Hz, 4H), 1.10 (t, J = 7.3 Hz, 6H); ^{13}C{^{1}H} NMR (CD_2Cl_2, 100 MHz) δ 147.2 (J_{PC} = 20.6 Hz), 135.0 (J_{PC} = 6.6 Hz), 134.0, 132.7, 131.9, 131.4, 129.5, 129.0, 125.1 (J_{PC} = 11.5 Hz), 122.5, 96.8, 82.1 (J_{PC} = 2.5 Hz), 38.8 (J_{PC} = 4.9 Hz), 14.1 (J_{PC} = 3.3 Hz); ^{31}P{^{1}H} NMR (CD_2Cl_2, 162

MHz) δ 17.92; λ_{abs} (THF) nm (ε/ M^{-1} cm^{-1}) 383 (9.6×10^3); HRMS (EI, positive mode) found 483.0880 (M^+), $C_{28}H_{22}NOPS_2$ requires 483.0880.

*Compound **PP***. Hydrochloric acid (12 N; 7.0 mL, 0.084 mol) was added to a solution of **3** (30.0 mg, 0.0621 mmol) in THF (15 mL) at 0°C. The reaction mixture was stirred for 4.5 h at room temperature, and extracted with CH_2Cl_2. The organic layer was washed with brine and separated from aqueous phase. The solvent was removed, and washing with water following precipitation from CH_2Cl_2/hexane gave **PP** as a pale yellow solid (24 mg, 0.056 mmol, 90%): mp 203–204 °C; ^{1}H NMR (DMSO-d_6, 400 MHz) δ 7.65 (d, J_{HP} = 1.5 Hz, 2H), 7.59–7.57 (m, 4H), 7.45–7.43 (m, 6H); ^{13}C{^{1}H} NMR (DMSO-d_6, 100 MHz) δ 134.0, 131.9 (J_{PC} = 4.0 Hz), 131.8, 130.0, 129.7, 129.4, 127.9, 126.2 (J_{PC} = 10.9 Hz), 122.1 (J_{PC} = 16.9 Hz), 121.8, 95.9, 83.1; ^{31}P{^{1}H} NMR (DMSO-d_6, 162 MHz) δ 0.31; λ_{abs} (THF) nm (ε/ M^{-1} cm^{-1}) 371 (1.5×10^4); HRMS (FAB, positive mode) found 428.0090 (M^+), $C_{24}H_{13}O_2PS_2$ requires 428.0095.

Density Functional Theory (DFT) Calculations. Geometry optimization and electronic structure calculations of the dyes were performed using B3LYP functional and 3-21G* basis set implemented in the Gaussian 03 program package. Molecular orbitals were visualized by Molstudio 3.0 software.[28] Electron densities of HOMO and LUMO were calculated using molecular orbital coefficients on each atoms.[29]

Electrochemical Measurements. Electrochemical measurements were made using an ALS 630a electrochemical analyzer. First one-electron oxidation potentials were determined by differential pulse voltammetry (DPV) in THF containing 0.1M tetrabutylammonium hexafluorophosphate (Bu_4NPF_6). A glassy carbon (3 mm diameter) working electrode, $Ag/AgNO_3$ reference electrode, and Pt wire counter electrode were employed. Ferrocene (0.64 V vs NHE) was used as an internal standard for the DPV measurements.

Fabrication of Dye-Sensitized TiO_2 Electrode. Nanoporous TiO_2 films were prepared from colloidal suspension of TiO_2 nanoparticles (P-25, Nippon Aerosil) dispersed in deionized water and Triton X-100. The suspension was deposited on a transparent conducting glass (FTO, SnO_2:F, 9.4 Ω/sq, Asahi Glass) by using doctor blade technique. The films were annealed at 723 K for 30 min, followed by similar deposition and annealing (723 K, 1 h) for the 10 μm thick TiO_2 films (0.25 cm^2 of projected area). The thickness of the films was determined using surface roughness/profile measuring instrument (SURFCOM 130A, ACCRETECH).[30] The TiO_2 electrodes were immersed into a 0.5 mM THF solution of the dye containing chenodeoxycholic acid (CDCA; 2.5 mM) at room temperature for 12 h. After dye adsorption, the dye-modified electrodes were rinsed with THF. The **TP** and **PP**-sensitized TiO_2 electrodes are denoted as TiO_2/**TP** and TiO_2/**PP**, respectively. The amounts of the **TP** or **PP** adsorbed onto TiO_2 films were determined by measuring the changes in the absorbance at 400 nm of the electrodes before and after modified with the dyes.

Optical Spectroscopy. UV-visible absorption spectra were obtained on a Perkin Elmer Lambda 900UV/vis/NIR spectrometer. Steady-state fluorescence spectra were recorded with a SPEX Fluoromax-3 spectrofluorometer (Horiba). Fluorescence quantum yields (Φ_f) of the samples in THF solutions were measured by using 9,10-diphenylanthracene (Φ_f = 90% in cyclohexane) as a standard.[31] The values were calculated using $\Phi_f = \Phi_S \times (I/I_S) \times (OD_S/OD) \times (n^2/ n_S^2)$, where Φ_S is a quantum yield of the standard, I is an integrated intensity, I_S is an integrated intensity of the standard, OD_S is an absorbance of the standard, OD is an absorbance of the sample, n is a refractive index of the solvent in which the sample is dissolved, and n_S is a refractive index of the solvent in which the standard is dissolved.[32]

Attenuated Total Reflectance-Fourier Transform Infrared (ATR-FTIR) Measurements. ATR-FTIR spectra were recorded by using Thermo Electron Corporation Nicolet 6700. The samples for ATR-FTIR measurements were made by the following method. First, TiO_2 electrodes were prepared by the same method as for the photovoltaic measurements (vide supra). Then, the TiO_2 electrodes were immersed into a 0.5 mM THF solution of the dye without CDCA at room temperature for 12 h. Finally, the dye-modified electrodes were rinsed with THF. The measurements of **TP** and **PP** powders were performed as control experiments.

X-ray Photoelectron Spectroscopy (XPS) Measurements. The XPS data were acquired using an ULVAC-PHI 5500MT system equipped with Mg Kα X-ray source (1253.6 eV) and a hemispherical energy analyzer. Samples were mounted on indium foil. The TiO_2/**TP** and TiO_2/**PP** powders were obtained by scratching **TP** and **PP**-adsorbed TiO_2 layer from TiO_2/**TP** and TiO_2/**PP** electrodes that were prepared by the same method as for the ATR-FTIR measurements (vide supra). The signals were fitted by Gaussian functions using the program OriginPro 7.0.

Photovoltaic Measurements. The photovoltaic measurements were performed in a sandwich cell consisting of the TiO_2/**TP** or TiO_2/**PP** electrode as the working electrode and a platinum-coated conducting glass as the counter electrode. The two electrodes were placed on top of each other using a thin transparent film of Surlyn polymer (Dupont) as a spacer to form the electrolyte space. A thin layer of electrolyte (0.5 M LiI and 0.01 M I_2 in acetonitrile) was introduced into the interelectrode space. Incident photon-to-current efficiency (IPCE) and photocurrent–voltage (I–V) performance were measured on an action spectrum measurement setup (PEC-S20) and a solar simulator (PEC-L10, Peccell Technologies, AM 1.5 (100 mW cm^{-2})), respectively. IPCE (%) = $100 \times 1240 \times i/(W_{in} \times \lambda)$, where i is a photocurrent density (A cm^{-2}), W_{in} is an incident light intensity (W cm^{-2}), and λ is an excitation wavelength (nm). APCE (%) = IPCE/$(1–10^{-A})$, where A is an absorbance.

References and Footnotes

(1) (a) Szuromi, P.; Jasny, B.; Clery, D.; Austin, J.; Hanson, B. *Science* **2007**, *315*, 781. (b) Clery, D. *Science* **2007**, *315*, 782.

(2) (a) Grätzel, M. *Phil. Trans. R. Soc. A* **2007**, *365*, 993. (b) Lewis, N. S. *Science* **2007**, *315*, 798. (c) Butler, D. *Nature* **2008**, *454*, 558. (d) Aberle, A. G. *Thin Solid Films* **2009**, *517*, 4706.

(3) (a) Tang, C. W. *Appl. Phys. Lett.* **1986**, *48*, 183. (b) Yu, G.; Gao, J.; Hummelen, J. C.; Wuldi, F.; Heeger, A. J. *Science* **1995**, *270*, 1789. (c) Mayer, A. C.; Scully, S. R.; Hardin, B. E.; Rowell, M. W.; McGehee, M. D. *Mater. Today* **2007**, *10*, 28.

(4) (a) O'Regan, B.; Grätzel, M. *Nature* **1991**, *353*, 737. (b) Nazeeruddin, M. K.; Kay, A.; Rodicio, I.; Humphry-Baker, R.; Müller, E.; Liska, P.; Vlachopoulos, N.; Grätzel, M. *J. Am. Chem. Soc.* **1993**, *115*, 6382. (c) Grätzel, M. *Acc. Chem. Res.* **2009**, *42*, 1788.

(5) Nazeeruddin, M. K.; Angelis, F. D.; Fantacci, S.; Selloni, A.; Viscardi, G.; Liska, P.; Ito, S.; Takeru, B.; Grätzel, M. *J. Am. Chem. Soc.* **2005**, *127*, 16835. (b) Gao, F.; Wang, Y.; Shi, D.; Zhang, J.; Wang, M.; Jing, X.; Humphry-Baker, R.; Wang, P.; Zakeeruddin, S. M.; Grätzel, M. *J. Am. Chem. Soc.* **2008**, *130*, 10720.

(6) (a) Mishra, A.; Fischer, M. K. R.; Bäuerle, P. *Angew. Chem., Int. Ed.* **2009**, *48*, 2474. (b) Ooyama, Y.; Harima, Y. *Eur. J. Org. Chem.* **2009**, 2903. (c) Imahori, H.; Umeyama, T.; Ito, S. *Acc. Chem. Res.* **2009**, *42*, 1809.

(7) (a) Hara, K.; Sayama, K.; Ohga, Y.; Shinpo, A.; Suga, S.; Arakawa, H. *Chem. Commun.* **2001**, 569. (b) Hara, K.; Kurashige, M.; Dan-oh, Y.; Kasada, C.; Shinpo, A.; Suga, S.; Sayama, K.; Arakawa, H. *New. J. Chem.* **2003**, *27*, 783. (c) Wang, Z.-S.; Cui, Y.; Dan-oh, Y.; Kasada, C.; Shinpo, A.; Hara, K. *J. Phys. Chem. C* **2007**, *111*, 7224. (d) Wang, Z.-S.; Cui, Y.; Dan-oh, Y.; Kasada, C.; Shinpo, A.; Hara, K. *J. Phys. Chem. C* **2008**, *112*, 17011.

(8) (a) Horiuchi, T.; Miura, H.; Uchida, S. *Chem. Commun.* **2003**, 3036. (b) Horiuchi, T.; Miura, H.; Sumioka, K.; Uchida, S. *J. Am. Chem. Soc.* **2004**, *126*, 12218. (c) Ito, S.; Zakeeruddin, S. M.; Humphry-Baker, R.; Liska, P.; Charvet, R.; Comte, P.; Nazeeruddin, M. K.; Péchy, P.; Takata, M.; Miura, H.; Uchida, S. Grätzel, M. *Adv. Mater.* **2006**, *18*, 1202. (d) Ito, S.; Miura, H.; Uchida, S.; Takata, M.; Sumioka, K.; Liska, P.; Comte, P.; Péchy, P.; Grätzel, M. *Chem. Commun.* **2008**, 5194.

(9) (a) Tanaka, K.; Takimiya, K.; Otsubo, T.; Kawabuchi, K.; Kajihara, S.; Harima, Y. *Chem. Lett.* **2006**, *35*, 592. (b) Liu, W.-H.; Wu, I-C.; Lai, C.-H.; Lai, C.-H.; Chou, P.-T.; Li, Y.-T.; Chen, C.-L.; Hsu, Y.-Y.; Chi, Y. *Chem. Commun.* **2008**, 5152. (c) Choi, H.; Baik, C.; Kang, S. O.; Ko, J.; Kang, M.-S.; Nazeeruddin, M. K.; Grätzel, M. *Angew. Chem., Int. Ed.* **2008**, *47*, 327. (d) Wang, Z.-S.; Koumura, N.; Cui, Y.; Takahashi, M.; Sekiguchi, H.; Mori, A.; Kubo, T.; Furube, A.; Hara, K. *Chem. Mater.* **2008**, *20*, 3993. (e) Zhang, G.; Bala, H.; Cheng, Y.; Shi, D.; Lv, X.; Yu, Q.; Wang, P. *Chem. Commun.* **2009**, 2198.

(10) (a) Ehret, A.; Stuhl, L.; Spitler, M. T. *Electrochim. Acta* **2000**, *45*, 4553. (b) Wu, W.; Hua, J.; Jin, Y.; Zhan, W.; Tian, H. *Photochem. Photobiol. Sci.* **2008**, *7*, 63.

(11) (a) Campbell, W. M.; Jolley, K. W.; Wagner, P.; Wagner, K.; Walsh, P. J.; Gordon, K. C.; Schmidt-Mende, L.; Nazeeruddin, M. K.; Wang, Q.; Grätzel, M.; Officer, D. L. *J. Phys. Chem. C* **2007**, *111*, 11760. (b) Tanaka, M.; Hayashi, S.; Eu, S.; Umeyama, T.; Matano, Y.; Imahori, H. *Chem. Commun.* **2007**, 2069. (c) Eu, S.; Hayashi, S.; Umeyama, T.; Matano, Y.; Araki, Y.; Imahori, H. *J. Phys. Chem. C* **2008**, *112*, 4396. (d) Lee, C.-W.; Lu, H.-P.; Lan, C.-M.; Huag, Y.-L.; Liang, Y.-R.; Yen, W.-N.; Liu, Y.-C.; Lin, Y.-S.; Diau, E. W.-G.; Yeh, C.-Y. *Chem.–Eur. J.* **2009**, *15*, 1403.

(12) (a) Kitamura, T.; Ikeda, M.; Shigaki, K.; Inoue, T.; Anderson, N. A.; Ai, X.; Lian, T.; Yanagida, S. *Chem. Mater.* **2004**, *16*, 1806. (b) Hwang, S.; Lee, J. H.; Park, C.; Lee, H.; Kim, C.; Park, C.; Lee, M.-H.; Lee, W.; Park, J.; Kim, K.; Park, N.-G.; Kim, C. *Chem. Commun.* **2007**, 4887. (c) Reddy, P. Y.; Giribabu, L.; Lyness, C.; Snaith, H. J.; Vijaykumar, C.; Chandrasekharam, M.; Lakshmikantam, M.; Y, J.-H.; Kalyanasundaram, K.; Grätzel, M.; Nazeeruddin, M. K. *Angew. Chem., Int. Ed.* **2007**, *46*, 373. (d) Shibano, Y.; Umeyama, T.; Matano, Y.; Imahori, H. *Org. Lett.* **2007**, *9*, 1971. (e) Yum, J.-H.; Walter, P.; Huber, S.; Rentsch, D.; Geiger, T.; Nüesch, F.; Angelis, F. D.; Grätzel, M.; Nazeeruddin, M. K. *J. Am. Chem. Soc.* **2007**, *129*, 10320. (f) Li, C.; Yum, J.-H.; Moon, S.-J.; Herrmann, A.; Eickemeyer, F.; Pschirer, N. G.; Erk, P.; Schöneboom, J.; Müllen, K.; Grätzel, M.; Nazeeruddin, M. K. *ChemSusChem.* **2008**, *1*, 615. (g) Ooyama, Y.; Shimada, Y.; Ishii, A.; Ito, G.; Kagawa, Y.; Imae, I.; Komaguchi, K.; Harima, Y. *J. Photochem. Photobiol. A* **2009**, *203*, 177.

(13) (a) Campbell, W. M.; Burrell, A. K.; Officer, D. L.; Jolley, K. W. *Coord. Chem. Rev.* **2004**, *248*, 1363. (b) Ernstorfer, R.; Gundlach, L.; Felber, S.; Storck, W.; Eichberger, R.; Willig, F. *J. Phys. Chem. B* **2006**, *110*, 25383. (c) Chen, R.; Yang, X.; Tian, H.; Wang, X.; Hagfeldt, A.; Sun, L. *Chem. Mater.* **2007**, *19*, 4007. (d) Wiberg, J.; Marinado, T.; Hagberg, D. P.; Sun, L.; Hagfeldt, A.; Albinsson, B. *J. Phys. Chem. C* **2009**, *113*, 3881.

(14) Heimer, T. A.; D'Arcangelis, S. T.; Farzad, F.; Stipkala, J. M.; Meyer, G. J. *Inorg. Chem.* **1996**, *35*, 5319.

(15) (a) Ma, T.; Inoue, K.; Noma, H.; Yao, K.; Abe, E. *J. Photochem. Photobiol. A* **2002**, *152*, 207. (b) Chen, Y.-S.; Li, C.; Zeng, Z.-H.; Wang, W.-B.; Wang, X.-S.; Zhang, B.-W. *J. Mater. Chem.* **2005**, *15*, 1654.

(16) (a) Odobel, F.; Blart, E.; Lagrée, M.; Villieras, M.; Boujtita, H.; Murri, N. E.; Caramori, S.; Bignozzi, C. A. *J. Mater. Chem.* **2003**, *13*, 502. (b) Nazeeruddin, M. K.; Humphry-Baker, R.; Officer, D. L.; Campbell, W. M.; Burrell, A. K.; Grätzel, M. *Langmuir* **2004**, *20*, 6514.

(17) (a) Dai, Q.; Rabani, J. *Chem. Commun.* **2001**, 2142. (b) Mosurkal, R.; He, J.-A.; Yang, K.; Samuelson, L. A.; Kumar, J. *J. Photochem. Photobiol. A* **2004**, *168*, 191. (c) Tae, E. L.; Lee, S. H.;

Lee, J. K.; Yoo, S. S.; Kang, E. J.; Yoon, K, B. *J. Phys. Chem. B* **2005**, *109*, 22513.

(18) Baik, C.; Kim, D.; Kang, M-S.; Kang, S. O.; Ko, J.; Nazeeruddin, M. K.; Grätzel, M. *J. Photochem. Photobiol. A* **2009**, *201*, 168.

(19) (a) Hissler, M.; Dyer, P. W.; Réau, R. *Coord. Chem. Rev.* **2003**, *244*, 1. (b) Dyer, P. W.; Réau, R. in *Functional Organic Materials*; Müller, T. J. J.; Bunz, U. H. F., Eds.; Wiley-VCH, Weinheim, 2007, pp 119–177. (c) Hissler, M.; Lescop, C.; Réau, R. *C. R. Chim.* **2008**, *11*, 628. (d) Hobbs, M. G.; Baumgartner, T. *Eur. J. Inorg. Chem.* **2007**, 3611. (e) Matano, Y.; Imahori, H. *Org. Biomol. Chem.* **2009**, *7*, 1258. (f) Matano, Y.; Imahori, H. *Acc. Chem. Res.* **2009**, *42*, 1193.

(20) (a) Quin, L. D. *The Heterocyclic Chemistry of Phosphorus,* Wiley, New York, 1981. (b) Mathey, F. *Chem. Rev.* **1988**, *88*, 429. (c) Quin, L. D. in *Comprehensive Heterocyclic Chemistry*; Katritzky, A. R.; Rees, C. W.; Scriven, E. F. V., Eds.; Elsevier, Oxford, 1996; Vol. 2. (d) Mathey, F. *Phosphorus-Carbon Heterocyclic Chemistry: The Rise of a New Domain,* Elsevier, Oxford, 2001. (e) Nyulászi, L. *Chem. Rev.* **2001**, *101*, 1229. (f) Mathey, F. *Angew. Chem., Int. Ed.* **2003**, *42*, 1578. (g) Quin, L. D. *Curr. Org. Chem.* **2006**, *10*, 43. (h) Baumgartner, T.; Réau, R. *Chem. Rev.* **2006**, *106*, 4681.

(21) It is well known that the localization of HOMO over the chromophore moieties except for carboxylic acid group as an anchoring group slows down the charge recombination. Xu, M.; Wenger, S.; Bala, H.; Shi, D.; Li, R.; Zhou, Y.; Zakeeruddin, S. M.; Grätzel, M.; Wang, P. *J. Phys. Chem. C* **2009**, *113*, 2966.

(22) Vicente, V.; Fruchier, A.; Taillefer, M.; Combes-Chamalet, C.; Scowen, I. J.; Plénat, F.; Cristau, H.-J. *New J. Chem.* **2004**, *28*, 418.

(23) (a) Rusu, C. N.; Yates, Jr. J. T.; *J. Phys. Chem. B* **2000**, *104*, 12292. (b) Guerrero, G.; Mutin, P. H.; Vioux, A. *Chem. Mater.* **2001**, *13*, 4367. (c) Al-Ali, F.; Brun, A.; Rodrigues, F.; Etemad-Moghadam, G.; Rico-Lattes, I. *Langmuir* **2003**, *19*, 6678. (d) Bae, E.; Choi, W.; Park, J.; Shin, H. S.; Kim, S. B.; Lee, J. S. *J. Phys. Chem. B* **2004**, *108*, 14093. (e) Wang, P.; Klein, C.; Moser, J.-E.; Humphry-Baker, R.; Cevey-Ha, N.-L.; Charvet, R.; Comte, P.; Zakeeruddin, S. M.; Grätzel, M. *J. Phys. Chem. B* **2004**, *108*, 17553. (f) Raman, A.; Dubey, M.; Gouzman, I.; Gawalt, E. S. *Langmuir* **2006**, *22*, 6469. (g) Paniague, S. A.; Hotchkiss, P. J.; Jones, S. C.; Marder, A. M.; Marrikar, F. S.; Pemberton, J. E.; Armstrong, N. R. *J. Phys. Chem. C* **2008**, *112*, 7809.

(24) (a) Hofer, R.; Textor, M.; Spencer, N. D. *Langmuir* **2001**, *17*, 4014. (b) Adden, N.; Gamble, L. J.; Castner, D. G.; Hoffmann, A.; Gross, G.; Menzel, H. *Langmuir* **2006**, *22*, 8197. (c) Gnauck, M.; Jaehne, E.; Blaettler, T.; Tosatti, S.; Textor, M.; Adler, H.-J. P. *Langmuir* **2007**, *23*, 377. (d) Spori, D. M.; Venkataraman, N. V.; Tosatti, S. G. P.; Durmaz, T. F.; Spencer, N. D.; Zürcher, S. *Langmuir* **2007**, *23*, 8053. (e) Zorn, G.; Adadi, R.; Brener, R.; Yakovlev, V. A.; Gotman, I.; Gutmanas, E. Y.; Sukenik, C. N. *Chem. Mater.* **2008**, *20*, 5368.

(25) Johansson, E. M. J.; Hedlund, M.; Siegbahn, H.; Rensmo, H. *J. Phys. Chem. B* **2005**, *109*, 22256.

(26) Imahori, H.; Hayashi, S.; Hayashi, H.; Oguro, A.; Eu, S.; Umeyama, T.; Matano, Y. *J. Phys. Chem. C* **2009**, *113*, 18406.

(27) Bilge, A.; Zen, A.; Forster, M.; Li, H.; Galbrecht, F.; Nehls, B. S.; Farrell, T.; Neher, D.; Scherf, U. *J. Mater. Chem.* **2006**, *16*, 3177.

(28) Frisch, M. J.; Trucks, G. W.; Schlegel, H. B.; Scuseria, G. E.; Robb, M. A.; Cheeseman, J. R.; Montgomery, Jr., J. A.; Vreven, T.; Kudin, K. N. ; Burant, J. C.; Millam, J. M.; Iyengar, S. S.; Tomasi, J.; Barone, V.; Mennucci, B.; Cossi, M.; Scalmani, G.; Rega, N.; Petersson, G. A.; Nakatsuji, H.; Hada, M.; Ehara, M.; Toyota, K.; Fukuda, R.; Hasegawa, J.; Ishida, M.; Nakajima, T.; Honda, Y.; Kitao, O.; Nakai, H.; Klene, M.; Li, X.; Knox, J. E.; Hratchian, H. P.; Cross, J. B.; Bakken, V.; Adamo, C.; Jaramillo, J.; Gomperts, R.; Stratmann, R. E.; Yazyev, O. ; Austin, A. J.; Cammi, R.; Pomelli, C.; Ochterski, J. W.; Ayala, P. Y.; Morokuma, K.; Voth, G. A.; Salvador, P.; Dannenberg, J. J.; Zakrzewski, V. G. ; Dapprich, S.; Daniels, A. D.; Strain, M. C.; Farkas, O.; Malick, D. K.; Rabuck, A. D.; Raghavachari, K.; Foresman, J. B.; Ortiz, J. V.; Cui, Q.; Baboul, A. G.; Clifford, S.; Cioslowski, J.; Stefanov, B. B.; Liu, G.; Liashenko, A.; Piskorz, P.; Komaromi, I.; Martin, R. L.; Fox, D. J.; Keith, T.; Al.Laham, M. A.; Peng, C. Y.; Nanayakkara, A.; Challacombe, M.; Gill, P. M. W.; Johnson, B.; Chen, W.; Wong, M. W.; Gonzalez, C.; Pople, J. A. *Gaussian 03*; Gaussian, Inc.: Wallingford, CT, 2004.

(29) (a) Lowe, J. P.; Peterson, K. A. *Quantum Chemistry*, 3rd ed.; Elsevier Academic Press: 2005; Chapter 10. (b) Kirgan, R. A.; Rillema, D. P. *J. Phys. Chem. A* **2007**, *111*, 13157.

(30) Eu, S.; Hayashi, S.; Umeyama, T.; Oguro, A.; Kawasaki, M.; Kadota, N.; Matano, Y.; Imahori, H. *J. Phys. Chem. C* **2007**, *111*, 3528.

(31) Hamai, S.; Hirayama, F. *J. Phys. Chem.* **1983**, *87*, 83.

(32) Ballesteros, E.; Moreno, D.; Gómez, T.; Rodríguez, T.; Rojo, J.; García-Valverde, G.; Torroba, T. *Org. Lett.* **2009**, *11*, 1269.

Chapter 2

Effects of π-Elongation and Fused Position of Quinoxaline-Fused Porphyrins as Sensitizers in Dye-Sensitized Solar Cells on Optical, Electrochemical, and Photovoltaic Properties

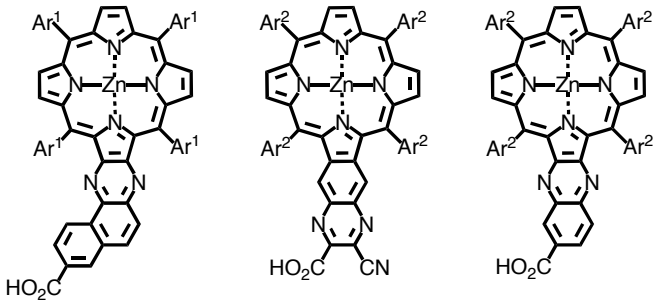

Abstract

Novel benzo[f]quinoxalino[2,3-β]porphyrin carboxylic acid (ZnBQA) and cyanoquinoxalino[6,7-β]porphyrin carboxylic acid (ZnQCA) have been synthesized to evaluate the effects of the π-elongation and the fused position of quinoxaline-fused porphyrins on the optical, electrochemical, and photovoltaic properties. ZnBQA showed intensified and red-shifted Soret band relative to that of quinoxalino[2,3-β]porphyrin acid (ZnQMA), while the Q bands are rather blue-shifted. On the other hand, both Soret and Q-bands of ZnQCA are red-shifted compared to those of ZnQMA. The ZnBQA cell exhibited a power conversion efficiency (η) of 5.1%, while the ZnQCA cell yielded a low η value of 0.80%. Both of the η values are smaller than those of reference cells under the optimized conditions (η = 6.3% for ZnQMA). The weak electronic coupling between the LUMO of ZnBQA and a conduction band (CB) of the TiO_2 may result in the low electron injection efficiency as well as the low incident photon-to-current efficiency (IPCE) for the ZnBQA cell (maximum IPCE = 60%) relative to the ZnQMA cell (maximum IPCE = 75%), leading to the lower η value of the ZnBQA cell than that of the ZnQMA cell. The ZnQCA cell exhibited the further low IPCE value up to 10% due to the short fluorescence lifetime comparable to the typical time scale (0.1–1 ps) of electron injection processes from dye excited states to a TiO_2 surface. In addition, the open circuit potential of the ZnQCA cell also significantly decreased by the effect of the charge recombination from the injected electrons in the CB of the TiO_2 to the I_3^- derived from the loose packing of ZnQCA molecules on the TiO_2 surface.

Introduction

Dye-sensitized solar cells (DSSC) with mesoporous TiO_2 electrodes have been regarded as one of the most promising candidates for solar energy conversion because of the potential of low-cost production and high power conversion efficiency (η).[1] Although ruthenium polypyridyl complexes have proven to be excellent TiO_2 sensitizers that have achieved the highest η value up to 11.5%, their extensive application would be hampered considerably owing to the limited availability and high cost of Ru metal.[2] In this context, studies on metal-free organic chromophores or inexpensive metal complexes for DSSC have progressed rapidly.[3] High-performance dyes for DSSC are requested to display broad light absorption capability that can cover the whole solar light spectrum, along with fast injection of electrons from the excited dyes to a conduction band (CB) of the TiO_2 electrode, and slow charge recombination between the injected electrons and resulting dye cations and/or I_3^- in the electrolyte. Organic dyes composed of π-conjugative molecules such as coumarin,[4] indoline,[5] polyene,[6] thiophene,[7] cyanine,[8] hemicyanine,[9] squaraine,[10] phthalocyanine,[11] and perylene[12] derivatives have been developed as potential sensitizers for DSSC.

Porphyrins have been frequently employed as sensitizers for DSSC due to their strong Soret (400–450 nm) and moderate Q bands (550–600 nm) as well as their primary role in natural photosynthetic systems.[13–17] They have demonstrated electron transfer kinetics indistinguishable from those of ruthenium polypyridyl complexes that are the most efficient dyes ever reported.[18] Moreover, the optical, photophysical, and electrochemical properties can be systematically tailored by the peripheral substitutions and/or inner metal complexations. Nevertheless, porphyrins typically showed inferior performances to ruthenium polypyridyl complexes as sensitizers because of the insufficient light-harvesting ability in the visible and near-infrared (NIR) regions, and the resulting low value of short circuit current. Broadening and red-shift of Soret and Q bands are promising strategy to tackle the above problem.[3c] For instance, a push-pull porphyrin with an electron-donating diarylamino group at the *meso*-position and an electron-withdrawing carboxyphenylethynyl anchoring group at the opposite *meso*-position materialized the improved η value up to 6.8%.[19] Extension of the porphyrin π-system by modifying a β position with olefinic linkage has been reported to be an effective method for the broadening of the absorption window,[20] and this concept has been successfully applied to design the best performing porphyrin sensitizers ($\eta = 7.1\%$).[21]

Imahori and co-workers have previously reported that quinoxalino[2,3-β]porphyrin acid (ZnQMA, Figure 1) showed broadened, red-shifted, and amplified light absorption properties compared to 5-(4-carboxyphenyl)-10,15,20-tris(2,4,6-trimethylphenyl)porphyrinatozinc (II) (ZnP-acid), leading to the higher η value of 5.2% for the ZnQMA cell than that of the ZnP-acid

cell (4.6%) using P-25 TiO_2 nanoparticle.[16e,g] Considering the fact that the unsymmetrical π-elongation of porphyrins allows one to match the porphyrin absorption with solar energy distribution on the earth more effectively,[16c,e,f] β,β'-edge quinoxaline fused porphyrins are highly promising as excellent sensitizers for DSSC. In this paper, the author reports the first synthesis and the optical, electrochemical, and photovoltaic properties of benzoquinoxalino[2,3-β]porphyrin (ZnBQA) and cyanoquinoxalino[6,7-β]porphyrin acid (ZnQCA) for DSSC (Figure 1). The author expected that ZnBQA would exhibit broadening and red-shift of the absorption compared with ZnQMA due to further π-elongation with low symmetry relative to ZnQMA. ZnQCA is an isomer of ZnQMA. Namely, β,β'-edge of the porphyrin was fused with 3-cyano-2-quinoxaline carboxylic acid at the 6,7-positions. In addition, an introduction of the cyano group as an electron-withdrawing substituent into the quinoxaline moiety close to the carboxylic acid anchoring group would be favorable for facile electron injection from the porphyrin excited singlet state to the CB of the TiO_2.[3] 3,5-Di-*tert*-butylphenyl groups or 2,4,6-trimethylphenyl groups were introduced to increase the solubility and to reduce the aggregation.[16] Overall, one can evaluate the effects of the π-elongation and the fused position of quinoxaline-fused porphyrins on the optical, electrochemical, and photovoltaic properties.

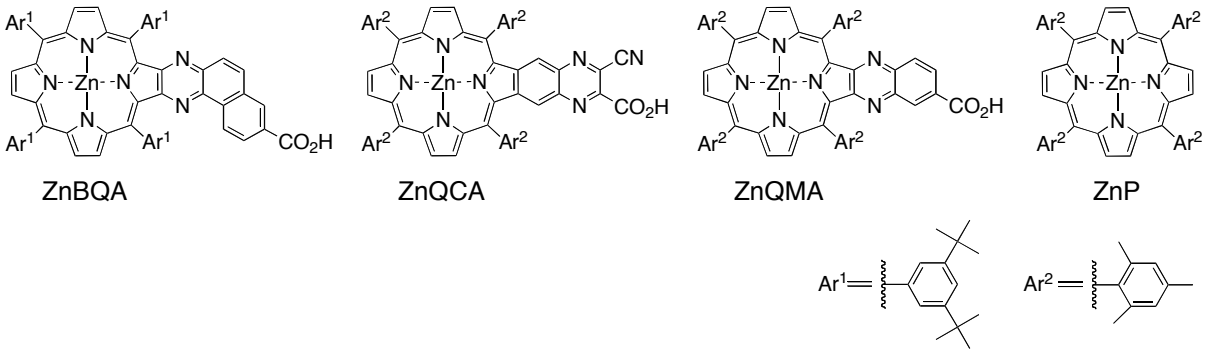

Figure 1. Structures of the porphyrins used in this study.

Results and Discussion

Synthesis. Synthetic routes to ZnBQA and ZnQCA are displayed in Scheme 1 and 2, respectively. 2-Amino-6-methoxycarbonylnaphthalene **1** was treated with acetic anhydride and nitric acid to yield 2-acetamido-6-methoxycarbonyl-1-nitronaphthalene **2**.[22] The hydrolysis of the acetamido group of **2** afforded 2-amino-6-methoxycarbonyl-1-nitronaphthalene **3**.[23] The reduction of the nitro group of **3** gave 1,2-diamino-6-methoxycarbonylnaphthalene **4**.[24] 12,13-Dioxo-5,10,15,20-tetrakis(3,5-di-*tert*-butylphenyl)chlorin **7** was prepared by

acetoxylation of **5** and subsequent oxidation of **6** according to the methods reported by Burn and co-workers.[25] The condensation of porphyrin **7** with **4** in pyridine afforded benzoquinoxaline-fused porphyrin **8**.[16e] Treatment of **8** with zinc acetate, followed by hydrolysis of **9**, gave ZnBQA. Initially, the author tried to synthesize benzoquinoxaline-fused porphyrin using 12,13-dioxo-5,10,15,20-tetrakis(2,4,6-trimethylphenyl) chlorin, but this chlorin was not fused with **4** probably due to steric hindrance between the ortho-methyl groups and the benzoquinoxaline moiety during the aromatic cyclization. Dicyanoquinoxalino [6,7-β]porphyrin **11** was synthesized from porphyrin **10**[16e] by the literature procedures describing Diels-Alder reaction between 5,10,15,20-tetraarylporphyrin and 2,3-bis (bromomethyl)-5,6-dicyano-1,4-pyrazine.[26] Dicyanoquinoxaline-fused porphyrin **11** was partially hydrolyzed with sulfuric acid to give porphyrin **12** bearing one carboxylic acid and the cyano group. The corresponding dicarboxyquinoxaline-fused porphyrin could not be obtained because of decarbonations during the hydrolysis. Finally, **12** was treated with zinc acetate to yield the corresponding ZnQCA. The author also prepared ZnQMA as a reference sensitizer.[16e]

Scheme 1. Synthesis of ZnBQA.

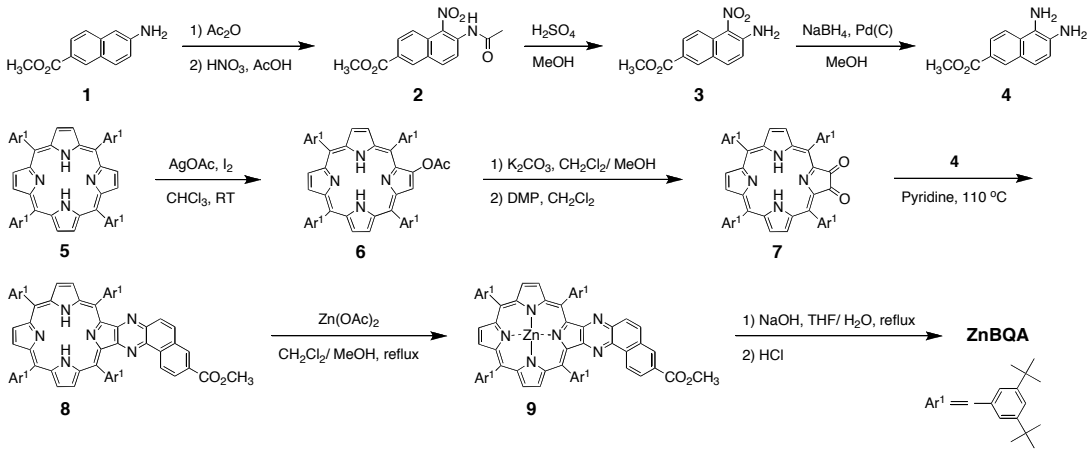

Scheme 2. Synthesis of ZnQCA.

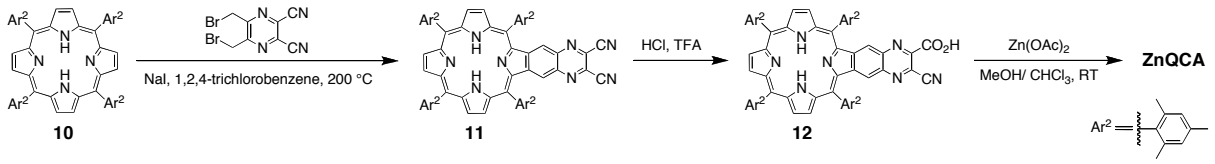

Optical and Electrochemical Properties. Figure 2 shows the UV-visible absorption spectra of ZnBQA, ZnQCA, and ZnQMA in dichloromethane. The peak positions and molar absorption coefficients (ε) of Soret and Q bands are listed in Table 1. The Soret and Q bands of ZnBQA are intensified compared with those of ZnQMA. Moreover, although the Soret

bands of ZnBQA are red-shifted, the Q bands are rather blue-shifted relative to those of ZnQMA. In contrast, both the Soret and Q bands of ZnQCA are broadened and red-shifted in comparison with those of ZnQMA. The absorption behavior will be discussed later on the basis of their molecular orbitals obtained by DFT calculations.

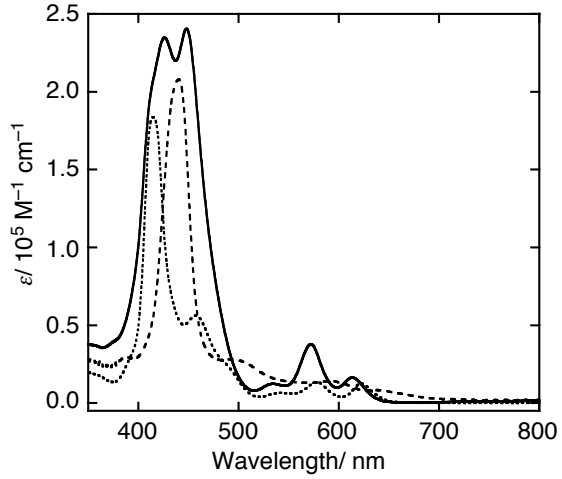

Figure 2. UV-visible absorption spectra of ZnBQA (solid line), ZnQCA (dashed line), and ZnQMA (dotted line) measured in dichloromethane.

Table 1. Optical and electrochemical data for porphyrins and driving forces for electron-transfer processes on TiO_2.

	λ_{abs}[a]/ nm (ε/ 10^3 M^{-1} cm^{-1})	λ_{em}[b]/ nm	E_{ox}[c]/ V	E_{red}[c]/ V	E_{0-0}/ eV	E_{ox}*[d]/ V	ΔG_{inj}[e]/ eV	ΔG_{reg}[f]/ eV
ZnBQA	426 (234.8)	632	0.97	–1.14	2.00	–1.03	–0.53	–0.47
	448 (240.6)	679						
	573 (37.8)							
	614 (16.4)							
ZnQCA	441 (208.0)	686	1.06	–0.54	1.87	–0.81	–0.31	–0.56
	503 (27.3)							
	600 (13.6)							
	642 (8.3)							
ZnQMA	415 (183.7)	645	0.98	–1.13	1.98	–1.00	–0.50	–0.48
	458 (56.2)							
	578 (13.6)							
	622 (12.6)							

[a] Wavelengths for Soret and Q bands maxima in CH_2Cl_2. [b] Wavelengths for emission maxima in CH_2Cl_2 by exciting at Soret wavelength. [c] Ground state redox potentials (vs NHE). [d] Excited-state oxidation potentials approximated from E_{ox} and E_{0-0} (vs NHE). [e] Driving forces for electron injection from the porphyrin singlet excited state (E_{ox}*) to the CB of TiO_2 (–0.5 V vs NHE). [f] Driving forces for the regeneration of porphyrin radical cation (E_{ox}) by I^-/I_3^- redox couple (+0.5 V vs NHE).

The steady-state fluorescence spectra of the porphyrins were measured in dichloromethane by exciting at the strongest peak positions of the Soret bands (Figure 3) and the wavelengths for emission maxima are listed in Table 1. In accordance with the trend of the absorption maximum on the longest wavelength side, the emission maximum of ZnBQA on the shortest wavelength side is blue-shifted relative to that of ZnQMA, whereas that of ZnQCA on the short wavelength side is red-shifted. From the intersection of the normalized absorption and emission spectra, the zero-zero excitation energies ($E_{0\text{–}0}$)[27] are determined to be 2.00 eV for ZnBQA, 1.87 eV for ZnQCA, and 1.98 eV for ZnQMA (Table 1).[16e] It is noteworthy that the fluorescence intensity of ZnQCA is much smaller than those of ZnBQA and ZnQMA. The fluorescence lifetimes (τ) of ZnBQA and ZnQMA were measured in dichloromethane by a time-correlated single photon counting technique, while that of ZnQCA was determined in benzonitrile by an up-conversion method.[28] The excitation wavelength was 405 nm and the fluorescence was monitored at the emission maximum for each porphyrin. The decay curves of the fluorescence intensity were fitted as a single exponential to give $\tau = 1.15 \pm 0.01$ ns for ZnBQA and $\tau = 0.99 \pm 0.01$ ns for ZnQMA, whereas the fluorescence lifetime for ZnQCA could be analyzed by two short components with $\tau = 0.2$ ps (88 %) and $\tau = 5$ ps (12 %). As electron injection processes from the excited dyes to the CB of TiO_2 are known to take place in a time scale of 0.1–1 ps,[18,29] the relatively slow fluorescence decays of ZnBQA and ZnQMA may have little influence on the electron injection efficiency (ϕ_{inj}). However, the fluorescence lifetime of ZnQCA is comparable to the typical time scale of the electron injection processes, which would affect the cell performance remarkably (vide infra).

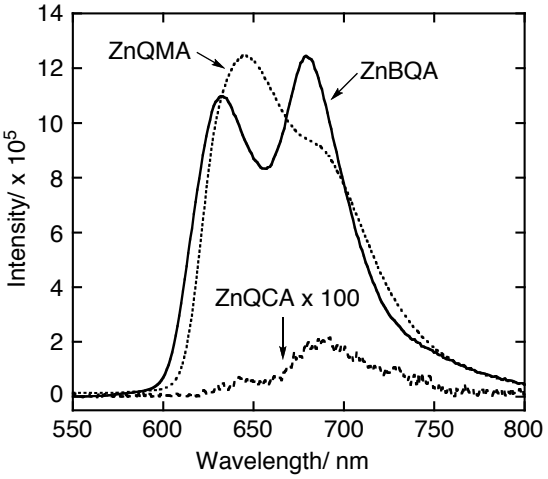

Figure 3. Steady-state fluorescence spectra of ZnBQA (solid line), ZnQCA (dashed line), and ZnQMA (dotted line) measured in dichloromethane (0.5 μM). The steady-state fluorescence spectra were obtained by exciting at the strongest peak positions of the Soret bands.

To determine the first oxidation potential (E_{ox}) and the first reduction potential (E_{red}) of the porphyrins in solutions, differntail pulse voltammetry measurements were performed in CH_2Cl_2 containing 0.1 M Bu_4NPF_6 as a supporting electrolyte (Table 1). The E_{ox} values of ZnBQA (0.97 V vs NHE) and ZnQMA (0.98 V vs NHE)[16e] are virtually the same, but that of ZnQCA (1.06 V vs NHE) is shifted to a positive direction slightly (Table 1). The E_{red} value of ZnBQA (–1.14 V vs NHE) is similar to that of ZnQMA (–1.13 V vs NHE),[16e] whereas the E_{red} value of ZnQCA (–0.54 V vs NHE) is shifted to a positive direction considerably. This suggests that the unsymmetrical π-elongation of the quinoxaline moiety by fusing an additional aromatic moiety has little effect on the redox properties. On the other hand, the fusion of β,β'-edge of the porphyrin with 3-cyano-2-quinoxaline carboxylic acid at the 6,7-positions affects mainly the lowest unoccupied molecular orbital (LUMO) of the porphyrin. The stabilization of the LUMO relative to the highest occupied molecular orbital (HOMO) leads to a decrease in the electrochemical HOMO-LUMO gaps.[30] The electrochemical HOMO-LUMO gaps are determined to be 2.11 eV for ZnBQA, 1.60 eV for ZnQCA, and 2.11 eV for ZnQMA,[16e] which largely agrees with the aforementioned trend of the optical HOMO-LUMO gaps.

From the spectroscopic and electrochemical measurements, driving forces for electron injection from the porphyrin excited singlet state to the CB of the TiO_2 (–0.5 V vs NHE) (ΔG_{inj}) and the regeneration of the porphyrin radical cation by I^-/I_3^- redox couple (+0.5 V vs NHE) (ΔG_{reg}) for the porphyrin-sensitized solar cells are evaluated (Table 1). Both of the processes are thermodynamically feasible.

DFT Calculations. DFT calculations were employed to gain the insight into the equilibrium geometry and electronic structures for the frontier orbitals of the porphyrins. The calculated structures do not show negative frequencies, implying that the optimized geometries are in the global energy minima.[31] Both ZnBQA and ZnQMA[16e] exhibit saddle structures, but the degree of deformation in ZnQMA is much larger than that in ZnQMA (Figure 4). In contrast, ZnQCA is found to adopt a planar structure.

Porphyrins with D_{4h} symmetry generally reveal energetically degenerate two LUMOs (LUMO+1, LUMO) and nearly degenerate two HOMOs (HOMO, HOMO-1). The degenerate energy levels of LUMO and LUMO+1 are split in both ZnBQA and ZnQCA, whereas the near degeneracy of HOMO and HOMO-1 remains intact by the quinoxaline substitutions (Table 2). A variation in energies by the structural modification for the LUMO of ZnQMA (–0.55 eV vs ZnP) is larger than that for the HOMO of ZnQMA (–0.19 eV vs ZnP).[16e] ZnBQA reveals similar, smaller variation in energies for the LUMO (–0.35 eV vs ZnP) and the HOMO (–0.10 eV vs ZnP). In contrast, ZnQCA exhibits analogous, larger variation in energies for the

LUMO (–0.74 eV vs ZnP) relative to that for the HOMO (–0.27 eV vs ZnP). The HOMO-LUMO gaps of the three porphyrins are as follows: ZnBQA (2.80 eV) > ZnQMA (2.69 eV) > ZnQCA (2.58 eV). This trend agrees well with that of the optical HOMO-LUMO gaps and rationalizes the unexpected blue-shift of the Q-bands in ZnBQA in comparison with ZnQMA (vide infra).

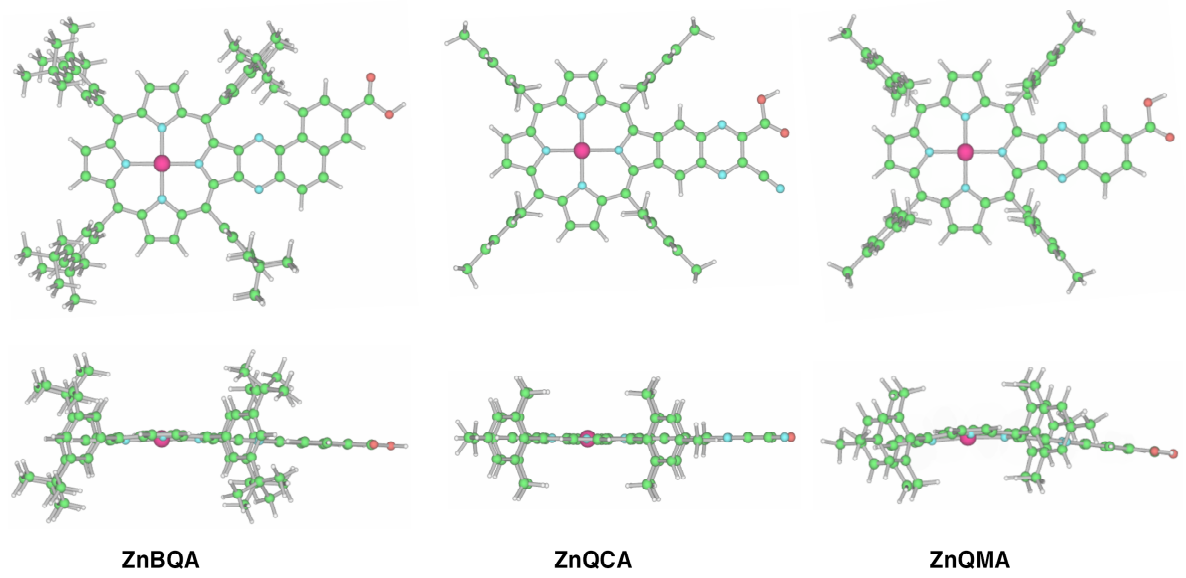

Figure 4. Optimized geometries for ZnBQA, ZnQCA, and ZnQMA determined by DFT calculations with B3LYP/3-21G(d) with various viewing angles.

Table 2. Molecular orbital energy levels for porphyrins.

	ZnBQA	ZnQCA	ZnQMA	ZnP
LUMO+1	–2.16	–2.45	–2.23	–2.01
LUMO	–2.36	–2.75	–2.56	–2.01
HOMO	–5.16	–5.33	–5.25	–5.06
HOMO-1	–5.17	–5.46	–5.28	–5.14

Some sets of molecular orbital energy levels for porphyrins were estimated by DFT calculations with B3LYP/3-21G(d). The energies in eV are quoted with respect to the vacuum (1 Hartree = 27.2116 eV).

Figure 5 illustrates the electron density distributions of ZnBQA, ZnQCA, and ZnQMA in their respective HOMOs and LUMOs. The electron density distribution of LUMOs around an anchoring group is known to influence the electronic coupling between the excited adsorbed dye and 3d orbital of TiO_2.[32] The bridging carbon atom with the carboxylic acid as well as the carboxylic acid in the LUMO of ZnBQA (Figure 5a) possesses lower electron densities than those in the LUMO of ZnQMA[16e] (Figure 5c). Accordingly, the author can anticipate that the low ϕ_{inj} value from the excited singlet state of ZnBQA to the CB of TiO_2 compared with that of

ZnQMA, leading to the low cell performance of ZnBQA relative to that of ZnQMA (vide infra). On the other hand, the electron densities of the bridging carbon atom with the carboxylic acid as well as of the carboxylic acid in the LUMO of ZnQCA (Figure 5b) are rather larger than those in the LUMO of ZnQMA.[16e] Although the fluorescence lifetime of ZnQCA is short, the large electron densities around the anchoring moiety in the LUMO would be favorable for the fast electron injection from the porphyrin excited singlet state to the CB of the TiO_2 electrode.

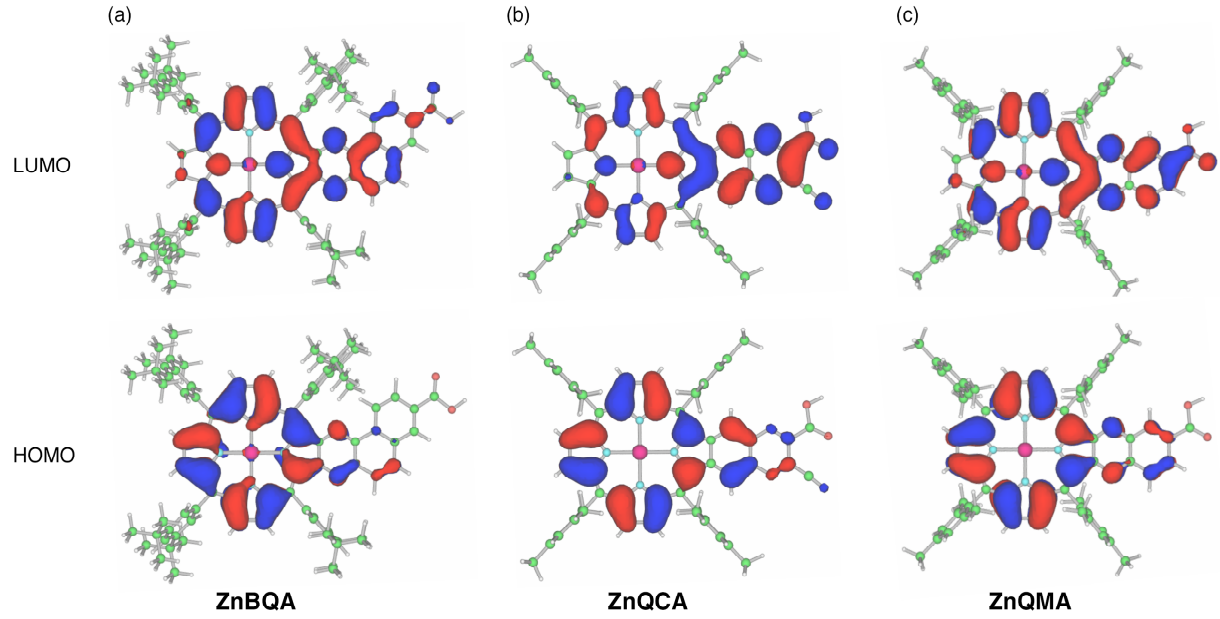

Figure 5. Some sets of molecular orbital diagrams for (a) ZnBQA, (b) ZnQCA, and (c) ZnQMA obtained by DFT calculations with B3LYP/3-21G(d).

Porphyrin Adsorption on TiO_2. The TiO_2 electrodes were immersed into 0.2 mM porphyrin solution to give the porphyrin-modified TiO_2 electrodes. The details on the adsorption conditions including the immersing solvent, time, and temperature are summarized in Table 3.

Table 3. Optimized conditions for the sensitization of the porphyrins on the TiO_2 electrodes.

	solvent	temperature/ °C	immersing time/ h	[dye]/ mM	[CDCA]/ mM
ZnBQA	EtOH	40	1	0.20	0.20
ZnQCA	MeOH	40	90	0.20	0.20
ZnQMA	MeOH	25	1	0.20	0.20
N719	*t*-BuOH:AcCN = 1:1 (v/v)	25	20	0.50	0.50

Total amounts of the porphyrins adsorbed on the TiO_2 films were determined by measuring the changes in the absorbances of the porphyrin solutions before and after immersing the TiO_2 films. After the immersion, both of ZnBQA in EtOH[33,34] and ZnQMA in MeOH reached saturated surface coverage (Γ) on the TiO_2 films in 1 h; the trend is very similar to the previous report on the Γ value of similar porphyrins on the TiO_2.[16b,e,g] The Γ values of ZnBQA and ZnQMA on the TiO_2 films are determined to be ca. 1.1×10^{-10} mol cm^{-2}. Assuming that the porphyrin monolayers are densely packed and vertically orientated to the TiO_2 surface, the Γ values of ZnBQA and ZnQMA are calculated to be 1.1×10^{-10} mol cm^{-2} and 1.2×10^{-10} mol cm^{-2}, respectively. Taking into account the good agreement between the calculated and experimental Γ values together with the saturated adsorption behavior of ZnBQA and ZnQMA, both of them form the densely packed monolayers of ZnBQA and ZnQMA on the TiO_2. By contrast, ZnQCA in MeOH reached the saturated surface coverage at an immersing time of 90 h. The experimental Γ value of ZnQCA is estimated to be 0.7×10^{-10} mol cm^{-2},[34] which is considerably lower than the calculated Γ values of 1.2×10^{-10} mol cm^{-2}, assuming the complete formation of similar porphyrin monolayer of ZnQCA on the TiO_2 surface. Accordingly, ZnQCA slowly binds to the TiO_2 surface, leading to the loose packing of ZnQCA on the TiO_2 surface.

To gain the detailed information on the adsorption modes of the porphyrins on the TiO_2 surface, X-ray photoelectron spectroscopy (XPS) measurements were performed for TiO_2/ZnBQA, TiO_2/ZnQCA, and TiO_2/ZnQMA (Figure 6). The O1s photoelectron spectra of TiO_2/ZnBQA (Figure 6a) and TiO_2/ZnQMA (Figure 6c) exhibit two distinct oxygen peaks. The peaks at 530.2 eV originate from the oxygen from the TiO_2 surface.[16e,35] The remaining peaks at around 532 eV can be assigned to the two oxygen atoms from the carboxylate, which are anchored to the TiO_2 surface with the same binding energy through bidentate

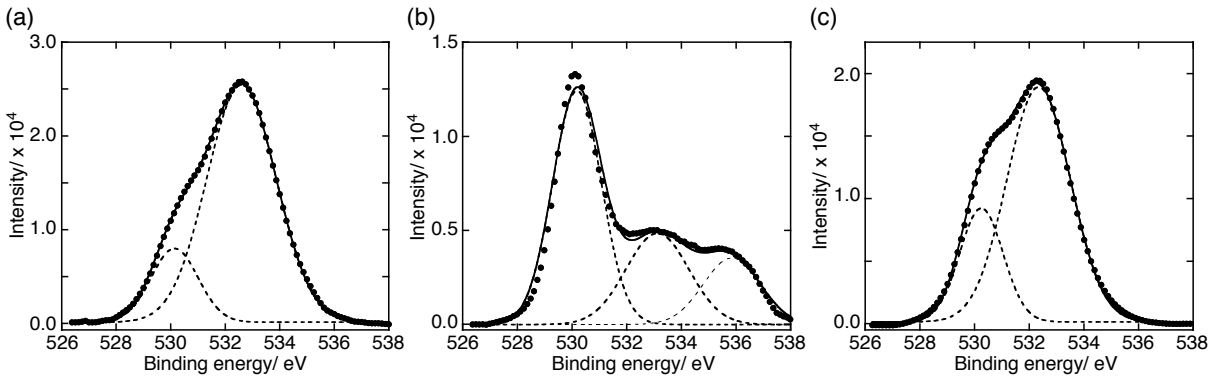

Figure 6. O1s XPS spectra for (a) ZnBQA, (b) ZnQCA, and (c) ZnQMA on the TiO2 surface without the light-scattering layers.

coordination.[16e,36] The O1s spectrum of TiO_2/ZnQCA (Figure 6b) shows three chemically nonequivalent oxygen signatures. One peak appeared at 530.2 eV is also assigned to the oxygen atom from the TiO_2; the remaining two peaks arising at 533.1 and 535.9 eV can be assigned to the two oxygen atoms of carboxylate, which coordinate weakly or adsorb physically on the TiO_2 by ester-like monodentate manner.[16e] Larger binding energy of the electron for monodentate O1s than that for bidentate O1s supports this interpretation.

To further shed light on adsorption state of the dyes on the TiO_2 surface, the N1s XPS spectra are compared for each porphyrin-sensitized TiO_2 surface (Figure 7). The N1s spectra of TiO_2/ZnBQA (Figure 7a) and TiO_2/ZnQMA (Figure 7c) have two peaks: the most intense peak at around 399 eV and another peak at around 397 eV. Considering that the peak intensity at the lower binding energy is approximately half of that at the higher binding energy and the four equivalent nitrogen atoms of the zinc porphyrins and nitrogen atom of C=N–C bonds such as pyridine are known to reveal their N1s peaks at around 398–399 eV,[37,38] the author can assign the peaks at 397 eV and at 399 eV to the nitrogen atoms of the pyrazine moieties and the four equivalent nitrogen atoms of the porphyrins, respectively. The N1s spectrum of TiO_2/ZnQCA was curve-fitted into four chemically different N1s subpeaks (Figure 7b). The peaks arising at 399.6 eV and 401.5 eV can be assigned to the nitrogen atoms of the porphyrin core and the cyano group substituted on the pyrazine moiety, respectively.[39] It is noteworthy

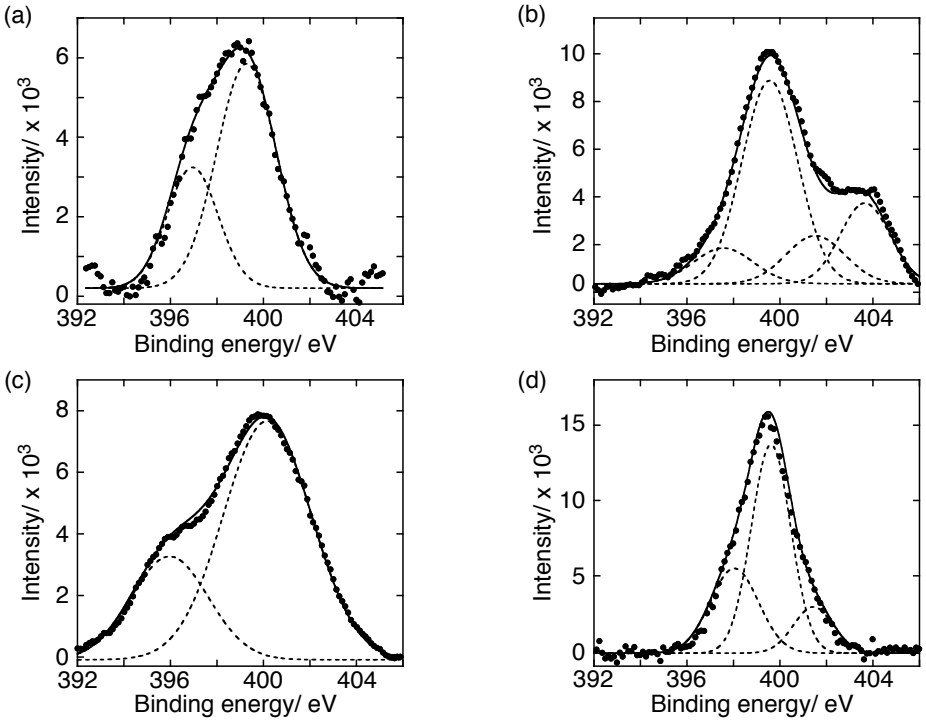

Figure 7. N1s XPS spectra for (a) ZnBQA, (b) ZnQCA, and (c) ZnQMA on the TiO_2 surface without the light-scattering layers, and (d) ZnQCA powder.

that the relative peak intensity at 397.6 eV derived from the nitrogen atoms of the pyrazine moiety is low and a new peak at around 404 eV is emerged. Meanwhile, N1s spectrum for ZnQCA powder as a reference depicts only three peaks at 398.0 eV, 399.6 eV and 401.4 eV without the additional peak at around 404 eV (Figure 7d). Positive shifts in the binding energy of N1s are known to be caused by the transfer of the lone pair on a pyridine-type nitrogen to acidic sites on a metal oxide surface.[38d,40] Thus, one can conclude that the N1s peak at 403.7 eV for TiO_2/ZnQCA stems from pyrazine-nitrogen atom closer to the carboxylic acid, which would interact with the TiO_2 surface. The remaining peak at 397.6 eV for TiO_2/ZnQCA may correspond to free pyrazine-nitrogen atom far from the carboxylic acid.

From the collective results of the surface coverage and the XPS measurements, the author propose the adsorption geometries of ZnBQA, ZnQCA, and ZnQMA on the TiO_2 surface as illustrated in Figure 8. Namely, carboxylic groups in ZnBQA and ZnQMA bind to the TiO_2 surface with bidentate coordination, leading to formation of the densely packed monolayers on the TiO_2 surface. In contrast, both of the pyrazine-nitrogen atom and the carboxylic group of ZnQCA interact with the TiO_2 surface, adopting relatively parallel orientation to the TiO_2 surface with monodentate binding of the carboxylic acid to the TiO_2, eventually yielding to the small surface coverage of ZnQCA (vide supra).

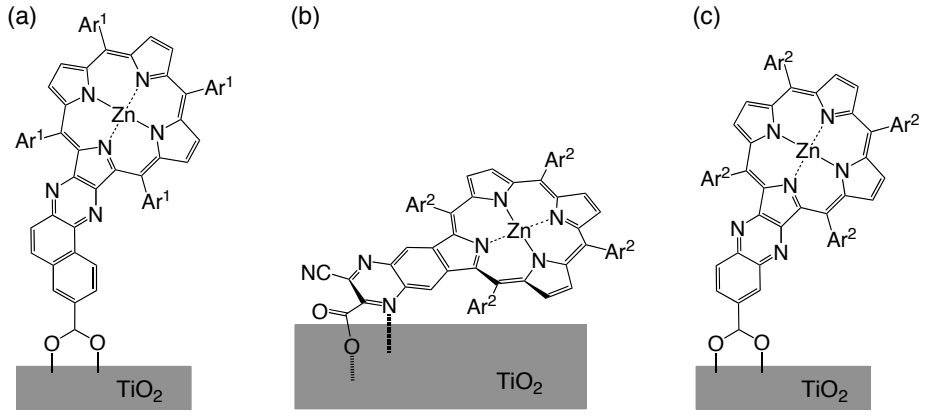

Figure 8. Proposed adsorption geometries of (a) ZnBQA, (b) ZnQCA, and (c) ZnQMA on the TiO_2 surface.

Photovoltaic Properties of Porphyrin-Sensitized TiO_2 Cells. The author evaluated the cell performances for TiO_2/ZnBQA, TiO_2/ZnQMA, and TiO_2/ZnQCA cells under the various porphyrin adsorption conditions. The TiO_2 electrodes were modified with each porphyrin by immersing TiO_2 electrodes into the porphyrin solutions for 0.5–120 h (see the Experimental Section). The η value is derived from the equation: $\eta = J_{SC} \times V_{OC} \times ff$, where V_{OC} is the open circuit potential, J_{SC} is the short circuit current, and ff is the fill factor. The η values of

TiO_2/ZnBQA, TiO_2/ZnQCA, and TiO_2/ZnQMA cells show the strong dependency on the immersing time, as observed in the immersing time dependence of η values of the TiO_2 cells modified with similar porphyrin carboxylic acids (Figure 9).[16] The maximal η values (ZnBQA: 3.7%; ZnQCA: 0.67%; ZnQMA: 5.4%) are noted with the immersing time of 1 h for TiO_2/ZnBQA and TiO_2/ZnQMA cells, and with that of 90 h for TiO_2/ZnQCA cell. To further optimize the cell performances, each porphyrin was sensitized onto the TiO_2 surface under the same adsorption conditions in which CDCA was added to reduce the porphyrin aggregation on the TiO_2 (see the Experimental Section). Actually, this coadsorption with CDCA improved the cell performances significantly. Figure 10a depicts the photocurrent-voltage characteristics of TiO_2/ZnBQA+CDCA, TiO_2/ZnQCA+CDCA, and TiO_2/ZnQMA+CDCA cells under the respective maximal η conditions (Table 3).

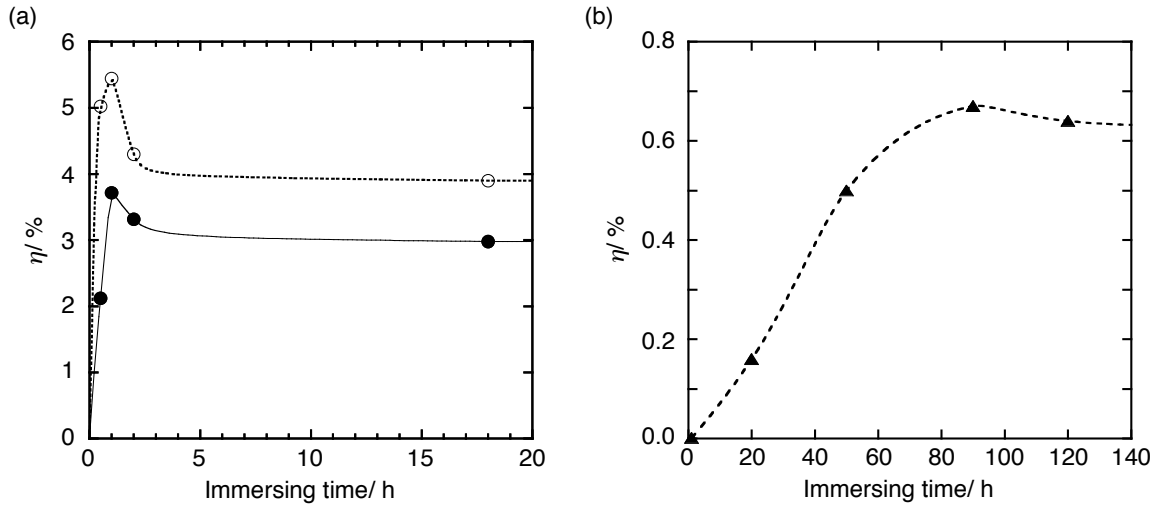

Figure 9. Immersing time dependence of the η values of (a) TiO_2/ZnBQA (solid line with filled circles) and TiO_2/ZnQMA (dotted line with open circles) cells and of (b) TiO_2/ZnQCA cell (dashed line with triangles). The porphyrin-sensitized TiO_2 electrodes were prepared under different immersing time for the porphyrin adsorption in the immersing solvents without CDCA.

TiO_2/ZnBQA+CDCA cell exhibits $\eta = 5.1\%$ with $J_{SC} = 11.1$ mA cm^{-2}, $V_{OC} = 0.68$ V, and $ff = 0.67$, while TiO_2/ZnQMA+CDCA cell yields $\eta = 6.3\%$ with $J_{SC} = 13.2$ mA cm^{-2}, $V_{OC} = 0.71$ V, and $ff = 0.67$. Both of the η values are smaller than that of N719-sensitized cell under the author's currently optimized conditions ($\eta = 8.4$ %, $J_{SC} = 15.7$ mA cm^{-2}, $V_{OC} = 0.80$ V, $ff = 0.67$, Figure 10b). The cell performances of TiO_2/ZnQMA+CDCA and N719 cells were improved compared to the previous results obtained by adsorption of the same dyes without CDCA on P-25 TiO_2 electrodes (see the Experimental Section).[16e] Difference in η values between the ZnBQA- and ZnQMA-sensitized solar cells primarily results from the nonparallel

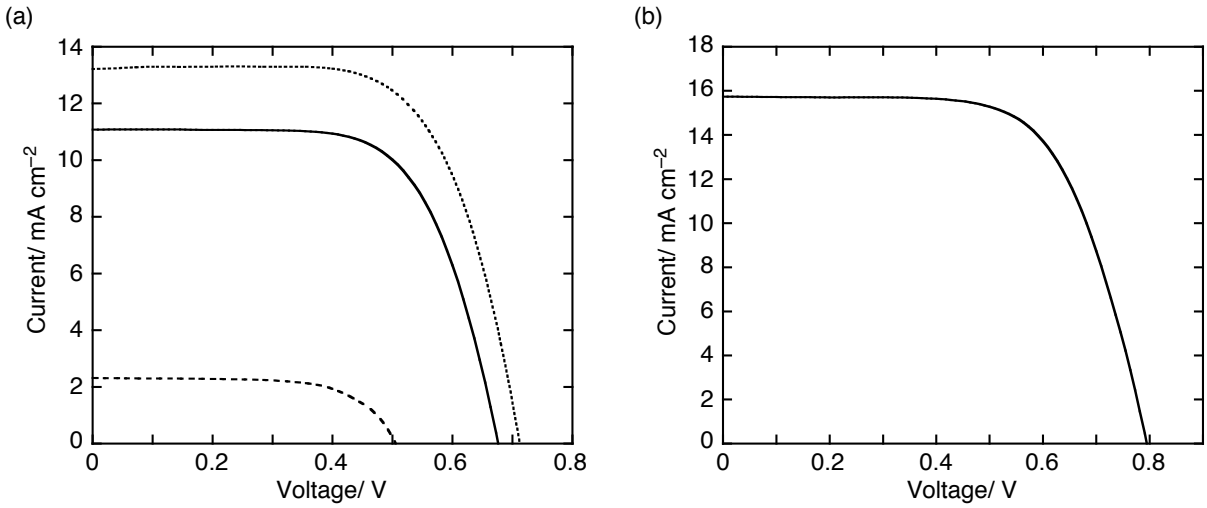

Figure 10. Photocurrent-voltage characteristics of (a) TiO_2/ZnBQA+CDCA cell (solid line), TiO_2/ZnQCA+CDCA cell (dashed line), TiO_2/ZnQMA+CDCA cell (dotted), and (b) N719-sensitized cell. Conditions: electrolyte 0.1 M LiI, 0.05 M I_2, 0.6 M 2,3-dimethyl-1-propyl imidazolium iodide, and 0.5 M 4-*tert*-butylpyridine in CH_3CN; input power: AM 1.5 under simulated solar light (100 mW cm^{-2}). $\eta = J_{sc} \times V_{oc} \times ff$.

values of J_{SC}. Each of the photocurrent action spectra (Figure 11a) follows the absorption features of the corresponding porphyrin adsorbed on the electrodes (Figure 12a), indicating that the porphyrin is the main source for the photocurrent generation. The IPCE is divided into three components as the following equation (1).

$$\text{IPCE} = \text{LHE} \times \phi_{inj} \times \eta_{col} \qquad (1)$$

where LHE (light-harvesting efficiency) is the number of absorbed photons per the number of incident photons, ϕ_{inj} is the quantum yield for electron injection from the porphyrin excited state to the CB of the TiO_2 electrode, and η_{col} is the efficiency of charge collection. TiO_2/ZnQMA+CDCA cell discloses superior IPCE values to TiO_2/ZnBQA+CDCA cell in all wavelength regions, although the LHE are rather comparable for the two cells (Figure 12b). This implies that the lower electron injection efficiency and/or electron collection efficiency of TiO_2/ZnBQA+CDCA cell than those of TiO_2/ZnQMA+CDCA cell are responsible for the difference in the IPCE and resulting η values. The maximal IPCE values at Soret bands are 60% for TiO_2/ZnBQA+CDCA cell and 75% for TiO_2/ZnQMA+CDCA cell, which are smaller than the maximal IPCE value of N719-sensitized cell ($IPCE_{max}$ = 77% at 525 nm, Figure 11b). The lower electron injection efficiency for TiO_2/ZnBQA+CDCA cell relative to that for TiO_2/ZnQMA+CDCA cell can be attributed to the weak electronic coupling between the LUMO of ZnBQA and the CB of the TiO_2 due to the smaller electron density of the carboxyl group in the LUMO of ZnBQA compared with that of ZnQMA (vide supra).

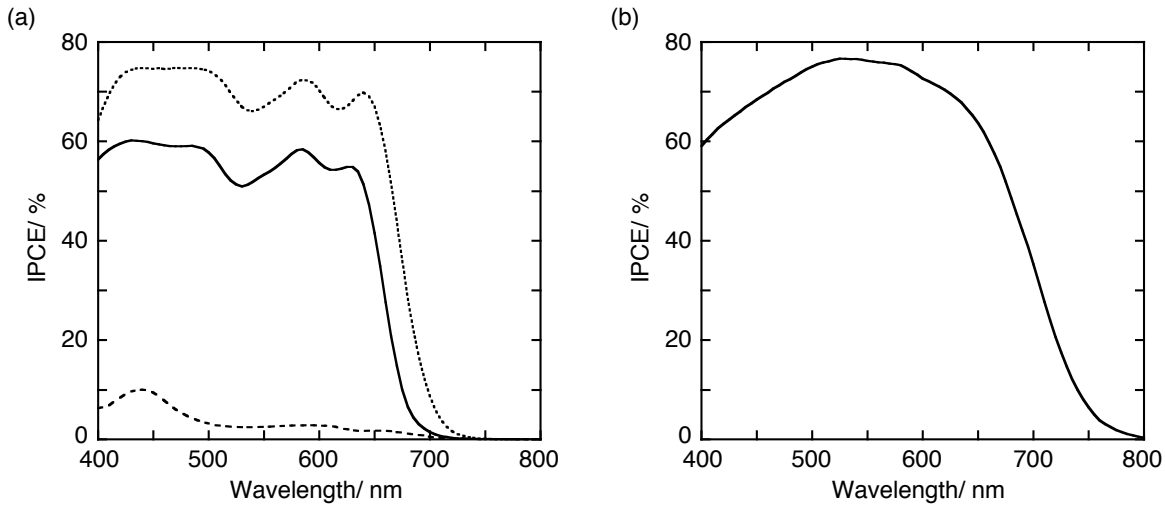

Figure 11. Photocurrent action spectra of TiO_2/ZnBQA+CDCA (solid line), TiO_2/ZnQCA+CDCA (dashed line), TiO_2/ZnQMA+CDCA (dotted line), and (b) N719-sensitized cell.

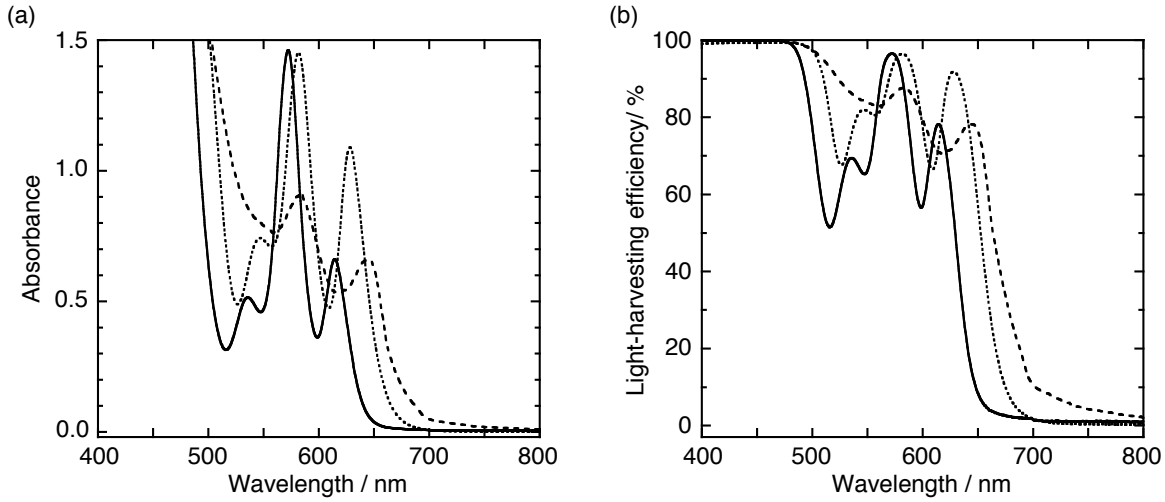

Figure 12. (a) Absorption spectra and (b) light-harvesting efficiencies of TiO_2/ZnBQA+CDCA (solid line), TiO_2/ZnQCA+CDCA (dashed line), and TiO_2/ZnQMA+CDCA (dotted line). The scattering TiO_2 layers were not applied to the TiO_2 electrodes to measure absorbance accurately.

On the other hand, considerably low J_{SC} of 2.3 mA cm^{-2} and V_{OC} of 0.51 V were obtained for TiO_2/ZnQCA+CDCA cell, resulting in a low η value of 0.80% with $ff = 0.68$. The maximal IPCE value at the Soret band is 10% that is also much lower than those of TiO_2/ZnBQA+CDCA and TiO_2/ZnQMA+CDCA cells. The influence of electronic coupling between the LUMO of ZnQCA and the CB of the TiO_2 on the electron injection efficiency for TiO_2/ZnQCA+CDCA cell may be excluded since the large electron density in the LUMO of ZnQCA is distributed on the carboxyl group. In contrast, the fluorescence lifetime of ZnQCA is short and comparable to the time scale of electron injection processes from the porphyrin

excited singlet state to TiO_2 surface (vide supra). Therefore, the reduced fluorescence lifetime of ZnQCA would have a large impact on the electron injection efficiency, leading to the low IPCE and resulting η values.[19e] The plausible tilted geometry of ZnQCA on the TiO_2 surface may also lower the electron injection efficiency because of fast charge recombination from the electrons in the CB of the TiO_2 to the porphyrin radical cation by the short separation distance between the porphyrin and the TiO_2. According to the literature, the adsorption of pyrazine molecules induces a negative shift of the Fermi level of the TiO_2 nanoparticle.[41] Nevertheless, the rather low V_{OC} value is observed for cells sensitized with ZnQCA molecules which adsorb on the TiO_2 surface through coordination bonding of the pyrazine moieties and carboxyl groups. To examine the reason for the low V_{OC} value of TiO_2/ZnQCA+CDCA cell, the author measured the current-voltage characteristics under dark conditions (Figure 13).

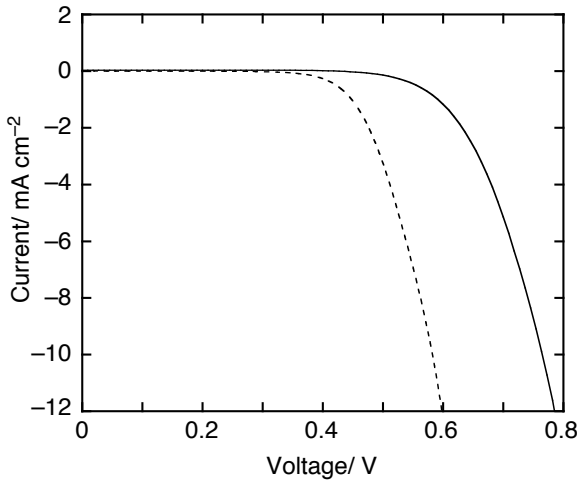

Figure 13. Current-voltage characteristics of TiO_2/ZnBQA+CDCA (solid line) and TiO_2/ZnQCA+CDCA (dashed line) cells under dark conditions.

Obviously, the onset for TiO_2/ZnQCA+CDCA cell appears at more negative value than that for TiO_2/ZnBQA+CDCA cell, indicating that the degree of the charge recombination between the injected electrons on the CB of the TiO_2 and the I_3^- for TiO_2/ZnQCA+CDCA cell is higher than that for TiO_2/ZnBQA+CDCA cell.[42] Considering that the η_{col} primarily depends on the relative rates of charge transport against charge recombination, the higher charge recombination rate for TiO_2/ZnQCA+CDCA cell also indicates the low charge collection efficiency, resulting the low IPCE values. The key factor for the frequent charge recombination for ZnQCA cell may originate from the packing structures of ZnQCA molecules on the TiO_2 surface. ZnQCA molecules may form a loosely packed monolayer due to the plausible adsorption mode of relatively parallel orientation to the TiO_2 surface (vide supra). Consequently, the I_3^- in the

electrolyte can approach to the TiO_2 surface, allowing the direct charge recombination from the electrons on the CB of the TiO_2 and the I_3^-.

Conclusion

Novel benzo[f]quinoxalino[2,3-β]porphyrin acid (ZnBQA) and quinoxalino[6,7-β] porphyrin acid (ZnQCA) have been synthesized and evaluated as photosensitizers for DSSC. ZnBQA showed the slight blue-shift of Q bands relative to that of quinoxalino[2,3-β]porphyrin acid (ZnQMA) by introducing the substituents with a benzoquinoxaline, while the Q bands of ZnQCA are red-shifted compared to those of ZnQMA. The optical HOMO-LUMO gaps are parallel to those estimated by DFT calculations. The photovoltaic properties were compared under the present optimized conditions in which a sealed device structure with $TiCl_4$-treated, TiO_2 double layers was used. The ZnBQA cell exhibited relatively high η value of 5.1% with J_{SC} = 11.1 mA cm^{-2}, V_{OC} = 0.68 V, and *ff* = 0.67, while the ZnQCA cell yielded low η value of 0.80% with J_{SC} of 2.3 mA cm^{-2}, V_{OC} = 0.51 V, and *ff* = 0.68. Both η values are smaller than those of reference cells under the currently optimized conditions (η = 6.3%, J_{SC} = 13.2 mA cm^{-2}, V_{OC} = 0.71 V, and *ff* = 0.67 for ZnQMA; η = 8.4 %, J_{SC} = 15.7 mA cm^{-2}, V_{OC} = 0.80 V, *ff* = 0.67 for N719). Nevertheless, the cell performances of the ZnQMA and N719 cells were improved considerably compared to the previous results obtained by adsorption of the same dyes without CDCA on P-25 TiO_2 electrodes. The weak electronic coupling between the LUMO of ZnBQA and the CB of the TiO_2 may result in the lower electron injection efficiency for ZnBQA-sensitized TiO_2 cell relative to ZnQMA-sensitized TiO_2 cell, leading to the lower η value of ZnBQA cell than that of ZnQMA cell. The ZnQCA-sensitized cell exhibited the further lower electron injection efficiency due to the short lifetime of the excited singlet state comparable to the time scale of electron injection processes from the dye excited states to the TiO_2 surface. In addition, the V_{OC} value of ZnQCA also significantly decreases by the effect of the charge recombination from the injected electrons in the CB of the TiO_2 to the I_3^- derived from the loose packing of ZnQCA molecules on the TiO_2 surface. Overall, the author has successfully examined the effects of the π-elongation and the fused position of quinoxaline-fused porphyrins on their photovoltaic properties, which may be useful information to design molecular structures of porphyrins for highly efficient DSSC.

Experimental Section

General. All solvents and chemicals were of reagent grade quality, purchased, and used without further purification unless otherwise noted. All of the reactions were carried out under nitrogen atmosphere in the dark. Column chromatography and thin-layer chromatography (TLC) were performed with UltraPure Silica Gel (230-400 mesh, SiliCycle) and Silica gel 60 F_{254} (Merck), respectively. ^{1}H-NMR spectra were measured on a JEOL EX-400 (400 MHz) or an ECX-400P (400 MHz) spectrometer. Matrix assisted laser desorption/ionization time-of-flight (MALDI-TOF) mass spectra were made on a Shimadzu KOMPACT MALDI II using CHCA as a matrix. High-resolution mass spectra (HRMS) were recorded on a JEOL JMS-MS700 spectrometer or a JEOL JMS-HX110A spectrometer. UV-vis absorption spectra were measured using a Perkin-Elmer Lambda 900 UV/VIS/NIR Spectrometer. FT-IR spectra were acquired using by a JASCO FT/IR-470 plus spectrometer with a KBr pellet.

Synthesis. 2-Amino-6-methoxycarbonylnaphthalene (**1**) (Tokyo Chemical Industry: TCI) was used as received. 5,10,15,20-Tetrakis(3,5-di-*tert*-butylphenyl)porphyrin (**5**),[43] 2-acetoxy-5,10,15,20-tetrakis(3,5-di-*tert*-butylphenyl)porphyrin, (**6**),[25] 12,13-dioxo-5,10,15,20-tetrakis(3,5-di-*tert*-butylphenyl)chlorin (**7**),[25] 5,10,15,20-tetrakis(2,4,6-trimethylphenyl) porphyrin (**10**),[44] 2,3-bis(bromomethyl)-5,6-dicyano-1,4-pyrazine,[45] and ZnQMA were prepared according to the known procedures.[16e] N719 was purchased from Solaronics, Inc. and purified according to the literature.[2a]

2-Acetamido-6-methoxycarbonyl-1-nitronaphthalene (2). This procedure was based upon the literature protocol for analogous compound.[22] A solution of **1** (813 mg, 4.05 mmol) in acetic anhydride (20 mL) was stirred at room temperature 5 min. To the stirred suspension of **1** was added acetic acid (20 mL) and then kept at 0 °C. The solution was added dropwise to a stirred mixture of fuming nitric acid (2.2 mL) and acetic acid (20 mL) and stirring was continued for 3 h. To the reaction mixture was added dichloromethane, and the extract was washed with $NaHCO_3$ aqueous solution and then water three times. The organic layer was collected, dried over anhydrous Na_2SO_4 and the solvent was removed in vacuo. Purification by silica gel column chromatography ($CHCl_3$:EtOAc = 5:1) and reprecipitation from methanol afforded **2** as a white solid (515 mg, 1.82 mmol, 45%): mp 154–157 °C; HRMS (EI, positive mode) found 288.0741 (M^+), $C_{14}H_{12}N_2O_5$ requires 288.0746; ^{1}H NMR (400 MHz, $CDCl_3$) δ 8.63 (d, J = 9.3 Hz 1H, Ar-H), 8.57 (d, J = 1.5 Hz, 1H, Ar-H), 8.21 (dd, J = 8.8 and 2.0 Hz, 1H, Ar-H), 8.15 (dd, J = 8.8 Hz and 1.5 Hz, 1H, Ar-H), 7.92 (s, 1H), 7.89 (d, J = 9.3 Hz, 1H, Ar-H), 7.38 (s, 1H), 3.99 (s, 3H, ester-H), 2.32 (s, 3H, amide-H); FT-IR (KBr) ν_{max} 3120 (br), 3075, 3008, 2955, 1828, 1712, 1662, 1609, 1533, 1287, 1204, 998, 824, 750 cm^{-1}.

2-Amino-6-methoxycarbonyl-1-nitronaphthalene (3). This procedure was based upon

the literature protocol for analogous compound.[23] To a solution of **2** (489 mg, 1.70 mmol) in MeOH (60 mL) was added concentrated sulfuric acid (3 mL). The solution was heated at reflux for 7 h. After pouring into ice water, the resulting precipitate was filtered off and dried in vacuo to afford **3** as an yellow solid (400 mg, 1.62 mmol, 96% yield): mp 184–186 °C; HRMS (EI, positive mode) found 246.0643 (M^+), $C_{12}H_{10}N_2O_4$ requires 246.0641; ^{1}H NMR (400 MHz, $CDCl_3$) δ 8.70 (d, J = 9.3 Hz, 1H, Ar-H), 8.41 (s, 1H, Ar-H), 8.18 (d, J = 9.3 Hz, 1H, Ar-H), 7.83 (d, J = 9.3 Hz, 1H, Ar-H), 6.81 (d, J = 9.3 Hz, 1H, Ar-H), 6.54 (s, 2H, amine-H), 3.97 (s, 3H, ester-H); FT-IR (KBr) ν_{max} 3435 (br), 3313 (br), 3162, 3074, 2991, 2948, 1713, 1635, 1507, 1305, 1287, 1248, 1208, 1113, 822, 755 cm^{-1}.

1,2-Diamino-6-methoxycarbonylnaphthalene (4). This procedure was based upon the literature protocol for analogous compound.[24] An oven dried two-neck flask was charged with **3** (350 mg, 1.42 mmol), dry methanol (90 mL) and palladium carbon (Pd 10%, 200 mg). The solution was purged with argon for 1 h and the flask was placed into ice bath. To the stirred solution was added sodium tetrahydroborate (191 mg, 5.0 mmol) in small portions over 20 min. After stirring for 30 min, the solution was evaporated. The residue was purified by passing through a plug of Celite using dichloromethane as eluent to give **4** as a pale red solid (264 mg, 1.22 mmol, 86%): mp 110–112 °C; HRMS (FAB, positive mode) found 216.0901 (M^+), $C_{12}H_{12}N_2O_2$ requires 216.0899; ^{1}H NMR (400 MHz, $CDCl_3$) δ 8.48 (s, 1H, Ar-H), 7.99 (d, J = 8.8 Hz, 1H, Ar-H), 7.73 (d, J = 8.8 Hz, 1H, Ar-H), 7.42 (d, J = 8.4 Hz, 1H, Ar-H), 7.07 (d, J = 8.4 Hz, 1H, Ar-H), 3.96 (s, 3H, ester-H), 3.76 (s, 4H, amine-H); FT-IR (KBr) ν_{max} 3250 (br), 3019, 2991, 2949, 1706, 1617, 1487, 1387, 1297, 1225, 1109, 798 cm^{-1}.

5,10,15,20-Tetrakis(3,5-di-*tert*-butylphenyl)-7'-methoxycarbonylbenzo[f]quinoxalino[2,3-β]porphyrin (8). This procedure was based upon the literature protocol for analogous compound.[16e] An oven dried Schlenk tube was charged with **4** (15.3 mg, 0.071 mmol), 12,13-dioxo-5,10,15,20-tetrakis(3,5-di-*tert*-butylphenyl)chlorin (**7**) (61.1 mg, 0.056 mmol) and dry pyridine (1.5 mL). After heating at 110°C for 8 h, the solution was evaporated. Column chromatography on silica gel (CH_2Cl_2/hexane = 1:1) afforded **8** (48.4 mg, 0.038 mmol, 68%) as a green solid: mp > 300 °C; HRMS (FAB, positive mode) found 1272.7854 (M^+), $C_{88}H_{100}N_6O_2$ requires 1272.7908; ^{1}H NMR (400 MHz, $CDCl_3$) δ 9.12 (d, J = 4.9 Hz, 1H, β-H), 9.02 (d, J = 4.9 Hz, 2H, β-H), 9.01 (s, 1H, β-H), 8.81 (s, 2H, Ar-H), 8.65 (s, 1H, Ar-H), 8.64 (d, J = 7.8 Hz, 1H, Ar-H), 8.24 (d, J = 8.8 Hz, 1H, Ar-H), 8.11 (m, 7H, Ar-H), 8.06 (d, J = 8.8 Hz, 1H, Ar-H), 8.24 (s, 2H, Ar-H), 8.01 (s, 2H, Ar-H), 7.96 (s, 1H, Ar-H), 7.81 (s, 2H, Ar-H), 7.72 (d, J = 8.8 Hz, 1H, Ar-H), 4.07 (s, 3H, methyl-H), 1.60–1.30 (m, 72H, *tert*-butyl-H), –2.53 (s, 2H, N-H).

5,10,15,20-Tetrakis(3,5-di-*tert*-butylphenyl)-7'-methoxycarbonylbenzo[f]quinoxalino[2,3-β]porphyrinatozinc (II) (9). To a solution of **8** (47.1 mg, 0.037 mmol) in

dichloromethane (10 mL) was added a solution of zinc acetate dihydrate (200 mg, 0.93 mmol) in methanol (10 mL). The reaction mixture was refluxed for 1 h. The solvent was removed by rotary evaporator, and purification by column chromatography on silica gel (CH_2Cl_2/hexane = 1:1) gave **9** (45.6 mg, 0.034 mmol, 92%) as a green solid: mp > 300 °C; MS (MALDI-TOF, positive mode) found 1337 (M^+), $C_{88}H_{98}N_6O_2Zn$ requires 1337; ^{1}H NMR (400 MHz, CD_2Cl_2) δ 9.10 (d, J = 4.9 Hz, 1H, β-H), 9.04 (d, J = 4.9 Hz, 1H, β-H), 9.03 (d, J = 4.9 Hz, 1H, β-H), 8.98 (d, J = 4.9 Hz, 1H, β-H), 8.94 (s, 2H, β-H), 8.70 (d, J = 8.8 Hz, 1H, Ar-H), 8.67 (s, 1H, Ar-H), 8.26 (dd, J = 8.8 and 1.5 Hz, 1H, Ar-H), 8.11–8.08 (m, 8H, Ar-H), 8.00 (d, J = 1.5 Hz, 2H, Ar-H), 7.95 (t, J = 1.7 Hz, 1H, Ar-H), 7.80 (t, J = 1.7 Hz, 2H, Ar-H), 7.77 (d, J = 8.8, 1H, Ar-H), 4.08 (s, 3H, methyl-H), 1.53–1.45 (m, 72H, *tert*-butyl-H); FT-IR (KBr) ν_{max} 2966, 2908, 2866, 1730, 1700, 1653, 1477, 1363, 1273, 1194, 1115, 1010, 940, 900, 799 cm^{-1}.

5,10,15,20-Tetrakis(3,5-di-*tert*-butylphenyl)-7'-carboxybenzo[f]quinoxalino[2,3-β]porphyrinatozinc (II) (ZnBQA). To a solution of **9** (45.6 mg, 0.034 mmol) in THF (10 mL) was added a solution of NaOH (194 mg, 5.0 mmol) in H_2O (5 mL). The reaction mixture was refluxed for 24 h. After cooling to room temperature, the reaction mixture was treated with 1 M HCl aqueous solution and passed through the filter paper. The filtrate was washed with water to give a crude product. Purification by column chromatography on silica gel (CH_2Cl_2/EtOAc = 10:1) and reprecipitation from CH_2Cl_2/MeOH gave ZnBQA (32.5 mg, 0.025 mmol, 72%) as a green solid: mp > 300 °C; HRMS (FAB, positive mode) found 1320.6909 (M^+), $C_{88}H_{96}N_6O_2Zn$ requires 1320.6886; ^{1}H NMR (400 MHz, CD_2Cl_2) δ 9.11 (d, J = 4.9 Hz, 1H, β-H), 9.04 (d, J = 4.9 Hz, 1H, β-H), 9.03 (d, J = 4.9 Hz, 1H, β-H), 8.98 (d, J = 4.9 Hz, 1H, β-H), 8.94 (s, 2H, β-H), 8.74 (d, J = 8.3 Hz, 1H, Ar-H), 8.74 (s, 1H, Ar-H), 8.30 (dd, J = 8.3 and 2.0 Hz, 1H, Ar-H), 8.13–8.09 (m, 8H, Ar-H), 8.00 (d, J = 1.5 Hz, 2H, Ar-H), 7.96 (t, J = 1.7 Hz, 1H, Ar-H), 7.80 (m, 3H, Ar-H), 1.54 (s, 36H, *tert*-butyl-H), 1.50 (s, 18H, *tert*-butyl-H), 1.48 (s, 18H, *tert*-butyl-H); FT-IR (KBr) ν_{max} 3400 (br), 3057, 2964, 2947, 2866, 1717, 1594, 1478, 1363, 1248, 1120, 1068, 1008, 939, 900, 797 cm^{-1}.

5,10,15,20-Tetrakis(2,4,6-trimethylphenyl)-2',3'-dicyanoquinoxalino[6,7-β]porphyrin (11). This procedure was based upon the literature protocol for analogous compound.[26] 5,10,15,20-Tetrakis(2,4,6-trimethylphenyl)porphyrin (**10**) (500 mg, 0.639 mmol), 2,3-bis(bromomethyl)-5,6-dicyano-1,4-pyrazine (2.02 g, 6.39 mmol), and NaI (2.87 g, 19.2 mmol) were dissolved in 1,2,4-trichlorobenzene (185 mL) and the mixture was refluxed for 9 h. The reaction mixture was diluted with $CHCl_3$, washed with an aqueous solution of $Na_2S_2O_3$, and then the organic layer was dried over Na_2SO_4. The solvent was removed by rotary evaporator, and purification by column chromatography on silica gel (CH_2Cl_2/hexane = 5:1) and reprecipitation from hexane gave **11** (125 mg, 0.134 mmol, 21%) as a purple solid: mp >

300 °C; HRMS (FAB, positive mode) found 934.4493 (M^+), $C_{64}H_{54}N_8$ requires 934.4471; ^{1}H NMR (400 MHz, CD_2Cl_2) δ 8.74 (d, J = 3.4 Hz, 2H, β-H), 8.72 (d, J = 3.4 Hz, 2H, β-H), 8.49 (s, 2H, β-H), 8.06 (s, 2H, quinoxalino-H), 7.51 (s, 4H, Ar-H), 7.30 (s, 4H, Ar-H), 2.79 (s, 6H, methyl-H), 2.61 (s, 6H, methyl-H), 1.88 (s, 12H, methyl-H), 1.81 (s, 12H, methyl-H), –2.31 (s, 2H, N-H); FT-IR (KBr) ν_{max} 3350 (br), 3000, 2954, 2916, 2857, 2245, 1436, 1412, 1177, 1096, 970, 825, 801, 724 cm^{-1}.

5,10,15,20-Tetrakis(2,4,6-trimethylphenyl)-2'-carboxy-3'-cyanoquinoxalino[6,7-β]porphyrin (12). To a solution of **11** (150 mg, 0.160 mmol) in trifluoroacetic acid (10 mL) was added 1N HCl aqueous solution (10 mL) and water (2 mL). The solution was stirred at room temperature for 4 h. The reaction mixture was neutralized with saturated $NaHCO_3$ aqueous solution at 0°C and then extracted with dichloromethane. The extract was washed with brine and dried over Na_2SO_4, and concentrated in vacuo. Purification by column chromatography on silica gel (CH_2Cl_2/EtOAc = 20:1) gave **12** (60.0 mg, 0.0629 mmol, 39%) as a purple solid: mp > 300 °C; HRMS (FAB, positive mode) found 953.4430 (M^+), $C_{64}H_{55}N_7O_2$ requires 953.4417; ^{1}H NMR (400 MHz, CD_2Cl_2) δ 8.73–8.68 (m, 4H, β-H), 8.53–8.46 (m, 2H, β-H), 8.10 (s, 1H, quinoxalino-H), 7.97 (s, 1H, quinoxalino-H), 7.53–7.51 (m, 4H, Ar-H), 7.32–7.29 (m, 4H, Ar-H), 2.81 (s, 3H, methyl-H), 2.77 (s, 3H, methyl-H), 2.62 (s, 6H, methyl-H), 1.88 (s, 12H, methyl-H), 1.82 (s, 12H, methyl-H), –2.31 (s, 2H, N-H); FT-IR (KBr) ν_{max} 3500 (br), 3350 (br), 2986, 2968, 2916, 2222, 1700, 1560, 1448, 1416, 1174, 1098, 970, 825, 801, 724 cm^{-1}.

5,10,15,20-Tetrakis(2,4,6-trimethylphenyl)-2'-carboxy-3'-cyanoquinoxalino[6,7-β]porphyrinatozinc (II) (ZnQCA). To a solution of **12** (50.7 mg, 0.0531 mmol) in chloroform (10 mL) was added a solution of zinc acetate dihydrate (1.0 g, 4.7 mmol) in methanol (10 mL). The reaction mixture was stirred at room temperature for 48 h. The solvent was removed by rotary evaporator, and purification by column chromatography on silica gel (CH_2Cl_2/EtOAc = 20:1) gave ZnQCA (28.2 mg, 0.0277 mmol, 52%) as a green solid: mp > 300 °C; HRMS (FAB, positive mode) found 1015.3559 (M^+), $C_{64}H_{53}N_7O_2Zn$ requires 1015.3552; ^{1}H NMR (400 MHz, CD_2Cl_2) δ 8.73–8.63 (m, 4H, β-H), 8.61–8.59 (m, 2H, β-H), 8.31 (s, 1H, quinoxalino-H), 8.17 (s, 1H, quinoxalino-H), 7.52–7.50 (m, 4H, Ar-H), 7.32–7.25 (m, 4H, Ar-H), 2.80 (s, 3H, methyl-H), 2.77 (s, 3H, methyl-H), 2.62 (s, 6H, methyl-H), 1.87 (s, 12H, methyl-H), 1.81 (s, 12H, methyl-H); FT-IR (KBr) ν_{max} 3470 (br), 2996, 2918, 2848, 2222, 1700, 1590, 1448, 1419, 1340, 1153, 1000, 825, 800, 724 cm^{-1}.

Optical Spectroscopy. UV-visible absorption spectra of the porphyrins in CH_2Cl_2 and the porphyrin monolayers on TiO_2 electrodes without light-scattering layer (vide infra) were recorded using a Perkin Elmer Lambda 900 UV/VIS/NIR Spectrometer. Steady-state fluorescence spectra were acquired by using a SPEX Fluoromax-3 Spectrofluorometer. A

time-correlated single photon counting (TCSPC) method was used for the time-resolved fluorescence measurements in the nanosecond and subnanosecond time-scale and the time resolution was ~ 80 ps (FWHM).[46] An up-conversion technique for fluorescence was used to detect the fast processes with a time resolution shorter than 0.2 ps. The excitation wavelength was 405 nm.[46]

Electrochemistry. Electrochemical measurements were made using an ALS 630a electrochemical analyzer. Redox potentials of the porphyrins in solution were determined by differential pulse voltammetry (DPV) in dichloromethane containing 0.1 M tetrabutylammonium hexafluorophosphate (Bu_4NPF_6) as a supporting electrolyte. A glassy carbon working electrode (3 mm diameter), $Ag/AgNO_3$ (0.01M in acetonitrile) reference electrode, and Pt wire counter electrode, were employed. Ferrocene/ferrocenium (+0.642 V vs NHE) was used as an internal standard for all measurements. All of the measured potentials were converted to the NHE scale.

Density Functional Theory (DFT) Calculations. Geometry optimization and electronic structure calculations of the porphyrins were performed using B3LYP functional and 3-21G* basis set implemented in the Gaussian 03 program package.[47] Molecular orbitals were visualized by Molstudio 3.0 software.

Preparation of Porphyrin- or N719-Sensitized TiO_2 Electrode and Photovoltaic Measurements. The preparation of TiO_2 electrodes and the fabrication of the sealed cells for photovoltaic measurements were performed by following the procedures previously reported by Grätzel and co-workers.[48] The details of this work was described as below.

The author used two types of TiO_2 pastes: one composed of nanocrystalline-TiO_2 particles (20 nm, CCIC:PST18NR, JGC-CCIC) and another containing submicrocrystalline-TiO_2 particles (400 nm, CCIC:PST400C, JGC-CCIC), to form the transparent and the light-scattering layers of the photoanode, respectively. To prepare the working electrodes, FTO glasses (Solar 4 mm thickness, 10Ω/□, Nippon Sheet Glass) were first cleaned in a detergent solution using an ultrasonic bath for 10 min, and then rinsed with distilled water and ethanol. After UV-O_3 irradiation for 18 min, the FTO glass plates were immersed into a 40 mM aqueous $TiCl_4$ solution at 70°C for 30 min and washed with distilled water and ethanol. A layer of the nanocrystalline-TiO_2 paste was coated on the FTO glass plate by screen-printing method, kept in a clean box for a few minutes and then dried over 6 min at 125°C. This screen-printing procedure with the nanocrystalline-TiO_2 paste was repeated to reach a thickness of 12 μm. After drying the films at 125°C, a layer of the submicrocrystalline-TiO_2 paste was deposited by screen-printing in the same method as the fabrication of the nanocrystalline-TiO_2 layer, resulting in a light-scattering TiO_2 film of 4–5 μm. Finally, the electrodes coated with

the TiO_2 pastes were gradually heated under an airflow at 325°C for 5 min, at 375°C for 5 min, at 450°C for 15min, and at 500°C for 15 min. The thickness of the films was determined using surface profiler (SURFCOM 130A, ACCRETECH). The size of the TiO_2 film was 0.25 cm^2 (5 × 5 mm). The TiO_2 electrode was treated again with 40 mM $TiCl_4$ solution as mentioned above, then rinsed with distilled water and ethanol, sintered at 500°C for 30 min, and allowed to cool under 70°C before dipping into the dye solution. The TiO_2 electrode was immersed into 0.20 mM porphyrin solution. As an immersing solvent the author used ethanol for ZnBQA[33] and methanol for ZnQCA and ZnQMA. The temperatures during immersion of the TiO_2 electrodes into the porphyrin solutions were kept at 40°C for ZnBQA and ZnQCA and at 25°C for ZnQMA.[34] The TiO_2 electrodes adsorbed with ZnBQA, ZnQCA, and ZnQMA are denoted as TiO_2/ZnBQA, TiO_2/ZnQCA, and TiO_2/ZnQMA, respectively. To reduce the aggregation, the TiO_2 electrodes were immersed into 0.20 mM porphyrin solution containing chenodeoxycholic acid (CDCA: 0.20 mM). The solvents and the temperatures during the immersion into the porphyrin solutions containing CDCA were identical to those used for the sensitization without CDCA. The TiO_2 electrodes adsorbed with ZnBQA, ZnQCA, and ZnQMA containing CDCA are denoted as TiO_2/ZnBQA+CDCA, TiO_2/ZnQCA+CDCA, and TiO_2/ZnQMA+CDCA respectively. N719-sensitized TiO_2 electrode as a reference was prepared by immersing the TiO_2 electrode into a mixture of *t*-BuOH/acetonitrile (v/v = 1:1) containing 0.50 mM N719 and 0.5 mM CDCA at 25°C for 20 h. The porphyrin densities adsorbed on the TiO_2 films (mol cm^{-2}) were determined by measuring the difference in the absorbances of the porphyrin solutions before and after immersion of the TiO_2 films (TiO_2 area of 0.25 cm^2 with a thickness of 12 μm) without the scattering layer.

To prepare a counter electrode, a small hole was drilled in an FTO glass (Solar 1 mm thickness, 10Ω/□, Nippon Sheet Glass). The perforated plate was rinsed with distilled water and ethanol, and then treated with 0.1 M HCl solution in 2-propanol using an ultrasonic bath for 5 min to remove an iron contamination source. The FTO glass was washed by rinsing with distilled water and ethanol, and ultrasound in acetone bath for 10 min. After heating in air for 15 min at 400°C, the Pt catalyst was deposited on the FTO glass by coating with a drop of H_2PtCl_6 solution (2 mg Pt in 1 mL ethanol) twice. Finally, the FTO glass was heated at 400°C for 15 min to obtain the counter Pt-electrode.

A sandwich cell was prepared by using the dye-anchored TiO_2 film as a working electrode and a counter Pt-electrode, which were assembled with a hotmelt-ionomer film of Surlyn polymer gasket (DuPont), and the superimposed electrodes were tightly held and heated at 130 °C to seal the two electrodes. The aperture of the Surlyn frame was 2 mm larger than that of the area of TiO_2 film and its width was 1 mm. The hole in the counter electrode was sealed

by a film of Surlyn. A hole was then made in the film of Surlyn covered on the hole by a needle. A drop of an electrolyte was put on the hole in the back of the counter electrode. It was introduced into the cell via vacuum backfilling. Finally, the hole was sealed using Surlyn film and a cover glass (0.13–0.17 mm thickness). The edge of the FTO outside of the cell was roughened with sandpaper. A solder was applied on each edge of the FTO electrodes. An electrolyte solution used was 0.60 M 2,3-dimethyl-1-propyl imidazolium iodide, 0.05 M I_2, 0.10 M LiI, and 0.50 M 4-*tert*-butylpyridine in an acetonitrile.

Incident photon-to-current efficiency (IPCE) and photocurrent–voltage (*I–V*) performance were measured on an action spectrum measurement setup (PEC-S20) and a solar simulator (PEC-L10, Peccell Technologies) with a simulated sunlight of AM 1.5 (100 mW cm^{-2}), respectively: IPCE (%) = 100 × 1240 × i/(W_{in} × λ), where i is the photocurrent density (A cm^{-2}), W_{in} is the incident light intensity (W cm^{-2}), and λ is the excitation wavelength (nm). During the photovoltaic measurements, a black plastic tape was attached on the back of the TiO_2 electrode except for the TiO_2 film region to reduce scattering light.

X-ray Photoelectron Spectroscopy (XPS) Measurements. The XPS data were acquired using an ULVAC-PHI 5500MT system equipped with Mg Kα X-ray source (1253.6 eV) and a hemispherical energy analyzer. The powders of samples were mounted on indium foil. The powders of TiO_2/ZnBQA, TiO_2/ZnQCA, and TiO_2/ZnQMA were obtained by scratching each porphyrin- adsorbed TiO_2 layer from the corresponding porphyrin-sensitized TiO_2 electrodes without scattering layer (vide supra). All spectra were referenced to the C1s major peak at 284.5 eV. The signals were fitted by Gaussian functions using the program OriginPro 7.0.

References and Footnote

(1) (a) O'Regan, B.; Grätzel, M. *Nature* **1991**, *353*, 737. (b) Nazeeruddin, M. K.; Kay, A.; Rodicio, I.; Humphry-Baker, R.; Müller, E.; Liska, P.; Vlachopoulos, N.; Grätzel, M. *J. Am. Chem. Soc.* **1993**, *115*, 6382. (c) Grätzel, M. *Acc. Chem. Res.* **2009**, *42*, 1788.

(2) (a) Nazeeruddin, M. K.; Angelis, F. D.; Fantacci, S.; Selloni, A.; Viscardi, G.; Liska, P.; Ito, S.; Takeru, B.; Grätzel, M. *J. Am. Chem. Soc.* **2005**, *127*, 16835. (b) Gao, F.; Wang, Y.; Shi, D.; Zhang, J.; Wang, M.; Jing, X.; Humphry-Baker, R.; Wang, P.; Zakeeruddin, S. M.; Grätzel, M. *J. Am. Chem. Soc.* **2008**, *130*, 10720. (c) Chen, C.-Y.; Wang, M.; Li, J.-Y.; Pootrakulchote, N.; Alibabaei, L.; Ngoc-le, C.; Decoppet, J.-D.; Tsai, J.-H.; Grätzel, C.; Wu, C.-G.; Zakeeruddin, S. M.; Grätzel, M. *ACS Nano* **2009**, *3*, 3103. (d) Chiba, Y.; Islam, A.; Watanabe, Y.; Komiya, R.; Koide, N.; Han, L. *Jpn. J. Appl. Phys.* **2006**, *45*, L638.

(3) (a) Mishra, A.; Fischer, M. K. R.; Bäuerle, P. *Angew. Chem., Int. Ed.* **2009**, *48*, 2474. (b)

Ooyama, Y.; Harima, Y. *Eur. J. Org. Chem.* **2009**, 2903. (c) Imahori, H.; Umeyama, T.; Ito, S. *Acc. Chem. Res.* **2009**, *42*, 1809.

(4) (a) Hara, K.; Sayama, K.; Ohga, Y.; Shinpo, A.; Suga, S.; Arakawa, H. *Chem. Commun.* **2001**, 569. (b) Hara, K.; Kurashige, M.; Danoh, Y.; Kasada, C.; Shinpo, A.; Suga, S.; Arakawa, H. *New. J. Chem.* **2003**, *27*, 783. (c) Wang, Z.-S.; Cui, Y.; Dan-oh, Y.; Kasada, C.; Shinpo, A.; Hara, K. *J. Phys. Chem. C* **2007**, *111*, 7224. (d) Wang, Z.-S.; Cui, Y.; Dan-oh, Y.; Kasada, C.; Shinpo, A.; Hara, K. *J. Phys. Chem. C* **2008**, *112*, 17011.

(5) (a) Horiuchi, T.; Miura, H.; Uchida, S. *Chem. Commun.* **2003**, 3036. (b) Horiuchi, T.; Miura, H.; Sumioka, K.; Uchida, S. *J. Am. Chem. Soc.* **2004**, *126*, 12218. (c) Ito, S.; Zakeeruddin, S. M.; Humphry-Baker, R.; Liska, P.; Charvet, R.; Comte, P.; Nazeeruddin, M. K.; Péchy, P.; Takata, M.; Miura, H.; Uchida, S. Grätzel, M. *Adv. Mater.* **2006**, *18*, 1202. (d) Ito, S.; Miura, H.; Uchida, S.; Takata, M.; Sumioka, K.; Liska, P.; Comte, P.; Péchy, P.; Grätzel, M. *Chem. Commun.* **2008**, 5194.

(6) (a) Hara, K.; Kurashige, M.; Ito, S.; Shinpo, A.; Suga, S.; Sayama, K.; Arakawa, H. *Chem. Commun.* **2003**, 252. (b) Kitamura, T.; Ikeda, M.; Shigaki, K.; Inoue, T.; Anderson, N. A.; Ai, X.; Lian, T.; Yanagida, S. *Chem. Mater.* **2004**, *16*, 1806. (c) Hwang, S.; Lee, J. H.; Park, C.; Lee, H.; Kim, C.; Park, C.; Lee, M.-H.; Lee, W.; Park, J.; Kim, K.; Park, N.-G.; Kim, C. *Chem. Commun.* **2007**, 4887. (d) Kim, C.; Choi, H.; Kim, S.; Baik, C.; Song, K.; Kang, M.-S.; Kang, S. O.; Ko, J. *J. Org. Chem.* **2008**, *73*, 7072. (e) Im, H.; Kim, S.; Park, C.; Jang, S.-H.; Kim, C-J.; Kim, K.; Park, N.-G.; Kim, C. *Chem. Commun.* **2010**, DOI: 10.1039/b917065k.

(7) (a) Tan, S.; Zhai, J.; Fang, H.; Jiu, T.; Ge, J.; Li, Y.; Jiang, L.; Zhu, D. *Chem.-Eur. J.* **2005**, *11*, 6272. (b) Liu, W.-H.; Wu, I-C.; Lai, C.-H.; Lai, C.-H.; Chou, P.-T.; Li, Y.-T.; Chen, C.-L.; Hsu, Y.-Y.; Chi, Y. *Chem. Commun.* **2008**, 5152. (c) Choi, H.; Baik, C.; Kang, S. O.; Ko, J.; Kang, M.-S.; Nazeeruddin, M. K.; Grätzel, M. *Angew. Chem., Int. Ed.* **2008**, *47*, 327. (d) Wang, Z.-S.; Koumura, N.; Cui, Y.; Takahashi, M.; Sekiguchi, H.; Mori, A.; Kubo, T.; Furube, A.; Hara, K. *Chem. Mater.* **2008**, *20*, 3993. (e) Zhang, G.; Bala, H.; Cheng, Y.; Shi, D.; Lv, X.; Yu, Q.; Wang, P. *Chem. Commun.* **2009**, 2198.

(8) (a) Ehret, A.; Stuhl, L.; Spitler, M. T. *Electrochim. Acta* **2000**, *45*, 4553. (b) Wu, W.; Hua, J.; Jin, Y.; Zhan, W.; Tian, H. *Photochem. Photobiol. Sci.* **2008**, *7*, 63.

(9) (a) Wang, Z.-S.; Li, F.-Y.; Huang, C.-H.; Wang, L.; Wei, M.; Jin, L.-P.; Li, N.-Q. *J. Phys. Chem. B* **2000**, *104*, 9676. (b) Yao, Q.-H.; Shan, L.; Li, F.-Y.; Yin, D.-D.; Huang, C.-H. *New J. Chem.* **2003**, *27*, 1277. (c) Chen, Y.-S.; Li, C.; Zeng, Z.-H.; Wang, W.-B.; Wang, X.-S.; Zhang, B.-W. *J. Mater. Chem.* **2005**, *15*, 1654.

(10) (a) Chen, Y.; Zeng, Z.; Li, C.; Wang, W.; Wang, X.; Zhang, B. *New J. Chem.* **2005**, *29*,

773. (b) Yum, J.-H.; Walter, P.; Huber, S.; Rentsch, D.; Geiger, T.; Nüesch, F.; Angelis, F. D.; Grätzel, M.; Nazeeruddin, M. K. *J. Am. Chem. Soc.* **2007**, *129*, 10320.

(11) (a) Reddy, P. Y.; Giribabu, L.; Lyness, C.; Snaith, H. J.; Vijaykumar, C.; Chandrasekharam, M.; Lakshmikantam, M.; Y, J.-H.; Kalyanasundaram, K.; Grätzel, M.; Nazeeruddin, M. K. *Angew. Chem., Int. Ed.* **2007**, *46*, 373. (b) Cid, J.-J.; Yum, J.-H.; Jang, S.-R.; Nazeeruddin, M. K.; Martínez-Ferrero, E.; Palomares, E. J.; Ko, J.; Grätzel, M.; Torres, T. *Angew. Chem., Int. Ed.* **2007**, *46*, 8358. (c) Eu, S.; Katoh, T.; Umeyama, T.; Matano, Y.; Imahori, H. *Dalton Trans.* **2008**, 5476. (d) Cid, J.-J.; García-Iglesias, M.; Yum, J.-M.; Forneli, A.; Albero, J.; Martínez-Ferrero, E.; Vázquez, P.; Grätzel, M.; Nazeeruddin, M. K.; Palomares, E.; Torres, T. *Chem.-Eur. J.* **2009**, *15*, 5130.

(12) (a) Ferrere, S.; Zaban, A.; Gregg, B. A. *J. Phys. Chem. B* **1997**, *101*, 4490. (b) Shibano, Y.; Umeyama, T.; Matano, Y.; Imahori, H. *Org. Lett.* **2007**, *9*, 1971. (c) Li, C.; Yum, J.-H.; Moon, S.-J.; Herrmann, A.; Eickemeyer, F.; Pschirer, N. G.; Erk, P.; Schöneboom, J.; Müllen, K.; Grätzel, M.; Nazeeruddin, M. K. *ChemSusChem.* **2008**, *1*, 615.

(13) (a) Kay, A.; Grätzel, M. *J. Phys. Chem.* **1993**, *97*, 6272. (b) Ma, T.; Inoue, K.; Noma, H.; Yao, K.; Abe, E. *J. Photochem. Photobiol. A* **2002**, *152*, 207. (c) Nazeeruddin, M. K.; Humphry-Baker, R.; Officer, D. L.; Campbell, W. M.; Burrell, A. K.; Grätzel, M. *Langmuir* **2004**, *20*, 6514. (d) Schmidt-Mende, L.; Campbell, W. M.; Wang, Q.; Jolley, K. W.; Officer, D. L.; Nazeeruddin, M. K.; Grätzel, M. *ChemPhysChem* **2005**, *6*, 1253. (e) Mozer, A. J.; Griffith, M. J.; Tsekouras, G.; Wagner, P.; Wallace, G. G.; Mori, S.; Sunahara, K.; Miyashita, M.; Earles, J. C.; Gordon, K. C.; Du, L.; Katoh, R.; Furube, A.; Officer, D. L. *J. Am. Chem. Soc.* **2009**, *131*, 15621. (f) Park, J. K.; Lee, H. R.; Chen, J.; Shinokubo, H.; Osuka, A.; Kim, D. *J. Phys. Chem. C* **2008**, *112*, 16691.

(14) (a) Cherian, S.; Wamser, C. C. *J. Phys. Chem. B* **2000**, *104*, 3624. (b) Watson, D. F.; Marton, A.; Stux, A. M.; Meyer, G. J. *J. Phys. Chem. B* **2003**, *107*, 10971. (c) Watson, D. F.; Marton, A.; Stux, A. M.; Meyer, G. J. *J. Phys. Chem. B* **2004**, *108*, 11680. (d) Rochford, J.; Chu, D.; Hagfeldt, A.; Galoppini, E. *J. Am. Chem. Soc.* **2007**,*129*, 4655. (e) Rochford, J.; Galoppini, E. *Langmuir* **2008**, *24*, 5366.

(15) (a) Boschloo, G. K.; Goossens, A. *J. Phys. Chem.* **1996**, *100*, 19489. (b) Koehorst, R. B. M.; Boschloo, G. K.; Savenije, T. J.; Goossens, A.; Schaafsma, T. J. *J. Phys. Chem. B* **2000**, *104*, 2371. (c) Clifford, J. N.; Yahioglu, G.; Milgrom, L. R.; Durrant, J. R. *Chem. Commun.* **2002**, 1260. (d) Odobel, F.; Blart, E.; Lagrée, M.; Villieras, M.; Boujtita, H.; El Murr, N.; Caramori, S.; Bignozzi, C. A. *J. Mater. Chem.* **2003**, *13*, 502. (e) Jasieniak, J.; Johnston, M.; Waclawik, E. R. *J. Phys. Chem. B* **2004**, *108*, 12962.

(16) (a) Imahori, H.; Hayashi, S.; Umeyama, T.; Eu, S.; Oguro, A.; Kang, S.; Matano, Y.;

Shishido, T.; Ngamsinlapasathian, S.; Yoshikawa, S. *Langmuir* **2006**, *22*, 11405. (b) Eu, S.; Hayashi, S.; Umeyama, T.; Oguro, A.; Kawasaki, M.; Kadota, N.; Matano, Y.; Imahori, H. *J. Phys. Chem. C* **2007**, *111*, 3528. (c) Tanaka, M.; Hayashi, S.; Eu, S.; Umeyama, T.; Matano, Y.; Imahori, H. *Chem. Commun.* **2007**, 2069. (d) Hayashi, S.; Matsubara, Y.; Eu, S.; Hayashi, H.; Umeyama, T.; Matano, Y.; Imahori, H. *Chem. Lett.* **2008**, *37*, 846. (e) Eu, S.; Hayashi, S.; Umeyama, T.; Matano, Y.; Araki, Y.; Imahori, H. *J. Phys. Chem. C* **2008**, *112*, 4396. (f) Hayashi, S.; Tanaka, M.; Hayashi, H.; Eu, S.; Umeyama, T.; Matano, Y.; Araki, Y.; Imahori, H. *J. Phys. Chem. C* **2008**, *112*, 15576. (g) Imahori, H.; Hayashi, S.; Hayashi, H.; Oguro, A.; Eu, S.; Umeyama, T.; Matano, Y. *J. Phys. Chem. C* **2009**, *113*, 18406. (h) Kira, A.; Tanaka, M.; Umeyama, T.; Matano, Y.; Yoshimoto, N.; Zhang, Y.; Ye, S.; Lehtivuori, H.; Tkachenko, N. V.; Lemmetyinen, H.; Imahori, H. *J. Phys. Chem. C* **2007**, *111*, 13618. (i) Imahori, H.; Umeyama, T. *J. Phys. Chem. C* **2009**, *113*, 9029.

(17) (a) Amao, Y.; Yamada, Y. *Langmuir* **2005**, *21*, 3008. (b) Stromberg, J. R.; Marton, A.; Kee, H. L.; Kirmaier, C.; Diers, J. R.; Muthiah, C.; Taniguchi, M.; Lindsey, J. S.; Bocian, D. F.; Meyer, G. J.; Holten, D. *J. Phys. Chem. C* **2007**, *111*, 15464. (c) Wang, X.-F.; Kitao, O.; Zhou, H.; Tamiaki, H.; Sasaki, S. *J. Phys. Chem. C* **2009**, *113*, 7954.

(18) Tachibana, Y.; Haque, S. A.; Mercer, I. P.; Durrant, J. R.; Klug, D. R. *J. Phys. Chem. B* **2000**, *104*, 1198.

(19) (a) Lee, C.-W.; Lu, H.-P.; Lan, C.-M.; Huag, Y.-L.; Liang, Y.-R.; Yen, W.-N.; Liu, Y.-C.; Lin, Y.-S.; Diau, E. W.-G.; Yeh, C.-Y. *Chem.–Eur. J.* **2009**, *15*, 1403. (b) Lin, C.-Y.; Lo, C.-F.; Luo, L.; Lu, H.-P.; Hung, C.-S.; Diau, E. W.-G. *J. Phys. Chem. C* **2009**, *113*, 755. (c) Lu, H.-P.; Tsai, C.-Y.; Yen, W.-N.; Hsieh, C.-P.; Lee, C.-W.; Yeh, C.-Y.; Diau, E. W.-G. *J. Phys. Chem. C* **2009**, *113*, 20990. (d) Lu, H.-P.; Mai, C.-L.; Tsia, C.-Y.; Hsu, S.-J.; Hsieh, C.-P.; Chiu, C.-L.; Yeh, C.-Y.; Diau, E. W.-G. *Phys. Chem. Chem. Phys.* **2009**, *11*, 10270. (e) Lin, C.-Y.; Wang, Y.-C.; Hsu, S.-J.; Lo, C.-F.; Diau, E. W.-G. *J. Phys. Chem. C* **2010**, *114*, 687.

(20) Chen, C.-T.; Yeh, H.-C.; Zhang, X.; Yu, J. *Org. Lett.* **1999**, *1*, 1767.

(21) (a) Wang, Q.; Campbell, W. M.; Bonfantani, E. E.; Jolley, K. W.; Officer, D. L.; Walsh, P. J.; Gordon, K.; Humphry-Baker, R.; Nazeeruddin, M. K.; Grätzel, M. *J. Phys. Chem. B* **2005**, *109*, 15397. (b) Campbell, W. M.; Jolley, K. W.; Wagner, P.; Wagner, K.; Walsh, P. J.; Gordon, K. C.; Schmidt-Mende, L.; Nazeeruddin, Md. K.; Wang, Q.; Grätzel, M.; Officer, D. L. *J. Phys. Chem. C* **2007**, *111*, 11760.

(22) (a) Stuart, D. R.; Bertrand-Laperle, M.; Burgess, K. M. N.; Fagnou, K. *J. Am. Chem. Soc.* **2008**, *130*, 16474. (b) Buckles, R. E.; Bellis, M. P. In *Organic Syntheses Collective*; Kamm, O., Rabjohn, N., Eds.; Wily: New York, 1963; Vol. 4, p 722.

(23) Aguirre, G.; Boiani, L.; Cerecetto, H.; Maio, R. D.; González, M.; Porcal, W.; Denicola, A.; Möller, M.; Thomson, L.; Tórtora, V. *Bioorg. Med. Chem.* **2005**, *13*, 6324.

(24) Baldwin, J. E.; Crossley, M. J.; Debernardis, J. *Tetrahedron* **1982**, *38*, 685.

(25) Zhang, W.; Wicks, M. N.; Burn, P. L. *Org. Biomol. Chem.* **2008**, *6*, 879.

(26) Zhao, S.; Neves, M. G. P. M. S.; Tomé, A. C.; Silva, A. M. S.; Cavaleiro, J. A. S.; Domingues, M. R. M.; Correia, A. J. F. *Tetrahedron Lett.* **2005**, *46*, 2189.

(27) Gierschner, J.; Cornil, J.; Egelhaaf, H.-J. *Adv. Mater.* **2007**, *19*, 173.

(28) The fluorescence decay of ZnQCA could not be measured in dichloromethane because of the degradation of the sample during the measurement. Thus, the fluorescence lifetime measurement for ZnQCA was carried out in benzonitrile.

(29) (a) Rehm, J. M.; McLendon, G. L.; Nagasawa, Y.; Yoshihara, K.; Moser, J.; Grätzel, M. *J. Phys. Chem.***1996**, *100*, 9577. (b) Burfeindt, B.; Hannappel, T.; Storck, W.; Willig, F. *J. Phys. Chem.* **1996**, *100*, 16463. (c) Hilgendorff, M.; Sundström, V. *J. Phys. Chem. B.* **1998**, *102*, 10505. (d) Asbury, J. B.; Hao, E.; Wang, Y.; Ghosh, H. N.; Lian, T. *J. Phys. Chem. B* **2001**, *105*, 4545.

(30) Kadish, K. M.; Wenbo. E.; Sintic, P. J.; Ou, Z.; Shao, J.; Ohkubo, K.; Fukuzumi, S.; Govenlock, L. J.; McDonald, J. A.; Try, A. C.; Cai, Z.-L.; Reimers, J. R.; Crossley, M. J. *J. Phys. Chem. B* **2007**, *111*, 8762.

(31) Foresman, J. B.; Frisch, A. In *Exploring Chemistry with Electronic Structure Methods*; Gaussian Inc.: Pittsburgh, 1995.

(32) Hagberg, D. P.; Edvinsson, T.; Marinado, T.; Boschloo, G.; Hagfeldt, A.; Sun, L. *Chem. Commun.* **2006**, 2245.

(33) Imahori and co-workers have shown that porphyrin carboxylic acids exhibit the high cell performance after the sensitization in protic solvents.[16g] Specifically, the cell performance is in the order of MeOH>EtOH. Unfortunately, ZnBQA was found to be insoluble in MeOH. Thus, the cell performance of ZnBQA was evaluated after the sensitization in EtOH.

(34) ZnBQA was sensitized on the TiO_2 surface at 40°C due to the low solubility in EtOH at 25°C. The sensitization of ZnQCA at 25°C yielded the lower surface coverage (0.4×10^{-10} mol cm^{-2}) than the sensitization at 40°C (0.7×10^{-10} mol cm^{-2}).

(35) Johansson, E. M. J.; Hedlund, M.; Siegbahn, H.; Rensmo, H. *J. Phys. Chem. B* **2005**, *109*, 22256.

(36) Patthey, L.; Rensmo, H.; Persson, P.; Westermark, K.; Vayssieres, L.; Stashans, A.; Petersson, Å.; Bruhwiler, P. A.; Siegbahn, H.; Lunell, S.; Martensson, N. *J. Chem. Phys.* **1999**, *110*, 5913.

(37) (a) Polzonetti, G.; Ferri, A.; Russo, M. V.; Iucci, G.; Licoccia, S.; Paolesse, R. *J. Vac. Sci. Technol. A* **1999**, *17*, 832. (b) Sarno, D. M.; Matienzo, L. J.; Jones, Jr., W. E. *Inorg. Chem.* **2001**, *40*, 6308. (c) Lu, M.; Chen, B.; He, T.; Li, Y.; Tour, J. M. *Chem. Mater.* **2007**, *19*, 4447. (d) Vilmercati, P.; Castellarin-Cudia, C.; Gebauer, R.; Ghosh, P.; Lizzit, S.; Petaccia, L.; Cepek, C.; Larciprete, R.; Verdini, A.; Floreano, L.; Morgante, A.; Goldoni, A. *J. Am. Chem. Soc.* **2009**, *131*, 644.

(38) (a) Condorelli, G. G.; Motta, A.; Favazza, M.; Fragalà, I. L.; Busi, M.; Menozzi, E.; Dalcanale, E.; Cristofolini, L. *Langmuir* **2006**, *22*, 11126. (b) Shen, C.; Haryono, M.; Grohmann, A.; Buck, M.; Weidner, T.; Ballav, N.; Zharnikov, M. *Langmuir* **2008**, *24*, 12883. (c) Yu, S.; Ahmadi, S.; Palmgren, P.; Hennies, F.; Zuleta, M.; Göthelid, M. *J. Phys. Chem. C* **2009**, *113*, 13765. (d) Bhargava, G.; Ramanarayanan, T. A.; Bernasek, S. L. *Langmuir* **2010**, *26*, 215.

(39) (a) He, Q.; Liu, Z.; Xiao, P.; Liang, R.; He, N.; Lu, Z. *Langmuir* **2003**, *19*, 6982. (b) Higo, M.; Futagawa, T.; Mitsushio, M.; Yoshidome, T.; Ozono, Y. *J. Phys. Chem. B* **2003**, *107*, 5871. (c) Ameur, S.; Bureau, C.; Charlier, J.; Palacin, S. *J. Phys. Chem. B* **2004**, *108*, 13042. (d) Yoshida, H.; Sato, N. *J. Phys. Chem. B* **2006**, *110*, 4232. (e) Palma, R. D.; Peeters, S.; Van Bael, M. J.; Van den Rul, H.; Bonroy, K.; Laureyn, W.; Mullens, J.; Borghs, G.; Maes, G. *Chem. Mater.* **2007**, *19*, 1821.

(40) Olivares-Xometl, O.; Likhanova, N. V.; Domínguez-Aguilar, M. A.; Hallen, J. M.; Zamudio, L. S.; Arce, E. *Appl. Surf. Sci.* **2006**, *252*, 2139.

(41) Kusama, H.; Orita, H.; Sugihara, H. *Langmuir* **2008**, *24*, 4411.

(42) (a) Hara, K.; Miyamoto, K.; Abe, Y.; Yanagida, M. *J. Phys. Chem. B* **2005**, *109*, 23776. (b) Chen, R.; Yang, X.; Tian, H.; Wang, X.; Hagfeldt, A.; Sun, L. *Chem. Mater.* **2007**, *19*, 4007.

(43) Smith, K. M. *Porphyrins and Metalloporphyrins*; Elsevier: Amsterdam, 1975.

(44) Lindsey, J. S.; Wagner, R. W. *J. Org. Chem.* **1989**, *54*, 828.

(45) Wang, C.; Bryce, M. R.; Batsanov, A. S.; Howard, J. A. K. *Chem.–Eur. J.* **1997**, *3*, 1679.

(46) (a) Maligaspe, E.; Tkachenko, N. V.; Subbaiyan, N. K.; Chitta, R.; Zandler, M. E.; Lemmetyinen, H.; D'Souza, F. *J. Phys. Chem. A* **2009**, *113*, 8478. (b) Tkachenko, N. V.; Rantala, L.; Tauber, A. Y.; Helaja, J.; Hynninen, P. H.; Lemmetyinen, H. *J. Am. Chem. Soc.* **1999**, *121*, 9378. (c) Vehmanen, V.; Tkachenko, N. V.; Imahori, H.; Fukuzumi, S.; Lemmetyinen, H. *Spectrochim. Acta. A* **2001**, *57*, 2229. (d) Isosomppi, M.; Tkachenko, N. V.; Efimov, A.; Lemmetyinen, H. *J. Phys. Chem. A* **2005**, *109*, 4881.

(47) (a) Binkley, J. S.; Pople, J. A.; Hehre, W. J. *J. Am. Chem. Soc.* **1980**, *102*, 939. (b) Frisch, M. J.; Trucks, G. W.; Schlegel, H. B.; Scuseria, G. E.; Robb, M. A.; Cheeseman, J. R.;

Montgomery, Jr., J. A.; Vreven, T.; Kudin, K. N.; Burant, J. C.; Millam, J. M.; Iyengar, S. S.; Tomasi, J.; Barone, V.; Mennucci, B.; Cossi, M.; Scalmani, G.; Rega, N.; Petersson, G. A.; Nakatsuji, H.; Hada, M.; Ehara, M.; Toyota, K.; Fukuda, R.; Hasegawa, J.; Ishida, M.; Nakajima, T.; Honda, Y.; Kitao, O.; Nakai, H.; Klene, M.; Li, X.; Knox, J. E.; Hratchian, H. P.; Cross, J. B.; Bakken, V.; Adamo, C.; Jaramillo, J.; Gomperts, R.; Stratmann, R. E.; Yazyev, O. ; Austin, A. J.; Cammi, R.; Pomelli, C.; Ochterski, J. W.; Ayala, P. Y.; Morokuma, K.; Voth, G. A.; Salvador, P.; Dannenberg, J. J.; Zakrzewski, V. G. ; Dapprich, S.; Daniels, A. D.; Strain, M. C.; Farkas, O.; Malick, D. K.; Rabuck, A. D.; Raghavachari, K.; Foresman, J. B.; Ortiz, J. V.; Cui, Q.; Baboul, A. G.; Clifford, S.; Cioslowski, J.; Stefanov, B. B.; Liu, G.; Liashenko, A.; Piskorz, P.; Komaromi, I.; Martin, R. L.; Fox, D. J.; Keith, T.; Al.Laham, M. A.; Peng, C. Y.; Nanayakkara, A.; Challacombe, M.; Gill, P. M. W.; Johnson, B.; Chen, W.; Wong, M. W.; Gonzalez, C.; Pople, J. A. *Gaussian 03*; Gaussian, Inc.: Wallingford, CT, 2004.

(48) Ito, S.; Murakami, T. N.; Comte, P.; Liska, P.; Grätzel, C.; Nazeeruddin, M. K.; Grätzel, M. *Thin Solid Films* **2008**, *516*, 4613.

Chapter 3

Structure and Photoelectrochemical Properties of Phthalocyanine and Perylene Diimide Composite Clusters Deposited Electrophoretically on Nanostructured SnO_2 Electrodes

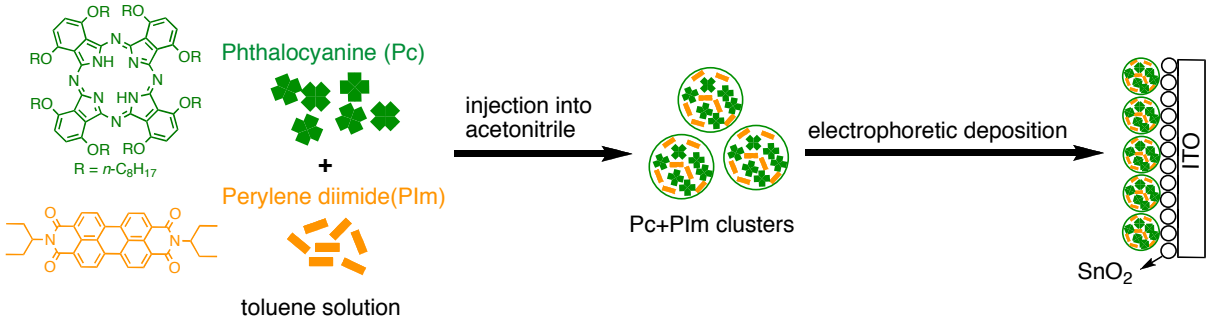

Abstract

Clusters of phthalocyanine and phthalocyanine-perylene diimide have been prepared and electrophoretically deposited on nanostructured SnO_2 electrodes. The structure and photoelectrochemical properties of the clusters have been investigated by using UV-visible absorption, dynamic light scattering (DLS), atomic force microscopy (AFM), transmission electron microscopy (TEM), photoelectrochemical, and photodynamical measurements. Enhancement of the photocurrent generation efficiency in the composite system has been achieved relative to the phthalocyanine reference system without the perylene diimide. Such information will be valuable for the design of molecular photoelectrochemical devices which exhibit efficient photocurrent generation.

Introduction

In recent years, organic photovoltaic materials have received particular attention because of their substantial potential for efficient solar energy conversion.[1–10] In particular, significant efforts have been made to explore the photovoltaic and photoelectrochemical properties of porphyrins.[9–11] Porphyrins have a high light-collecting property in the visible region and the potential ability to accept or release an electron because of the delocalized π system in the macrocycles. In addition, it is possible to modulate the redox properties of the porphyrins dramatically by changing the inserted metals in the core, modifying substituents in the periphery of the porphyrin ring, coordinating axial ligands onto the metals, and exciting the chromophore with visible light. However, taking into account solar energy distribution on the earth surface, the light-harvesting property of porphyrins in the long-wavelength region is insufficient as organic photovoltaic materials.

Phthalocyanines possess intensive absorption in the visible and near-IR regions (600–900 nm) and exhibit excellent chemical, light, and thermal stability compared to porphyrins.[12] Thus, phthalocyanines are highly promising materials for solar cell application. The photoelectrochemical properties of phthalocyanine-modified electrodes have been investigated to improve the cell performance.[7,13–17]

The surface morphology of organic photovoltaic materials on electrodes also affects the device performance greatly. A variety of methods have been pursued to obtain a favorable threedimensional architecture of organic thin films on the electrodes. However, because of the poor solubility of phthalocyanines in organic solvents, the technique for the preparation of phthalocyanine films on electrodes has been mainly limited to vacuum deposition.[7,13] Both proper choice of soluble substituents at the periphery of the macrocycles and other fabrication methods are required to surmount the problem. Such phthalocyanine fabrication onto electrode surfaces is a crucial process for controlling the morphology of phthalocyanine assemblies in the molecular scale, leading to the improvement of the cell performance. Versatile methods such as chemical adsorption,[14] spin coating,[15] Langmuir-Blodgett films,[16] and electrochemical deposition of dye-semiconductor composites[17] have been applied to construct photoelectrochemical devices involving phthalocyanines.

As has been shown by Kamat, Imahori and co-workers, the nanoclusters of fullerene derivatives,[18] aniline-linkedC_{60} dyad,[19] and porphyrin-C_{60} composites[10,20,21] in toluene/acetonitrile mixed solutions can be deposited electrophoretically onto nanostructured SnO_2 electrodes to exhibit efficient photocurrent generation. The advantage of the electrophoretic deposition is the step-by-step fabrication of molecules on electrodes: from molecules to clusters of the molecules and, subsequently, from the clusters to bulk thin films on the electrodes. This allows me to control film morphology on the molecular level. Despite this advantage, phthalocyanine clusters have yet to be prepared in toluene/acetonitrile mixtures to examine the photoelectrochemical properties of the clusters deposited

electrophoretically onto nanostructured SnO_2 electrodes. As such, no photoelectrochemical properties of the composite clusters of phthalocyanines with an electron acceptor have been investigated.

The author reports herein the structure and photoelectrochemical properties of the clusters of phthalocyanine and phthalocyanine-perylene diimide electrophoretically deposited on nanostructured SnO_2 electrodes on the basis of UV-visible absorption, dynamic light scattering (DLS), atomic force microscopy (AFM), transmission electron microscopy (TEM), and photoelectrochemical and photodynamical measurements. Perylene diimide is chosen as an acceptor because of its excellent electron-accepting and light-harvesting (400–600 nm) abilities and chemical, light, and thermal stability. To increase the solubility of phthalocyanine and perylene diimide, the author designed phthalocyanine C*n*Pc (*n* = 4,8) and perylene diimide PIm (Figure 1) where eight 1-octyl (or 1-butyl) and two 3-pentyl groups are introduced into the phthalocyanine and the perylene diimide moieties, respectively.[17]

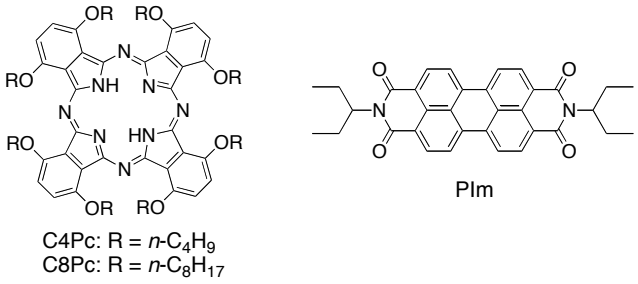

Figure 1. Phthalocyanine (C4Pc, C8Pc) and perylene diimide (PIm) used in this study.

Results and Discussion

Preparation and Characterization of Phthalocyanine Clusters. Phthalocyanines C*n*Pc (*n* = 4, 8) form optically transparent clusters in a mixture of toluene/acetonitrile after rapid injection of the toluene solution into acetonitrile [denoted as $(C_nPc)_m$]. Figure 2 displays the absorption spectra of C8Pc (0.25 mM) in toluene (dotted line) and in a toluene/acetonitrile (1:5, v/v) mixture (solid line). The phthalocyanine C8Pc in toluene has a relatively strong UV band at 300–500 nm and a strong near-IR band at 700–800 nm. The clusters of C8Pc in the toluene-acetonitrile mixture exhibit structureless broad absorption in the 300–500 nm and 700–800 nm ranges with lower molar coefficients, compared to those of the monomeric form in toluene.[22] Similar spectral behavior is observed for C8Pc with a high concentration of [C8Pc] = 0.5 mM. These results confirm that the phthalocyanine molecules aggregate and form clusters in the mixed solvents, as in the cases of porphyrins and/or fullerenes.[18,20,21] In contrast, phthalocyanine C4Pc does not reveal such a spectral change under the same conditions. This indicates that the longer alkyl chains of C8Pc relative to C4Pc have a large impact on the formation of clusters in the mixed solvents. Absorption spectra of the mixture of C8Pc

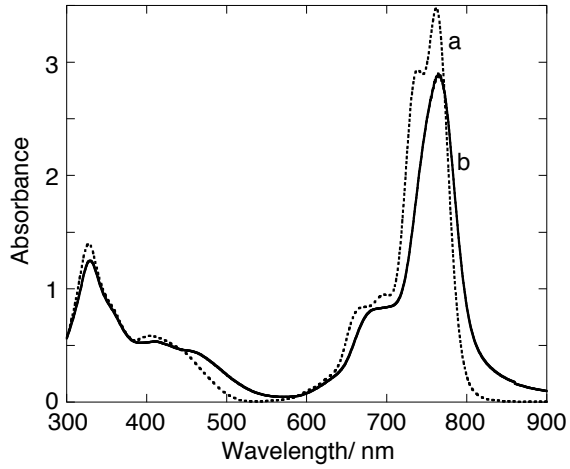

Figure 2. Absorption spectra of (a) C8Pc (0.25 mM) in toluene (dotted line) and (b) C8Pc cluster solutions (0.25 mM in 1:5(v/v) toluene/acetonitrile, solid line). 1 mm cell was used for all measurements.

and PIm as well as those of PIm are also compared in toluene and in a toluene/acetonitrile (1:5, v/v) mixture (Figure 3). No apparent spectral change is noted for the absorption spectrum of PIm in the mixed solvent (dotted line in Figure 3B) relative to that in toluene (dotted line in Figure 3A). This indicates that perylene diimide molecules do not form $(PIm)_m$ clusters or form small ones in the mixed solvents under the present conditions (vide infra).[23] In the absorption spectrum of the mixture of C8Pc and PIm in the toluene/acetonitrile (1:5, v/v) mixture (solid line in Figure 3B), absorption arising from the phthalocyanine moiety exhibits structureless broad absorption in the 300–500 nm and 700–800 nm regions, as seen for the cluster formation of C8Pc in the mixed solvents. In contrast, absorption arising

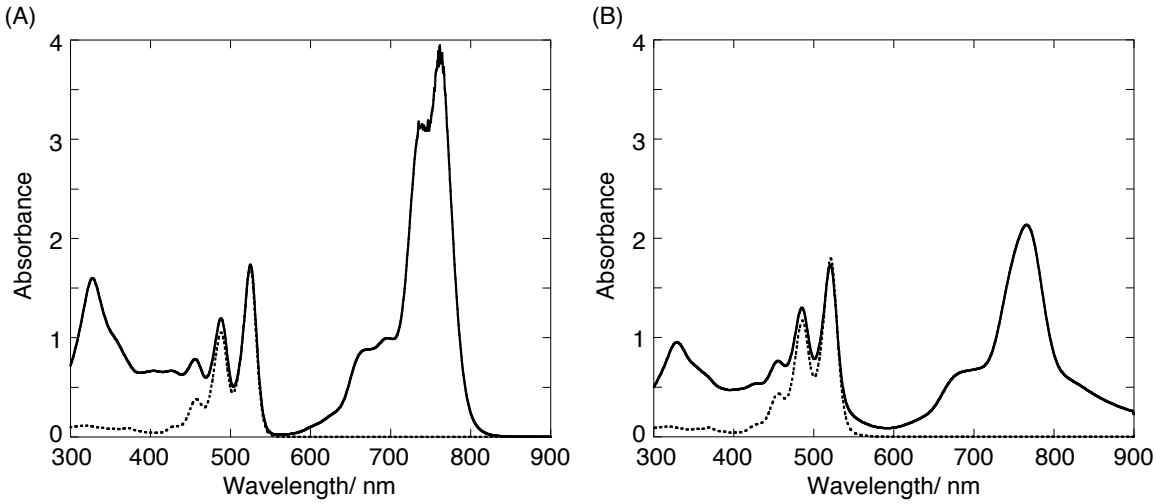

Figure 3. (A) Absorption spectra of the mixture of C8Pc and PIm (0.25 mM, solid line) and PIm (0.25 mM, dotted line) in toluene. (B) Absorption spectra of the mixture of C8Pc and PIm (0.25 mM, solid line) and PIm (0.25 mM, dotted line) in 1:5(v/v) toluene/acetonitrile. 1 mm cell was used for all measurements.

from the PIm moiety reveals no significant change in toluene and the mixed solvents. This demonstrates that at least C8Pc molecules form clusters in the mixture of C8Pc and PIm in the toluene/acetonitrile mixture (vide infra).

To determine the particle size of these clusters in the mixed solvent, DLS measurements were carried out. In a mixture (1:5) of toluene/acetonitrile at an incubation time of 1 min after the rapid injection, the size distribution of clusters of $(C8Pc)_m$ is relatively narrow with different mean diameters (*D*M) of 110 nm (0.25 mM) and 150 nm (0.5 mM) for $(C8Pc)_m$ (Figure 4). The size distribution of clusters of $(C8Pc)_m$ virtually remains constant with increasing the incubation time. Contrastively, the *D*M of $(PIm)_m$ clusters is found to be extremely small (13 nm).[23] This agrees well with no apparent change in the absorption spectra of PIm in toluene and toluene/acetonitrile (1:5, v/v) mixture (vide supra). Unfortunately, however, rapid precipitation of the clusters precludes the determination of the particle size of the clusters prepared from the mixture of C8Pc and PIm.

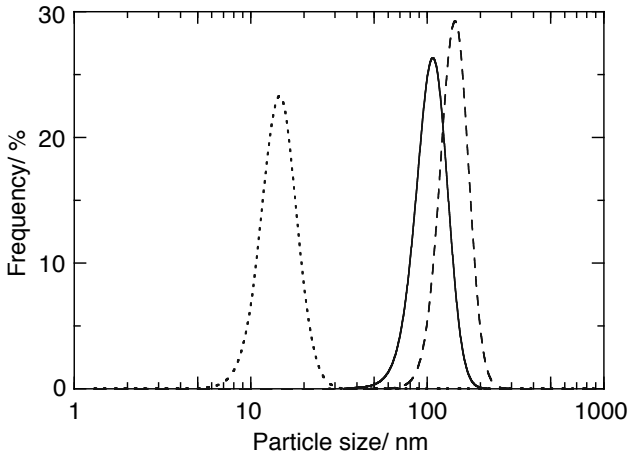

Figure 4. Particle size distribution of clusters of C8Pc (0.25 mM, solid line; 0.5 mM, dashed line) and PIm (0.5 mM, dotted line) in 1:5(v/v) toluene/acetonitrile mixture at 1 min after rapid injection of the toluene solutions into acetonitrile.

To evaluate the shapes and morphology of the clusters of $(C8Pc)_m$, $(PIm)_m$, and $(C8Pc+PIm)_m$, the author performed TEM measurements. Figure 5 reveals the TEM images of the clusters prepared by the deposition of $(C8Pc)_m$, $(PIm)_m$, and $(C8Pc+PIm)_m$ in toluene/acetonitrile mixed solvents on a carbon-coated copper grid. The clusters of $(C8Pc)_m$ are rather spherical with moderate size (100–300 nm; Figure 5a). The sizes of the small particles for $(C8Pc)_m$ (~100 nm) are similar to the corresponding values determined from DLS measurements (vide supra). The clusters of $(PIm)_m$ are cubic with small size (20–100 nm; Figure 5b), which is in good agreement with the results from the DLS measurements (vide supra). These results also indicate that, as solvent evaporates on the grid,

secondary aggregation occurs in an orderly fashion to form large aggregates compared to the size of the clusters in the mixed solvents. It is noteworthy that the clusters of $(C8Pc+PIm)_m$ exhibit a large cuboid (Figure 5c), the shape of which is quite different from those of $(C8Pc)_m$ and $(PIm)_m$. This demonstrates that PIm molecules are incorporated into C8Pc aggregates to make the large composite clusters (vide supra).

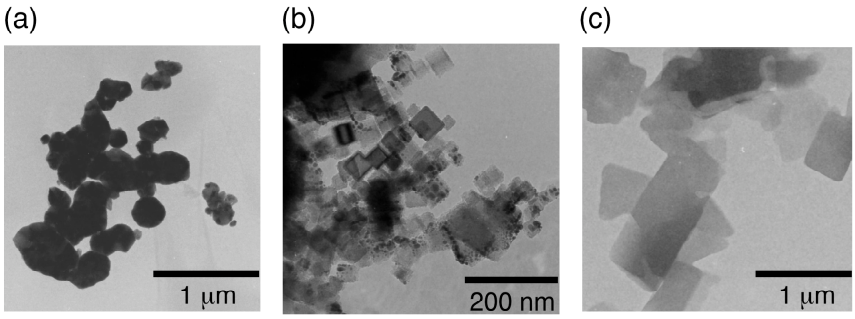

Figure 5. TEM images of (a) $(C8Pc)_m$([C8Pc] = 0.50 mM), (b) $(PIm)_m$ ([PIm] = 0.50 mM), and (c) $(C8Pc+PIm)_m$ ([C8Pc] = [PIm] = 0.50 mM). A toluene/acetonitrile solution of the samples was applied to a carbon-coated copper grid for the TEM measurements.

Electrophoretic Deposition of Phthalocyanine and Phthalocyanine-Perylene Diimide Clusters. The clusters of $(C8Pc)_m$ and $(C8Pc+PIm)_m$ were attached onto ITO/SnO_2 electrodes by the electrophoretic deposition method[18–21] [denoted as ITO/SnO_2/$(C8Pc)_m$ and ITO/SnO_2/$(C8Pc+PIm)_m$, respectively]. Under application of a high dc electric field (250 V for 2 min), the clusters of $(C8Pc)_m$ and $(C8Pc+PIm)_m$, which are positively charged in toluene/acetonitrile, are driven toward the negatively charged electrode surface.[18–21,24] With increasing time of deposition, the ITO/SnO_2 electrodes turn green and brownish green, respectively, whereas discoloration of the cluster solution takes place. On the other hand, the clusters of $(PIm)_m$ could not be deposited onto the ITO/SnO_2 electrode because of the small size. The absorption spectra of the cluster films on nanostructured SnO_2 electrodes are shown in Figure 6. The absorption features of ITO/SnO_2/$(C8Pc)_m$ and ITO/SnO_2/$(C8Pc+PIm)_m$ are largely similar to those observed for the cluster solutions in the toluene/acetonitrile mixture (solid lines in Figures 2b and 3B). The broad absorption of these films as well as the high molar absorptivity in the visible and near-IR regions makes these films suitable for harvesting solar energy.

AFM was used to evaluate the topology of ITO/SnO_2/$(C8Pc)_m$ and ITO/SnO_2/$(C8Pc+PIm)_m$ films, as shown in Figure 7. The AFM image of ITO/SnO_2/$(C8Pc)_m$ film shows a relatively smooth morphology without the apparent appearance of the cluster packing. Notably, the ITO/SnO_2/$(C8Pc+PIm)_m$ film reveals rather random packing of long rod structures, which is in good agreement with the TEM image of $(C8Pc+PIm)_m$ clusters (vide supra). These results support the successful electrophoretic deposition of the clusters on the ITO/SnO_2 electrode.

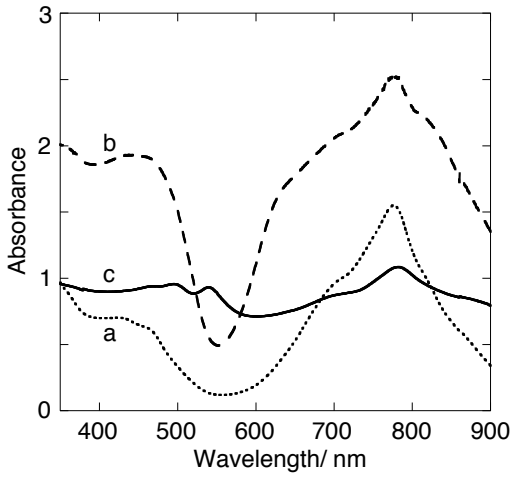

Figure 6. The absorption spectra of ITO/SnO_2/$(C8Pc)_m$, prepared from the cluster solution ((a) 0.25 mM, dotted line; (b) 0.50 mM, dashed line), and of ITO/SnO_2/$(C8Pc+PIm)_m$, prepared from the cluster solution ((c) [C8Pc] = [PIm] = 0.50 mM, solid line).

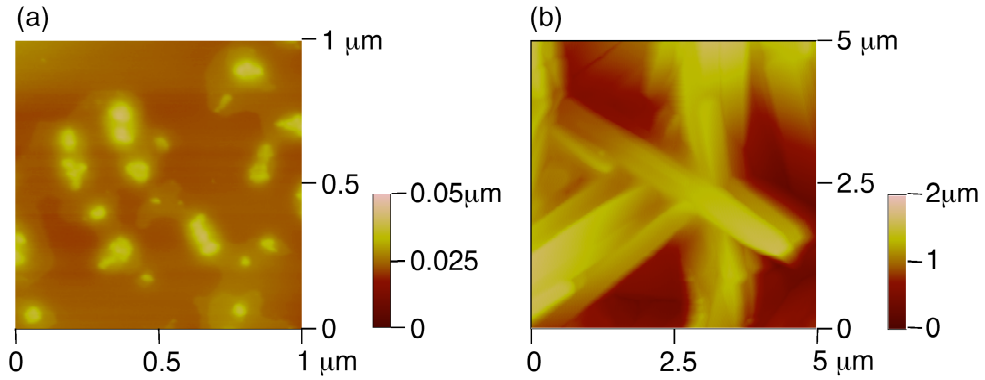

Figure 7. Tapping mode atomic force micrography of (a) ITO/SnO_2/$(C8Pc)_m$ and (b) ITO/SnO_2/$(C8Pc+PIm)_m$ electrodes in air. The samples were prepared from the cluster solutions ((a) [C8Pc] = 0.50 mM) and ((b) [C8Pc] = [PIm] = 0.50 mM), respectively.

Photoelectrochemical Measurements. Photoelectrochemical measurements were performed in acetonitrile containing 0.5 M LiI and 0.01 M I_2 with ITO/SnO_2/$(C8Pc)_m$ or ITO/SnO_2/$(C8Pc+PIm)_m$ as a working electrode, a platinum counter electrode, and a reference electrode. Figure 8a displays anodic photocurrent responses of the ITO/SnO_2/$(C8Pc+PIm)_m$ films, prepared from the cluster solution ([C8Pc] = [PIm] = 0.50 mM), illuminated at an excitation wavelength of 788 nm (input power: 44 μcm^{-2}) at 0.15 V versus SCE. The photocurrent responses are prompt, steady, and reproducible during repeated on/off cycles of the visible light illumination. Control experiments conducted with the ITO/SnO_2/$(C8Pc)_m$ electrode produce a much smaller photocurrent under similar experimental conditions. These results demonstrate the role of phthalocyanine-perylene diimide composite assemblies toward harvesting light energy and generating a photocurrent during the operation of a photoelectrochemical device. Figure 8b displays the current versus potential characteristics of the

ITO/SnO_2/(C8Pc+PIm)$_m$ device under white light illumination ($\lambda > 380$ nm; input power: 110 mW cm^{-2}). With increasing positive bias (–0.1 to +0.15 V) the photocurrent increases compared to the dark current. Increased charge separation and the facile transport of charge carriers under positive bias are responsible for the enhanced photocurrent generation.

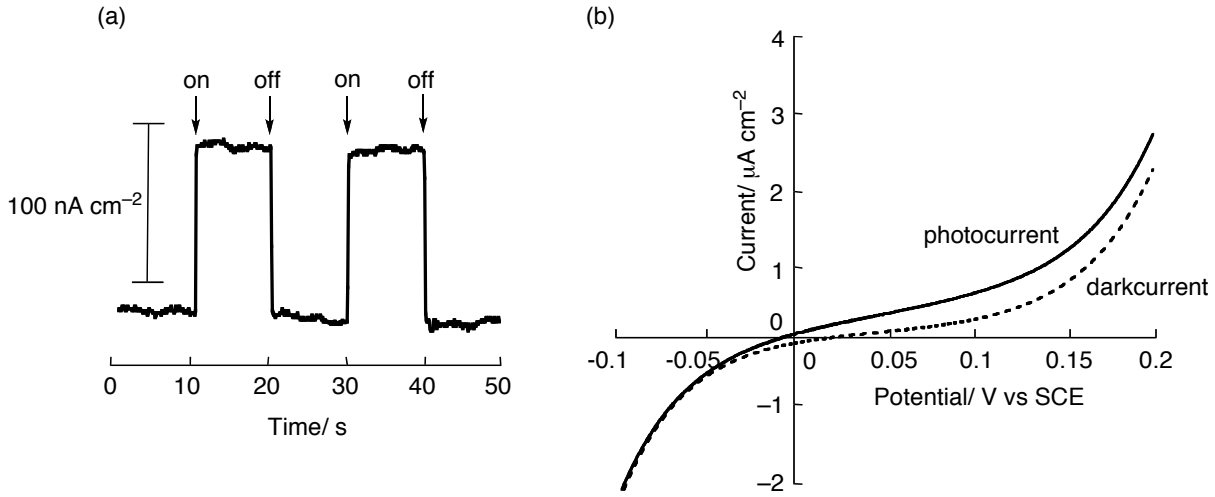

Figure 8. (a) The photocurrent response of ITO/SnO_2/(C8Pc+PIm)$_m$ electrode prepared from the cluster solution ([C8Pc] = [PIm] = 0.50 mM) at the excitation wavelength of 788 nm. Potential: +0.15 V vs SCE; 0.5 M LiI and 0.01 M I_2 in acetonitrile; Input power: 44 μW cm^{-2}. (b) Potential versus current characteristics of ITO/SnO_2/(C8Pc+PIm)$_m$ electrode prepared from the cluster solution ([C8Pc] = [PIm] = 0.50 mM) under white light illumination ($\lambda > 380$ nm). Potential: +0.15 V vs SCE; 0.5 M LiI and 0.01 M I_2 in acetonitrile; Input power: 110 mW cm^{-2}.

To evaluate the response of phthalocyanine-perylene diimide composite clusters toward photocurrent generation, photocurrent action spectra are compared against the absorption spectra on ITO/SnO_2. The photocurrent action spectra of the ITO/SnO_2/(C8Pc+PIm)$_m$ and ITO/SnO_2/(C8Pc)$_m$ devices are shown in Figure 9. Incident photon-to-current efficiency (IPCE) values are calculated by normalizing the photocurrent densities for incident light energy and intensity and using the expression

$$\text{IPCE}\ (\%) = 100 \times 1240 \times i/(W_{in} \times \lambda)$$

where i is the photocurrent density (A cm^{-2}), W_{in} is the incident light intensity (W cm^{-2}), and λ is the excitation wavelength (nm). The overall responses of the ITO/SnO_2/(C8Pc+PIm)$_m$ devices parallel the broad absorption features, indicating the involvement of the phthalocyanine and perylene diimide moieties in the photocurrent generation. The disagreement between the action and absorption spectra at 400–500 nm can be rationalized by the photocurrent generation stemming from the direct excitation of the ITO/SnO_2 electrode. It should be noted here that the IPCE values at 400–600 nm arising from the absorption of the PIm moiety and those at 700–800 nm from that of C8Pc moiety increase with increasing the concentration of PIm. This also supports the involvement of the phthalocyanine and

perylene diimide moieties in the photocurrent generation. Specifically, the significant enhancement of the photocurrent generation at around 400 nm and at 700–800 nm indicates photoinduced electron transfer from the excited singlet state of C8Pc to PIm followed by electron injection from the reduced PIm to the conduction band (CB) of SnO_2 or electron transfer from iodide ion to the excited singlet state of C8Pc followed by stepwise electron injection from the reduced C8Pc to the CB band via PIm (vide infra).

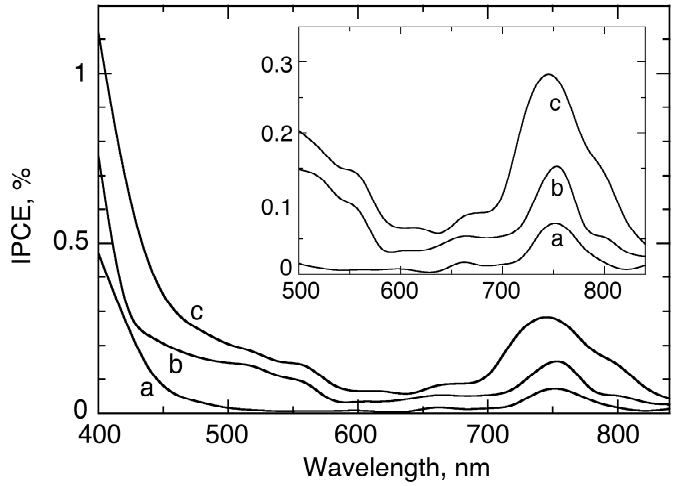

Figure 9. The photocurrent action spectra of (a) ITO/SnO_2/$(C8Pc)_m$ ([C8Pc] = 0.5 mM), (b) ITO/SnO_2/$(C8Pc+PIm)_n$ ([C8Pc] = 0.5 mM, [PIm] = 0.25 mM), and (c) ITO/SnO_2/$(C8Pc+PIm)_n$ ([C8Pc] = [PIm] = 0.5 mM) electrodes. Potential: +0.15 V vs SCE; 0.5 M LiI and 0.01 M I_2 in acetonitrile.

Photocurrent Generation Mechanism. On the basis of the previous studies on a similar photoelectrochemical system consisting of porphyrin and C_{60},[10,20,21] a photocurrent generation diagram is schematically illustrated in Schemes 1 and 2 and 3. First, the oxidation and reduction potentials of C8Pc (0.79 V, –0.56 V vs normal hydrogen electrode (NHE)) and PIm (2.05 V, –0.31 V vs NHE) were determined by using cyclic voltammetry in CH_2Cl_2 containing 0.1 M tetrabutylammonium hexafluorophosphate. Photocurrent generation mechanisms involving C8Pc (Scheme 1) and PIm (Scheme 2) are presented for better understanding of the more complex composite system. Scheme 1 illustrates the photocurrent generation pathway for C8Pc: (i) electron injection from the excited singlet state of C8Pc (^{1}C8Pc*/C8Pc$^{\bullet+}$ = –0.82 V vs NHE) to the CB of SnO_2 (E_{CB} = 0 V vs NHE)[18–21] followed by electron transfer from the iodide ion (I_3^-/I^- = 0.5 V vs NHE)[18–21] to the resulting phthalocyanine radical cation (C8Pc$^{\bullet+}$/C8Pc = 0.79 V) (pathway 1) and (ii) electron transfer from the iodide ion to the excited singlet state of C8Pc (^{1}C8Pc*/C8Pc$^{\bullet-}$)1.05Vvs NHE) followed by electron injection from the reduced phthalocyanine (C8Pc/C8Pc$^{\bullet-}$ = –0.56V vs NHE) to the CB band (pathway 2). Scheme 2

exemplifies the photocurrent generation pathway for PIm: (iii) electron injection from the excited singlet state of PIm (^{1}PIm*/PIm$^{\bullet+}$ = –0.21 V vs NHE) to the CB of SnO_2 (E_{CB}) 0 V vs NHE)[18–21] followed by electron transfer from the iodide ion (I^{3-}/I^-) 0.5 V vs NHE)[18–21] to the resulting perylene diimide radical cation (PIm/PIm$^{\bullet+}$ = 2.05 V vs NHE) (pathway 3) and (iv) electron transfer from the iodide ion to the excited singlet state of PIm (^{1}PIm*/PIm$^{\bullet-}$ = 1.95 V vs NHE) followed by electron injection from the reduced perylene diimide (PIm/PIm$^{\bullet-}$ = –0.31VvsNHE) to the CB band (pathway 4). In both cases, the electrons transferred to the semiconductor nanocrystallines are driven to the counter electrode via an external circuit to regenerate the redox couple.

Scheme 1

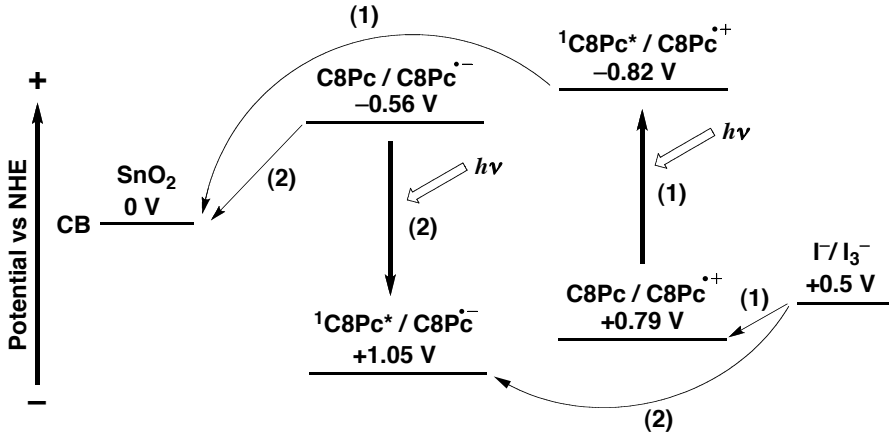

Scheme 2

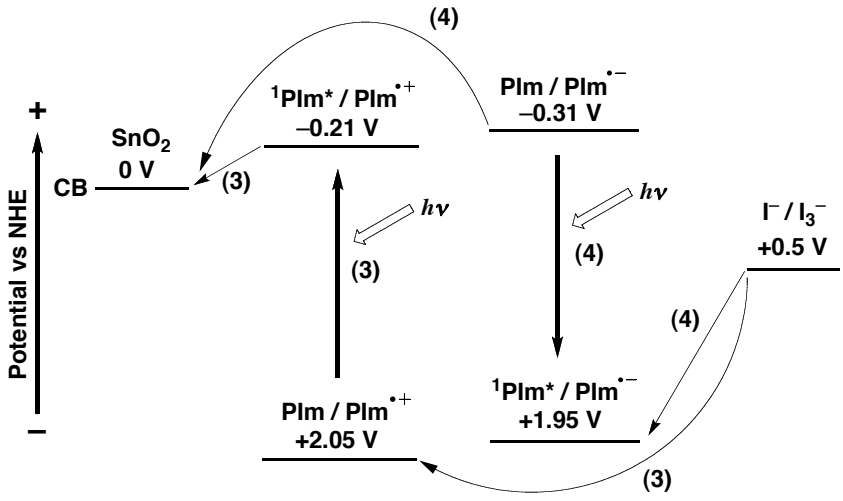

In addition to the photocurrent generation mechanism in Schemes 1 and 2, four additional photocurrent generation pathways are proposed for the ITO/SnO_2/$(C8Pc+PIm)_m$ device (Scheme 3): (v) electron injection from the excited singlet state of C8Pc to the CB of SnO_2 via intermediate PIm, followed by electron transfer from the iodide ion to the resulting phthalocyanine radical cation (pathway 5), vi) electron transfer from the iodide ion to the excited singlet state of C8Pc, followed by electron injection from the reduced phthalocyanine to the CB band via intermediate PIm (pathway 6), (vii) electron injection from the excited singlet state of PIm to the CB band of SnO_2, followed by electron transfer from the iodide ion to the resulting perylene diimide radical cation via C8Pc (pathway 7), and (viii) electron transfer from the iodide ion to the excited singlet state of PIm via C8Pc, followed by electron injection from the reduced perylene diimide to the CB band (pathway 8). In all cases, the electrons transferred to the semiconductor nanocrystallines are driven to the counter electrode via an external circuit to regenerate the redox couple.

Scheme 3

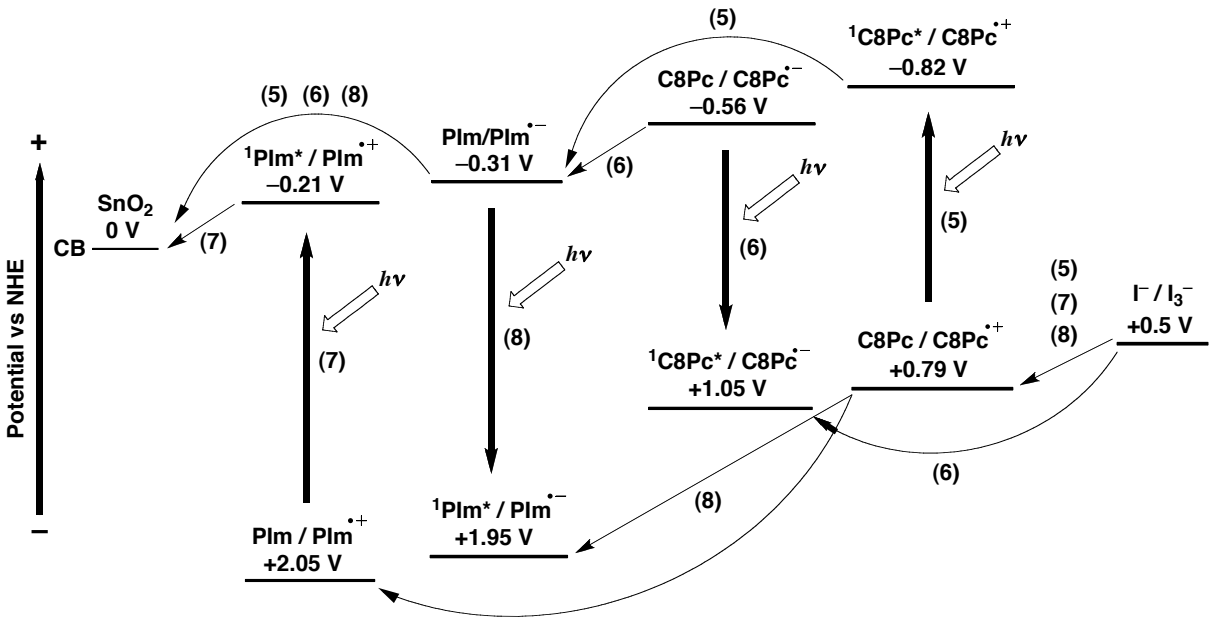

The occurrence of the ultrafast relaxation process of the phthalocyanine singlet excited state by interaction with PIm in the composite cluster in the mixed solvent was further examined by femtosecond time-resolved transient absorption spectroscopy. Figure 10 shows transient absorption component spectra of $(C8Pc+PIm)_m$ in the mixed solvents ([C8Pc] = 0.12 mM; [PIm] = 0.06 mM) with a laser excitation wavelength of 415 nm, which ensures the selective formation of the phthalocyanine excited singlet state rather than perylene excited singlet state (excitation ratio of [C8Pc]:[PIm] = 17:1). The three components (0.3, 10, and 670 ps) are obtained by global analysis. The absorption shape and lifetime of the longest component are similar to those (780 ps) observed for the $(C8Pc)_m$ in the mixed

solvents ([C8Pc] = 0.12 mM), which corresponds to the decay of the phthalocyanine excited singlet state. The lifetime (670 ps) is much shorter than that of the phthalocyanine excited singlet state in solutions (~6 ns),[25] possibly because of the self-quenching occurring in the $(C8Pc)_m$ clusters. The middle component is quite weak and may originate from minor deactivation pathways involving phthalocyanine and perylene diimide excited singlet states. The negative amplitude of the fastest component can be assigned tentatively to the formation of the phthalocyanine radical cation, which exhibits characteristic absorption at 915 nm.[25] The red-shift of the peak position (~940 nm) relative to the phthalocyanine radical cation may originate from the unique environment of the phthalocyanine radical cation in the composite clusters. Unfortunately, the instrument used in this study does not allow the author to probe absorption due to the perylene radical anion at 750–850 nm[23] because of disturbance from the laser fundamental harmonic (~800 nm) and the strong signal from the phthalocyanine moiety due to the bleaching of the Q-band. These results indicate the involvement of the excited singlet state of C8Pc for the photocurrent generation. A small fraction of the excited singlet state of C8Pc would undergo electron transfer to yield the charge-separated state in the composite clusters, leading to the enhancement of the IPCE value in the composite system.

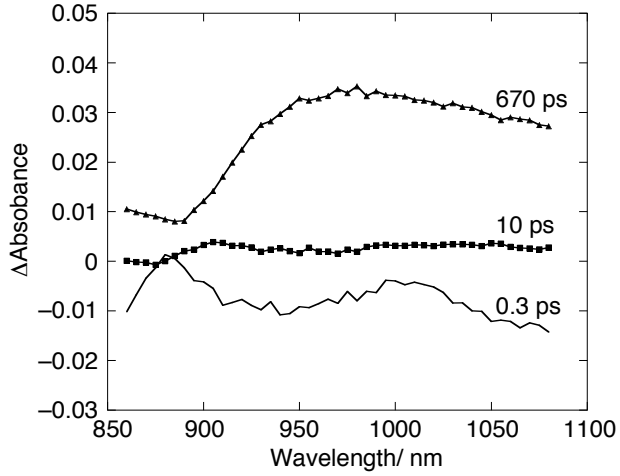

Figure 10. Transient absorption decay component spectra of $(C8Pc+PIm)_m$ ([C8Pc] = 0.12 mM, [PIm] = 0.06 mM) in toluene/acetonitrile = 1:5 (v/v) obtained from global three-component fit of the data. The excitation wavelength is 415 nm. The fitted time constants are displayed on the plots.

It is intriguing to compare the IPCE values of the present system with those of similar porphyrin-based systems,[10,20,21] where clusters of the porphyrins are deposited electrophoretically onto ITO/SnO_2 electrode. The IPCE value of the phthalocyanine device (0.1–1%) is smaller than those of the porphyrin devices (1–3%). In the case of the porphyrins, bulky *tert*-butyl groups are introduced into the *meta* positions of the *meso*-phenyl groups of the porphyrins to avoid undesirable aggregation leading to the self-quenching of the porphyrin excited singlet state. On the other hand, the present

phthalocyanine (C*n*Pc) possesses relatively long alkoxy chains, which induce π-π stacking of the phthalocyanine rings, resulting in the relatively strong self-quenching of the excited singlet state (vide supra). Such differences in the photophysics of the phthalocyanine and the porphyrins may be responsible for the difference in the IPCE values. This matches the strong tendency of phthalocyanines to aggregate on the semiconductor surface, leading to low IPCE values of phthalocyanine-sensitized solar cells (< 4%).[14,26]

Conclusion

The author has successfully prepared clusters of phthalocyanine and phthalocyanine-perylene diimide composite deposited electrophoretically on a nanostructured semiconductor electrode. The structures of the clusters and their photoelectrochemical properties have been examined in detail. Although the photocurrent generation efficiency of the present phthalocyanine system is rather low compared to similar porphyrin systems,[10,20,21] an enhancement of the photocurrent generation efficiency of the composite system is achieved relative to that of the phthalocyanine reference system without the perylene diimide. This is another example of dye-sensitized bulk heterojunction solar cells in addition to the combination of porphyrins and fullerenes.[10,20,21] Such knowledge will provide fundamental information for the design of molecular photoelectrochemical devices that exhibit efficient photocurrent generation.

Experimental Section

Materials and Methods. C_{60} (99.98%) was obtained from MTR Ltd. Porous nanostructured SnO_2 film was prepared by spraying a dilute (1.5%) SnO_2 colloidal solution (particle size: 15 nm; Chemat Technology, Inc.) onto an optically transparent indium-tin oxide electrode (ITO; Tokyo Sanyo Sinku), which was washed by sonicating in 2-propanol and cleaning in O_3 atmosphere in advance, and finally it was annealed at 673 K for 1 h (denoted as ITO/SnO_2). Phthalocyanine (C*n*Pc (n = 4,8))[27] and perylene diimide (PIm)[28] were prepared by following the same procedure described previously. All the other chemicals were of analytical grade and used as received.

Preparation of Cluster Solutions and Films. The cluster suspensions of phthalocyanine (C*n*Pc) or the mixture of Pc and perylene diimide (PIm) were prepared in a 1 cmcuvette by injecting 0.3 mL of toluene solution of C*n*Pc or C*n*Pc-PIm into 1.5 mL of acetonitrile (toluene/acetonitrile = 1:5 (v/v)). Two electrodes (ITO and ITO/SnO_2) were kept at a distance of 6 mm using a Teflon spacer and set in the cuvette, and then a direct current (dc) voltage (250 V) was applied for 2 min between these two electrodes using a power supply (ATTA model AE-8750). The deposition of the film could

be confirmed visibly as the solution became colorless.

Characterization. UV-visible spectra of solutions and films on ITO/SnO_2 were recorded using a Lambda 900 spectrophotometer (Perkin-Elmer, Boston, MA). The distribution of cluster size was evaluated by a DLS method using a LB-550 particle size analyzer (Horiba, Japan). TEM micrographs were measured by applying a drop of the sample to a carbon-coated copper grid. Images were recorded using a JEM-200CX transmission electron microscope (JEOL, Japan). The surface morphology of the films was observed by AFM measurements using a Digital Nanoscope III (Veeco, Santa Barbara, CA) in the tapping mode.

Electrochemical and Photoelectrochemical Measurements. All electrochemical measurements were carried out in a standard three-electrode system using an ALS 630a electrochemical analyzer. For the photoelectrochemical measurements, the cluster film as a working electrode was immersed into the electrolyte solution containing 0.5 M LiI and 0.01 M I_2 in acetonitrile. A Pt wire covered with a glass ruggin capillary whose tip was located near the working electrode and a Pt coil were used as quasi-reference and counter electrodes, respectively. The potential measured was converted to the saturated calomel electrode (SCE) scale by adding +0.05 V. The stability of the reference electrode potential was confirmed under the experimental conditions. A 500 W xenon lamp (XB-50101AA-A; Ushio, Japan) was used as a light source. Potential versus current characteristics were obtained using a 380 nm cutoff filter. The monochromatic light through a monochromator (MC-10N; Ritsu, Japan) was illuminated on the modified area of the working electrode (0.20 cm^2) from the backside. The light intensity was monitored by an optical power meter (ML9002A; Anritsu, Japan) and corrected.

Spectral Measurements. Femtosecond to picosecond timeresolved absorption spectra were collected using a pump-probe technique as described elsewhere.[29] The femtosecond pulses of the Ti:sapphire generator were amplified by using a multipass amplifier (CDP-Avesta, Moscow, Russia) pumped by a second harmonic of the Nd:YAG Q-switched laser (model LF114, Solar TII, Minsk, Belorussia). The amplified pulses were used to generate a second harmonic (415 nm) for sample excitation (pump beam) and a white continuum for time-resolved spectrum detection (probe beam). The samples were placed into 1 mm rotating cuvette, and an average of 100 pulses at 10 Hz repetition rate was used to improve the signalto-noise ratio. The wavelength range for a single measurement was 227 nm, and typically three regions were studied: 480–670, 540–760, and 860–1080 nm. The typical response time of the instrument was 150 fs (full width at half-maximum (FWHM)). A global multi exponential fitting procedure was applied to process the data. The procedure takes into account the instrument time response function and the group velocity dispersion of the white continuum, and allows one to calculate the decay time constants and dispersion compensated transient absorption spectra.

References and Footnotes

(1) (a) *Organic Photovoltaics*; Sun, S.S., Sariciftci, N. S., Eds.; CRC: Boca Raton, 2005. (b) *Organic Photovoltaics*; Brabec, C., Dyakonov, V., Parisi, J., Sariciftci, N. S., Eds.; Springer: Berlin, 2003.

(2) (a) Tang, C. W. *Appl. Phys. Lett.* **1986**, *48*, 183. (b) Peumans, P.; Yakimov, A.; Forrest, S. R. *J. Appl. Phys.* **2003**, *93*, 3693. (c) Gregg, B. A. *J. Phys. Chem. B* **2003**, *107*, 4688.

(3) (a) Hagfeldt, A.; Grätzel, M. *Acc. Chem. Res.* **2000**, *33*, 269. (b) Grätzel, M. *Nature* **2001**, *414*, 338. (c) Bignozzi, C. A.; Argazzi, R.; Kleverlaan, C. J. *Chem. Soc. Rev.* **2000**, *29*, 87.

(4) (a) Hirata, N.; Lagref, J.-J.; Palomares, E. J.; Durrant, J. R.; Nazeeruddin, M. K.; Grätzel, M.; Di Censo, D. *Chem. Eur. J.* **2004**, *10*, 595. (b) Piotrowiak, P.; Galoppini, E.; Wei, Q.; Meyer, G. J.; Wiewior, P. *J. Am. Chem. Soc.* **2003**, *125*, 5278. (c) Kamat, P. V.; Haria, M.; Hotchandani, S. *J. Phys. Chem. B* **2004**, *108*, 5166.

(5) (a) Yu, G.; Gao, J.; Hummelen, J. C.; Wudl, F.; Heeger, A. J. *Science* **1995**, *270*, 1789. (b) Padinger, F.; Rittberger, R. S.; Sariciftci, N. S. *Adv. Funct. Mater.* **2003**, *13*, 85. (c) Wienk, M. M.; Kroon, J. M.; Verhees, W. J. H.; Knol, J.; Hummelen, J. C.; van Hal, P. A.; Janssen, R. A. J. *Angew. Chem. Ind. Ed.* **2003**, *42*, 3371.

(6) (a) Halls, J. J. M.; Walsh, C. A.; Greenham, N. C.; Marseglia, E. A.; Friend, R. H.; Moratti, S. C.; Holmes, A. B. *Nature* **1995**, *376*, 498. (b) Schmidt-Mende, L.; Fechtenkötter, A.; Müllen, K.; Moons, E.; Friend, R. H.; MacKenzie, J. D. *Science* **2001**, *293*, 1119. (c) Nierengarten, J.-F. *New J. Chem.* **2004**, *28*, 1177.

(7) (a) Hiramoto, M.; Fujiwara, H.; Yokoyama, M. *Appl. Phys. Lett.* **1991**, *58*, 1062. (b) Tsuzuki, T.; Shirota, Y.; Rostalski, J.; Meissner, D. *Solar Energy Mater. Solar Cells* **2000**, *61*, 1. (c) Xue, J.; Uchida, S.; Rand, B. P.; Forrest, S. R. *Appl. Phys. Lett.* **2004**, *84*, 3013.

(8) (a) Huynh, W. U.; Dittmer, J. J.; Alivisatos, A. P. *Science* **2002**, *295*, 2425. (b) Liu, J.; Tanaka, T.; Sivula, K.; Alivisatos, A. P.; Fréchet, J. M. J. *J. Am. Chem. Soc.* **2004**, *126*, 6550.

(9) (a) Gregg, B. A.; Fox, M. A.; Bard, A. J. *J. Phys. Chem.* **1990**, *94*, 1586. (b) Wang, Q.; Cambell, W. M.; Bonfantani, E. E.; Jolley, K. W.; Officer, D. L.; Walsh, P. J.; Gordon, K.; Humphry-Baker, R.; Nazeeruddin, M. K.; Grätzel, M. *J. Phys. Chem. B* **2005**, 109, 15397. (c) Brune, A.; Jeong, G.; Liddell, P. A.; Sotomura, T.; Moore, T. A.; Moore, A. L.; Gust, D. *Langmuir* **2004**, *20*, 8366.

(10) (a) Imahori, H. *J. Phys. Chem. B* **2004**, *108*, 6130. (b) Imahori, H.; Fukuzumi, S. *Adv. Funct. Mater.* **2004**, *14*, 525. (c) Hasobe, T.; Imahori, H.; Kamat. P. V.; Fukuzumi, S. *J. Am. Chem. Soc.* **2003**, *125*, 14962. (d) Hasobe, T.; Imahori, H.; Kamat, P. V.; Ahn, T. K.; Kim, S. K.; Kim, D.; Fujimoto, A.; Hirakawa, T.; Fukuzumi, S. *J. Am. Chem. Soc.* **2005**, *127*, 1216.

(11) *The Porphyrin Handbook*; Kadish, K. M., Smith, K. M., Guilard, R., Eds.; Academic Press: San Diego, 2003.

(12) *Phthalocyanines: Properties and Applications*; Leznoff, C. C., Lever, A. B. P., Eds.; VCH: New

York; 1993, Vols. 1-3; 1996, Vol. 4.

(13) (a) Danziger, J.; Dodelet, J.-P.; Lee, P.; Nebesny, K. W.; Armstrong, N. R. *Chem. Mater.* **1991**, *3*, 821. (b) Yanagi, H.; Douko, S.; Ueda, Y.; Ashida, M.; Wöhrle, D. *J. Phys. Chem.* **1992**, *96*, 1366. (c) Santerre, F.; Cöté, R.; Veilleux, G.; Saint-Jacques, R. G.; Dodelet, J. P. *J. Phys. Chem.* **1996**, *100*, 7632. (d) Huisman, C. L.; Goossens, A.; Schoonman, J. *J. Phys. Chem. B* **2002**, *106*, 10578.

(14) (a) He, J.; Hagfeldt, A.; Lindquist, S.-E.; Grennberg, H.; Korodi, F.; Sun, L.; Åkermark, B. *Langmuir* **2001**, *17*, 2743. (b) He, J.; Benko,G.; Korodi, F.; Polívka, T.; Lomoth, R.; Åkermark, B.; Sun, L.; Hagfeldt, A.; Sundström, V. *J. Am. Chem. Soc.* **2002**, *124*, 4922. (c) Amao, Y.; Komori, T. *Langmuir* **2003**, *19*, 8872. (d) Palomares, E.; Martínez-Díaz, M. V.; Haque, S. A.; Torres, T.; Durrant, J. R. *Chem. Commun.* **2004**, 2112.

(15) Loi, M. A.; Denk, P.; Hoppe, H.; Neugebauer, H.; Winder, C.; Meissner, D.; Brabec, C.; Sariciftci, N. S.; Gouloumis, A.; Vázquez, P.; Torres, T. *J. Mater. Chem.* **2003**, *13*, 700.

(16) Yang, S.; Fan, L.; Yang, S. *J. Phys. Chem. B* **2003**, *107*, 8403.

(17) Schlettwein, D.; Oekermann, T.; Yoshida, T.; Tochimoto, M.; Minoura, H. *J. Electroanal. Chem.* **2000**, *481*, 42.

(18) (a) Kamat. P. V.; Barazzouk, S.; Thomas, K. G.; Hotchandani S. *J. Phys. Chem. B* **2000**, *104*, 4014. (b) Kamat. P. V.; Haria, M.; Hotchandani S. *J. Phys. Chem. B* **2004**, *108*, 5166. (c) Hotta, H.; Kang, S.; Umeyama, T.; Matano, Y.; Yoshida, K.; Isoda, S.; Imahori, H. *J. Phys. Chem. B* **2005**, *109*, 5700.

(19) Kamat. P. V.; Barazzouk, S.; Hotchandani S.; Thomas, K. G. *Chem. Eur. J.* **2000**, *6*, 3914.

(20) (a) Hasobe, T.; Imahori, H.; Fukuzumi, S.; Kamat. P. V. *J. Phys. Chem. B* **2003**, *107*, 12105. (b) Hasobe, T.; Kashiwagi, Y.; Absalom, M. A.; Hosomizu, K.; Crossley, M. J.; Imahori, H.; Kamat, P. V.; Fukuzumi, S. *Adv. Mater.* **2004**, *16*, 975. (c) Hasobe, T.; Kamat, P. V.; Absalom, M. A.; Kashiwagi, Y.; Sly, J.; Crossley, M. J.; Hosomizu, K.; Imahori, H.; Fukuzumi, S. *J. Phys. Chem. B*, **2004**, *108*, 12865.

(21) (a) Hasobe, T.; Kamat, P. V.; Troiani, V.; Solladie, N.; Ahn, T. K.; Kim, S. K.; Kim, D.; Kongkanand, A.; Kuwabata, S.; Fukuzumi, S. *J. Phys. Chem. B* **2005**, *109*, 19. (b) Imahori, H.; Fujimoto, A.; Kang, S.; Hotta, H.; Yoshida, K.; Umeyama, T.; Matano, Y.; Isoda, S. *Adv. Mater.* **2005**, *17*, 1727.

(22) In the case of fullerenes, clustering results in an enhancement in molar extinction coefficient. The strong π-π interaction between the phthalocyanines may lead to the formation of clusters in which some of the phthalocyanines adopt face-to-face orientation, thereby decreasing the molar absorption coefficients. Large size of fullerene clusters (200–300 nm) relative to that of the present system may also cause light scattering in the visible region, increasing the apparent molar absorption coefficient of fullerene clusters.

(23) (a) Giaimo, J. M.; Gusev, A. V.; Wasielewski, M. R. *J. Am. Chem. Soc.* **2002**, *124*, 8530. (b) Fuller, M. J.; Sinks, L. E.; Rybtchinski, B.; Giaimo, J. M.; Li, X.; Wasielewski, M. R. *J. Phys. Chem. A* **2005**, *109*, 970.

(24) Under application of a high dc electric field, the clusters of C_{60} and C_{60} derivatives, which tend to be negatively charged in toluene/acetonitrile, are driven towards the positively charged electrode surface.[18,20,21] This is in sharp contrast with electrophoretic deposition of positively charged $(C_n\text{Pc})_m$ onto negatively charged electrode surface. As such, the composite clusters of the phthalocyanines and fullerenes could not be deposited onto ITO/SnO_2 electrode.

(25) Guldi, D. M.; Zilbermann, I.; Gouloumis, A.; Vázquez, P.; Torres, T. *J. Phys. Chem. B* **2004**, *108*, 18485.

(26) (a) Fang, J.; Su, L.; Wu, J.; Shen, Y.; Lu, Z. *New J. Chem.* **1997**, *21*, 1303. (b) Shen, Y.; Wang, L.; Lu, Z.; Wei, Y.; Zhou, Q.; Mao, H.; Xu, H. *Thin Solid Films* **1995**, *257*, 144. (c) Fang, J.; Wu, J.; Lu, X.; Shen, Y.; Lu, Z. *Chem. Phys. Lett.* **1997**, *270*, 145. (d) Yanagi, H.; Chen, S.; Lee, P. A.; Nebesny, K. W.; Armstrong, N. R.; Fujishima, A. *J. Phys. Chem.* **1996**, *100*, 5447. (e) Deng, H.; Lu, Z.; Mao, H.; Xu, H. *Chem. Phys.* **1997**, *221*, 323.

(27) (a) Cook, M. J.; Dunn, A. J.; Howe, S. D.; Thomason, A. J.; Harrison, K. J. *J. Chem. Soc. Perkin Trans. I* **1988**, 2453. (b) Rihter, B. D.; Kenney, M. E.; Ford, W. E.; Rodgers, M. A. *J. Am. Chem. Soc.* **1990**, *112*, 8064.

(28) Demmig, S.; Langhals, H. *Chem. Ber.* **1988**, *121*, 225.

(29) (a) Tkachenko, N. V.; Rantala, L.; Tauber, A. Y.; Helaja, J.; Hynninen, P. H.; Lemmetyinen, H. *J. Am. Chem. Soc.* **1999**, 121, 9378. (b) Kesti, T. J.; Tkachenko, N. V.; Vehmanen, V.; Yamada, H.; Imahori, H.; Fukuzumi, S.; Lemmetyinen, H. *J. Am. Chem. Soc.* **2002**, *124*, 8067. (c) Tkachenko, N. V.; Lemmetyinen, H.; Sonoda, J.; Ohkubo, K.; Sato, T.; Imahori, H.; Fukuzumi, S. *J. Phys. Chem. A* **2003**, *107*, 8834.

Chapter 4

Hydrogen Bonding Effects on the Surface Structure and Photoelectrochemical Properties of Nanostructured SnO_2 Electrodes Modified with Porphyrin and Fullerene Composites

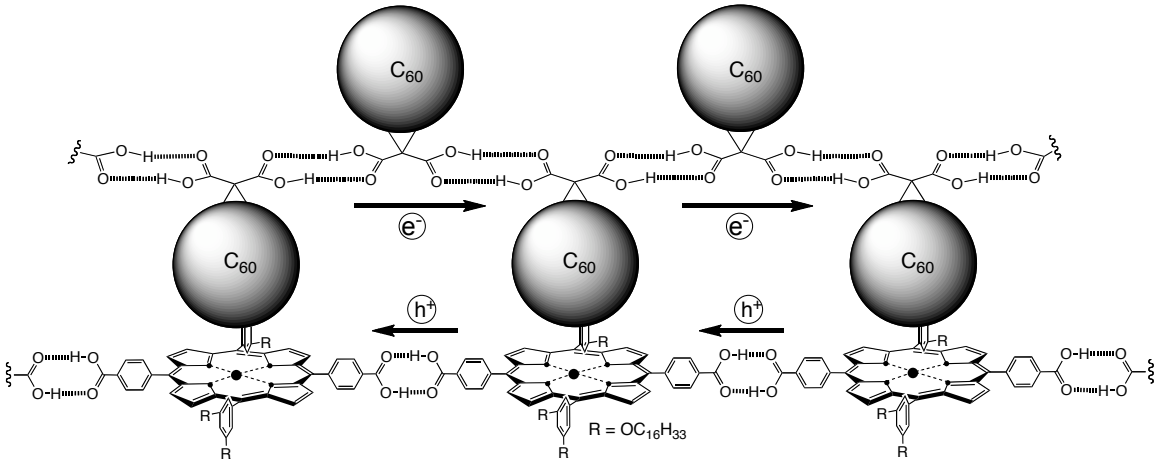

Abstract

Hydrogen bonding effects on surface structure, photophysical, and photoelectrochemistry have been examined in a mixed film of porphyrin and fullerene composites with and without hydrogen bonding on ITO and nanostructured SnO_2 electrodes. The nanostructured SnO_2 electrodes modified with the mixed films of porphyrin and fullerene composites with hydrogen bonding exhibited efficient photocurrent generation compared to the reference systems without hydrogen bonding. Atomic force microscopy, infrared reflection absorption and ultraviolet-visible absorption spectroscopies, and time-resolved fluorescence lifetime and transient absorption spectroscopic measurements disclosed the relationship between the surface structure, photophysical, and photoelectrochemical properties relating to the formation of hydrogen bonding between the porphyrins and/or the C_{60} moieties in the films on the electrode surface. These results show that hydrogen bonding is a highly promising methodology for the fabrication of donor and acceptor composites on nanostructured semiconducting electrodes, which exhibit high photoelectrochemical properties.

Introduction

Non-covalent bonding such as hydrogen-bonding, coordination bonding, electrostatic interaction, van der Waals interaction, and π-π interaction plays an important role in biological activities in nature. For instance, photosynthesis employs such weak interaction to arrange donor-acceptor (D-A) molecules in a protein matrix precisely, exhibiting a vectorial cascade of energy and electron transfer processes.[1] Stimulated by this vision, the utilization of weak interaction has recently merited increasing attention as sophisticated methodology to assemble supramolecular photosynthetic architectures.[2] A variety of non-covalently bonded donor-acceptor (D-A) systems have been constructed in fluid media to mimic photoinduced energy and electron transfer processes in photosynthesis.[3–11]

Along this line, achieving efficient solar energy conversion at low cost is one of the most important technological challenges for the near future. During the last decade, organic solar cells have been discussed as promising alternative to inorganic semiconductors for renewable energy production. Specifically, considerable attention has been drawn towards developing the dye-sensitized[12] and bulkheterojunction[13–18] solar cells. The distinguishing characteristic of these cells is that excitations are generated upon light absorption, and within 100 fs charge carriers are generated and simultaneously separated across the dye-semiconductor or donor-acceptor heterointerface. Typically, bulk heterojunction solar cells possess an interpenetrating network of donor (D) and acceptor (A) molecules in the blend film revealing photoinduced charge separation and the transport of created charges to the electrodes. Thus, design and construction of electron- and hole-transporting, nanostructured highways in the D-A interpenetrating network are pivotal to enhance both charge separation efficiency and charge carrier mobility. Supramolecular assembly of D-A molecules is a potential approach to create such bulk heterojunction layer with a phase-separated, interpenetrating network involving nanostructured electron and hole highways. However, there have so far been few examples where non-covalent bonding strategy has been employed in a mixed film of donor and acceptor to improve photocurrent generation efficiency in photoelectrochemical devices.[15a,19,20]

Here, the author reports the first mixed films of porphyrin and fullerene with hydrogen bonding on tin oxide (SnO_2) as well as indium tin oxide (ITO) electrodes to reveal efficient photocurrent generation. The compounds used in this study are shown in Figure 1. A combination of porphyrin as a donor as well as a sensitizer with fullerene as an acceptor was chosen, because such a D-A system is known to exhibit a long-lived charge-separated state with a high quantum yield via photoinduced electron transfer.[21,22] Given the fact that porphyrins tend to make a complex with fullerenes in a solid state due to the π-π interaction[23–25] and the small reorganization energy of porphyrin and fullerene system,[21,22] one can expect fast photoinduced charge separation and slow charge recombination in the mixed film. More importantly, the resulting electron and hole pair must be separated through tailored

network of the acceptors and the donors, respectively, to suppress charge recombination. Such electron or hole-transporting highway would be constructed with the help of hydrogen bonding. To evaluate the hydrogen bonding effect on the photoelectrochemical properties of the D-A systems, carboxyl and alkoxycarbonyl groups were introduced to porphyrin and C_{60} to yield zincporphyrin (ZnP) acid and ester as a donor (denoted as ZnP-acid and ZnP-ester) and C_{60} acid and C_{60} ester as an acceptor (denoted as C_{60}-acid and C_{60}-ester), respectively (Figure 1).

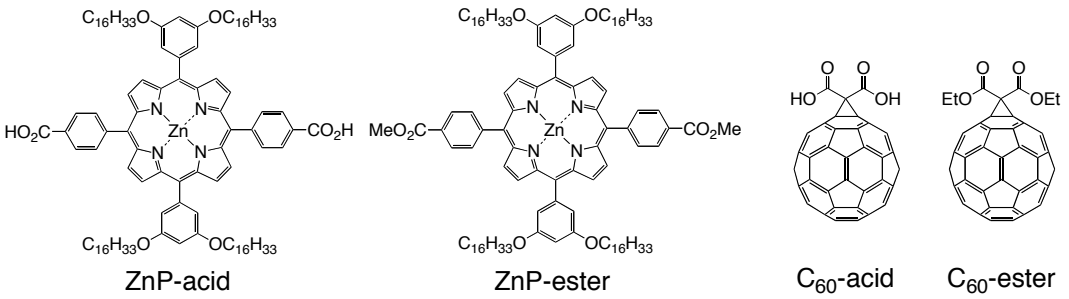

Figure 1. Porphyrin and fullerene derivatives used in this study.

Results and Discussion

Synthesis. Synthetic strategy of porphyrin derivatives with carboxyl groups is shown in Scheme 1. 3,5-Dihexadecyloxybenzyl alcohol was oxidized using PCC to yield benzaldehyde **1**.[26] Porphyrin **2** was synthesized by the condensation of 5-(4-methoxycarbonylphenyl)dipyrromethane with **1** in the presence of BF_3•OEt_2.[27] Porphyrin diester **2** was hydrolyzed to give porphyrin dicarboxylic acid **3**. ZnP-acid was obtained by treatment of **3** with $Zn(OAc)_2$. ZnP-ester was prepared from porphyrin diester **2** in the same manner. C_{60}-ester and C_{60}-acid were synthesized by following previously reported procedures.[28]

Scheme 1. Synthesis of ZnP-acid and ZnP-ester.

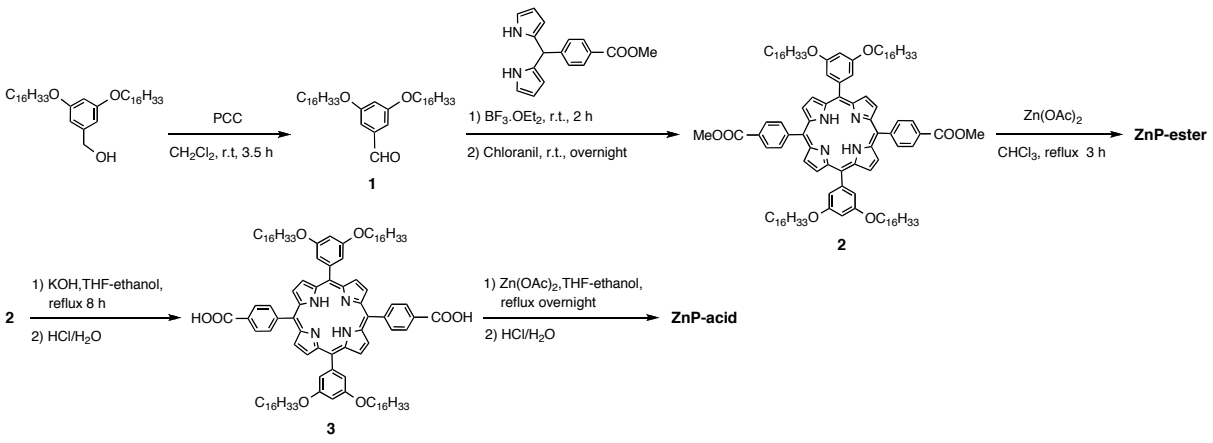

Characterization and Surface Structure of SnO_2/ITO and ITO Electrodes Modified with Porphyrin and Fullerene Composites. The author has successfully observed enhanced photocurrent generation in ITO electrode modified with the mixed film of porphyrin and hydrogen-bonded C_{60} derivative relative to the reference system without hydrogen-bonding.[19b] To improve the photovoltaic properties of the previous system, hydrogen bonding strategy has been also applied to the porphyrin moiety in addition to the C_{60} moiety (Figure 1). More importantly, ITO electrode is replaced by SnO_2/ITO electrode to suppress charge recombination. Once the separated electron is injected into the conduction band (CB) of SnO_2, there would be less chance to recombine the electron in the conduction band and the hole in porphyrin radical cation or electron carrier in the electrolyte solution, leading to the remarkable improvement of photocurrent generation efficiency.

SnO_2/ITO electrodes were immersed into an equimolar THF solution (1.5 mM) of porphyrin (ZnP-acid, ZnP-ester) and/or fullerene (C_{60}-acid, C_{60}-ester) to give modified SnO_2/ITO electrodes. Figure 2 shows absorption spectra of a mixed film of ZnP-acid and C_{60}-acid (denoted as ZnP-acid+C_{60}-acid/SnO_2/ITO), a film of ZnP-acid (denoted as ZnP-acid/SnO_2/ITO), and the equimolar THF solution of ZnP-acid and C_{60}-acid (denoted as ZnP-acid+C_{60}-acid). The Soret bands of ZnP-acid+C_{60}-acid/SnO_2/ITO and ZnP-acid/SnO_2/ITO are broadened and red-shifted relative to that of ZnP-acid+C_{60}-acid in THF due to the interaction between the porphyrins. In addition, the broad long wavelength absorption of ZnP-acid+C_{60}-acid/SnO_2/ITO in the 600–700 nm regions is

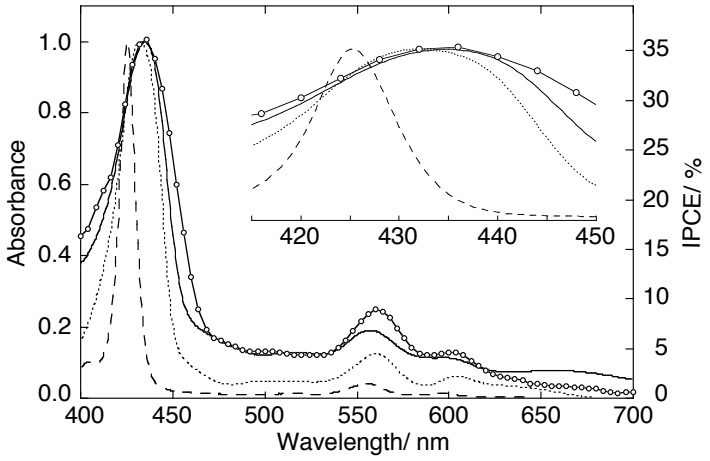

Figure 2. UV-visible absorption spectra of a mixed film of ZnP-acid and C_{60}-acid (ZnP-acid+C_{60}-acid/SnO_2/ITO, solid line), a film of ZnP-acid (ZnP-acid/SnO_2/ITO, dotted line), an equimolar THF solution of ZnP-acid and C_{60}-acid (ZnP-acid+C_{60}-acid, dashed line), and action spectrum of ZnP-acid+C_{60}-acid/SnO_2/ITO system (solid line with open circles). Input power: 85 μW cm^{-2} (λ_{ex}= 435 nm); applied potential: 0.15 V vs SCE; 0.5 M LiI and 0.01 M I_2 in acetonitrile. The spectra were normalized at the Soret band for comparison. Expanded spectra in the Soret band region are shown as an inset. The modified SnO_2/ITO electrodes were prepared by immersing SnO_2/ITO electrodes into an equimolar THF solution (1.5 mM) of ZnP-acid and C_{60}-acid.

diagnostic of the charge-transfer absorption band due to the π-complex formed between the porphyrin and the C_{60}.[20,25] Similar spectral behavior was observed for the modified SnO_2/ITO electrodes prepared by the spin-coating method.

Figure 3 shows IRRA spectra in the C=O stretching region (1850–1650 cm^{-1}) for the thin films of porphyrin and/or fullerene spin-coated on gold surface as (a) ZnP-ester, (b) ZnP-acid, (c) C_{60}-ester, (d) C_{60}-acid, (e) ZnP-acid+C_{60}-acid, (f) ZnP-acid+C_{60}-ester, (g) ZnP-ester+C_{60}-acid and (h) ZnP-ester+C_{60}-ester. Detailed peak information was summarized in Table 1. As shown in Figure 3a, ZnP-ester gives an IR peak at 1725 cm^{-1} which can be assigned to the free C=O stretching mode of the ester moiety. In contrast with ZnP-ester, ZnP-acid shows an IR absorption peak from C=O stretching at lower wavenumber (1688 cm^{-1}, Figure 3b). Normally, it is known that the peak from C=O stretching mode shifts to lower frequency region when the hydrogen bonding is formed between carbonyl group and a hydrogen-bonding donor.[29–33] Thus, the red-shift in peak position of the C=O stretching can be attributed to the formation of intermolecular hydrogen bonding between ZnP-acid molecules, possibly dimer or some higher aggregates.

Furthermore, C_{60}-ester shows an IR peak at 1748 cm^{-1} with a shoulder at 1729 cm^{-1} (Figure 3c), while C_{60}-acid gives a broad IR peak around 1720 cm^{-1} (Figure 3d), suggesting the formation of hydrogen bonding between C_{60}-acid molecules. The reason for the relatively broad shape of the IRRA spectrum of C_{60}-acid is not clear at this stage and may be related to the un-uniform aggregates of C_{60}-acid on the substrate.

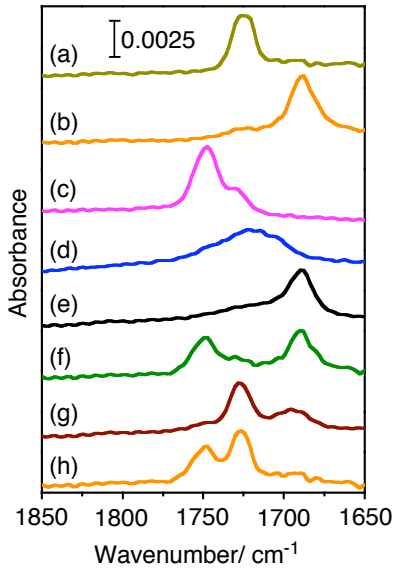

Figure 3. IRRA spectra in the C=O stretching region (1850–1650 cm^{-1}) for the thin films of porphyrin and/or fullerene spin-coated on gold surface as (a) ZnP-ester, (b) ZnP-acid, (c) C_{60}-ester, (d) C_{60}-acid, (e) ZnP-acid+C_{60}-acid, (f) ZnP-acid+C_{60}-ester, (g) ZnP-ester+C_{60}-acid and (h) ZnP-ester+C_{60}-ester. IR intensities for mixed films were normalized to the same concentration as those for single component films.

On the other hand, useful structural information about the hydrogen bonding interaction between different types of molecules can be obtained from the IRRA spectra of mixed films of porphyrin and fullerene composites. As shown in Figures 3e and 3f, an IR peak at 1688 cm^{-1} was clearly observed for ZnP-acid mixed with C_{60}-acid or C_{60}-ester. It is unlikely that the hydrogen bonding interaction between ZnP-acid and C_{60}-acid or C_{60}-ester is strong since these IR spectra look like a superimposition of IR spectra of two single respective components. For example, C=O stretching mode of C_{60}-ester in the equimolar mixture film with ZnP-acid shows nearly the same feature as that of single C_{60}-ester component and obvious changes in peak position and intensity were not observed (Figure 3f), indicating that interaction between ZnP-acid and C_{60}-ester species is very limited. At the same time, the author still expects that a small part of ZnP-acid molecules may form hydrogen-bonding with C_{60}-acid molecules, although the hydrogen bonding interaction between the same types of molecules (i.e., ZnP-acid and ZnP-acid, C_{60}-acid and C_{60}-acid) seemed to be stronger. It is noteworthy that equimolar mixture of ZnP-ester and C_{60}-acid shows slightly different behavior (Figure 3g), where the peak position of C=O stretching from C_{60}-acid in the mixture film was narrower and was shifted to 1694 cm^{-1} in comparison with that of single C_{60}-acid component, suggesting that the hydrogen bonding in C_{60}-acid was intensified in the mixture with ZnP-ester (vide infra). As expected, no change was observed in the mixture of ZnP-ester molecules and C_{60}-ester molecules (Figure 3h) since there is no hydrogen-bonding donor.

Table 1. IRRA frequencies, IPCE values, and Fluorescence Lifetimes.

system	IRRA frequency/cm^{-1}	IPCE/% [a] (dipping method)	IPCE/% [b] (spin-coating method)	fluorescence lifetime/ ps [c]
ZnP-acid+C_{60}-acid	1688, 1720	36	18	*d*
ZnP-acid+C_{60}-ester	1689, 1749	28	8.2	*d*
ZnP-ester+C_{60}-acid	1694, 1727	15	7.1	40
ZnP-ester+C_{60}-ester	1726, 1749	7	2.6	62
ZnP-acid	1688	26	3.5	*d*
ZnP-ester	1725	6	1.2	380
C_{60}-acid	1720	*e*	*e*	*e*
C_{60}-ester	1748, 1729	*e*	*e*	*e*

[a]Input power: 85 μW cm^{-2} (λ_{ex} = 435 nm); absorbance: 1.00±0.05 at excitation wavelength; thickness of SnO_2 layer: 1.1 μm; applied potential: 0.15 V vs SCE. [b]Input power: 92 μW cm^{-2} (λ_{ex} = 435 nm); absorbance: 0.25±0.03 at excitation wavelength; thickness of SnO_2 layer: 0.4 μm; applied potential: 0.15 V vs SCE. [c]The samples were prepared by dipping method. The fluorescence decays were measured by time-correlated single photon counting method (λ_{ex} = 590 nm), monitoring wavelength was at 660 nm. [d]The decay was too fast to give the fluorescence lifetime accurately. [e]Not measured.

As demonstrated above, the formation of hydrogen bonding was confirmed in the mixed film of ZnP-acid+C_{60}-acid, ZnP-acid+C_{60}-ester as well as ZnP-ester+C_{60}-acid but not in ZnP-ester+C_{60}-ester. The hydrogen bonding interaction between the ZnP-acid molecules or C_{60}-acid molecules seems to be more important than that between different types of molecules.

AFM measurements were performed for the SnO_2/ITO electrodes modified with the compounds by spin-coating method (Figures 4 and 5). The images of ZnP-acid/SnO_2/ITO (Figure 4a) and ZnP-ester/SnO_2/ITO (Figure 4b) are similar to that of bare SnO_2/ITO, which exhibit arrays of spherical particles with 20 nm size. In contrast, the images of C_{60}-acid/SnO_2/ITO (Figure 4c) and C_{60}-ester/SnO_2/ITO (Figure 4d) show arrays of spherical particles with 30–40 nm size, which is larger than that of ZnP-acid/SnO_2/ITO and ZnP-ester/SnO_2/ITO. These results together with the IRRA spectra suggest that the C_{60} molecules are more aggregative than the porphyrins (vide supra).

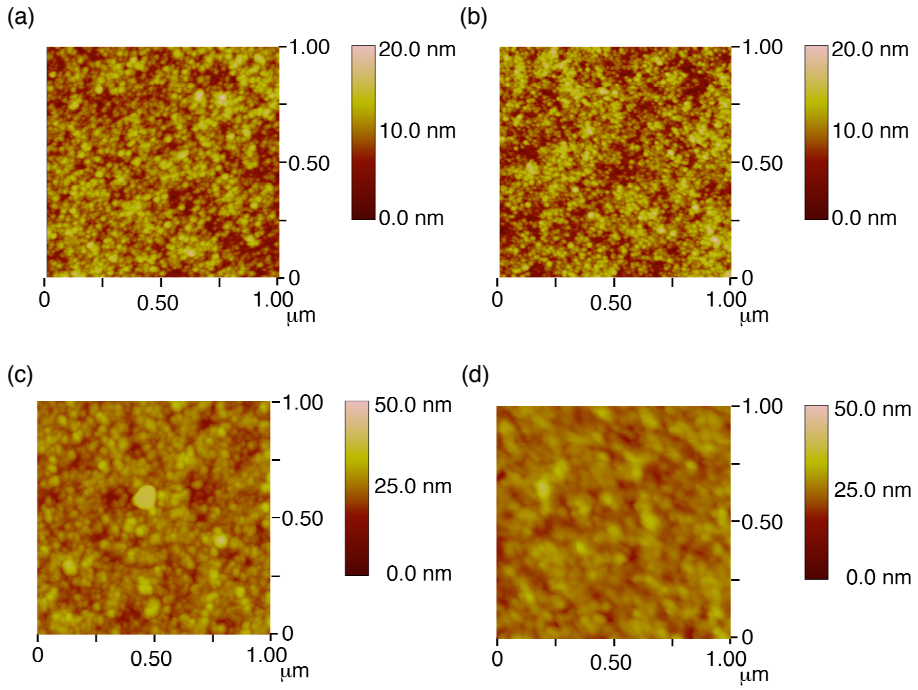

Figure 4. AFM images of (a) ZnP-acid/SnO_2/ITO, (b) ZnP-ester/SnO_2/ITO, (c) C_{60}-acid/SnO_2/ITO, and (d) C_{60}-ester/SnO_2/ITO electrodes.

The AFM images of the porphyrin and C_{60} mixed system are quite different from those of either the porphyrin or the C_{60} system. The AFM images of ZnP-acid+C_{60}-acid/SnO_2/ITO (Figure 5a), ZnP-acid+C_{60}-ester/SnO_2/ITO (Figure 5b), and ZnP-ester+C_{60}-acid/SnO_2/ITO (Figure 5c) are much smoother than those of ZnP-ester+C_{60}-ester/SnO_2/ITO (Figure 5d) as well as of ZnP-acid/SnO_2/ITO, ZnP-ester/SnO_2/ITO, C_{60}-acid/SnO_2/ITO, and C_{60}-ester/SnO_2/ITO (Figure 6). Similar trend was observed for the AFM images on ITO and mica surfaces. These results demonstrate that both the

intermolecular interaction between the porphyrin and the C_{60} and the hydrogen bonding from either the porphyrin or the C_{60} moieties are required for the smooth morphology on the surface in which the porphyrin and the C_{60} molecules would be self-assembled with a phase-separated, interpenetrating network involving hydrogen-bonded electron and/or hole transporting nanostructures (vide infra).

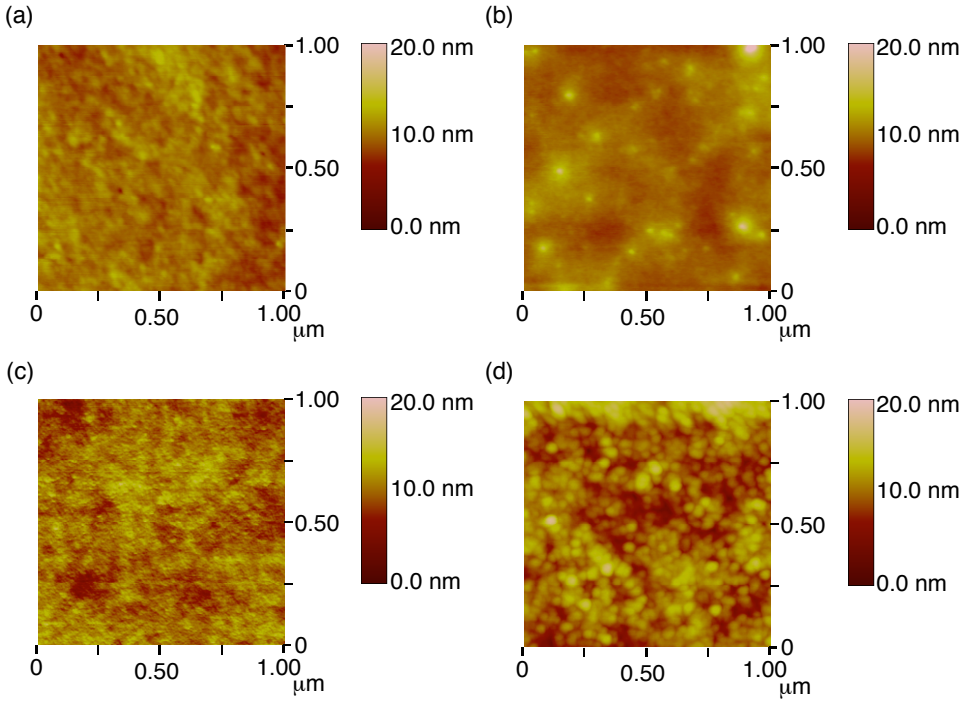

Figure 5. AFM images of (a) ZnP-acid+C_{60}-acid/SnO_2/ITO, (b) ZnP-acid+C_{60}-ester/SnO_2/ITO, (c) ZnP-ester+C_{60}-acid/SnO_2/ITO, and (d) ZnP-ester+C_{60}-ester/SnO_2/ITO ([ZnP]:[C_{60}] = 1:1) electrodes.

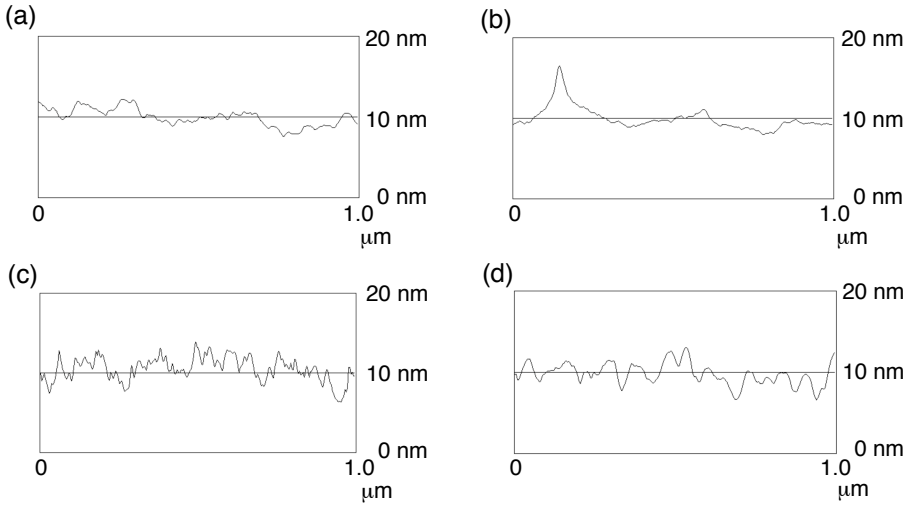

Figure 6. Section profiles of AFM images of (a) ZnP-acid+C_{60}-acid/SnO_2/ITO, (b) ZnP-ester+C_{60}-acid/SnO_2/ITO, (c) ZnP-acid+C_{60}-ester/SnO_2/ITO, and (d) ZnP-ester+C_{60}-ester/SnO_2/ITO ([ZnP]:[C_{60}] = 1:1) electrodes prepared by the spin-coating method.

Photoelectrochemical Properties of SnO_2/ITO and ITO Electrodes Modified with Porphyrin and Fullerene Composites. Photoelectrochemical measurements were performed in a nitrogen-saturated acetonitrile solution containing 0.5 M LiI and 0.01 M I_2 using the modified SnO_2/ITO as the working electrode, a platinum counter electrode, and a I^-/I_3^- reference electrode. For instance, a stable anodic photocurrent from the electrolyte to ZnP-acid+C_{60}-acid/SnO_2/ITO electrode, prepared by the dipping method, appeared immediately upon irradiation of the modified SnO_2/ITO electrode (Figure 7). The photocurrent fell down instantly when the illumination was cut off. The intensity of the photocurrent was maintained almost constant during the irradiation at least one hour. The anodic photocurrent increases with increasing positive bias to the ITO electrode from –0.05 V to 0.4 V vs SCE, as shown in Figure 7. The agreement of the action spectrum with the absorption spectrum of ZnP-acid+C_{60} acid/SnO_2/ITO, which is largely similar to that of ZnP-acid/SnO_2/ITO (Figure 2), demonstrates that the direction of the electron flow is from the electrolyte to the ITO via the excited singlet state of the porphyrin moiety (vide infra). Similar photoelectrochemical behavior was observed for ZnP-acid+C_{60}-ester/SnO_2/ITO, ZnP-ester+C_{60}-acid/SnO_2/ITO, ZnP-ester+C_{60}-ester/SnO_2/ITO, ZnP-acid/SnO_2/ITO, and ZnP-ester/SnO_2/ITO systems.

The IPCE (incident photon-to-current efficiency) values were compared for ZnP-acid+C_{60}-acid/SnO_2/ITO, ZnP-acid+C_{60}-ester/SnO_2/ITO, ZnP-ester+C_{60}-acid/SnO_2/ITO, ZnP-ester+C_{60}-ester/SnO_2/ITO, ZnP-acid/SnO_2/ITO, and ZnP-ester/SnO_2/ITO systems under the same conditions (applied potential: 0.15 V vs SCE, λ_{ex} = 435 nm). The excitation wavelength at the Soret band guarantees the

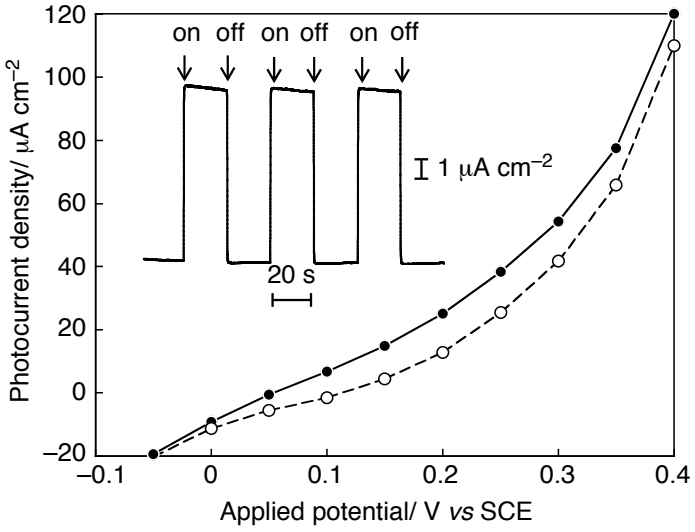

Figure 7. Photocurrent vs applied potential curves of ZnP-acid+C_{60}-acid/SnO_2/ITO system. The dark currents are shown as dashed line with open circles. Experimental conditions were as follows; excitation power: 85 μW cm^{-2} (λ_{ex} = 435 nm); absorbance: 1.00 at excitation wavelength; thickness of SnO_2 layer: 1.1 μm; 0.5 M LiI and 0.01 M I_2 in acetonitrile. The photoelectrochemical response at applied potential of 0.15 V vs SCE is shown as an inset.

selective excitation of the porphyrin rather than that of C_{60} moiety. The IPCE values obtained by the dipping method are in the order of ZnP-acid+C_{60}-acid/SnO_2/ITO (36%) > ZnP-acid+C_{60}-ester/SnO_2/ITO (28%) > ZnP-acid/SnO_2/ITO (26%) > ZnP-ester+C_{60}-acid/SnO_2/ITO (15%) > ZnP-ester+C_{60}-ester/ SnO_2/ITO (7%) > ZnP-ester/SnO_2/ITO (6%) systems (Table 1). The IPCE values are larger by 1–2 orders of magnitudes than those of similar porphyrin-hydrogen-bonded C_{60} system on ITO electrode.[19b] The IPCE values from ZnP-acid systems are much larger than those from ZnP-ester systems. This difference may result from direct adsorption of ZnP-acid onto the SnO_2 surface where an electron is directly injected into the conduction band of the SnO_2 surface from the excited singlet state of the porphyrin to generate photocurrent.[34,35] In both the porphyrin carboxylic acid system and the porphyrin ester system, IPCE values increase significantly when C_{60} acid rather than C_{60} ester is employed. This suggests that not only the direct electron injection takes place, but also a competitive electron transfer occurs from the porphyrin excited singlet state to C_{60} acid, followed by the electron injection from the reduced C_{60} to the conduction band of the SnO_2 surface (vide infra). Besides, electron and hole relay may occur in the arrays of hydrogen-bonded C_{60}-acid and ZnP-acid, respectively, as indicated from the dominant hydrogen bonding interaction between the identical ZnP-acid molecules or C_{60}-acid molecules rather than between different types of molecules (vide supra). It is noteworthy that the IPCE value is improved in the mixed system with hydrogen bonding as compared to the reference system. Although the largest IPCE value (36%) is achieved in ZnP-acid+C_{60}-acid/SnO_2/ITO system,[36,37] the hydrogen bonding effect on photocurrent generation is not prominent in comparison with ZnP-acid+C_{60}-ester/SnO_2/ITO and ZnP-acid/SnO_2/ITO systems. It may be originated from the dipping method in which ZnP-acid and C_{60}-acid tend to adsorb onto the SnO_2 surface rather than make hydrogen bonding each other. To differentiate the two competitive processes, the fabrication of these molecules on the SnO_2/ITO electrodes were carried out by using spin-coating method, which reduces the possibility of adsorbing ZnP-acid and C_{60}-acid onto the SnO_2/ITO electrodes significantly. Although the IPCE values obtained by the spin-coating method are smaller than those obtained by the dipping method, the former trend for the IPCE values is unambiguous: ZnP-acid+C_{60}-acid/SnO_2/ITO (18%) > ZnP-acid+C_{60}-ester/SnO_2/ITO (8.2%) > ZnP-ester+C_{60}-acid/SnO_2/ITO (7.1%) > ZnP-acid/ SnO_2/ITO (3.5%) > ZnP-ester+C_{60}-ester/SnO_2/ITO (2.6%) > ZnP-ester/SnO_2/ITO (1.2%) systems. The trend for the IPCE values is in good agreement with the results on the IRRA spectra and the AFM measurements. For instance, the IPCE value (18%) of ZnP-acid+C_{60}-acid/SnO_2/ITO system is much larger than those of ZnP-acid+C_{60}-ester/SnO_2/ITO (8.2%) and ZnP-acid/SnO_2/ITO (3.5%) systems (Table 1). Furthermore, a prominent effect for the photocurrent generation was also observed for ZnP-ester+C_{60}-acid/SnO_2/ITO (7.1%) in comparison with those of ZnP-ester+C_{60}-ester/SnO_2/ITO (2.6%) and ZnP-ester/SnO_2/ITO (1.2%) systems. The increase may be attributed to the enhancement

of hydrogen bonding between C_{60}-acid molecules in the mixed film, as shown in Figure 3g. These results demonstrate that photocurrent generation is much enhanced in hydrogen-bonded porphyrin-fullerene system compared with the reference system without hydrogen bonding.

Photophysical studies. At first, steady-state fluorescence spectra (λ_{ex} = 430 nm) were measured for the better understanding of the photodynamical behavior of the porphyrin-fullerene system on the SnO_2 electrodes prepared by the dipping method (Figure 8). Fluorescence from the porphyrin is strongly quenched in ZnP-acid+C_{60}-acid/SnO_2/ITO and ZnP-acid+C_{60}-ester/SnO_2/ITO relative to ZnP-acid/SnO_2/ITO. In the ZnP-acid system, no emission from the C_{60} moiety (720 nm) is seen except the case of ZnP-acid+C_{60}-acid/SnO_2/ITO (Figure 8a).[38] Intensity of the fluorescence due to the porphyrin moiety in the ZnP-acid system is in the order of ZnP-acid+C_{60}-acid/SnO_2/ITO < ZnP-acid+C_{60}-ester/SnO_2/ITO < ZnP-acid/SnO_2/ITO, which is consistent with that of the IPCE values. Similar porphyrin fluorescence quenching was observed for ZnP-ester+C_{60}-acid/SnO_2/ITO and ZnP-ester+C_{60}-ester/SnO_2/ITO in comparison with ZnP-ester/SnO_2/ITO (Figure 8b). These results suggest the occurrence of photoinduced electron transfer or partial charge-transfer (i.e., exciplex formation) from the porphyrin excited singlet state to the C_{60} moiety (vide infra).[39] It is noteworthy that ZnP-ester+C_{60}-acid/SnO_2/ITO reveals the emission from both the porphyrin and the C_{60} moieties,[38] which agrees with the results on the IRRA spectrum (Figure 3g). On the other hand, ZnP-ester+C_{60}-ester/SnO_2/ITO exhibit CT emission (800 nm),[25] in addition to the weak emission from the porphyrin. In the case of ZnP-ester+C_{60}-ester/SnO_2/ITO, ZnP-ester and C_{60}-ester molecules are

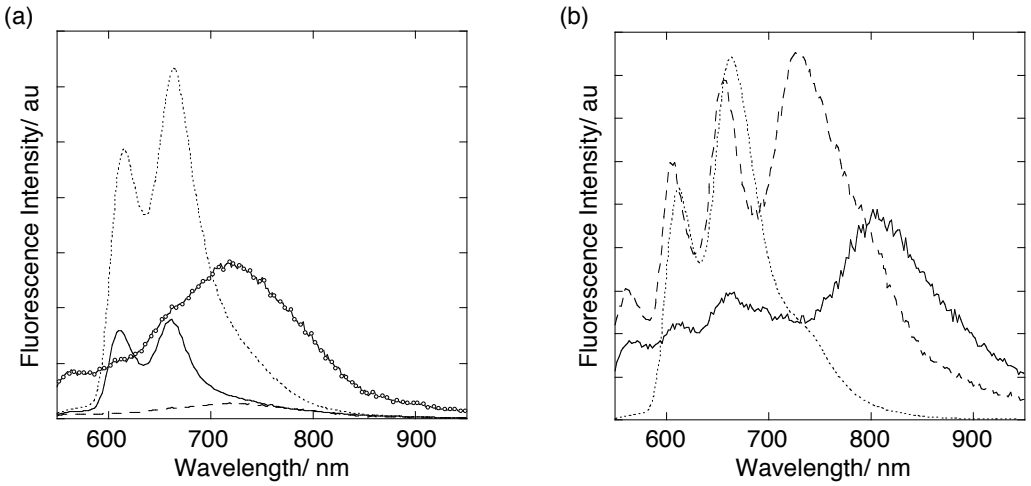

Figure 8. Steady-state fluorescence spectra of (a) ZnP-acid/SnO_2/ITO (dotted line), ZnP-acid+C_{60}-ester/SnO_2/ITO (solid line, [ZnP]:[C_{60}] = 1:1), and ZnP-acid+C_{60}-acid/SnO_2/ITO (dashed line and solid line with white circles (× 10); [ZnP]:[C_{60}] = 1:1) electrodes. (b) ZnP-ester/SnO_2/ITO (dotted line (× 10^{-2})), ZnP-ester+C_{60}-ester/SnO_2/ITO (solid line, [ZnP]:[C_{60}] = 1:1), and ZnP-ester+C_{60}-acid/SnO_2/ITO (dashed line, [ZnP]:[C_{60}] = 1:1) electrodes. The excitation wavelength was 430 nm.

susceptible to make close contact due to the π-π interaction because of the absence of hydrogen-bonding. Accordingly, most of the ZnP-ester and C_{60}-ester make the supramolecular complex to exhibit CT emission, whereas the minor, uncomplex ZnP-ester and C_{60}-ester reveals the quenching of fluorescence from the porphyrin moiety via photoinduced ET (vide infra).

Photoinduced electron transfer process was confirmed by the comparison of picosecond fluorescence lifetime measurements for ZnP-acid+C_{60}-acid/SnO_2/ITO, ZnP-acid+C_{60}-ester/SnO_2/ITO, ZnP-ester+C_{60}-acid/SnO_2/ITO, ZnP-ester+C_{60}-ester/SnO_2/ITO, ZnP-acid/SnO_2/ITO, and ZnP-ester/SnO_2/ITO systems prepared by the dipping method. The fluorescence lifetimes on the SnO_2/ITO surfaces were measured by a time-correlated single-photon counting technique at emission wavelength of 660 nm due to the porphyrin moiety with excitation at 590 nm. The decay curves of the fluorescence intensity were fitted by 3-exponentials (Figure 9). However, in all cases, the fastest component was the dominating one (> 80%). The lifetimes of the fastest component are summarized in Table 1. The fluorescence lifetimes of ZnP-acid+C_{60}-acid/SnO_2/ITO, ZnP-acid+C_{60}-ester/SnO_2/ITO, and ZnP-acid/SnO_2/ITO are much shorter than the time resolution of the present system (< 40 ps).[40] This is in accordance with the stepwise electron transfer from the porphyrin excited singlet state to the C_{60}, followed by electron injection to the CB of the SnO_2 electrode, in addition to the fast, direct electron injection of the porphyrin singlet excited state to the conduction band (CB) of the SnO_2 electrode through the chemical adsorption of carboxylic acid group onto the SnO_2 surface.[34,35] The fluorescence lifetimes of ZnP-ester+C_{60}-acid/SnO_2/ITO (40 ps) and ZnP-ester+C_{60}-ester/SnO_2/ITO (62 ps) are shorter than that of ZnP-ester/ITO systems (380 ps) where direct electron injection process

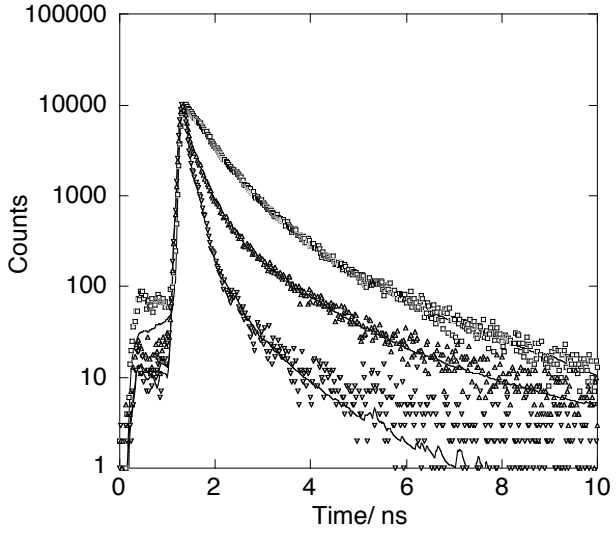

Figure 9. Fluorescence decay curves of (a) ZnP-ester/SnO_2/ITO (square), (b) ZnP-ester+C_{60}-ester/SnO_2/ITO (upper triangle, [ZnP]:[C_{60}] = 1:1), and (c) ZnP-ester+C_{60}-acid/SnO_2/ITO (downward triangle, [ZnP]:[C_{60}] = 1:1) electrodes observed at 660 nm by the single photon counting method. The excitation wavelength is 590 nm.

from the porphyrin excited singlet state to the CB of the SnO_2 electrode is suppressed due to the absence of chemical adsorption of the porphyrin onto the SnO_2 surface. These results support the occurrence of photoinduced electron transfer or partial charge transfer from the porphyrin singlet excited state to the C_{60} moiety rather than self-quenching of the porphyrin excited state due to the aggregation to yield the charge-separated state, which eventually leads to the photocurrent generation.

The formation of the charge-separated state in the mixed films was detected using femtosecond pump-probe method for ZnP-ester+C_{60}-ester/SnO_2/ITO, ZnP-acid/SnO_2/ITO, and ZnP-ester/SnO_2/ITO systems with the excitation wavelength of 555 nm. The transient absorption spectrum of ZnP-ester+ C_{60}-ester/SnO_2/ITO, prepared by dipping method, reveals the characteristic bands around 650 nm due zinc porphyrin radical cation[25] and 1000 nm due to C_{60} radical anion[25] (Figure 10), which thus can be assigned to the charge-separated state or to the exciplex state.[21,25,39] With time resolution of the instrument used an instant formation of the bands was observed, which indicates that the primary exciplex formation in the sample can be as fast as 10^{13} s^{-1}. This is consistent with the observation of CT emission due to the π-complexation between the porphyrin and the C_{60} in the steady-state fluorescence spectrum of ZnP-ester+C_{60}-ester/SnO_2/ITO. The decay of the transient absorption was a complex process with the fastest relaxation rate of 10^{11} s^{-1}, which followed by a slower relaxation with the rates constant even smaller than 10^{9} s^{-1}. This can be understood in terms of different types of structures formed and a variety of charge-separation pathways realized in the system. In contrast, the transient absorption spectra of ZnP-acid/SnO_2/ITO and ZnP-ester/SnO_2/ITO exhibit the characteristic bleaching around 590 nm due to the porphyrin excited singlet state.[21,25,39,41]

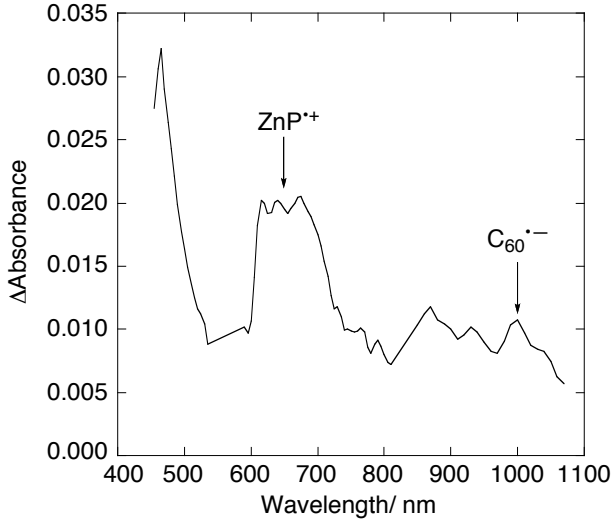

Figure 10. Transient absorption spectrum of ZnP-ester+C_{60}-ester/SnO_2/ITO at time delay of 10 ps excited at 555 nm.

Based on the energetics of the photoactive and radical ion species involved in ZnP-aicd+C_{60}-acid/ SnO_2/ITO system, the mechanism of anodic photocurrent generation is proposed (Scheme 2). First, an electron transfer takes place from $^1ZnP^*$ (ZnP-acid: –0.97 V; ZnP-ester: –0.96 V (vs NHE)) to the conduction band of SnO_2 (0 V vs NHE)[20] or C_{60} (C_{60}-acid: –0.43 V; C_{60}-ester: –0.32 V (vs NHE))[20] yielding the porphyrin radical cation ($ZnP^{\bullet+}$) and the electron in the conduction band or $ZnP^{\bullet+}$ and C_{60} radical anion ($C_{60}^{\bullet-}$).[42] In the latter case, the reduced $C_{60}^{\bullet-}$ gives an electron to the conduction band of SnO_2 (0 V vs SCE)[20] to yield the same state. On the other hand, I^- (0.5 V vs NHE)[20] donates an electron to $ZnP^{\bullet+}$ (ZnP-acid: 1.08 V; ZnP-ester: 1.09 V (vs NHE))[20] to generate anodic photocurrent. The hydrogen bonding in the porphyrin or the C_{60} molecules or the both may be responsible for the large IPCE values in comparison with the reference system without the hydrogen bonding. Such hydrogen bonding would facilitate the initial charge separation between the porphyrin and the C_{60} and the separated electron and hole relay through the hydrogen-bonded arrays which suppress the undesirable charge recombination. It is well known that the use of acid functionalized dyes helps in adsorbing the dye to the metal oxide.[12] The advantage of this approach compared to such conventional dye-sensitized solar cells is the acid groups can contribute both binding to SnO_2 and binding the molecules to one another. Although the present system is rather complex relative to the dye-sensitized solar cells, such binding properties would be modulated by varying the chemical modification conditions (i.e., spin-coating, dipping, and electrophoretic deposition methods) to optimize the photoelectrochemical properties.

Scheme 2. Photocurrent generation diagram for ZnP-acid+C_{60}-acid/SnO_2/ITO system.

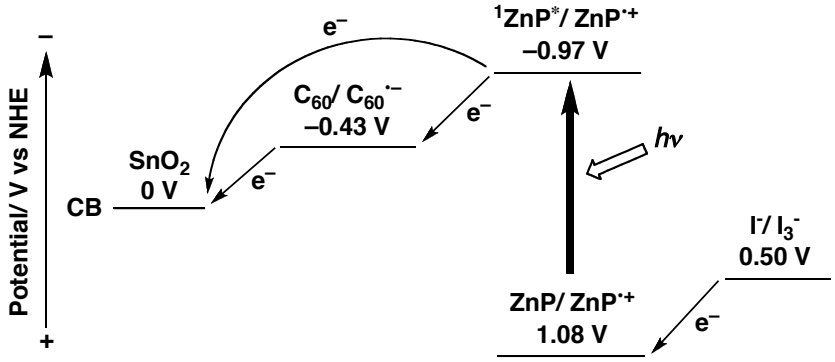

Conclusion

Hydrogen bonding effects on photocurrent generation have been examined in the mixed films of porphyrin and/or fullerene with and without hydrogen bonding on nanostructured SnO_2 electrodes. The nanostructured SnO_2 electrodes modified with the mixed films of porphyrin and fullerene with hydrogen bonding exhibit efficient photocurrent generation (up to IPCE value of 36%) as compared

to the reference systems without hydrogen bonding. Atomic force microscopy, infrared reflection absorption and ultraviolet-visible absorption spectroscopies, and time-resolved fluorescence lifetime and transient absorption measurements support the significant contribution of hydrogen bonding interaction between the porphyrins or the C_{60} moieties or the both in the films on the electrode surface for the photocurrent generation efficiency. These results show that hydrogen bonding is a highly promising methodology for the construction of molecular photoelectrochemical devices.

Experimental Section

General. Melting points were recorded on a Yanagimoto micro-melting point apparatus and not corrected. ^{1}H NMR spectra were measured on a JEOL EX-400 spectrometer. Matrix-assisted laser desorption/ionization (MALDI) time-of-flight mass spectra (TOF) were measured on a Kratos Compact MALDI I (Shimadzu). UV-visible absorption spectra were obtained on a Perkin Elmer Lambda 900UV/vis/NIR spectrometer. Infrared reflection absorption (IRRA) spectra were recorded by a Bio-Rad FTS 575C FT-IR spectrometer equipped with a liquid-N_2 cooled MCT detector and a Harrick Reflector™ grazing angle reflectance unit.[43] The samples for IRRA observation were prepared by direct deposition of these functional molecules on a slide glass (2×2 cm^2) covered by a 200 nm-thick gold film for IRRA observation, by spin-coating method. The IRRA spectrum of a bare gold film was used as the reference. The spectral resolution used was 4 cm^{-1}. AFM measurements were carried out using a Digital Nanoscope III in the tapping mode. Steady-state fluorescence spectra were measured on a Fluorolog 3 spectrofluorimeter (ISA Inc.) equipped with a cooled IR sensitive photomultiplier (R2658). All solvents and chemicals were of reagent grade quality, purchased commercially and used without further purification unless otherwise noted. Tetrabutylammonium hexafluorophosphate used as a supporting electrolyte for the electrochemical measurements was obtained from Fluka and recrystallized from methanol. Thin-layer chromatography and flash column chromatography were performed with Alt. 5554 DC-Alufolien Kieselgel 60 F_{254} (Merck) and Silica-gel 60N (Kanto Chemicals), respectively. ITO electrodes (190–200 nm ITO on transparent glass slides) were commercially available from Tokyo Sanyo Sinku. The roughness factor (R = 1.3) was estimated by AFM measurement with tapping mode.

Synthesis and Characterization.

Compound **1.** To solution of 3,5-dihexadecyloxybenzyl alcohol[26] (5.8 g, 9.85 mmol) in dried dichloromethane (90 mL), was added a suspension of PCC (5.5 g) in dried dichloromethane (20 mL) with stirring for 3.5 h at room temperature. The resulting mixture was filtered and the residue was washed with dichloromethane for several times. The filtrate was collected and the solvent was removed under reduced pressure. Flash column chromatography on silica gel (hexane/ethyl acetate =

96:4) afforded **1** as a white solid (4.4 g, 7.5 mmol, 76%): mp 54–55 °C; IR (KBr) 3100, 2953 2917, 2851, 1710, 1683, 1596, 1472, 1392, 1325, 1319, 1180, 1059, 943, 848, 834, 734, 717, 675 cm^{-1}; ^1H NMR (400 MHz, $CDCl_3$) δ 0.88 (t, J = 6.8 Hz, 6H), 1.26 (m, 52H), 1.79 (m, 4H), 3.98 (t, J = 6.4 Hz, 4H), 6.70 (t, J = 2.0 Hz, 1H), 6.98 (d, J = 2.0 Hz, 2H), 9.89 (s, 1H); MS (MALDI-TOF, positive mode) found 588 ($M+H^+$); Anal. Calcd for $C_{39}H_{70}O_3$: C, 79.80; H, 12.02. Found: C, 79.59; H, 12.05.

Compound **2.** A solution of 5-(4-methoxycarbonylphenyl)dipyrromethane[27] (1.40 g, 5 mmol) and **1** (2.93g, 5 mmol) in chloroform (500 mL) with stirring at room temperature under nitrogen was treated with boron trifluoride diethyl etherate (0.64 mL, 5.06 mmol).[27] After 2 hour, *p*-chloranil (1.86 g, 7.6 mmol) was added and the reaction mixture was stirred overnight. Triethylamine (2.1 mL, 15.2 mmol) was added and the resulting mixture was concentrated. Subsequent flash column chromatography on silica gel (hexane/toluene = 3:1→1:3) yielded **2** as a reddish purple solid (0.41 g, 0.24 mmol, 9.7%): mp 127–128 °C; IR (KBr) 3315, 2921, 2852, 1725, 1590, 1471, 1430, 1394, 1354, 1311, 1276, 1256, 1155, 1109, 1100, 1054, 1022, 974, 927, 848, 799, 778, 732, 720, 633 cm^{-1}; ^1H NMR (400 MHz, $CDCl_3$) δ –2.83 (br s, 2H), 0.85 (t, J = 6.8 Hz, 12H), 1.22 (m, 104H), 1.85 (m, 8H), 4.11 (t, J = 6.4 Hz, 8H), 4.12 (s, 6H), 6.88 (t, J = 2.0 Hz, 2H), 7.36 (d, J = 2.0 Hz, 4H), 8.30 (d, J = 8.4 Hz, 4H), 8.44 (d, J = 8.4 Hz, 4 H), 8.77 (d, J = 4.8 Hz, β-H, 4H), 8.98 (d, J = 4.8 Hz, β-H, 4H); MS (MALDI-TOF, positive mode) found 1693 ($M+H^+$).

Compound **3.** A mixture of **2** (0.17 g, 0.1 mmol) in 100 mL of THF/ethanol (1:1) and potassium hydroxide (0.513 g) in water (5 mL) was refluxed for 8 h. After cooling and the removal of solvent, the residue was diluted with water (100 mL) and desired porphyrin dipotassium salt was filtered. Acidification (pH 2) of an aqueous suspension of the porphyrin dipotassium salt with concentrated hydrochloric acid and subsequent filtration gave **3** as a reddish purple power (0.16 g, 0.1 mmol, 96%): mp > 300°C; IR (KBr) 3318, 3090, 2921, 2852, 2533, 1690, 1599, 1589, 1541 1467, 1430, 1383, 1354, 1310, 1292, 1250, 1162 1129, 1057, 1020, 974, 928, 849, 830, 799, 778, 724, 711, 699 cm^{-1}; ^1H NMR (400 MHz, $CDCl_3$/DMSO-d_6 = 3:2) δ –2.91 (br s, 2H), 0.83 (t, J = 6.0 Hz, 12H), 1.18 (m, 104H), 1.81 (m, 8H), 4.10 (t, J = 6.0 Hz, 8H), 6.86 (t, J = 2.0 Hz, 2H), 7.31 (d, J = 2.0 Hz, 4H), 8.20 (d, J = 8.0 Hz, 4H), 8.41(d, J = 8.0 Hz, 4H), 8.83 (d, J = 4.8 Hz, β-H, 4H), 8.95 (d, J = 4.8 Hz, β-H, 4H); MS (MALDI-TOF, positive mode) found 1665 ($M+H^+$).

ZnP-acid. To the solution of **3** (0.30 g, 0.18 mmol) in 300 mL of THF/ethanol (1:1) was added a solution of zinc acetate dihydrate (0.20 g, 0.91 mmol) in methanol (4 mL). The reaction mixture was refluxed for overnight. After cooling and following removal of solvent, the residue was treated with 150 mL of 1M HCl aqueous solution and 500 mL of $CHCl_3$ with stirring for overnight. The $CHCl_3$ layer was collected, washed with water for several times, dried over anhydrous Na_2SO_4, and concentrated in vacuo. The resulting solid was purified by chromatography on silica gel eluting with CH_2Cl_2/THF (95:5) to yield ZnP-acid as a purple red solid (0.30 g, 0.17 mmol, 96%): mp

281–282 °C; IR (KBr) 3096, 2923, 2852, 2667, 2542, 1691 1602, 1466, 1457, 1430, 1419, 1387, 1350, 1312, 1287, 1205, 1166, 1127, 1071, 1057, 998, 946, 796, 719, 698 cm^{-1}; ^1H NMR (400 MHz, $CDCl_3$) δ 0.85 (t, J = 6.8 Hz 12H), 1.22 (m, 104 H), 1.86 (m, 8H), 4.22 (t, J = 6.0 Hz, 8H), 6.90 (t, J = 2.0 Hz, 2H), 7.38 (d, J = 2.0 Hz, 4H), 8.34 (d, J = 8.4 Hz, 4H), 8.50 (d, J = 7.6 Hz, 4 H), 8.89 (d, J = 4.8 Hz, β-H, 4H), 9.11 (d, J = 4.8 Hz, β-H, 4H); MS (MALDI-TOF, positive mode) found 1727 ($M+H^+$).

ZnP-ester. To the solution of **2** (0.10 g, 0.06 mmol) in 100 mL of $CHCl_3$ was added a solution of zinc acetate dihydrate (0.10 g, 0.46 mmol) in methanol (2 mL). The mixture was refluxed for 3 h. After cooling, the resulting solution was washed with saturated sodium bicarbonate aqueous solution and water successively and dried over Na_2SO_4, and then the solvent was evaporated. The resulting solid was purified by chromatography on silica gel eluting with CH_2Cl_2 to yield ZnP-ester as a red purple solid (0.09 g, 0.05 mmol, 90%): mp 86–87 °C; IR (KBr) 3440, 2921, 2852, 1724, 1696, 1591, 1470 1433, 1394, 1348, 1273, 1154, 1111, 1099, 1053, 998, 945, 797, 719 cm^{-1}; ^1H NMR (400 MHz, $CDCl_3$) δ 0.85 (t, J = 6.8 Hz, 12H), 1.21 (m, 104H), 1.84 (m, 8H), 4.09 (t, J = 6.4 Hz, 8H), 4.10 (s, 6H), 6.86 (t, J = 2.0 Hz, 2H), 7.36 (d, J = 2.0 Hz, 4H), 8.29 (d, J = 8.4 Hz, 4H), 8.42 (d, J = 8.0 Hz, 4H), 8.87 (d, J = 4.8 Hz, β-H, 4H), 9.08 (d, J = 4.8 Hz, β-H, 4H); MS (MALDI-TOF, positive mode) found 1754 ($M+H^+$).

Preparation of Films. Porous nanostructured SnO_2 films were fabricated by repeated spin-coating of 10% colloidal solution (pH 10, Chemat Technology) onto optically transparent ITO electrode, followed by drying at 473 K for 10 minutes.[20] Finally, the dried films were annealed at 673 K for one hour. The nanostructured SnO_2 film electrode is referred as SnO_2/ITO. The thickness of SnO_2 layer was determined using surface roughness/profile measuring instrument (SURFCOM 130A, ACCRETECH). The thicknesses of SnO_2 layer on the ITO electrode prior to chemical modification were 0.4 μm and 1.1 μm in this study where organic layers were further deposited by spin-coating and dipping methods, respectively. A known amount of ZnP, C_{60} or the mixed solution in THF was spin-coated onto ITO or SnO_2/ITO or gold electrodes (spin-coating method). Modification of ITO or SnO_2/ITO electrode was also carried out by immersing the SnO_2/ITO electrode into the THF solution containing the compounds, followed by washing the substrate with THF repeatedly (dipping method). The characterization of photochemical behavior was carried out on the ITO and/or SnO_2/ITO substrates, while that of IRRA absorption was performed on the gold substrate.

Photoelectrochemical Measurements. Photoelectrochemical measurements were performed in a one-compartment Pyrex UV cell (5 mL) with nitrogen-saturated electrolyte solution containing 0.5 M LiI and 0.01 M I_2 in acetonitrile. The samples were excited with monochromatic light using a 500 W Xe arc lamp (Ritsu UXL-500D-0) coupled with a monochromator (Ritsu MC-10N). The illuminated area on the modified surface was 0.20 cm^2. The light intensity was modulated with

neutral density filters (HOYA). The casting film was immersed into the electrolyte solution containing 0.5 M LiI and 0.01 M I_2 in acetonitrile as a working electrode. The photocurrent was measured in a three-electrode arrangement, a modified SnO_2/ITO working electrode, a platinum wire counter electrode (the distance between the electrodes is 0.3 mm), and an I^-/I_3^- reference electrode using an ALS 630a electrochemical analyzer. The light intensity was monitored by an optical power meter (Anritsu ML9002A) and corrected. The I^-/I_3^- reference electrode was made from platinum wire covered with glass ruggin capillary filled with the acetonitrile solution containing 0.5 M LiI and 0.01 M I_2. The potential measured was converted to the saturated calomel electrode (SCE) scale by adding +0.05 V. The stability of the reference electrode potential was confirmed under the experimental conditions.

Spectral Measurements. A pump-probe method was used to measure transient absorption spectra in sub-picosecond-nanosecond time domain. The measurements were carried out using the instrument described previously.[39] The transient spectra were recorded by a CCD detector coupled with a monochromator in the visible and near infrared ranges. The second harmonic (420 nm) of Ti:sapphire laser was used for the excitation. In addition, the samples were excited at 555 nm using an optical parametric amplifier (CDP 2017, CDP Inc., Russia) after multipass femtosecond amplifier and mixing base harmonic with idle beam of the parametric amplifier. A typical time resolution of the instrument was 200–300 fs (FWHM). Emission decays were measured using a time-correlated single photon counting (TCSPC) technique. The excitation wavelength was 590 nm and the time resolution was 40 ps.

References and Footnotes

(1) (a) *The Photosynthetic Reaction Center*; Deisenhofer, J., Norris, J. R., Eds.; Academic Press: San Diego, 1993. (b) *Anoxygenic Photosynthetic Bacteria*; Blankenship, R. E., Madigan, M. T., Bauer, C. E., Eds.; Kluwer Academic Publishers: Dordrecht, 1995.

(2) (a) Lehn, J.-M. *Supramolecular Chemistry: Concepts and Perspectives*; VCH, Weinheim, 1995. (b) Sessler, J. L.; Wang, B.; Springs, S. L.; Brown, C. T. In *Comprehensive Supramolecular Chemistry*; Atwood, J. L., Davies, J. E. D., Eds.; Pergamon, 1996. (c) Chang, C. J.; Brown, J. D. K.; Chang, M. C. Y.; Baker, E. A.; Nocera, D. G. In *Electron Transfer in Chemistry*; Balzani, V. Ed.; Wiley-VCH: Weinheim, 2001; Vo. 2, pp 408–461. (d) *Molecular Catenanes, Rotaxanes and Knots*, Sauvage, J.-P., Dietrich-Buchecker, C. Eds.; Wiley-VCH: Weinheim, 1999.

(3) (a) Hunter, C. A.; Sanders, J. K. M.; Beddard, G. S.; Evans, S. *Chem. Commun.* **1989**, 1765. (b) Anderson, H. L.; Hunter, C. A.; Sanders, J. K. M. *J. Chem. Soc., Chem. Commun.* **1989**, 226. (c) McClenaghan, N. D.; Grote, Z.; Darriet, K.; Zimine, M.; Williams, R. M.; De Cola, L.; Bassani,

D. M. *Org*. *Lett*. **2005**, *7*, 807. (d) Smitha, M. A.; Prasad, E.; Gopidas, K. R. *J*. *Am*. *Chem*. *Soc*. **2001**, *123*, 1159. (e) Prasad, E.; Gopidas, K. R. *J*. *Am*. *Chem*. *Soc*. **2000**, *122*, 3191.

(4) (a) de Rege, P. J. F.; Williams, S. A.; Therien, M. J. *Science* **1995**, *269*, 1409. (b) Harriman, A.; Magda, D. J.; Sessler, J. L. *Chem*. *Commun*. **1991**, 345. (c) Sessler, J. L.; Wang, B.; Harriman, A. *J*. *Am*. *Chem*. *Soc*. **1995**, *117*, 704. (d) Berman, A.; Izraeli, E. S.; Levanon, H.; Wang, B.; Sessler, J. L. *J*. *Am*. *Chem*. *Soc*. **1995**, *117*, 8252.

(5) (a) Hayashi, T.; Ogoshi, H. *Chem*. *Soc*. *Rev*. **1997**, *26*, 355. (b) Blanco, M.-J.; Jiménez, M. C.; Chambron, J.-C.; Heitz, V.; Linke, M.; Sauvage, J.-P. *Chem*. *Soc*. *Rev*. **1999**, *28*, 293. (c) Willner, I.; Kaganer, E.; Joselevich, E.; Dürr, H.; David, E.; Günter, M. J.; Johnston, M. R. *Coord*. *Chem*. *Rev*. **1998**, *171*, 261. (d) Jensen, H.; Kakkassery, J. J.; Nagatani, H.; Fermin, D. J.; Girault, H. H. *J*. *Am*. *Chem*. *Soc*. **2000**, *122*, 10943.

(6) (a) D'Souza, F.; Rath, N. P.; Deviprasad, G. R.; Zandler, M. E. *Chem*. *Commun*. **2001**, 267. (b) D'Souza, F.; Deviprasad, G. R.; El-Khouly, M. E.; Fujitsuka, M.; Ito, O. *J*. *Am*. *Chem*. *Soc*. **2001**, *123*, 5277. (c) D'Souza, F.; Deviprasad, G. R.; Rahman, M. S.; Choi, J. *Inorg*. *Chem*. **1999**, *38*, 2157. (d) D'Souza, F.; Zandler, M. E.; Smith, P. M.; Deviprasad, G. R.; Arkady, K.; Fujitsuka, M.; Ito, O. *J*. *Phys*. *Chem*. *A* **2002**, *106*, 649. (e) D'Souza, F.; Deviprasad, G. R.; Zandler, M. E.; El-Khouly, M. E.; Fujitsuka, M.; Ito, O. *J*. *Phys*. *Chem*. *A* **2003**, *107*, 4801. (f) D'Souza, F.; Smith, P. M.; Zandler, M. E.; McCarty, A. L.; Itou, M.; Araki, Y.; Ito, O. *J*. *Am*. *Chem*. *Soc*. **2004**, *126*, 7898.

(7) (a) Otsuki, J.; Harada, K.; Toyama, K.; Hirose, Y.; Araki, K.; Seno, M.; Takatera, K.; Watanabe, T. *Chem*. *Commun*. **1998**, 1515. (b) Imahori, H.; Yoshizawa, E.; Yamada, K.; Hagiwara, K.; Okada, T.; Sakata, Y. *Chem*. *Commun*. **1995**, 1133. (c) Imahori, H.; Yamada, K.; Yoshizawa, E.; Hagiwara, K.; Okada, T.; Sakata, Y. *J*. *Porphyrins and Phthalocyanines* **1997**, *1*, 55. (d) Yamada, K.; Imahori, H.; Yoshizawa, E.; Gosztola, D.; Wasielewski, M. R.; Sakata, Y. *Chem*. *Lett*. **1999**, 235.

(8) (a) Da Ros, T.; Prato, M.; Guldi, D. M.; Ruzzi, M.; Pasimeni, L. *Chem*. *Eur*. *J*. **2001**, *7*, 816. (b) Armaroli, N.; Diederich, F.; Echegoyen, L.; Habicher, T.; Flamigni, L.; Marconi, G.; Nierengarten, J.-F. *New*. *J*. *Chem*. **1999**, 77. (c) D'Souza, F. *J*. *Am*. *Chem*. *Soc*. **1996**, *118*, 923.

(9) (a) Guldi, D. M.; Martín, N. *J*. *Mater*. *Chem*. **2002**, *12*, 1978. (b) Segura, M.; Sanchez, L.; de Mendoza, J.; Martín, N.; Guldi, D. M. *J*. *Am*. *Chem*. *Soc*. **2003**, *125*, 15093. (c) Fang, H.; Wang, S.; Xiao, S.; Yang, J.; Liu, Y.; Shi, Z.; Li, H.; Liu, H.; Xiao, S.; Zhu, D. *Chem*. *Mater*. **2003**, *15*, 1593.

(10) (a) Beckers, E. H. A.; Schenning, A. P. H. J.; van Hal, P. A.; El-ghayoury, A.; Sanchez, L.; Hummelen, J. C.; Meijer, E. W.; Janssen, R. A. J. *Chem*. *Commun*. **2002**, 2888. (b) Beckers, E. H. A.; van Hal, P. A.; Schenning, A. P. H. J.; El-ghayoury, A.; Peeters, E.; Rispens, M. T.;

Hummelen, J. C.; Meijer, E. W.; Janssen, R. A. J. *J. Mater. Chem.* **2002**, 2054. (c) Neuteboom, E. E.; Beckers, E. H. A.; Meskers, S. C. J.; Meijer, E. W.; Janssen, R. A. J. *Org. Biomol. Chem.* **2003**, *1*, 198.

(11) (a) Li, K.; Schuster, D. I.; Guldi, D. M.; Herranz, M. A.; Echegoyen, L. *J. Am. Chem. Soc.* **2004**, *126*, 3388. (b) Li, K.; Bracher, P. J.; Guldi, D. M.; Herranz, M. A.; Echegoyen, L.; Schuster, D. I. *J. Am. Chem. Soc.* **2004**, *126*, 9156.

(12) (a) Hagfeldt, A.; Grätzel, M. *Acc. Chem. Res.* **2000**, 33, 269. (b) Grätzel, M. *Nature* **2001**, *414*, 338. (c) Bignozzi, C. A.; Argazzi, R.; Kleverlaan, C. J. *Chem. Soc. Rev.* **2000**, *29*, 87.

(13) (a) Yu, G.; Gao, J.; Hummelen, J. C.; Wudl, F.; Heeger, A. J. *Science* **1995**, *270*, 1789. (b) Wudl, F. *J. Mater. Chem.* **2002**, *12*, 1959.

(14) (a) Shaheen, S. E.; Brabec, C. J.; Sariciftci, N. S.; Padinger, F.; Fromherz, T.; Hummelen, J. C. *Appl. Phys. Lett.* **2001**, *78*, 841. (b) Padinger, F.; Rittberger, R. S.; Sariciftci, N. S. *Adv. Funct. Mater.* **2003**, *13*, 85.

(15) (a) Schmidt-Mende, L.; Fechtenkötter, A.; Müllen, K.; Moons, E.; Friend, R. H.; MacKenzie, J. D. *Science* **2001**, *293*, 1119. (b) Halls, J. J. M.; Walsh, C. A.; Greenham, N. C.; Marseglia, E. A.; Friend, R. H.; Moratti, S. C.; Holmes, A. B. *Nature* **1995**, *376*, 498. (c) Granström, M.; Petritsch, K.; Arias, A. C.; Lux, A.; Andersson, M. R.; Friend, R. H. *Nature* **1998**, *395*, 257. (d) Huynh, W. U.; Dittmer, J. J.; Alivisatos, A. P. *Science* **2002**, *295*, 2425. (e) Liu, J.; Tanaka, T.; Sivula, K.; Alivisatos, A. P.; Fréchet, J. M. J. *J. Am. Chem. Soc.* **2004**, *126*, 6550.

(16) (a) Tsuzuki, T.; Shirota, Y.; Rostalski, J.; Meissner, D. *Solar Energy Mater. Solar Cells* **2000**, *61*, 1. (b) Xue, J.; Rand, B. P.; Uchida, S.; Forrest, S. R. *Adv. Mater.* **2005**, *17*, 66.

(17) (a) Wienk, M. M.; Kroon, J. M.; Verhees, W. J. H.; Knol, J.; Hummelen, J. C.; van Hal, P. A.; Janssen, R. A. J. *Angew. Chem. Ind. Ed.* **2003**, *42*, 3371. (b) Dhanabalan, A.; van Duren, J. K. J.; van Hal, P. A.; van Dongen, J. L. J.; Janssen, R. A. J. *Adv. Funct. Mater.* **2001**, *11*, 255.

(18) (a) Eckert, J.-F.; Nicoud, J.-F.; Nierengarten, J.-F.; Liu, S.-G.; Echegoyen, L.; Barigelletti, F.; Armaroli, N.; Ouali, L.; Krasnikov, V.; Hadziioannou, G. *J. Am. Chem. Soc.* **2000**, *122*, 7467. (b) Lahav, M.; Heleg-Shabtai, V.; Wasserman, J.; Katz, E.; Willner, I.; Dürr, H.; Hu, Y.-Z.; Bossmann, S. H. *J. Am. Chem. Soc.* **2000**, *122*, 11480.

(19) (a) Liu, Y.; Xiao, S.; Li, H.; Li, Y.; Liu, H.; Lu, F.; Zhuang, J.; Zhu, D. *J. Phys. Chem. B* **2004**, *108*, 6256. (b) Imahori, H.; Liu, J.-C.; Hosomizu, K.; Sato, T.; Mori, Y.; Hotta, H.; Matano, Y. Araki, Y.; Ito, O.; Maruyama, N.; Fujita, S. *Chem. Commun.* **2004**, 2066.

(20) (a) Hasobe, T.; Imahori, H.; Fukuzumi, S.; Kamat, P. V. *J. Phys. Chem. B* **2003**, *107*, 12105. (b) Hasobe, T.; Kashiwagi, Y.; Absalom, M. A.; Sly, J.; Hosomizu, K.; Crossley, M. J.; Imahori, H.; Kamat, P. V.; Fukuzumi, S. *Adv. Mater.* **2004**, *16*, 975. (c) Hasobe, T.; Imahori, H.; Kamat, P. V.; Fukuzumi, S. *J. Am. Chem. Soc.* **2003**, *125*, 14962. (d) Imahori, H. *J. Phys. Chem. B* **2004**, *108*,

6130. (e) Imahori, H.; Fukuzumi, S. *Adv. Funct. Mater.* **2004**, *14*, 525.

(21) (a) Imahori, H.; Sakata, Y. *Adv. Mater.* **1997**, *9*, 537. (b) Imahori, H.; Sakata, Y. *Eur. J. Org. Chem.* **1999**, 2445. (c) Imahori, H.; Mori, Y.; Matano, Y. *J. Photochem. Photobiol. C* **2003**, 4, 51. (d) Imahori, H. *Org. Biomol. Chem.* **2004**, *2*, 1425.

(22) (a) Fukuzumi, S.; Guldi, D. M. In *Electron Transfer in Chemistry*; Balzani, V., Ed.; Wiley-VCH: Weinheim, 2001; Vol. 2, pp 270–337. (b) Guldi, D. M.; Prato, M. *Acc. Chem. Res.* **2000**, *33*, 695. (c) Gust, D.; Moore, T. A.; Moore, A. L. *Acc. Chem. Res.* **2001**, *34*, 40.

(23) (a) Evans, D. R.; Fackler, N. L. P.; Xie, Z.; Rickard, C. E. F.; Boyd, P. D. W.; Reed, C. A. *J. Am. Chem. Soc.* **1999**, *121*, 8466. (b) Sun, D.; Tham, F. S.; Reed, C. A.; Chaker, L.; Boyd, P. D. W. *J. Am. Chem. Soc.* **2002**, *124*, 6604. (c) Tashiro, K.; Aida, T.; Zheng, J.-Y.; Kinbara, K.; Saigo, K.; Sakamoto, S.; Yamaguchi, K. *J. Am. Chem. Soc.* **1999**, *121*, 9477.

(24) (a) Yamaguchi, T.; Ishii, N.; Tashiro, K.; Aida, T. *J. Am. Chem. Soc.* **2003**, *125*, 13934. (b) Kimura, M.; Saito, Y.; Ohta, K.; Hanabusa, K.; Shirai, H.; Kabayashi, N. *J. Am. Chem. Soc.* **2002**, *124*, 5274. (c) Shirakawa, M.; Fujita, N.; Shinkai, S. *J. Am. Chem. Soc.* **2003**, *125*, 9902.

(25) (a) Imahori, H.; Hagiwara, K.; Aoki, M.; Akiyama, T.; Taniguchi, S.; Okada, T.; Shirakawa, M.; Sakata, Y. *J. Am. Chem. Soc.* **1996**, *118*, 11771. (b) Imahori, H.; Tkachenko, N. V.; Vehmanen, V.; Tamaki, K.; Lemmetyinen, H.; Sakata, Y.; Fukuzumi, S. *J. Phys. Chem. A* **2001**, *105*, 1750. (c) Tkachenko, N. V.; Guenther, C.; Imahori, H.; Tamaki, K.; Sakata, Y.; Fukuzumi, S.; Lemmetyinen, H. *Chem. Phys. Lett.* **2000**, *326*, 344. (d) Vehmanen, V.; Tkachenko, N. V.; Imahori, H.; Fukuzumi, S.; Lemmetyinen, H. *Spectrochimica Acta, Part A* **2001**, *57*, 2229. (e) Guldi, D. M.; Luo, C.; Prato, M.; Troisi, A.; Zerbetto, F.; Scheloske, M.; Dietel, E.; Bauer, W.; Hirsch, A. *J. Am. Chem. Soc.* **2001**, *123*, 9166.

(26) Nierengarten, J.-F.; Eckert, J.-F.; Rio, Y.; del Pilar Carreon, M. P.; Gallani, J.-L.; Guillon, D. *J. Am. Chem. Soc.* **2001**, *123*, 9743.

(27) Luo, C.; Guldi, D. M.; Imahori, H.; Tamaki, K.; Sakata, Y. *J. Am. Chem. Soc.* **2000**, *122*, 6535.

(28) (a) Pasimeni, L.; Hirsch, A.; Lamparth, I.; Maggini, M.; Prato, M. *J. Am. Chem. Soc.* **1997**, *119*, 12902. (b) Camps, X.; Hirsch, A. *J. Chem. Soc., Perkin Trans. 1* **1997**, 1595.

(29) Colthup, N. B.; Daly, L. H.; Wiberley, S. E. *Introduction to Infrared and Raman Spectroscopy*. 3rd ed.; Academic Press, Inc.: San Diego, CA, 1990.

(30) Génin, F.; Quilès, F.; Burneau, A. *Phys. Chem. Chem. Phys.* **2001**, *3*, 932.

(31) Dong, J.; Ozaki, Y. *Macromolecules* **1997**, *30*, 286.

(32) Ye, S.; Morita, S.; Li, G.; Noda, H.; Tanaka, M.; Uosaki, K.; Osawa, M., *Macromolecules* **2003**, 36, 5694.

(33) Li, G.; Ye, S.; Morita, S.; Nishida, T.; Osawa, M. *J. Am. Chem. Soc.* **2004**, *126*, 12198.

(34) (a) Durrant, J. R.; Haque, S. A.; Palomares, E. *Coord. Chem. Rev.* **2004**, *248*, 1247. (b) Gregg, B.

A. *Coord. Chem. Rev.* **2004**, *248*, 1215. (c) Katoh, R.; Furube, A.; Barzykin, A. V.; Arakawa, H.; Tachiya, M. *Coord. Chem. Rev.* **2004**, *248*, 1195. (d) Tachibana, Y.; Moser, J. E.; Grätzel, M.; Klug, D. R.; Durrant, J. R. *J. Phys. Chem.* **1996**, *100*, 20056. (e) Kay, A.; Humphry-Baker, R.; Grätzel, M. *J. Phys. Chem.* **1994**, *98*, 952. (f) Clifford, J. N.; Palomares, E.; Nazeeruddin, M. K.; Grätzel, M.; Nelson, J.; Li, X.; Long, N. J.; Durrant, J. R. *J. Am. Chem. Soc.* **2004**, *126*, 5225.

(35) (a) Ellingson, R. J.; Asbury, J. B.; Ferrere, S.; Ghosh, H. N.; Sprague, J. R.; Lian, T. Q.; Nozik, A. J. *J. Phys. Chem. B* **1998**, *102*, 6455. (b) Fessenden, R. W.; Kamat, P. V. *J. Phys. Chem.* **1995**, *99*, 12902. (c) Asbury, J. B.; Hao, E.; Wang, Y. Q.; Ghosh, H. N.; Lian, T. Q. *J. Phys. Chem. B* **2001**, *105*, 4545. (d) Watson, D. F.; Marton, A.; Stux, A. M.; Meyer, G. J. *J. Phys. Chem. B* **2004**, *108*, 11680. (e) Wienke, J.; Schaafsma, T. J.; Goossens, A. *J. Phys. Chem. B* **1999**, *103*, 2702. (g) Koehorst, R. B. M.; Boschloo, G. K.; Savenije, T. J.; Goossens, A.; Schaafsma, T. J. *J. Phys. Chem. B* **2000**, *104*, 2371. (h) Fungo, F.; Otero, L.; Durantini, E. N.; Silber, J. J.; Sereno, L. E. *J. Phys. Chem. B* **2000**, *104*, 7644.

(36) The author also examined the effect of the relative ratios of ZnP-acid and C_{60}-acid on the IPCE values under the same experimental conditions. The largest IPCE value (36%) was obtained when a mixed solution with the relative ratio of [ZnP-acid]:[C_{60}-acid] = 1:1 was employed for the preparation of the modified SnO_2 electrode.

(37) Thickness of the SnO_2 layer (0.1–1.1 μm) on the ITO electrode was also varied to optimize the IPCE value. The largest IPCE value (36%) was achieved when the thickness of the SnO_2 layer was 1.1 μm. Further increase of the thickness of the SnO_2 layer resulted in the formation of extremely rough SnO_2 layer.

(38) The weak emission from the C_{60} moiety (C_{60}-acid) may be attributed to the direct excitation of the C_{60} moiety in which some part of the identical C_{60}-acid molecules form hydrogen-bonded aggregates without making a supramolecular complex with the zincporphyrin, as suggested from the IRRA spectra.

(39) (a) Tkachenko, N. V.; Rantala, L.; Tauber, A. Y.; Helaja, J.; Hynninen, P. H.; Lemmetyinen, H. *J. Am. Chem. Soc.* **1999**, 121, 9378. (b) Kesti, T. J.; Tkachenko, N. V.; Vehmanen, V.; Yamada, H.; Imahori, H.; Fukuzumi, S.; Lemmetyinen, H. *J. Am. Chem. Soc.* **2002**, *124*, 8067. (c) Tkachenko, N. V.; Lemmetyinen, H.; Sonoda, J.; Ohkubo, K.; Sato, T.; Imahori, H.; Fukuzumi, S. *J. Phys. Chem. A* **2003**, *107*, 8834.

(40) The author also tried to measure the fluorescence lifetimes on SnO_2 electrodes using up-conversion method (time resolution, ~100 fs), but it was not possible because the excitation light destroys the sample at the excitation spot very quickly.

(41) Reliable conclusion could not be drawn from the transient absorption spectra of ZnP-acid+C_{60}-acid/SnO_2/ITO, ZnP-acid+C_{60}-ester/SnO_2/ITO, and ZnP-ester+C_{60}-acid/SnO_2/ITO

systems because of the weak signals and the degradation of the samples under laser irradiation.

(42) The first reduction and oxidation potentials were determined by using cyclic voltammetric measurements in THF containing 0.1 M Bu_4NPF_6. The energy level of porphyrin excited singlet state was estimated to be 2.05 eV in THF from the absorption and emission spectra.

(43) Li, G.; Morita, S.; Ye, S.; Tanaka, M.; Osawa, M. *Anal. Chem.* **2004**, *76*, 788.

Chapter 5

Hydrogen Bonding Effects on Film Structure and Photoelectrochemical Properties of Porphyrin and Fullerene Composites on Nanostructured TiO_2 Electrodes

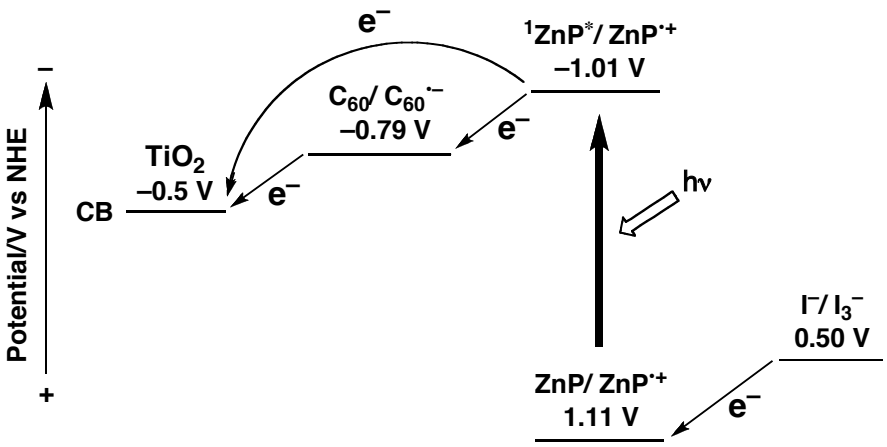

Abstract

Hydrogen bonding effects on film structures and photophysical, photoelectrochemical and photovoltaic properties have been examined in mixed films of porphyrin and fullerene composites with and without hydrogen bonding on nanostructured TiO_2 electrodes. The nanostructured TiO_2 electrodes modified with the mixed films of porphyrin and fullerene composites with hydrogen bonding exhibited efficient photocurrent generation compared to the reference systems without hydrogen bonding. Atomic force microscopy, infrared reflection absorption and ultraviolet-visible absorption spectroscopies, and time-resolved fluorescence lifetime and transient absorption spectroscopic measurements disclosed the relationship between the film structures and optical and photoelectrochemical properties relating to the formation of hydrogen bonding between the porphyrins and/or the C_{60} moieties in the films on the electrode surface. These results show that hydrogen bonding is a potential methodology for the fabrication of donor and acceptor composites on a nanostructured TiO_2 electrode, which exhibits high open circuit potential relative to that of the corresponding SnO_2 electrode.

Introduction

Fullerenes have exhibited excellent electron transfer (ET) properties as acceptors (A) owing to small reorganization energies of ET.[1,2] The small reorganization energies have allowed us to accelerate photoinduced charge separation (CS) and charge-shift and decelerate charge recombination (CR) in donor (D)-fullerene linked systems.[1–3] The unique ET properties also rationalize the frequent utilization of fullerenes and their derivatives in organic electronics including organic transistors and photovoltaic devices exhibiting high performance characteristics.[4] Specifically, typical bulk heterojunction solar cells involve an active photovoltaic layer consisting of a blend of conjugated polymer and fullerene derivative[5] or of small donor molecule and pristine fullerene.[6] It has been well recognized that an intimate mixing of the components leads to increases in both interface area and percolation of the donor-acceptor (D-A) components. The desirable bulk heterojunction architectures have been prepared by changing spin-coating solvents and annealing the blend films.[7]

Another potential approach to construct such D-A architectures is based on supramolecular assembly of preprogrammed D-A molecules on electrodes. Weak noncovalent interactions such as hydrogen bonding, π-π interaction, and coordination bonding can be introduced into D-A molecules to create bulk heterojunction layers with a phase-separated, interpenetrating network involving nanostructured hole- and electron-transporting highways. Although noncovalently-linked donor-fullerene systems have been prepared to reveal photoinduced energy transfer and ET in solutions,[8–12] there have been few examples where non-covalent bonding strategy has been employed in a mixed film of donor and fullerene to improve photocurrent generation efficiency in photoelectrochemical devices and photovoltaics.[13,14]

The author has applied step-by-step self-assembly to porphyrin and fullerene single components and the composites to construct a novel organic solar cell (dye-sensitized bulk heterojunction solar cell), possessing both the dye-sensitized and bulk heterojunction characteristics.[15–19] The author has already found that there is specific π-π interaction between porphyrin and fullerene in the ground and excited states.[20,21] The specific interaction between porphyrin and fullerene is suitable for electrophoretic deposition of the composite clusters. Bearing this in mind, the author prepares a supramolecular complex of porphyrin and fullerene in toluene employing the π-π interaction (step 1).[15–19] Then, the supramolecular complexes are self-assembled into larger clusters in a mixture of toluene and acetonitrile due to lyophobic interaction between the complex and the mixed solvent (step 2). Finally, the larger clusters can be further associated onto a nanostructured SnO_2 electrode using the electrophoretic deposition technique.[22] The self-assembled composite cluster films assembled by this bottom-up technique have exhibited an incident photon-to-current efficiency (IPCE) of up to 50–60% and a power conversion efficiency (η) of up to 1.5%.[15–19] However, taking into account the fact that the open circuit potential (V_{OC}) of dye-sensitized solar cells depends on the difference in the

conduction band (CB) edge energies (E_{CB}) of semiconducting electrodes and the redox potential of I^-/I_3^- couple, replacement of the SnO_2 electrode by other semiconducting electrodes bearing more negative E_{CB} values is an appealing approach to improve the cell performance.

Here, the author reports the first mixed films of porphyrin and fullerene with hydrogen bonding on a titanium oxide (TiO_2) electrode of which the E_{CB} value is more negative than that of the SnO_2 electrode. The porphyrin and fullerene compounds used in this study are shown in Figure 1. It is important to note that the energy level of $C_{60}^{\bullet-}$ (–0.2 V vs NHE)[15–19] is higher than the CB of SnO_2 electrode (0 V vs NHE),[15–19] but lower by 0.3 V than the CB of TiO_2 electrode (–0.5 V vs NHE).[23] Thus, no pristine C_{60} can be applied to the dye-sensitized bulk heterojunction solar cell with TiO_2 electrode instead of SnO_2 electrode. To realize stepwise electron injection from the porphyrin excited singlet state (–1.0 V vs NHE)[23] to the CB of TiO_2 electrode via C_{60}, the author focused on bis(ethoxycarbonyl)methylene polyadducts and the corresponding malonic acids of C_{60}.[24] The first reduction potential of C_{60} ($E_{red}^{0/-1}$ = –0.2 V vs NHE)[15–19] is shifted to a negative direction by ca. 0.1 V with an increase in the number of the addition sites on a C_{60} surface.[24] Thus, the hexakisadduct of C_{60} malonic acids (denoted as C_{60}-acid) was chosen by reason of the suitable reduction potential ($E_{red}^{0/-1}$ = –0.79 V vs NHE), the multiple hydrogen-bonding sites, and the T_h high symmetry, together with the C_{60} reference without hydrogen-bonding moiety (denoted as C_{60}-ester, $E_{red}^{0/-1}$ = –0.80 V vs NHE). Four carboxyl and methoxycarbonyl groups were also introduced to *para*-positions of the *meso*-phenyl groups in 5,10,15,20-tetraphenylporphyrinatozinc (II) to yield zincporphyrin (ZnP) acid and ester as a donor (denoted as ZnP-acid and ZnP-ester, respectively).[25] Single components of ZnP-acid, ZnP-ester, C_{60}-acid, and C_{60}-ester and the combinations will allow us to evaluate the hydrogen bonding effects on the film structures and optical, photoelectrochemical, and photovoltaic properties of the D-A composites on TiO_2 electrodes.

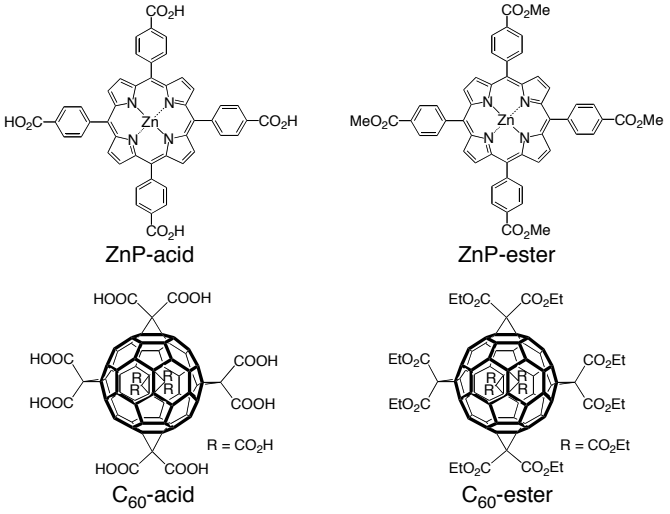

Figure 1. Porphyrin and fullerene derivatives used in this study.

Results and Discussion

Characterization of TiO_2 Electrodes Modified with Porphyrin and Fullerene Composites. An equimolar DMF solution (1.0 mM) of porphyrin (ZnP-acid, ZnP-ester) and/or fullerene (C_{60}-acid, C_{60}-ester) was spin-coated onto a TiO_2 electrode to give a modified TiO_2 electrode. Figure 2 shows absorption spectra of a mixed film of ZnP-acid and C_{60}-acid (denoted as TiO_2/ZnP-acid+C_{60}-acid), a film of ZnP-acid (denoted as TiO_2/ZnP-acid), and the equimolar DMF solution of ZnP-acid and C_{60}-acid (denoted as ZnP-acid+C_{60}-acid). The Q bands of TiO_2/ZnP-acid+C_{60}-acid and TiO_2/ZnP-acid are broadened and red shifted relative to that of ZnP-acid+C_{60}-acid in DMF due to the interaction between the porphyrins in the films. It is noteworthy that the absorption of TiO_2/ZnP-acid+C_{60}-acid is almost linear combination of absorption spectra of TiO_2/ZnP-acid and of C_{60}-acid film (denoted as TiO_2/C_{60}-acid) (Figure 3a). Therefore, no broad absorption at around 600–800 nm due to the charge-transfer (CT) interaction between ZnP-acid and C_{60}-acid[20,21] is observed for the absorption spectrum of TiO_2/ZnP-acid+C_{60}-acid. This implies that no CT complexes are formed, because the large steric hindrance on the C_{60} surface due to the six substituents does not allow the porphyrin molecule to make direct contact between the porphyrin and C_{60} molecules (vide infra). Similar results are obtained for the absorption spectrum of TiO_2/ZnP-acid+C_{60}-ester (Figure 3b).

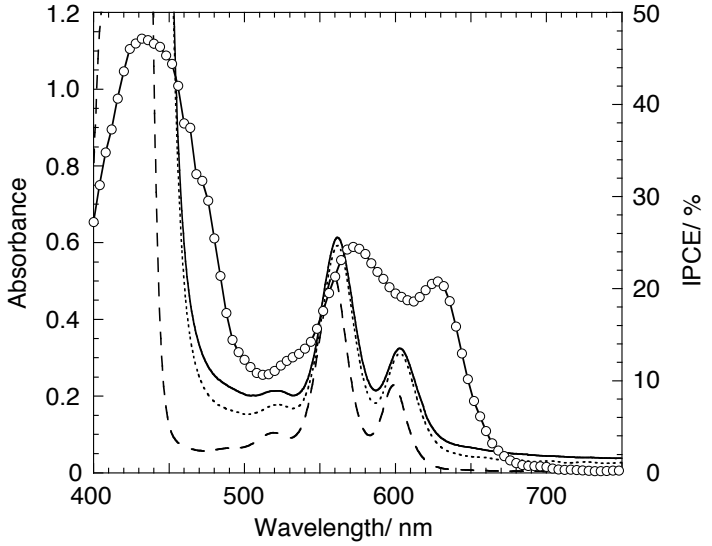

Figure 2. UV-visible absorption spectra of a mixed film of ZnP-acid and C_{60}-acid (TiO_2/ZnP-acid+C_{60}-acid, solid line), a film of ZnP-acid (TiO_2/ZnP-acid, dotted line), an equimolar DMF solution of ZnP-acid and C_{60}-acid (ZnP-acid+C_{60}-acid, dashed line), and action spectrum of TiO_2/ZnP-acid+C_{60}-acid system (solid line with open circles); applied potential: 0.10 V vs SCE; 0.5 M LiI and 0.01 M I_2 in acetonitrile. The modified TiO_2 electrodes were prepared by spin-coating an equimolar DMF solution (1.0 mM) of ZnP-acid and/or C_{60}-acid onto a TiO_2 electrode.

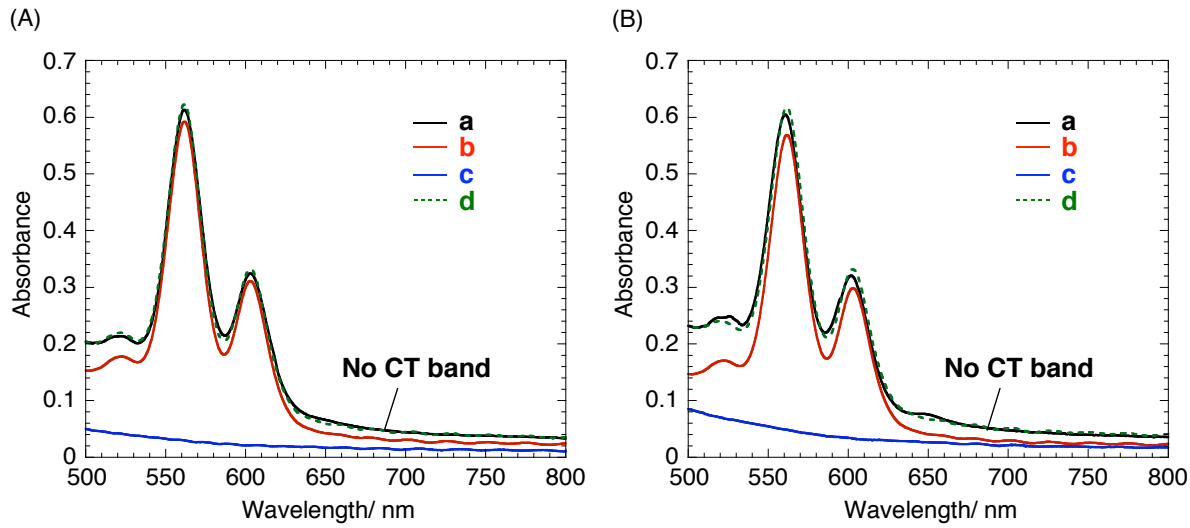

Figure 3. (A) UV-visible absorption spectra of (a) a mixed film of ZnP-acid and C_{60}-acid (TiO_2/ZnP-acid+C_{60}-acid, black line), (b) a film of ZnP-acid (TiO_2/ZnP-acid, red line), (c) a film of C_{60}-acid (TiO_2/C_{60}-acid, blue line), and (d) a sum of (b) and (c) (dashed green line). (B) UV-visible absorption spectra of (a) a mixed film of ZnP-acid and C_{60}-ester (TiO_2/ZnP-acid+C_{60}-ester, black line), (b) a film of ZnP-acid (TiO_2/ZnP-acid, red line), (c) a film of C_{60}-ester (TiO_2/C_{60}-ester, blue line), and (d) a sum of (b) and (c) (dashed green line). The modified TiO_2 electrodes were prepared by spin-coating a DMF solution (1.0 mM) of porphyrin and/or fullerene onto a TiO_2 electrode.

Figure 4 shows IRRA spectra in the C=O stretching region (1900–1650 cm^{-1}) for the thin films of porphyrin and/or fullerene spin-coated on gold surface as (a) ZnP-acid, (b) ZnP-ester, (c) C_{60}-acid, (d) C_{60}-ester, (e) ZnP-acid+C_{60}-acid, (f) ZnP-acid+C_{60}-ester, (g) ZnP-ester+C_{60}-acid and (h) ZnP-ester+C_{60}-ester. The peak frequencies are listed in Table 1. As shown in Figure 4b, ZnP-ester gives an IRRA peak at 1730 cm^{-1} which can be assigned to the free C=O stretching mode of the ester moiety. In contrast with ZnP-ester, ZnP-acid shows a broad IRRA peak due to the C=O stretching at lower wavenumber region (1700 cm^{-1}, Figure 4a). It is well known that the peak from C=O stretching mode shifts to lower wavenumber region by forming a hydrogen bond at the carbonyl oxygen atom.[26] Thus, the red-shift in peak position of the C=O stretching can be attributed to the formation of intermolecular hydrogen bonds between ZnP-acid molecules, possibly higher hydrogen-bonded aggregates. For the C_{60} derivatives, C_{60}-ester shows a rather sharp IRRA peak at 1750 cm^{-1} (Figure 4d) which corresponds to the free C=O stretching mode.[24b] In contrast, C_{60}-acid gives a broad IRRA peak at 1730–1740 cm^{-1} with a shoulder at 1800 cm^{-1} (Figure 4c). Similar IRRA peaks without the peak at 1800 cm^{-1} were reported for the monoadduct of C_{60} malonic acids.[14] Taking into account the fact that malonic acid displays the infrared band at 1740 cm^{-1} corresponding to stretching mode of inter- and intra-molecularly hydrogen-bonded carbonyl group and the band around 1800 cm^{-1} is assigned to the free carbonyl group,[27] the IRRA peak at 1730–1740 cm^{-1} of C_{60}-acid stems from the stretching mode of the inter- and intra-molecular hydrogen-bonded carbonyl group,

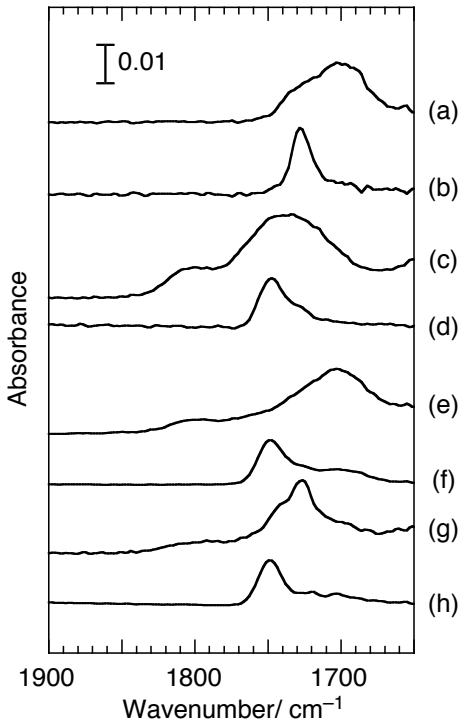

Figure 4. IRRA spectra in the C=O stretching region (1900–1650 cm^{-1}) for the thin films of porphyrin and/or fullerene spin-coated on gold surface as (a) ZnP-acid, (b) ZnP-ester, (c) C_{60}-acid, (d) C_{60}-ester, (e) ZnP-acid+C_{60}-acid, (f) ZnP-acid+C_{60}-ester, (g) ZnP-ester+C_{60}-acid and (h) ZnP-ester+ C_{60}-ester. An equimolar DMF solution of porphyrin (ZnP-acid, ZnP-ester) and/or fullerene (C_{60}-acid, C_{60}-ester) was spin-coated onto gold surfaces.

while the IRRA peak at 1800 cm^{-1} originates from that of the free carbonyl group. From comparison of the peak intensities, most of carboxylic acid groups form inter- and intra-molecular hydrogen bonds in the C_{60}-acid single film.

On the other hand, useful structural information on the hydrogen bonding interaction between different types of molecules can be obtained from the IRRA spectra of mixed films of porphyrin and fullerene composites. The samples were prepared by spin-coating a DMF solution containing an equimolar mixture of porphyrin and fullerene onto the gold surface. The compositions of porphyrin and fullerene in each mixed films were estimated by dissolving each component into DMF from the mixed films and measuring the absorbances due to the porphyrin and C_{60} moieities: [ZnP]:[C_{60}] = 1:1 in ZnP-acid+C_{60}-acid film, [ZnP]:[C_{60}] = 1:4 in ZnP-acid+C_{60}-ester film, [ZnP]:[C_{60}] = 1:2 in ZnP-ester+C_{60}-acid film, [ZnP]:[C_{60}] = 1:3 in ZnP-ester+C_{60}-ester film. ZnP-acid+C_{60}-acid (Figure 4e) and ZnP-acid+C_{60}-ester (Figure 4f) show the IRRA peak at the same position as that in ZnP-acid, implying that Zn-acid molecules form hydrogen bonds in the mixed films similar to ZnP-acid solely. The IRRA spectrum of ZnP-acid+C_{60}-acid shows the weak peak at 1800 cm^{-1} arising from the free carbonyl group of C_{60}-acid, while the peak at 1730–1740 cm^{-1} arising from the inter- and intra-molecular hydrogen-bonded carbonyl group of C_{60}-acid is not evident probably due to the

overlapping with the strong peak stemming from the intermolecular hydrogen-bonded carbonyl group of ZnP-acid. Nevertheless, the relative peak intensity at 1730–1740 cm^{-1} versus at 1800 cm^{-1} for the ZnP-acid+ C_{60}-acid film is lower than the corresponding value at 1730–1740 cm^{-1} versus at 1800 cm^{-1} for the C_{60}-acid single film. Therefore, ZnP-acid would interpenetrate into the inter- and intra-molecular hydrogen bonding network of the C_{60}-acid, weakening the inter- and intra-molecular hydrogen bonding of the C_{60}-acid in the ZnP-acid+C_{60}-acid film. Totally, the existence of ZnP-acid would suppress inter- and intra-molecular hydrogen bonding in C_{60}-acid, leading to the formation of intermolecular hydrogen bonding between ZnP-acid and C_{60}-acid molecules in addition to that between C_{60}-acid molecules. In contrast, ZnP-ester+C_{60}-acid displays the IRRA peak due to ZnP-ester (1730 cm^{-1}) and the IRRA peaks at 1730–1740 cm^{-1} and 1800 cm^{-1} (Figure 4g), which match those of C_{60}-acid (Figure 4c). This implies that C_{60}-acid does not form hydrogen bond with ZnP-ester, making inter- and intra-molecular hydrogen bonding between C_{60}-acid molecules. ZnP-acid+C_{60}-ester (Figure 4f) and ZnP-ester+C_{60}- ester (Figure 4h) yield the evident IRRA peak (1750 cm^{-1}) due to the C_{60}-ester, and the peak intensity is much larger than that due to the porphyrin. These result from the fact that the both mixed films contain more C_{60}-ester molecules than the porphyrin molecules. Overall, hydrogen-bonding interaction between the same molecules is dominant for all the mixed films except the ZnP-acid+ C_{60}-acid system in which additional hydrogen-bonding interaction between ZnP-acid and C_{60}-acid molecules exists (vide infra).

AFM measurements were performed for mica substrates modified with the compounds by spin-coating method (Figures 5 and 6).[28] The image of ZnP-acid (Figure 5a) shows smooth surface morphology, while that of ZnP-ester exhibits domain structure with 40 ± 10 nm size (Figure 5b). The image of C_{60}-acid (Figure 5c) reveals domain structure with 60 ± 10 nm size, whereas that of C_{60}-ester

Table 1. IRRA frequencies and IPCE and APCE values.

system	IRRA frequency/cm^{-1}	IPCE /% [a]	APCE/% [b]
ZnP-acid+C_{60}-acid	1700, 1800	31 ± 2	37 ± 3
ZnP-acid+C_{60}-ester	1700, 1750	26 ± 1	30 ± 1
ZnP-ester+C_{60}-acid	1730, 1730–40, 1800	7.8 ± 2.2[b]	14 ± 1
ZnP-ester+C_{60}-ester	1750	7.7 ± 0.5[b]	13 ± 3
ZnP-acid	1700	23 ± 1	27 ± 1
ZnP-ester	1730	6.6 ± 1.7[b]	12 ± 2
C_{60}-acid	1730–40, 1800	*c*	*c*
C_{60}-ester	1750	*c*	*c*

[a] Prepared by the adsorption-spin-coating method: input power: 68 μW cm^{-2} (λ_{ex} = 444 nm); absorbance: 0.86±0.13 at excitation wavelength; thickness of TiO_2 layer: 4.0 μm; applied potential: 0.10 V vs SCE. [b] Absorbance: 0.37 ± 0.19 at excitation wavelength. [C] Not measured.

exhibits partial domain structure with 90 ± 20 nm size (Figure 5d). The AFM images of the porphyrin and C_{60} mixed system are quite different from those of either the porphyrin or the C_{60} system. In typical donor-acceptor blend films such as conjugated polymer and PCBM ([6,6]-phenyl C61 butyric acid methyl ester) in bulk heterojunction solar cells, an intimate mixing of the components leads to smooth surface morphology of the blend film which can be confirmed by using AFM.[7a,c] The AFM images of ZnP-acid+C_{60}-acid (Figure 6a) and ZnP-acid+C_{60}-ester (Figure 6b) disclose smooth surface morphology, while those of ZnP-ester+C_{60}-acid (Figure 6c) and ZnP-ester+C_{60}-ester (Figure 6d) show island-shaped one. These results suggest that the ZnP-acid molecules tend to form extensive network structure due to the hydrogen-bonding interaction more effectively than the ZnP-ester molecules (vide supra). Furthermore, the AFM image of ZnP-acid+C_{60}-acid is more uniform than that of ZnP-acid+ C_{60}-ester. These results demonstrate that the hydrogen-bonding interaction between the different molecules as well as between the same molecules is required for the smooth morphology on the surface in which ZnP-acid and C_{60}-acid molecules would be self-assembled with a phase-separated, interpenetrating network involving hydrogen-bonded electron and/or hole transporting nanostructures (vide infra).

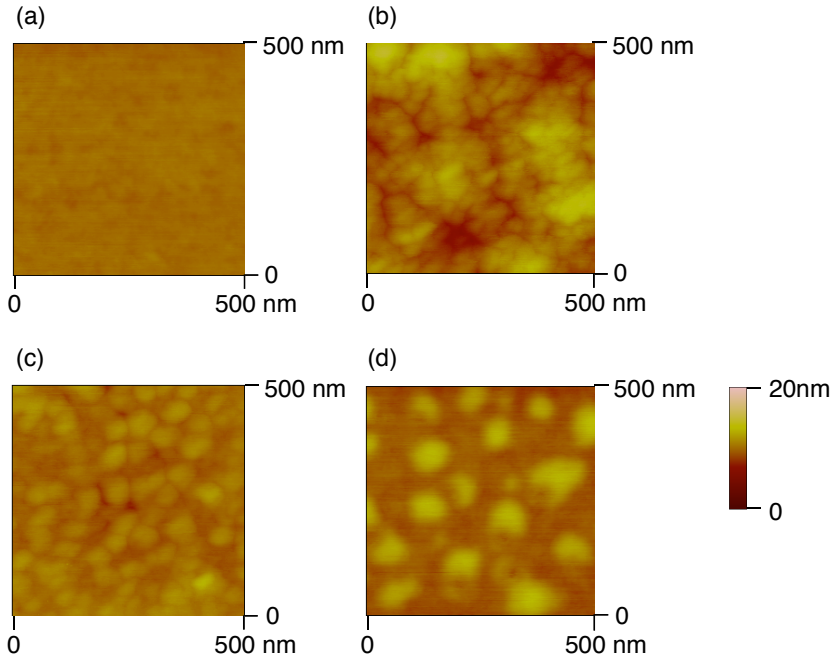

Figure 5. AFM images of (a) ZnP-acid, (b) ZnP-ester, (c) C_{60}-acid, and (d) C_{60}-ester on mica substrate. The color scale represents the height topography with bright and dark representing the highest and lowest features, respectively. An equimolar DMF solution of porphyrin (ZnP-acid, ZnP-ester) or fullerene (C_{60}-acid, C_{60}-ester) was spin-coated onto freshly cleaved mica.

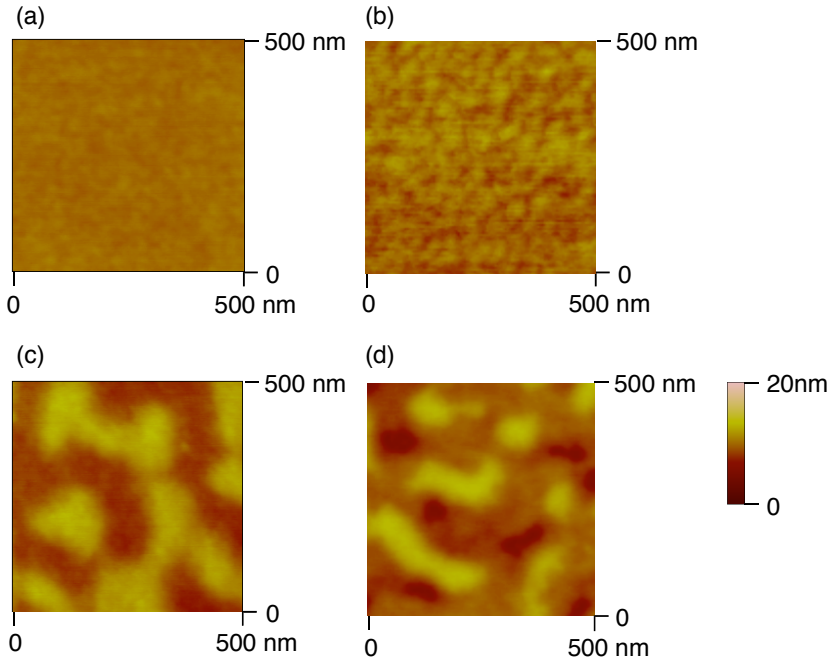

Figure 6. AFM images of (a) ZnP-acid+C_{60}-acid, (b) ZnP-acid+C_{60}-ester, (c) ZnP-ester+C_{60}-acid, and (d) ZnP-ester+C_{60}-ester on mica substrate. The color scale represents the height topography with bright and dark representing the highest and lowest features, respectively. An equimolar DMF solution of porphyrin (ZnP-acid, ZnP-ester) and fullerene (C_{60}-acid, C_{60}-ester) was spin-coated onto freshly cleaved mica.

Photoelectrochemical and Photovoltaic Properties of TiO_2 Electrodes Modified with Porphyrin and Fullerene Composites. Photoelectrochemical measurements were performed in a nitrogen-saturated acetonitrile solution containing 0.5 M LiI and 0.01 M I_2 using the modified TiO_2 as the working electrode, a platinum counter electrode, and an I^-/I_3^- reference electrode. For instance, a stable anodic photoinduced electron flow from the electrolyte to TiO_2/ZnP-acid+C_{60}-acid electrode, prepared by the spin-coating method, appears immediately upon irradiation of the modified TiO_2 electrode (inset of Figure 7). The photocurrent falls down instantly when the illumination is cut off. The anodic electron flow increases with increasing positive bias to the TiO_2 electrode from –0.1 V to 0.2 V vs SCE, showing the direction of electron flow from the electrolyte to the TiO_2 electrode. The action spectrum largely parallels the absorption spectrum of TiO_2/ZnP-acid+C_{60}-acid (Figure 2) except for the slight red-shift, demonstrating that the porphyrin excited singlet state is involved into the photocurrent generation. The slight red-shift of the action spectrum compared to the absorption spectrum may originate from the difference in the experimental conditions for the two measurements.[29] Namely, the absorption spectrum was measured in air using dry film, whereas the photocurrent action spectrum was obtained under the photoelectrochemical conditions in which the positive potential (0.1 V vs SCE) is applied to the film that is exposed to the electrolyte solution

(Figure 8).[29] Similar discrepancy between absorption and action spectra has been reported in many cases including phthalocyanine-sensitized TiO_2 electrodes and porphyrin-modified gold electrodes.[29a,b] Similar photoelectrochemical behavior is noted for TiO_2/ZnP-acid+C_{60}-ester, TiO_2/ZnP-ester+C_{60}-acid, TiO_2/ZnP-ester+C_{60}-ester, TiO_2/ZnP-acid, and TiO_2/ZnP-ester devices.

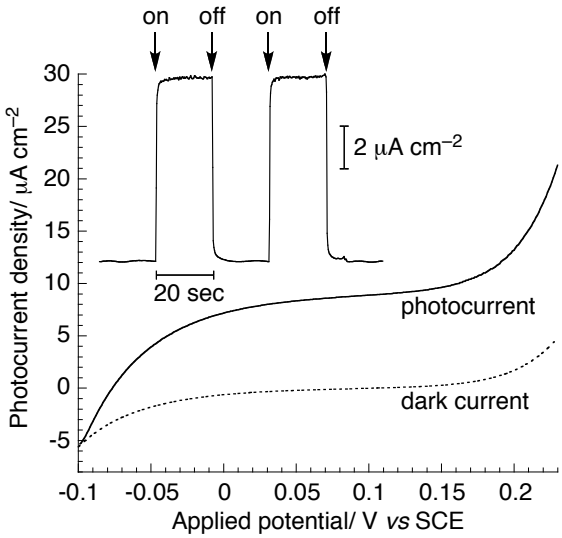

Figure 7. Photocurrent vs applied potential curves of FTO/TiO_2/ZnP-acid+C_{60}-acid system. The dark current is shown as a dotted line. The photoelectrochemical response of FTO/TiO_2/ZnP-acid+C_{60}-acid system at applied potential of 0.10 V vs SCE is shown as an inset; excitation power: 54 μW cm^{-2} (λ_{ex} = 440 nm); absorbance > 3 at excitation wavelength; 0.5 M LiI and 0.01 M I_2 in acetonitrile.

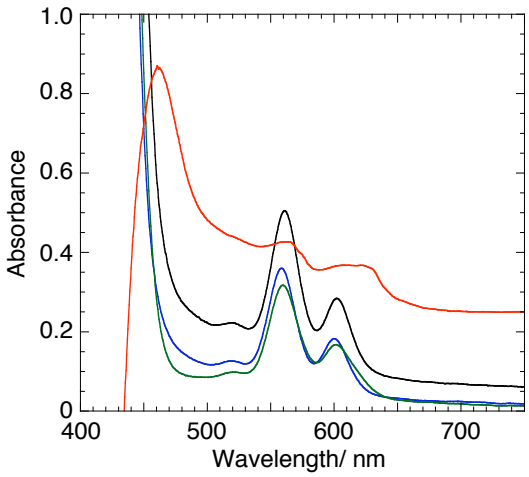

Figure 8. UV-visible absorption spectra of a mixed film of ZnP-acid and C_{60}-acid (TiO_2/ZnP-acid+C_{60}-acid) in air (black line), in acetonitrile (blue line), in electrolyte solution (green line), and under the photoelectrochemical conditions in which the positive potential (0.1 V vs SCE) is applied to the film that is in contact with the electrolyte solution (red line).

To evaluate the hydrogen bonding effects on the photocurrent generation, the IPCE values were compared for TiO_2/ZnP-acid+C_{60}-acid, TiO_2/ZnP-acid+C_{60}-ester, TiO_2/ZnP-ester+C_{60}-acid, TiO_2/ZnP-ester+C_{60}-ester, TiO_2/ZnP-acid, and TiO_2/ZnP-ester systems under the same conditions (applied potential: 0.10 V vs SCE, λ_{ex} = 436 nm). The excitation wavelength at the Soret band guarantees the selective excitation of the porphyrin rather than that of C_{60} moiety. At first, direct spin-coating of the DMF solution containing the compounds onto a bare TiO_2 electrode was employed to compare the IPCE values (Figure 9). The IPCE value of TiO_2/ZnP-acid+C_{60}-acid system (47 ± 5%) is significantly larger than that of TiO_2/ZnP-acid system (32 ± 2%). This demonstrates the involvement of C_{60} in the enhancement of the photocurrent generation efficiency. However, the IPCE value of TiO_2/ZnP-acid+C_{60}-acid system is slightly larger than that of TiO_2/ZnP-acid+C_{60}-ester system (40 ± 7%). Only minor effect of the hydrogen bonding may result from direct adsorption of ZnP-acid onto the TiO_2 surface through the carboxylic acid where an electron is directly injected into the CB of the TiO_2 surface from the porphyrin excited singlet state to generate photocurrent.[30,31] The efficient, direct electron injection would mask the rather inefficient, stepwise electron injection from the porphyrin excited singlet state to the CB of TiO_2 via C_{60}, depending on the amount of directly adsorbed porphyrin molecules on the TiO_2 surface. To minimize the direct adsorption of the ZnP-acid molecule onto the TiO_2 surface, the assembly of these molecules was carried out by spin-coating the DMF solution containing the compounds onto the pre-treated TiO_2 surface which is chemically modified with the C_{60}-acid molecules in advance (adsorption-spin-coating method).[32,33] Although the IPCE values obtained by the adsorption-spin-coating method (Table 1) are smaller than those obtained by the simple spin-coating method, the hydrogen bonding effects on the IPCE values are unambiguous for the ZnP-acid systems: TiO_2/ZnP-acid+C_{60}-acid (31 ± 2%) > TiO_2/ZnP-acid+C_{60}-ester (26 ± 1%) > TiO_2/ZnP-acid (23 ± 1%) systems.[34] The trend is more evident when one compare the absorbed photon-to-current efficiency (APCE): TiO_2/ZnP-acid+C_{60}-acid (37 ± 3%) > TiO_2/ZnP-acid+C_{60}-ester (30 ± 1%) > TiO_2/ZnP-acid (27 ± 1%) systems (Table 1).[35] The trend for the IPCE and APCE values is in good agreement with the results on the IRRA spectra and the AFM measurements. These results unequivocally corroborate that the photocurrent generation efficiency is much enhanced in hydrogen-bonded porphyrin-fullerene system compared with the reference system without hydrogen bonding. In contrast, the IPCE (5–10%) and APCE (11–16%) values are rather comparable for the ZnP-ester systems (Table 1), although the values are significantly lower than those for the ZnP-acid systems. These results lead to the conclusion that the hydrogen bonding between the different ZnP-acid and C_{60}-acid molecules as well as the same ZnP-acid molecules, together with the direct adsorption of ZnP-acid onto TiO_2, is essential for the efficient photocurrent generation.

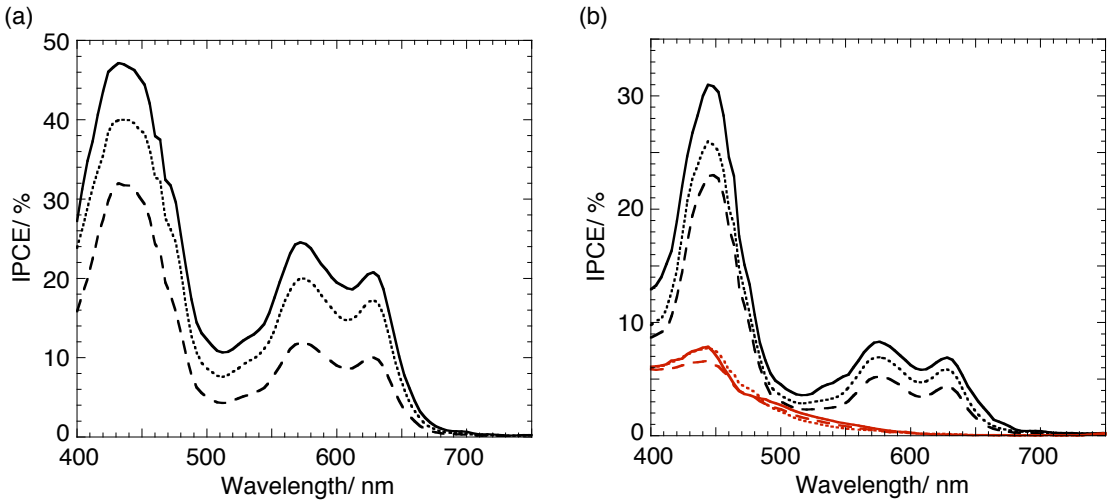

Figure 9. Photocurrent action spectra of (a) TiO_2/ZnP-acid+C_{60}-acid (solid line), TiO_2/ZnP-acid+C_{60}-ester (dotted line) and TiO_2/ZnP-acid (dashed line). The modified TiO_2 electrodes were prepared by the spin-coating method. (b) TiO_2/ZnP-acid+C_{60}-acid (solid black line), TiO_2/ZnP-acid+C_{60}-ester (dotted black line), TiO_2/ZnP-acid (dashed black line), TiO_2/ZnP-ester+C_{60}-acid (solid red line), TiO_2/ZnP-ester+C_{60}-ester (dotted red line) and TiO_2/ZnP-ester (dashed red line). The modified TiO_2 electrodes were prepared by the adsorption-spin-coating method. Applied potential: 0.10 V vs SCE; 0.5 M LiI and 0.01 M I_2 in acetonitrile.

To exemplify an increase in V_{OC} in the present system, the author examined the photovoltaic properties of TiO_2 and SnO_2 electrodes modified with the ZnP-acid and C_{60}-acid composite. Both TiO_2 and SnO_2 electrodes were modified by the spin-coating method. Note that the particle size of TiO_2 (20–25 nm) is slightly larger than that of SnO_2 (15 nm). The amount of the adsorbed ZnP-acid (3.5×10^{-11} mol cm^{-2}) in TiO_2/ZnP-acid+C_{60}-acid is 4 times larger than that (9.2×10^{-12} mol cm^{-2}) in SnO_2/ZnP-acid+C_{60}-acid. Current-voltage characteristics were measured using the modified electrode and a Pt counter electrode under AM 1.5 conditions. The η value is derived from the equation: $\eta = J_{SC} \times V_{OC} \times ff$, where J_{SC} is the short circuit current and ff is the fill factor. For the TiO_2 cell: $\eta = 2.1 \pm 0.1\%$ with $J_{SC} = 5.1 \pm 0.2$ mA cm^{-2}, $V_{OC} = 0.58 \pm 0.01$ V and $ff = 0.70 \pm 0.01$ (Figure 10), whereas for the SnO_2 cell: $\eta = 0.31 \pm 0.02\%$ with $J_{SC} = 2.3 \pm 0.2$ mA cm^{-2}, $V_{OC} = 0.36 \pm 0.02$ V and $ff = 0.39 \pm 0.03$.[36] The cell performance of the TiO_2 cell is higher than that of the SnO_2 cell. The large J_{SC} and ff values of the TiO_2 cell compared to those of the SnO_2 cell mainly result from the larger amount of the adsorbed dyes on the TiO_2 electrode in the TiO_2 cell. Nevertheless, the large V_{OC} value of the TiO_2 cell relative to that of the SnO_2 cell demonstrates the validity of our strategy in which the SnO_2 electrode is replaced by the TiO_2 electrode.

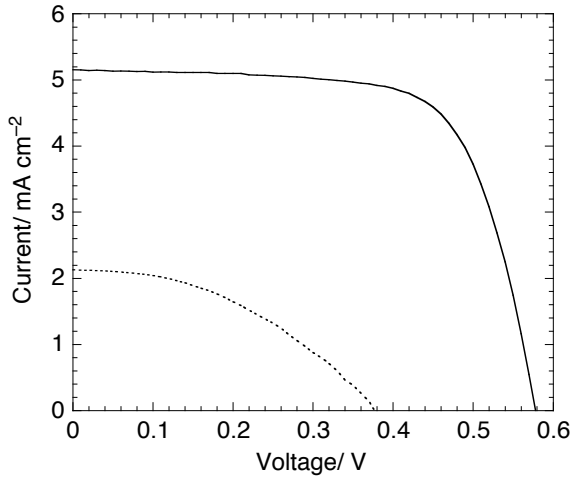

Figure 10. Photocurrent-voltage characteristics of TiO_2/ZnP-acid+C_{60}-acid cell ($\eta = 2.1 \pm 0.1\%$, $J_{sc} = 5.1 \pm 0.2$ mA cm^{-2}, $V_{oc} = 0.58 \pm 0.01$ V, $ff = 0.70 \pm 0.01$, solid line) and SnO_2/ZnP-acid+C_{60}-acid cell ($\eta = 0.31 \pm 0.02\%$, $J_{sc} = 2.3 \pm 0.2$ mA cm^{-2}, $V_{oc} = 0.36 \pm 0.02$ V, $ff = 0.39 \pm 0.03$, dotted line). Conditions: electrolyte 0.1 M LiI, 0.05 M I_2, 0.6 M 2,3-dimethyl-1-propyl imidazolium iodide, and 0.5 M 4-*t*-butylpyridine in CH_3CN; input power: AM 1.5 under simulated solar light (100 mW cm^{-2}). $\eta = J_{sc} \times V_{oc} \times ff$.

Optical studies. At first, steady-state fluorescence spectra (λ_{ex} = 430 nm) were measured for the better understanding of the photodynamical behavior of the porphyrin-fullerene system on the TiO_2 electrodes prepared by the spin-coating method. The ZnP-acid systems reveal very weak fluorescence with a maximum at 670 nm and a shoulder at 720 nm (Figure 11), which does not match that of ZnP-acid with maxima of 600 nm and 650 nm in solution. Taking into account the results on the photoelectrochemical properties, the porphyrin excited singlet state is strongly quenched by the TiO_2 and/or C_{60} via ET, exhibiting little zinc porphyrin fluorescence at 600–620 nm. Thus, the emission on the TiO_2 electrodes could originate from the impurities or degradation of the zinc porphyrins and the demetalated freebase porphyrins with maxima of 650 nm and 720 nm in solution. It is noteworthy that TiO_2/ZnP-acid+C_{60}-acid and TiO_2/ZnP-acid+C_{60}-ester exhibit no CT emission at 800–1000 nm, which is consistent with the no appreciable CT absorption in the absorption spectra of TiO_2/ZnP-acid+C_{60}-acid and TiO_2/ZnP-acid+C_{60}-ester (Figure 3).

The porphyrin excited singlet state was probed by the picosecond fluorescence lifetime measurements for TiO_2/ZnP-acid+C_{60}-acid, TiO_2/ZnP-acid+C_{60}-ester and TiO_2/ZnP-acid systems prepared by the spin-coating method. The emission decay measurements were carried out using time-correlated single photon counting method at the wavelength of 650 nm at which the zinc porphyrin and the demetalated freebase porphyrin emits. The time resolution is 60–70 ps on the basis of FWHM of instrument response function. As discussed in the steady-state fluorescence measurements, the porphyrin excited singlet state is strongly quenched by the TiO_2 and/or C_{60} via ET,

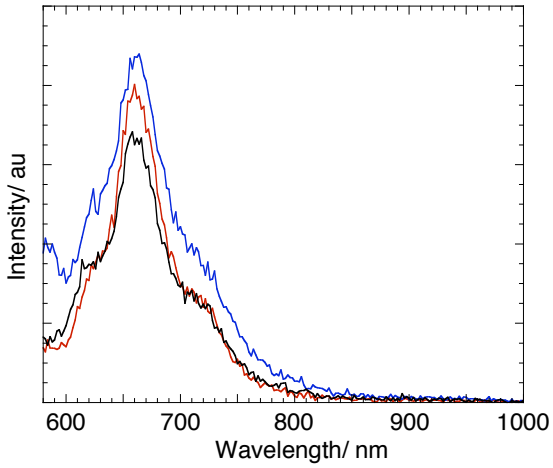

Figure 11. Steady-state fluorescence spectra of TiO_2/ZnP-acid+C_{60}-acid (black line, [ZnP-acid]:[C_{60}-acid] = 1:1), TiO_2/ZnP-acid+C_{60}-ester (blue line, [ZnP-acid]:[C_{60}-ester] = 1:1) and TiO_2/ZnP-acid (red line) electrodes with an excitation wavelength of 430 nm. The TiO_2 electrodes were prepared by the spin-coating method.

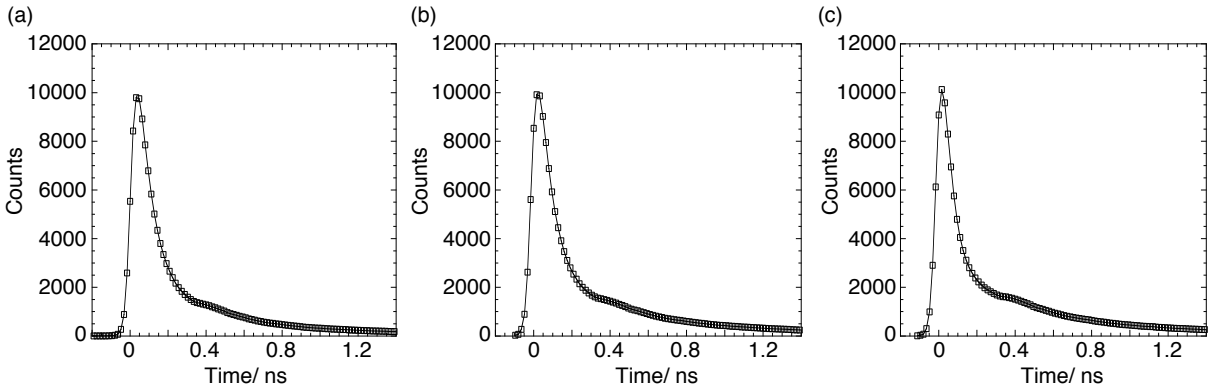

Figure 12. The fluorescence decay curves of (a) TiO_2/ZnP-acid+C_{60}-acid, (b) TiO_2/ZnP-acid+C_{60}-ester, and (c) TiO_2/ZnP-acid electrodes observed at 650 nm with an excitation wavelength of 405 nm. The TiO_2 electrodes were prepared by the spin-coating method. The decays were analyzed with 3-exponential fit (τ_1 = 0.14 ns (72%), τ_2 = 0.64 ns (26.5%), τ_3 = 2.3 ns (1.5%) for TiO_2/ZnP-acid+C_{60}-acid, τ_1 = 0.040 ns (80%), τ_2 = 0.39 ns (18%), τ_3 = 1.7 ns (2%) for TiO_2/ZnP-acid+C_{60}-ester, and τ_1 = 0.070 ns (83%), τ_2 = 0.46 ns (16%), τ_3 = 1.8 ns (1%) for TiO_2/ZnP-acid).

exhibiting little zinc porphyrin fluorescence at 650 nm. Thus, the multi-component fluorescence decays with rather long lifetimes of > 60 ps stem from the minor relaxation process probably due to the impurities or degradation of the zinc porphyrins and the demetalated freebase porphyrins (Figure 12).

The formation of the charge-separated state in the mixed films was detected using femtosecond pump-probe method for TiO_2/ZnP-acid+C_{60}-acid, TiO_2/ZnP-acid+C_{60}-ester, and TiO_2/ZnP-acid electrodes with the excitation wavelength of 420 nm. The transient absorption spectrum of TiO_2/ZnP-acid+C_{60}-acid, prepared by the spin-coating method, discloses the characteristic bands

around 500 nm and 650 nm due to zinc porphyrin radical cation (Figure 13).[20] The fingerprint of $C_{60}^{\bullet-}$ at 1000 nm could not be detected because of the low molar absorptivity of $C_{60}^{\bullet-}$ relative to $ZnP^{\bullet+}$ and the poor signal-to-noise ratio.[20] These results unequivocally demonstrate the occurrence of photoinduced ET from the porphyrin excited singlet state to the CB of TiO_2 electrode, yielding the porphyrin radical cation. Within the time resolution (200 fs) of the instrument used an instant formation of the bands was observed, which indicates that the formation of the charge-separated state in the sample can be as fast as ~10^{13} s^{-1}. Reliable decay profiles could not be obtained because of the sample degradation under the experimental conditions. The transient absorption spectra of TiO_2/ZnP-acid+C_{60}-ester and TiO_2/ZnP-acid electrodes exhibit similar behavior. In the transient absorbances of TiO_2/ZnP-acid+C_{60}-acid, TiO_2/ZnP-acid+C_{60}-ester, and TiO_2/ZnP-acid electrodes at 450–550 nm, the amount of ZnP-acid radical cations at 20 ps after laser excitation is in the order of TiO_2/ZnP-acid+C_{60}-acid > TiO_2/ZnP-acid+C_{60}-ester ≈ TiO_2/ZnP-acid (inset of Figure 13). The trend parallels the moderate difference in the photocurrent generation efficiencies of the three photoelectrochemical devices prepared by the spin-coating method, corroborating the significant contribution of stepwise ET from the porphyrin excited singlet state to the C_{60}, followed by electron injection from the C_{60} radical anion to the CB of the TiO_2 electrode, to the photocurrent generation.

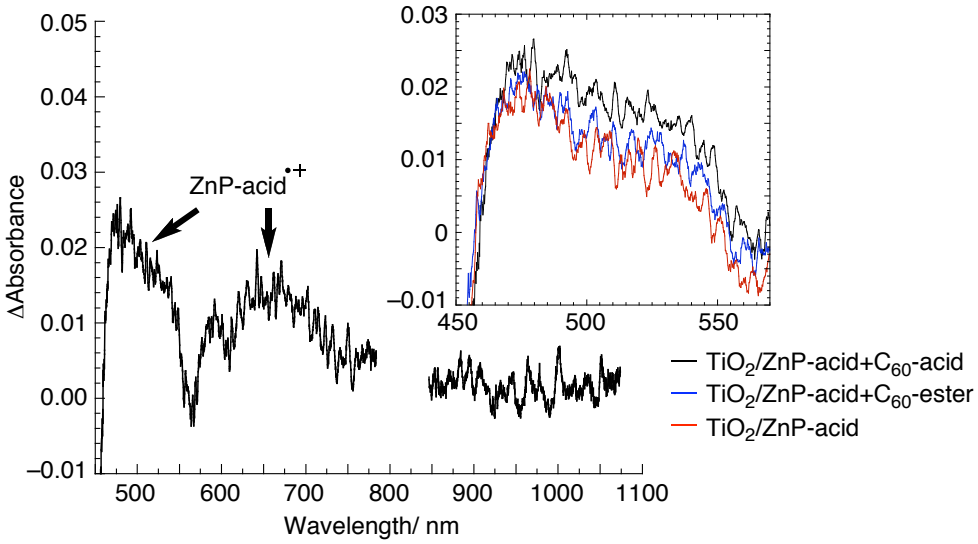

Figure 13. Transient absorption spectrum of TiO_2/ZnP-acid+C_{60}-acid at time delay of 20 ps excited at 420 nm. The inset shows the transient absorption spectra of TiO_2/ZnP-acid+C_{60}-acid (black line), TiO_2/ZnP-acid+C_{60}-ester (blue line) and TiO_2/ZnP-acid (red line) around 500 nm.

On the basis of the energetics of the photoactive and radical ion species involved in TiO_2/ZnP-acid+C_{60}-acid system, a mechanism of photocurrent generation is proposed (Scheme 1). First, ET takes place from $^1ZnP^*$ (ZnP-acid: –1.01 V vs NHE) to the CB of TiO_2 (–0.5 V vs NHE) or

C_{60} (C_{60}-acid: –0.79 V vs NHE) yielding the porphyrin radical cation ($ZnP^{\bullet+}$) and the electron in the CB of the TiO_2 electrode or $ZnP^{\bullet+}$ and C_{60} radical anion ($C_{60}^{\bullet-}$). In the latter case, the generated $C_{60}^{\bullet-}$ gives an electron to the CB of TiO_2 (–0.79 V vs NHE) to yield the same state. On the other hand, I^- (0.5 V vs NHE) donates an electron to $ZnP^{\bullet+}$ (ZnP-acid: 1.11 V vs NHE) to generate anodic photocurrent. The hydrogen bonding in the porphyrin or the C_{60} molecules or the both may be responsible for the large IPCE values in comparison with the reference system without the hydrogen bonding. Such hydrogen bonding would facilitate the initial CS between the porphyrin and the C_{60} and the separated electron and hole relay through the hydrogen-bonded arrays which suppress the undesirable CR.

Scheme 1. Photocurrent generation diagram for TiO_2/ZnP-acid+C_{60}-acid system.

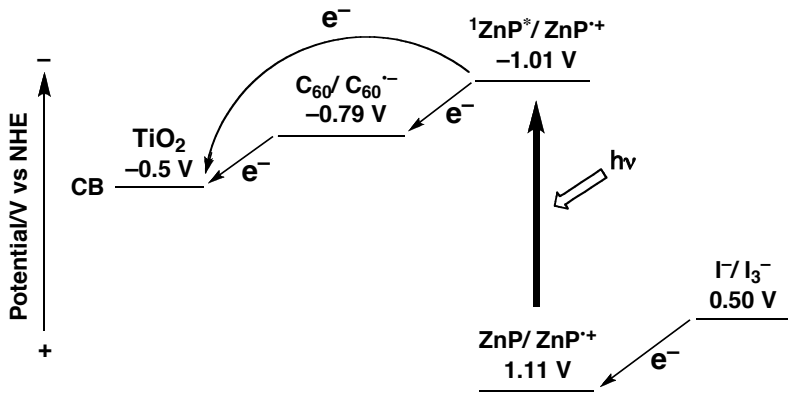

Conclusion

Hydrogen bonding effects on photocurrent generation have been examined in the mixed films of porphyrin and/or fullerene with and without hydrogen bonds on nanostructured TiO_2 electrodes for the first time. The nanostructured TiO_2 electrodes modified with the mixed films of porphyrin and fullerene with hydrogen bonds exhibit efficient photocurrent generation (IPCE value of up to 47 ± 5% for FTO/TiO_2/ZnP-acid+C_{60}-acid electrode prepared by simple spin-coating method) as compared to the reference systems without hydrogen bonds. Atomic force microscopy, infrared reflection absorption and ultraviolet-visible absorption spectroscopies, and time-resolved fluorescence lifetime and transient absorption measurements support the significant contribution of hydrogen bonding interaction between the porphyrins or the C_{60} moieties or the both in the films on the electrode surface for the photocurrent generation efficiency. These results show that hydrogen bonding is a potential methodology for the fabrication of donor and acceptor composites on a nanostructured TiO_2 electrode, which exhibit high open circuit potential relative to that of the corresponding SnO_2 electrode.

Experimental Section

General. Syntheses of the compounds ZnP-acid, ZnP-ester, C_{60}-acid, and C_{60}-ester were carried out according to the previously reported methods.[24,25] UV-visible absorption spectra were obtained on a Perkin Elmer Lambda 900UV/vis/NIR spectrometer. Infrared reflection absorption (IRRA) spectra were recorded by a Bio-Rad FTS 575C FT-IR spectrometer equipped with a liquid-N_2 cooled MCT detector and a Harrick Reflector™ grazing angle reflectance unit.[37] The samples for IRRA observation were prepared by direct deposition of the compounds on a slide glass (2×2 cm^2) covered by a 200 nm-thick gold film for IRRA observation, by spin-coating method. The IRRA spectrum of a bare gold film was used as the reference. The spectral resolution used was 4 cm^{-1}. AFM measurements were carried out using a Digital Nanoscope III in the tapping mode. Steady-state fluorescence spectra were measured on a Fluorolog 3 spectrofluorimeter (ISA Inc.) equipped with a cooled IR sensitive photomultiplier (R2658). All solvents and chemicals were of reagent grade quality, purchased commercially and used without further purification unless otherwise noted. Tetrabutylammonium hexafluorophosphate used as a supporting electrolyte for the electrochemical measurements was prepared by mixing equimolar aqueous solutions of *n*-tetrabutylammonium bromide and potassium hexafluorophosphate, followed by recrystallization of the precipitate from water/acetone. Transparent conducting glasses (FTO, SnO_2:F, 9.4 Ω/sq) were commercially available from Asahi Glass.

Preparation of Films. Nanoporous TiO_2 films were prepared from colloidal suspension of TiO_2 nanoparticles (P-25, Nippon Aerosil) dispersed in deionized water and Triton X-100.[38] The suspension was deposited on a FTO electrode by using doctor blade technique. The films were annealed at 723 K for 0.5 h. Nanostructured SnO_2 films were fabricated by repeated spin-coating of 10% colloidal solution (pH 10, Chemat Technology) onto FTO electrode, followed by drying at 473 K for 20 minutes.[16–19] Finally, the dried films were annealed at 673 K for one hour. The thicknesses of the TiO_2 and SnO_2 layers on the FTO electrode used in this study were determined as 4.0 μm and 1.1 μm, respectively, using surface roughness/profile measuring instrument (SURFCOM 130A, ACCRETECH). A known amount of ZnP, C_{60} or the mixed solution in DMF was spin-coated onto TiO_2, SnO_2 or gold electrodes (spin-coating method). Modification of TiO_2 or SnO_2 electrode was also carried out by immersing the bare electrode into the DMF solution containing C_{60}-acid, followed by washing the substrate with DMF repeatedly, and finally by spin-coating the ZnP, C_{60} or the mixed solution in DMF onto the C_{60}-acid pre-modified electrode (adsorption-spin-coating method).

Photoelectrochemical Measurements. Photoelectrochemical measurements were performed in a one-compartment Pyrex UV cell (5 mL) with nitrogen-saturated electrolyte solution containing 0.5 M LiI and 0.01 M I_2 in acetonitrile.[16–19] The samples were excited with monochromatic light using a 500 W Xe arc lamp (Ritsu UXL-500D-0) coupled with a monochromator (Ritsu MC-10N).

The illuminated area on the modified surface was 0.20 cm^2. The light intensity was modulated with neutral density filters (HOYA). The casting film was immersed into the electrolyte solution containing 0.5 M LiI and 0.01 M I_2 in acetonitrile as a working electrode. The photocurrent was measured in a three-electrode arrangement, a modified TiO_2 working electrode, a platinum wire counter electrode (the distance between the electrodes is 0.3 mm), and an I^-/I_3^- reference electrode using an ALS 630a electrochemical analyzer. The light intensity was monitored by an optical power meter (Anritsu ML9002A) and corrected. The I^-/I_3^- reference electrode was made from platinum wire covered with glass luggin capillary filled with the acetonitrile solution containing 0.5 M LiI and 0.01 M I_2. The potential measured was converted to the saturated calomel electrode (SCE) scale by adding +0.10 V. The stability of the reference electrode potential was confirmed under the experimental conditions.

The photovoltaic measurements were performed in a sandwich cell consisting of the modified TiO_2 or SnO_2 electrode as the working electrode and a platinum-coated conducting glass as the counter electrode.[23] The two electrodes were placed on top of each other using a thin transparent film of Surlyn polymer (Dupont) as a spacer to form the electrolyte space. A thin layer of electrolyte (0.1 M LiI, 0.05 M I_2, 0.6 M 2,3-dimethyl-1-propylimidazolium iodide, and 0.5 M 4-*t*-butylpyridine in acetonitrile) was introduced into the interelectrode space. The photocurrent-voltage characteristics were determined by using a potentiostat (Bunko-Keiki Co., Ltd., Model HCSSP-25) and irradiating the samples with simulated AM 1.5 solar light (100 mW cm^{-2}, Bunko-Keiki Co., Ltd., Model CEP-2000). All the experimental values were given as an average from five independent measurements.

Spectral Measurements. A pump-probe method was used to measure transient absorption spectra in sub-picosecond-nanosecond time domain. The measurements were carried out using the instrument described previously.[39] The transient spectra were recorded by a CCD detector coupled with a monochromator in the visible and near infrared ranges. The second harmonic (420 nm) of Ti:sapphire laser was used for the excitation. A typical time resolution of the instrument was 200 fs (FWHM). Emission decays were measured using a time-correlated single photon counting (TCSPC) technique. The excitation wavelength was 405 nm and the time resolution was 60–70 ps.

References and Footnotes

(1) (a) Imahori, H.; Hagiwara, K.; Akiyama, T.; Aoki, M.; Taniguchi, S.; Okada, T.; Shirakawa, M.; Sakata, Y. *Chem. Phys. Lett.* **1996**, *263*, 545. (b) Imahori, H.; Yamada, H.; Guldi, D. M.; Endo, Y.; Shimomura, A.; Kundu, S.; Yamada, K.; Okada, T.; Sakata, Y.; Fukuzumi, S. *Angew. Chem. Int. Ed.* **2002**, *41*, 2344. (c) Fukuzumi, S.; Ohkubo, K.; Imahori, H.; Guldi, D. M. *Chem. Eur. J.*

2003, *9*, 1585.

(2) (a) Imahori, H.; Sakata, Y. *Adv. Mater.* **1997**, *9*, 537. (b) Imahori, H.; Sakata, Y. *Eur. J. Org. Chem.* **1999**, 2445. (c) Imahori, H.; Mori, Y.; Matano, Y. *J. Photochem. Photobiol., C* **2003**, *4*, 51. (d) Imahori, H. *Org. Biomol. Chem.* **2004**, *2*, 1425. (e) Imahori, H. *Bull. Chem. Soc. Jpn.* **2007**, *80*, 621.

(3) (a) Martín, N.; Sánchez, L.; Illescas, B.; Pérez, I. *Chem. Rev.* **1998**, *98*, 2527. (b) Diederich, F.; Gómez-López, M. *Chem. Soc. Rev.* **1999**, *28*, 263. (c) Guldi, D. M.; Prato, M. *Acc. Chem. Res.* **2000**, *33*, 695. (d) Nierengarten, N.-F. *New J. Chem.* **2004**, *28*, 1177. (e) Armaroli, N. *Photochem. Photobiol. Sci.* **2003**, *2*, 73. (f) Armaroli, N.; Accorsi, G.; Gisselbrecht, J. P.; Gross, M.; Krasnikov, V.; Tsamouras, D.; Hadziioannou, G.; Gómez-Escalonilla, M. J.; Langa, F.; Eckert, J. F.; Nierengarten, J. F. *J. Mater. Chem.* **2002**, *12*, 2077. (g) El-Khouly, M. E.; Ito, O.; Smith, P. M.; D'Souza, F. *J. Photochem. Photobiol. C* **2004**, *5*, 79.

(4) (a) *Organic Photovoltaics*; Sun, S.S., Sariciftci, N. S., Eds.; CRC: Boca Raton, 2005. (b) *Organic Photovoltaics*; Brabec, C., Dyakonov, V., Parisi, J., Sariciftci, N. S., Eds.; Springer: Berlin, 2003.

(5) (a) Yu, G.; Gao, J.; Hummelen, J. C.; Wudl, F.; Heeger, A. J. *Science* **1995**, *270*, 1789. (b) Padinger, F.; Rittberger, R. S.; Sariciftci, N. S. *Adv. Funct. Mater.* **2003**, *13*, 85. (c) Hoppe, H.; Sariciftci, N. S. *J. Mater. Chem.* **2006**, *16*, 45. (d) Scharber, M. C.; Mühlbacher, D.; Koppe, M.; Denk, P.; Waldauf, C.; Heeger, A. J.; Brabec, C. J. *Adv. Mater.* **2006**, *18*, 789.

(6) (a) Tsuzuki, T.; Shirota, Y.; Rostalski, J.; Meissner, D. *Solar Energy Mater. Solar Cells* **2000**, *61*, 1. (b) Gebeyehu, D.; Maennig, B.; Drechsel, J.; Leo, K.; Pfeiffer, M. *Solar Energy Mater. Solar Cells* **2003**, *79*, 81. (c) Xue, J.; Rand, B. P.; Uchida, S.; Forrest, S. R. *Adv. Mater.* **2005**, *17*, 66. (d) Suemori, K.; Miyata, T.; Yokoyama, M.; Hiramoto, M. *Appl. Phys. Lett.* **2005**, *86*, 63509.

(7) (a) Shaheen, S. E.; Brabec, C. J.; Sariciftci, N. S.; Padinger, F.; Fromherz, T.; Hummelen, J. C. *Appl. Phys. Lett.* **2001**, *78*, 841. (b) Padinger, F.; Rittberger, R. S.; Sariciftci, N. S. *Adv. Funct. Mater.* **2003**, *13*, 85. (c) Van Duren, J. K. J.; Yang, X.; Loos, J.; Bulle-Lieuwma, C. W. T.; Sieval. A. B.; Hummelen, J. C.; Janssen, R. A. J. *Adv. Funct. Mater.* **2004**, *14*, 425. (d) Li, G.; Shrotriya, V.; Huang, J.; Yao, Y.; Moriarty, T.; Emery, K.; Yang, Y. *Nature Mater.* **2005**, *4*, 864. (e) Ma, W.; Yang, C.; Gong, X.; Lee, K.; Heeger, A. J. *Adv. Funct. Mater.* **2005**, *15*, 1617. (f) Kim, Y.; Cook, S.; Tuladhar, S. M.; Choulis, S. A.; Nelson, J.; Durrant, J. R.; Bradley, D. D. C.; Giles, M.; McCulloch, I.; Ha. C.-S.; Ree, M. *Nature Mater.* **2006**, *5*, 197.

(8) (a) D'Souza, F.; Rath, N. P.; Deviprasad, G. R.; Zandler, M. E. *Chem. Commun.* **2001**, 267. (b) D'Souza, F.; Deviprasad, G. R.; El-Khouly, M. E.; Fujitsuka, M.; Ito, O. *J. Am. Chem. Soc.* **2001**, *123*, 5277. (c) D'Souza, F.; Deviprasad, G. R.; Rahman, M. S.; Choi, J. *Inorg. Chem.* **1999**, *38*, 2157. (d) D'Souza, F.; Zandler, M. E.; Smith, P. M.; Deviprasad, G. R.; Arkady, K.; Fujitsuka, M.; Ito, O. *J. Phys. Chem. A* **2002**, *106*, 649. (e) D'Souza, F.; Deviprasad, G. R.; Zandler, M. E.;

El-Khouly, M. E.; Fujitsuka, M.; Ito, O. *J. Phys. Chem. A* **2003**, *107*, 4801. (f) D'Souza, F.; Smith, P. M.; Zandler, M. E.; McCarty, A. L.; Itou, M.; Araki, Y.; Ito, O. *J. Am. Chem. Soc.* **2004**, *126*, 7898.

(9) (a) Da Ros, T.; Prato, M.; Guldi, D. M.; Ruzzi, M.; Pasimeni, L. *Chem. Eur. J.* **2001**, *7*, 816. (b) Armaroli, N.; Diederich, F.; Echegoyen, L.; Habicher, T.; Flamigni, L.; Marconi, G.; Nierengarten, J.-F. *New. J. Chem.* **1999**, 77. (c) D'Souza, F. *J. Am. Chem. Soc.* **1996**, *118*, 923.

(10) (a) Guldi, D. M.; Martín, N. *J. Mater. Chem.* **2002**, *12*, 1978. (b) Segura, M.; Sanchez, L.; de Mendoza, J.; Martín, N.; Guldi, D. M. *J. Am. Chem. Soc.* **2003**, *125*, 15093. (c) Fang, H.; Wang, S.; Xiao, S.; Yang, J.; Liu, Y.; Shi, Z.; Li, H.; Liu, H.; Xiao, S.; Zhu, D. *Chem. Mater.* **2003**, *15*, 1593.

(11) (a) Beckers, E. H. A.; Schenning, A. P. H. J.; van Hal, P. A.; El-ghayoury, A.; Sanchez, L.; Hummelen, J. C.; Meijer, E. W.; Janssen, R. A. J. *Chem. Commun.* **2002**, 2888. (b) Beckers, E. H. A.; van Hal, P. A.; Schenning, A. P. H. J.; El-ghayoury, A.; Peeters, E.; Rispens, M. T.; Hummelen, J. C.; Meijer, E. W.; Janssen, R. A. J. *J. Mater. Chem.* **2002**, 2054. (c) Neuteboom, E. E.; Beckers, E. H. A.; Meskers, S. C. J.; Meijer, E. W.; Janssen, R. A. J. *Org. Biomol. Chem.* **2003**, *1*, 198.

(12) (a) Li, K.; Schuster, D. I.; Guldi, D. M.; Herranz, M. A.; Echegoyen, L. *J. Am. Chem. Soc.* **2004**, *126*, 3388. (b) Li, K.; Bracher, P. J.; Guldi, D. M.; Herranz, M. A.; Echegoyen, L.; Schuster, D. I. *J. Am. Chem. Soc.* **2004**, *126*, 9156.

(13) (a) Liu, Y.; Xiao, S.; Li, H.; Li, Y.; Liu, H.; Lu, F.; Zhuang, J.; Zhu, D. *J. Phys. Chem. B* **2004**, *108*, 6256. (b) Huang, C.-H.; McCenaghan, N. D.; Kuhn, A.; Hofstraat, J. W.; Bassani, D. M. *Org. Lett.*, **2005**, *7*, 3409.

(14) (a) Imahori, H.; Liu, J.-C.; Hosomizu, K.; Sato, T.; Mori, Y.; Hotta, H.; Matano, Y.; Araki, Y.; Ito, O.; Maruyama, N.; Fujita, S. *Chem. Commun.* **2004**, 2066. (b) Imahori, H.; Liu, J.-C.; Hotta, H.; Kira, A.; Umeyama, T.; Matano, Y.; Li, G.; Ye, S.; Isosomppi, M.; Tkachenko, N. V.; Lemmetyinen, H. *J Phys. Chem. B* **2005**, *109*, 18465.

(15) (a) Imahori, H. *J. Phys. Chem. B* **2004**, *108*, 6130. (b) Imahori, H.; Fukuzumi, S. *Adv. Funct. Mater.* **2004**, *14*, 525. (c) Imahori, H. *J. Mater. Chem.* **2007**, *13*, 31.

(16) (a) Hasobe, T.; Imahori, H.; Fukuzumi, S.; Kamat, P. V. *J. Phys. Chem. B* **2003**, *107*, 12105. (b) Kang, S.; Umeyama, T.; Ueda, M.; Matano, Y.; Hotta, H.; Yoshida, K.; Isoda, S.; Shiro, M.; Imahori, H. *Adv. Mater.* **2006**, *18*, 2549. (c) Kira, A.; Umeyama, T.; Matano, Y.; Yoshida, K.; Isoda, S.; Isosomppi, M.; Tkachenko, N. V.; Lemmetyinen, H.; Imahori, H. *Langmuir* **2006**, *22*, 5497. (d) Hosomizu, K.; Imahori, H.; Hahn, U.; Nierengarten, J.-F.; Listori, A.; Armaroli, N.; Nemoto, T.; Isoda, S. *J. Phys. Chem. C* **2007**, *111*, 2777.

(17) (a) Hasobe, T.; Kashiwagi, Y.; Absalom, M. A.; Sly, J.; Hosomizu, K.; Crossley, M. J.; Imahori,

H.; Kamat, P. V.; Fukuzumi, S. *Adv. Mater.* **2004**, *16*, 975. (b) Hasobe, T.; Kamat, P. V.; Absalom, M. A.; Kashiwagi, Y.; Sly, J.; Crossley, M. J.; Hosomizu, K.; Imahori, H.; Fukuzumi, S. *J. Phys. Chem. B* **2004**, *108*, 12865.

(18) Hasobe, T.; Kamat, P. V.; Troiani, V.; Solladié, N.; Ahn, T. K.; Kim, S. K.; Kim, D.; Kongkanand, A.; Kuwabata, S.; Fukuzumi, S. *J. Phys. Chem. B* **2005**, *109*, 19.

(19) (a) Hasobe, T.; Imahori, H.; Kamat, P. V.; Ahn, T. K.; Kim, S. K.; Kim, D.; Fujimoto, A.; Hirakawa, T.; Fukuzumi, S. *J. Am. Chem. Soc.* **2005**, *127*, 1216. (b) Imahori, H.; Fujimoto, A.; Kang, S. Hotta, H.; Yoshida, K.; Umeyama, T.; Matano, Y.; Isoda, S. *Adv. Mater.* **2005**, *17*, 1727. (c) Imahori, H.; Fujimoto, A.; Kang, S.; Hotta, H.; Yoshida, K.; Umeyama, T.; Matano, Y.; Isoda, S.; Isosomppi, M.; Tkachenko, N. V.; Lemmetyinen, H. *Chem. Eur. J.* **2005**, *11*, 7265. (d) Imahori, H.; Mitamura, K.; Umeyama, T.; Hosomizu, K.; Matano, Y.; Yoshida, K.; Isoda, S. *Chem. Commun.* **2006**, 406. (e) Imahori, H.; Mitamura, K.; Shibano, Y.; Umeyama, T.; Matano, Y.; Yoshida, K.; Isoda, S.; Araki, Y.; Ito, O. *J. Phys. Chem. B* **2006**, *110*, 11399. (f) Imahori, H.; Fujimoto, A.; Kang, S.; Hotta, H.; Yoshida, K.; Umeyama, T.; Matano, Y.; Isoda, S. *Tetrahedron* **2006**, *62*, 1955.

(20) (a) Imahori, H.; Hagiwara, K.; Aoki, M.; Akiyama, T.; Taniguchi, S.; Okada, T.; Shirakawa, M.; Sakata, Y. *J. Am. Chem. Soc.* **1996**, *118*, 11771. (b) Imahori, H.; Tkachenko, N. V.; Vehmanen, V.; Tamaki, K.; Lemmetyinen, H.; Sakata, Y.; Fukuzumi, S. *J. Phys. Chem. A* **2001**, *105*, 1750. (c) Tkachenko, N. V.; Guenther, C.; Imahori, H.; Tamaki, K.; Sakata, Y.; Fukuzumi, S.; Lemmetyinen, H. *Chem. Phys. Lett.* **2000**, *326*, 344. (d) Vehmanen, V.; Tkachenko, N. V.; Imahori, H.; Fukuzumi, S.; Lemmetyinen, H. *Spectrochimi. Acta, Part A* **2001**, *57*, 2229. (e) Wahadoszamen, M.; Nakabayashi, T.; Kang, S.; Imahori, H.; Ohta, N. *J. Phys. Chem. B* **2006**, *110*, 20354.

(21) (a) Evans, D. R.; Fackler, N. L. P.; Xie, Z.; Rickard, C. E. F.; Boyd, P. D. W.; Reed, C. A. *J. Am. Chem. Soc.* **1999**, *121*, 8466. (b) Sun, D.; Tham, F. S.; Reed, C. A.; Chaker, L.; Boyd, P. D. W. *J. Am. Chem. Soc.* **2002**, *124*, 6604. (c) Tashiro, K.; Aida, T.; Zheng, J.-Y.; Kinbara, K.; Saigo, K.; Sakamoto, S.; Yamaguchi, K. *J. Am. Chem. Soc.* **1999**, *121*, 9477. (d) Boyd, P. D. W.; Reed, C. A. *Acc. Chem. Res.* **2005**, *38*, 235.

(22) (a) Kamat, P. V.; Barazzouk, S.; Thomas, K. G.; Hotchandani, S. *J. Phys. Chem. B* **2000**, *104*, 4014. (b) Kamat, P. V.; Haria, M.; Hotchandani, S. *J. Phys. Chem. B* **2004**, *108*, 5166. (c) Kamat, P. V.; Barazzouk, S.; Hotchandani, S.; Thomas, K. G. *Chem. Eur. J.* **2000**, *6*, 3914.

(23) (a) Eu, S.; Hayashi, S.; Umeyama, T.; Oguro, A.; Kawasaki, M.; Kadota, N.; Matano, Y.; Imahori, H. *J. Phys. Chem. C* **2007**, *111*, 3528. (b) Imahori, H.; Hayashi, S.; Umeyama, T.; Eu, S.; Oguro, A.; Kang, S.; Matano, Y.; Shishido, T.; Ngamsinlapasathian, S.; Yoshikawa, S. *Langmuir*, **2006**, *22*, 11405.

(24) (a) Hirsch, A.; Lamparth, I.; Karfunkel, H. R. *Angew. Chem. Int. Ed. Engl.* **1994**, *33*, 437. (b) Hirsch, A.; Lamparth, I.; Grösser, T. *J. Am. Chem. Soc.* **1994**, *116*, 9385. (c) Lamparth, I.; Maichle-Mössmer, C.; Hirsch, A. *Angew. Chem. Int. Ed. Engl.* **1995**, *34*, 1607.

(25) (a) Lindsey, J. S.; Schreiman, I. C.; Hsu, H. C.; Kearney, P. C.; Marguerettaz, A. M. *J. Org. Chem.* **1987**, *52*, 827. (b) Harada, A.; Shiotsuki, K.; Fukushima, H.; Yamaguchi, H.; Kamachi, M. *Inorg. Chem.* **1995**, *34*, 1070. (c) Chudinov, A. V.; Rumyantseva, V. D.; Lobanov, A. V.; Chudinova, G. K.; Stomakhin, A. A.; Mironov, A. F. *Rus. J. Bioorg. Chem.* **2001**, *30*, 89.

(26) (a) Colthup, N. B.; Daly, L. H.; Wiberley, S. E. *Introduction to Infrared and Raman Spectroscopy*. 3rd ed.; Academic Press, Inc.: San Diego, CA, 1990. (b) Génin, F.; Quilès, F.; Burneau, A. *Phys. Chem. Chem. Phys.* **2001**, *3*, 932. (c) Dong, J.; Ozaki, Y. *Macromolecules* **1997**, *30*, 286. (d) Ye, S.; Morita, S.; Li, G.; Noda, H.; Tanaka, M.; Uosaki, K.; Osawa, M., *Macromolecules* **2003**, 36, 5694.

(27) (a) Maçôas, E. M. S.; Fausto, R.; Lundell, J.; Pettersson, M.; Khriachtchev, L.; Räsänen, M. *J. Phys. Chem. A* **2000**, *104*, 11725. (b) Wolfs, I.; Desseyn, H. O. *Applied Spectroscopy* **1996**, *50*, 1000.

(28) An equimolar DMF solution (1.0 mM) of porphyrin and/or fullerene was spin-coated (rotation rate = 500 rpm for 20 s and then 2000 rpm for 40 s) onto a mica substrate, followed by evaporation in air at room temperature. This procedure was repeated three times. Finally, the mica substrate was dried in a vacuum for 2 h.

(29) The author measured absorption spectra of TiO_2/ZnP-acid+C_{60}-acid film under four different conditions, that is, in air using dry film, in acetonitrile, in electrolyte solution (acetonitrile solution containing 63 mM LiI and 1.3 mM I_2), and under the photoelectrochemical conditions in which the positive potential (0.1 V vs SCE) is applied to the film that is in contact with the electrolyte solution (Figure 8). The three spectra taken in air, in acetonitrile, and in electrolyte solution revealed similar absorption with almost the same peak positions. On the other hand, the absorption spectrum under the photoelectrochemical conditions was red-shifted and broadened relative to the three spectra. These results are consistent with the red-shift and broadening of the action spectrum compared to the absorption spectrum in air. Moreover, CT interaction between the porphyrin and TiO_2 surface as well as between the porphyrin and the C_{60} molecules may also account for the difference in the absorption and action spectra. (a) He, J.; Hagfeldt, A.; Lindquist, S-E. *Langmuir* **2001**, *17*, 2743. (b) Imahori, H.; Hasobe, T.; Yamada, H.; Nishimura, Y.; Yamazaki, I.; Fukuzumi, S. *Langmuir* **2001**, *17*, 4925.

(30) (a) Durrant, J. R.; Haque, S. A.; Palomares, E. *Coord. Chem. Rev.* **2004**, *248*, 1247. (b) Gregg, B. A. *Coord. Chem. Rev.* **2004**, *248*, 1215. (c) Katoh, R.; Furube, A.; Barzykin, A. V.; Arakawa, H.; Tachiya, M. *Coord. Chem. Rev.* **2004**, *248*, 1195. (d) Tachibana, Y.; Moser, J. E.; Grätzel, M.;

Klug, D. R.; Durrant, J. R. *J. Phys. Chem.* **1996**, *100*, 20056. (e) Kay, A.; Humphry-Baker, R.; Grätzel, M. *J. Phys. Chem.* **1994**, *98*, 952. (f) Clifford, J. N.; Palomares, E.; Nazeeruddin, M. K.; Grätzel, M.; Nelson, J.; Li, X.; Long, N. J.; Durrant, J. R. *J. Am. Chem. Soc.* **2004**, *126*, 5225.

(31) (a) Ellingson, R. J.; Asbury, J. B.; Ferrere, S.; Ghosh, H. N.; Sprague, J. R.; Lian, T. Q.; Nozik, A. J. *J. Phys. Chem. B* **1998**, *102*, 6455. (b) Fessenden, R. W.; Kamat, P. V. *J. Phys. Chem.* **1995**, *99*, 12902. (c) Asbury, J. B.; Hao, E.; Wang, Y. Q.; Ghosh, H. N.; Lian, T. Q. *J. Phys. Chem. B* **2001**, *105*, 4545. (d) Watson, D. F.; Marton, A.; Stux, A. M.; Meyer, G. J. *J. Phys. Chem. B* **2004**, *108*, 11680. (e) Wienke, J.; Schaafsma, T. J.; Goossens, A. *J. Phys. Chem. B* **1999**, *103*, 2702. (g) Koehorst, R. B. M.; Boschloo, G. K.; Savenije, T. J.; Goossens, A.; Schaafsma, T. J. *J. Phys. Chem. B* **2000**, *104*, 2371. (h) Fungo, F.; Otero, L.; Durantini, E. N.; Silber, J. J.; Sereno, L. E. *J. Phys. Chem. B* **2000**, *104*, 7644.

(32) The surface coverage of C_{60}-acid in DMF is determined as 4.0 x 10^{-11} mol cm^{-2}, which corresponds to 24% of the actual surface area of the TiO_2 electrode, considering the molecular size (0.98 nm^2).

(33) When C_{60}-acid and ZnP-acid are adsorbed onto TiO_2 in MeOH separately, the adsorption rates are similar. However, the saturated surface coverage of C_{60}-acid (adsorption time = 12 h) is 17% of the complete monolayer coverage, whereas ZnP-acid yields the complete monolayer coverage (8.0×10^{-11} mol cm^{-2}) for the adsorption time of 12 h.

(34) ZnP-acid and C_{60}-acid were also assembled onto the TiO_2 electrode modified with the C_{60}-acid molecules by immersing the pre-treated TiO_2 electrode into the DMF solution of ZnP-acid and C_{60}-acid. The IPCE values are similar (ZnP-acid+C_{60}-acid system: 37%, ZnP-acid+C_{60}-ester system: 36%, ZnP-acid system: 34 % (input power: 68 μW cm^{-2}, λ_{ex} = 444 nm, applied potential: 0.10 V vs SCE)). Thus, the hydrogen bonding effects on the IPCE values are minor in this assembly method due to the direct adsorption of ZnP-acid onto the TiO_2 surface through the carboxylic acid.

(35) The estimation of the absorbed photon to current efficiency (APCE) at the Q band region, where the absorbance of the film is low (< 0.1), may contain large experimental error because of the small absorbance and the red-shift of action spectrum compared with the absorption spectrum. On the other hand, the absorbance at the Soret band region is almost saturated (> 1) so that the error in the APCE is small. Therefore, the author estimated the APCE values of each electrode at 444 nm for comparison.

(36) When ZnP-acid is directly adsorbed onto TiO_2 in MeOH which yielding the formation of complete porphyrin monolayer on the TiO_2 surface (adsorption time = 12 h), the cell performance (η = 2.0%, J_{sc} = 6.0 mA cm^{-2}, V_{oc} = 0.54 V, *ff* = 0.61) is comparable to that (η = 2.1%) of TiO_2/ZnP-acid+C_{60}-acid cell (Figure 7). This reveals that the role of carboxylic acid groups as

linkers to TiO_2 for photocurrent generation is more significant than that of the hydrogen bonding between porphyrin and fullerene.

(37) (a) Shen, Y. R. *The Principles of Nonlinear Optics*, Wiley, New York, 1984. (b) Ye, S.; Noda, H.; Morita, S.; Uosaki, K.; Osawa, M. *Langmuir* **2003**, *19*, 2238. (c) Li, G.; Ye, S.; Morita, S.; Nishida, T.; Osawa, M. *J. Am. Chem. Soc.* **2004**, *126*, 12198. (d) Holman, J.; Davies, P. B.; Nishida, T.; Ye, S.; Neivandt, D. J. *J. Phys. Chem. B* **2005**, *109*, 18723. (e) Nishida, T.; Johnson, C. M.; Holman, J.; Osawa, M.; Davies, P. B.; Ye, S. *Phys. Rev. Lett.* **2006**, *96*, 77402.

(38) Nakade, S.; Matsuda, M.; Kambe, S.; Saito, Y.; Kitamura, T.; Sakata, T.; Wada, Y.; Mori, H.; Yanagida, S. *J. Phys. Chem. B* **2002**, *106*, 10004.

(39) (a) Tkachenko, N. V.; Rantala, L.; Tauber, A. Y.; Helaja, J.; Hynninen, P. H.; Lemmetyinen, H. *J. Am. Chem. Soc.* **1999**, 121, 9378. (b) Kesti, T. J.; Tkachenko, N. V.; Vehmanen, V.; Yamada, H.; Imahori, H.; Fukuzumi, S.; Lemmetyinen, H. *J. Am. Chem. Soc.* **2002**, *124*, 8067. (c) Tkachenko, N. V.; Lemmetyinen, H.; Sonoda, J.; Ohkubo, K.; Sato, T.; Imahori, H.; Fukuzumi, S. *J. Phys. Chem. A* **2003**, *107*, 8834.

Chapter 6

Supramolecular Donor-Acceptor Heterojunctions by Vectorial Stepwise Assembly of Porphyrins and Coordination Bonded Fullerene Arrays for Photocurrent Generation

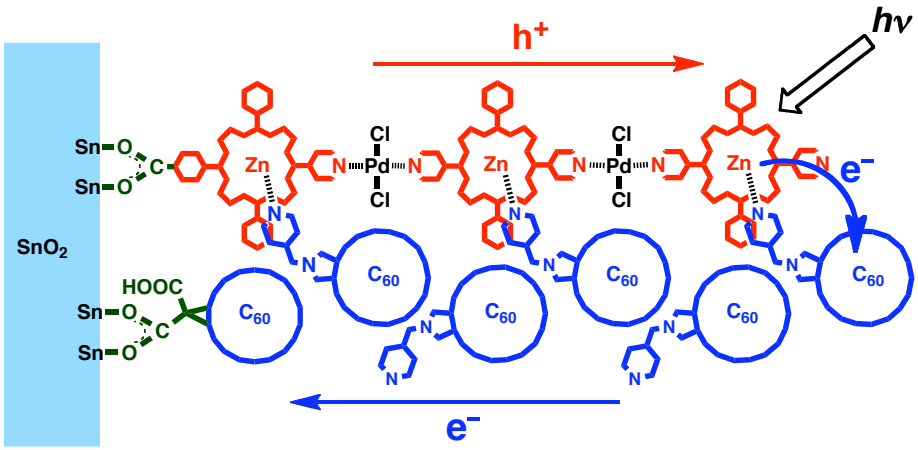

Abstract

A novel strategy has been developed to construct the vertical arrangement of bicontinuous donor-acceptor arrays on a semiconducting electrode with stepwise assembly of porphyrins and coordination bonded fullerene. The relationship between the film structure and photoelectrochemical properties has been elucidated as a function of the number of donor layer for the first time. The maximum IPCE value (21%) is comparable to the highest value (20%) among vertical arrangement of bicontinuous donor-acceptor arrays on electrodes.

Introduction

Bicontinuous donor-acceptor (D-A) arrays at molecular level have attracted increasing scientific and technological interest due to their potential applications in organic photovoltaics.[1] Such D-A arrays would yield efficient charge separation (CS) and transportation of separated charges to respective electrodes leading to enhanced photocurrent generation provided ideally vertical arrangement of the D-A arrays on the electrodes. Although nanostructures with bicontinuous D-A arrays have been obtained by self-assembly of D-A molecules,[2] it is still difficult to achieve desirable vertical arrangement of bicontinuous D-A arrays on an electrode.[3] Here the author reports a novel approach to construct vertical alignment of bicontinuous D-A arrays on a flat SnO_2 electrode for photoelectrochemical device (Figure 1). A palladium-mediated stepwise self-assembly of zincporphyrins (ZnP) as a donor ensures the vertical growth of porphyrin chains on the SnO_2 electrode.[4] Pyridylfullerenes (Py-C_{60}) as an acceptor are infiltrated into the porphyrin brush by using the coordination bonding of the pyridyl moiety to the zinc atom together with π-π interaction between Py-C_{60}.[5] Therefore, one can systematically investigate the relationship between the film structure and photoelectrochemical properties as a function of the number of porphyrin layer.

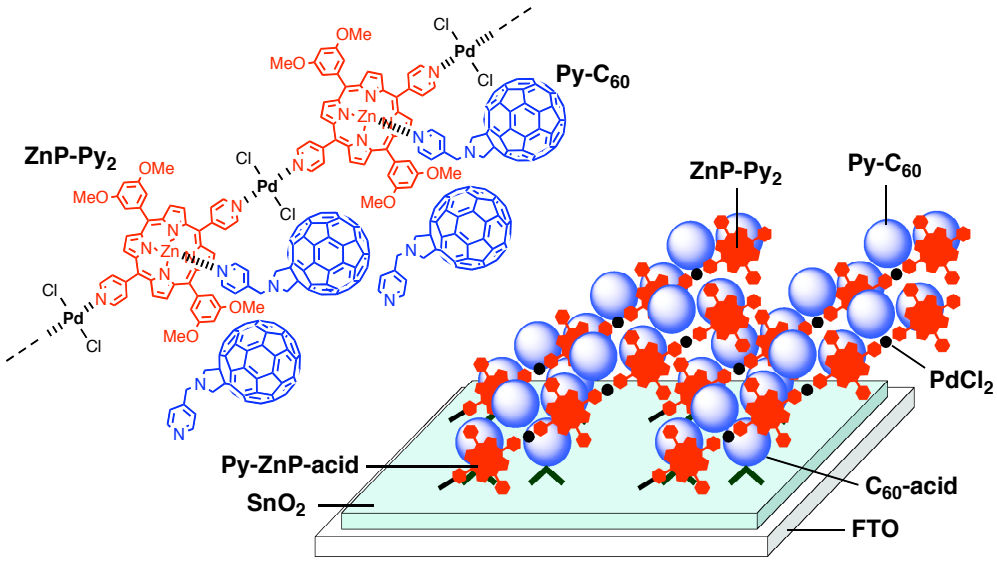

Figure 1. Schematic porphyrin-fullerene arrays on a SnO_2 electrode.

Results and Discussion

Preparation of Porphyrin-Fullerene Arrays on a SnO_2 Electrode. A SnO_2 electrode was modified with ZnP arrays as follows. A thin and nonporous SnO_2 film with a roughness factor of 1.1 was prepared on a FTO electrode.[6] The assembly of ZnP arrays on the SnO_2 electrode was performed by the similar procedure described by Qian et al (Scheme 1).[4b] First, pyridylporphyrin acid (Py-ZnP-acid, Figure 2) was adsorbed on the surface of the SnO_2 electrode through the carboxylic group. The porphyrin density (1.8×10^{-10} mol cm^{-2}) is comparable to the calculated value of the well-packed porphyrin monolayer (1.5×10^{-10} mol cm^{-2}) considering the occupied area (1.2 nm^2 $molecule^{-1}$) and the roughness factor (1.1) of the SnO_2 electrode. Then, Pd(II) was coordinated to the pyridyl group of the adsorbed Py-ZnP-acid, followed by coordination of bispyridylporphyrin ($ZnP\text{-}Py_2$) to the Pd atom. The number of the porphyrin layers could be controlled by that of cycles of $ZnP\text{-}Py_2$ deposition via coordination bonding between the pyridyl group and Pd(II). Consequently, ZnP arrays were formed on the SnO_2 electrode (denoted as $SnO_2/(ZnP)_n$, number of porphyrin layers (n) = 1–8). Figure 3a displays UV-vis absorption spectra measured after each assembly of the porphyrins on the electrode. The absorption due to the porphyrin was increased by the repeated number of the deposition cycles, implying the successive growth of porphyrin chains. The amounts of the assembled porphyrins exhibited a linear increase with increasing the layer numbers of porphyrins and leveled off at $n = 8$ (Figure 4).

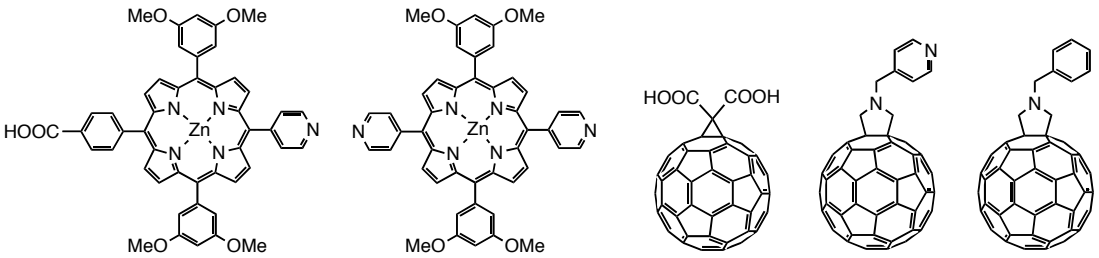

Figure 2. Porphyrin and fullerene derivatives used in this study.

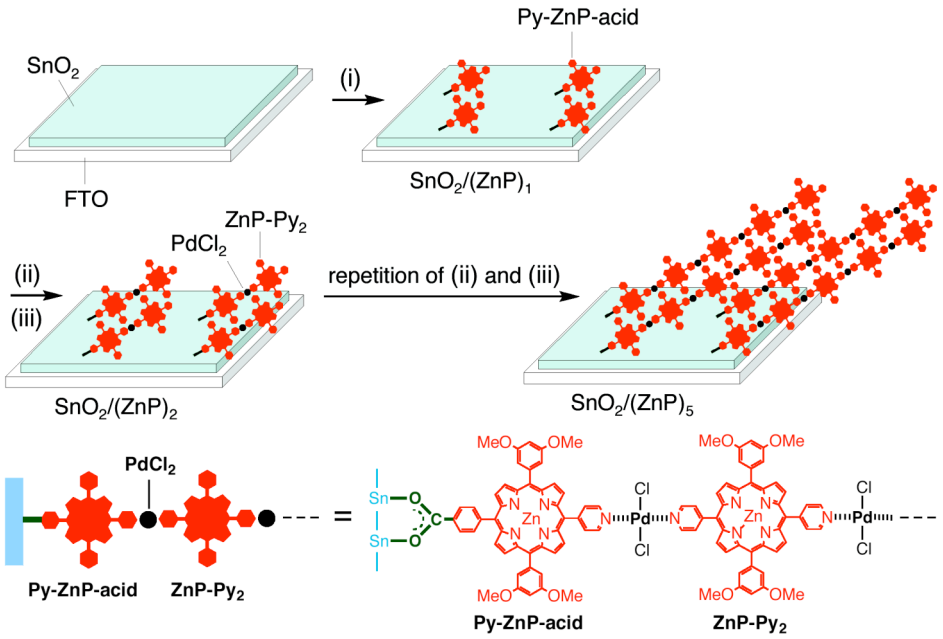

Scheme 1. Procedures for preparation of porphyrin arrays on a SnO_2 electrode. (i) A SnO_2 electrode was immersed into Py-ZnP-acid (0.2 mM in DMF) for 4 h, and then washed with DMF. (ii) The SnO_2 electrode modified with the porphyrins was immersed into K_2PdCl_4 (3.0 mM in water) for 20 min, and then washed with water and finally immersed into MeOH for 20 min. (iii) The SnO_2 electrode was immersed into ZnP-Py_2 (0.2 mM in $CHCl_3$/MeOH (3:1, v/v)) for 20 min, and then washed with $CHCl_3$, and finally immersed into MeOH for 20 min to yield $SnO_2/(ZnP)_n$ (n = 1–8) electrode.

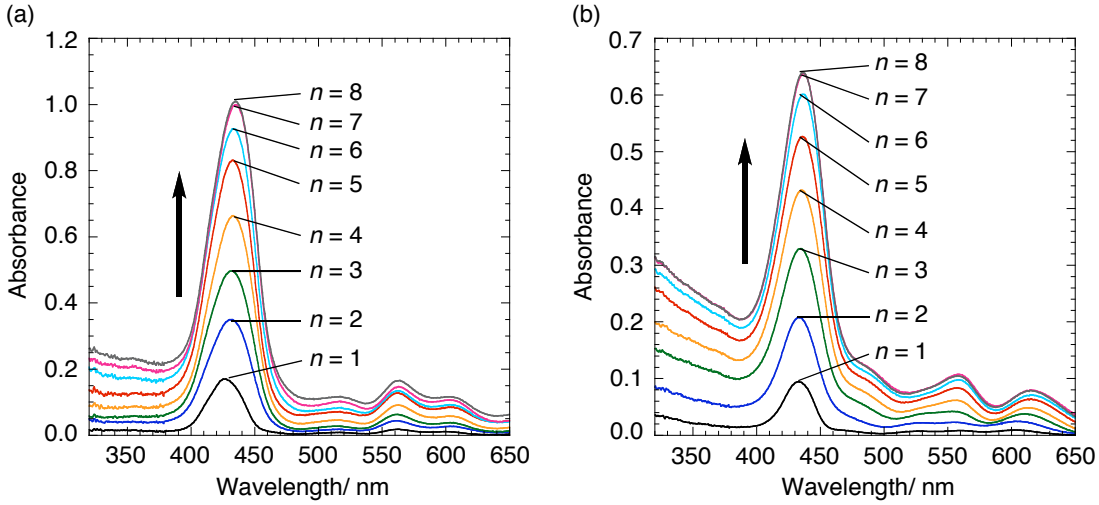

Figure 3. Spectral change in the absorption spectra of electrodes after successive assembly of ZnP-Py_2 on the electrode modified with (a) Py-ZnP-acid ($SnO_2/(ZnP)_n$) and (b) Py-ZnP-acid and C_{60}-acid (SnO_2/C_{60}-acid+$(ZnP)_n$). The absorption arising from the SnO_2 electrode was subtracted from the spectrum.

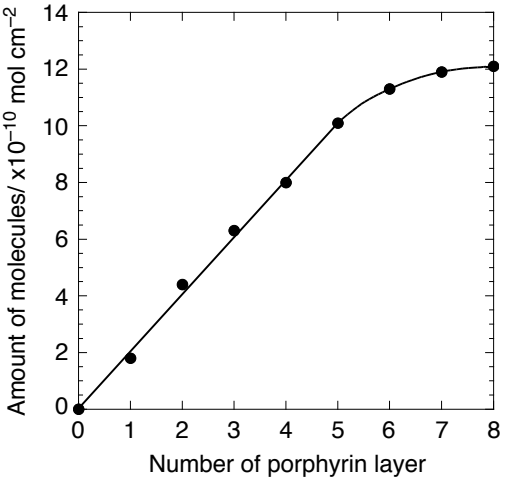

Figure 4. Plots for the amounts of the porphyrin molecules assembled on the SnO_2 electrode as a function of the number of porphyrin layer. See the Experimental for determination of the amounts of the porphyrin molecules.

Assembly of ZnP-C_{60} composites was also performed on the SnO_2 electrode following Scheme 2. First, Py-ZnP-acid and C_{60}-acid (Figure 2) were simultaneously adsorbed on the surface of the SnO_2 electrode, and then successive assembly of ZnP-Py_2 molecules was achieved (Figure 3b), as described above (denoted as SnO_2/C_{60}-acid+$(ZnP)_n$). The C_{60} density (2.0×10^{-10} mol cm^{-2}) is two times larger than the calculated value (C_{60}-acid: 1.0×10^{-10} mol cm^{-2}) for the well-packed porphyrin-C_{60} mixed monolayer considering the occupied area (C_{60}-acid: 0.8 nm^2 molecule^{-1}), the roughness factor (1.1) of the SnO_2 electrode, and the slope (Py-ZnP-acid: 1.0×10^{-10} mol cm^{-2}) of the plot for the amounts of the porphyrin assembled on the SnO_2 electrode as a function of the number of porphyrin layer (Figure 5). The ratio of Py-ZnP-acid and C_{60}-acid adsorbed on the surface of SnO_2 electrode was determined as [Py-ZnP-acid]:[C_{60}-acid] = 1:2. Besides, the SnO_2/C_{60}-acid+$(ZnP)_n$ electrodes were further immersed into the *o*-dichlorobenzene (ODCB) solution of Py-C_{60} which would form coordination bonding with the zincporphyrins,[5] incorporating Py-C_{60} into the porphyrin arrays (denoted as SnO_2/C_{60}-acid+$(ZnP)_n$+Py-C_{60}). Treatment of the SnO_2/C_{60}-acid+$(ZnP)_n$ electrodes with the solution of Py-C_{60} resulted in a significant rise in the absorption around 320–400 nm stemming from the absorption of Py-C_{60} together with the red-shift of Soret band (Figure 6a).[5] This demonstrates the complexation of Py-C_{60} and ZnP and the infiltration of Py-C_{60} from top to bottom of the ZnP brushes. The SnO_2/C_{60}-acid+$(ZnP)_n$ electrodes were also treated with the ODCB solution of Ph-C_{60} without the pyridyl moiety (Figure 2). A slight rise in the absorption around 320–400 nm and no red-shift were observed for the SnO_2/C_{60}-acid+$(ZnP)_n$+Ph-C_{60} electrode, suggesting the weak interpenetration of Ph-C_{60} into the ZnP arrays due to π-π interaction between Ph-C_{60} solely (Figure 6b).[1c] The infiltrated amounts of Py-C_{60} or Ph-C_{60} were determined by

measuring an increase in absorbance of the electrodes at 375 nm resulting from the modification with Py-C_{60} or Ph-C_{60}; [ZnP]:[Py-C_{60}] = 1:3–4 (n = 2–6) for the SnO_2/C_{60}-acid+$(ZnP)_n$+Py-C_{60} electrodes, [ZnP]:[Ph-C_{60}] = 1:1–2 (n = 2–6) for the SnO_2/C_{60}-acid+ $(ZnP)_n$+Ph-C_{60} electrodes (Figure 5). The increased ratio for Py-C_{60} relative to Ph-C_{60} implies that the coordination bonding in addition to the π-π interaction contributes to the infiltration greatly. The steady-state fluorescence experiments revealed intense quenching of the porphyrin fluorescence for the SnO_2/C_{60}-acid+$(ZnP)_n$+Py-C_{60} electrodes compared with that of the reference without the C_{60} molecules (Figure 7). These results suggest that the porphyrin excited singlet state (^{1}ZnP*) is quenched by Py-C_{60} interpenetrated into the ZnP arrays via electron transfer (ET).[1c,2e,5] A weak emission around 700–800 nm may be attributed to the direct excitation of the C_{60} molecules incorporated into ZnP arrays due to π-π interaction between C_{60} molecules.[7]

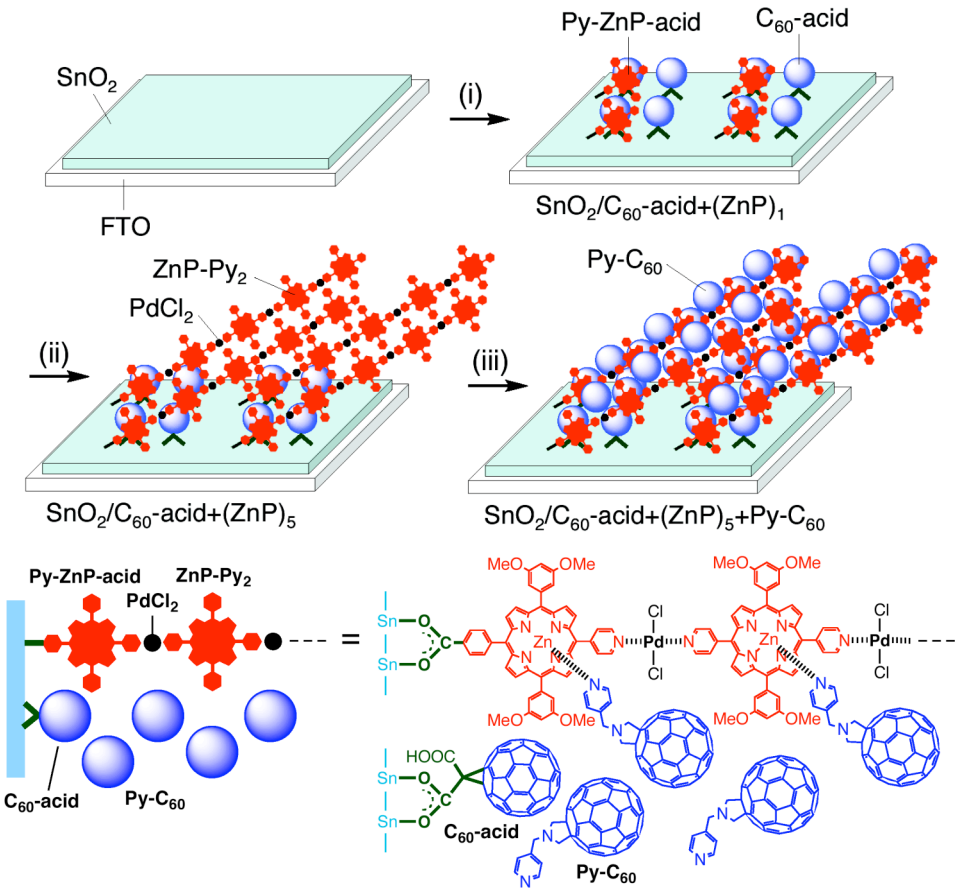

Scheme 2. Procedures for preparation of porphyrin-fullerene arrays on a SnO_2 electrode. (i) A SnO_2 electrode was immersed into an equimolar DMF solution (0.20 mM) of Py-ZnP-acid and C_{60}-acid for 4 h, and then washed with DMF to yield SnO_2/C_{60}-acid+$(ZnP)_1$ electrode. (ii) ZnP-Py_2 was sequentially deposited via coordination bonding with Pd(II), as illustrated in Scheme S1, to yield SnO_2/C_{60}-acid+$(ZnP)_n$ (n = 1–8) electrode. (iii) The SnO_2 electrode modified with C_{60}-acid and the porphyrin arrays was immersed into Py-C_{60} (1.0 mM in o-dichlorobenzene) for 4 h and washed with o-dichlorobenzene to yield SnO_2/C_{60}-acid+$(ZnP)_n$+Py-C_{60} (n = 1–8) electrode.

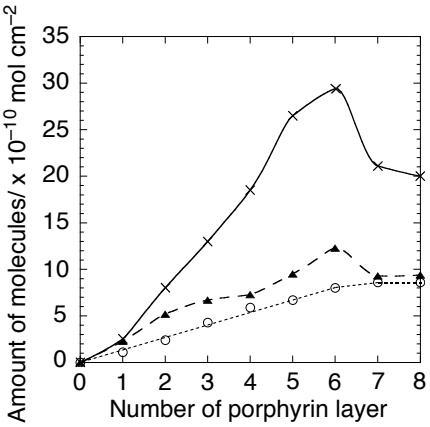

Figure 5. Plots for the amounts of the porphyrin (dotted line with open circles), Ph-C_{60} (dashed line with triangles), and Py-C_{60} (solid line with crosses) assembled on the SnO_2 electrode as a function of the number of porphyrin layer. The ε values of Py-C_{60} (1.0×10^4 cm^{-1} M^{-1}) and Ph-C_{60} (1.0×10^4 cm^{-1} M^{-1}) at 375 nm were used for the determination.

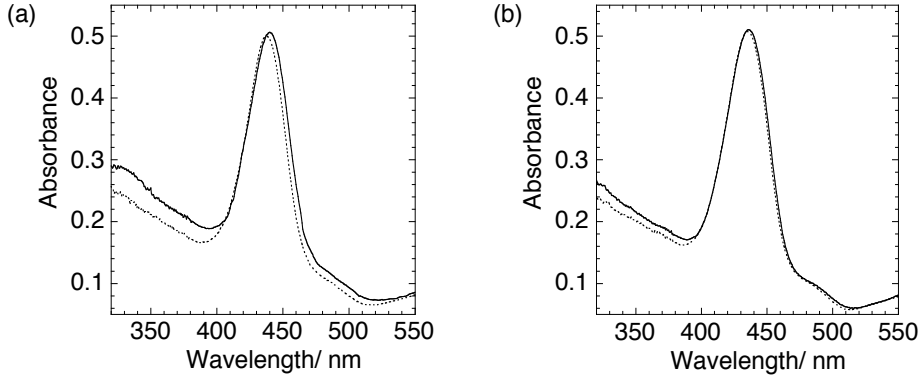

Figure 6. UV-visible absorption spectra of (a) SnO_2/C_{60}-acid+$(ZnP)_5$ (dotted line) and SnO_2/C_{60}-acid+$(ZnP)_5$+Py-C_{60} (solid line) and (b) SnO_2/C_{60}-acid+$(ZnP)_5$ (dotted line) and SnO_2/C_{60}acid+$(ZnP)_5$+Ph-C_{60} (solid line). The absorption arising from the SnO_2 electrode was subtracted from the spectrum.

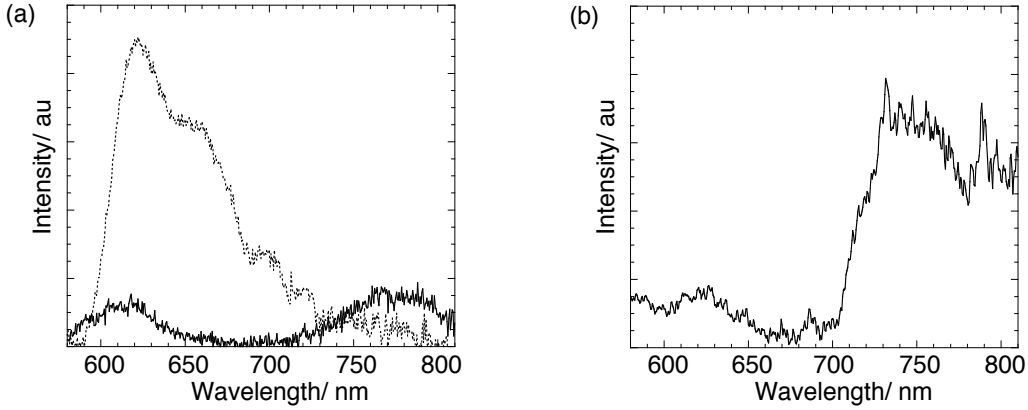

Figure 7. Steady-state fluorescence spectra of (a) SnO_2/$(ZnP)_2$ (dotted line) and SnO_2/C_{60}-acid+$(ZnP)_2$+Py-C_{60} (solid line) electrodes and (b) SnO_2/Py-C_{60} electrode with an excitation wavelength of 430 nm. The SnO_2/Py-C_{60} electrode was prepared by evaporation of Py-C_{60} solution (1.0 mM in *o*-dichlorobenzene) on a FTO/SnO_2 electrode.

Film Structures of the Porphyrin-Fullerene Arrays. The average thickness of the porphyrin arrays was evaluated by using transmission electron microscopy (TEM) measurements for the SnO_2 nanoparticles modified with the porphyrin arrays (Figure 8). The dark-fields in the TEM images were the SnO_2 nanoparticles, and the layers of porphyrin arrays were observed as the thin layers at the edge of the SnO_2 nanoparticles. Close inspection of the TEM images showed that the thickness linearly increased with increasing the number of the porphyrin layers, indicating the linear elongation of porphyrin chains. From the comparison of the film thicknesses and the length of porphyrin arrays estimated from the sizes of porphyrins and Pd complex (Table 1 and Figure 9), the orientation angle (θ) between the porphyrin arrays and the SnO_2 surface is estimated as 28 ± 5°, which is consistent with the value for similar porphyrin arrays on quartz substrates.[4b] Similar trend is noted for the SnO_2 nanoparticles further modified with C_{60}-acid and Py-C_{60} (Table 1).

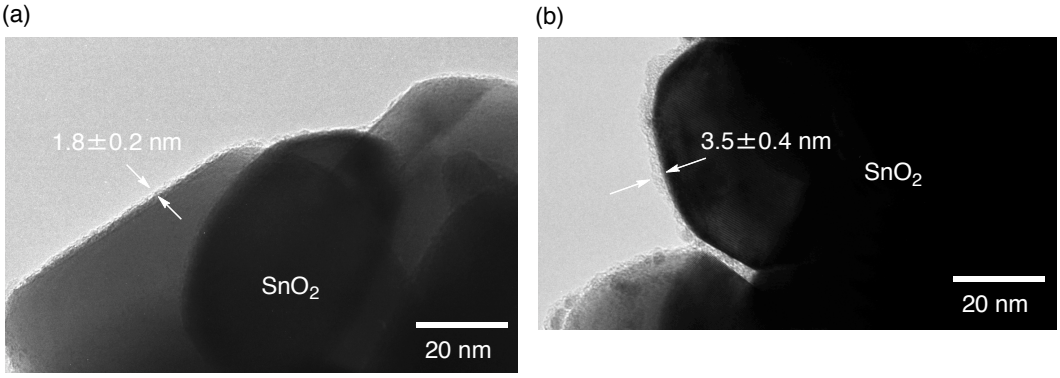

Figure 8. TEM images of SnO_2 nanoparticles (NPs) modified with porphyrin arrays. (a) SnO_2 NP/$(ZnP)_2$ and (b) SnO_2 NP/$(ZnP)_4$.

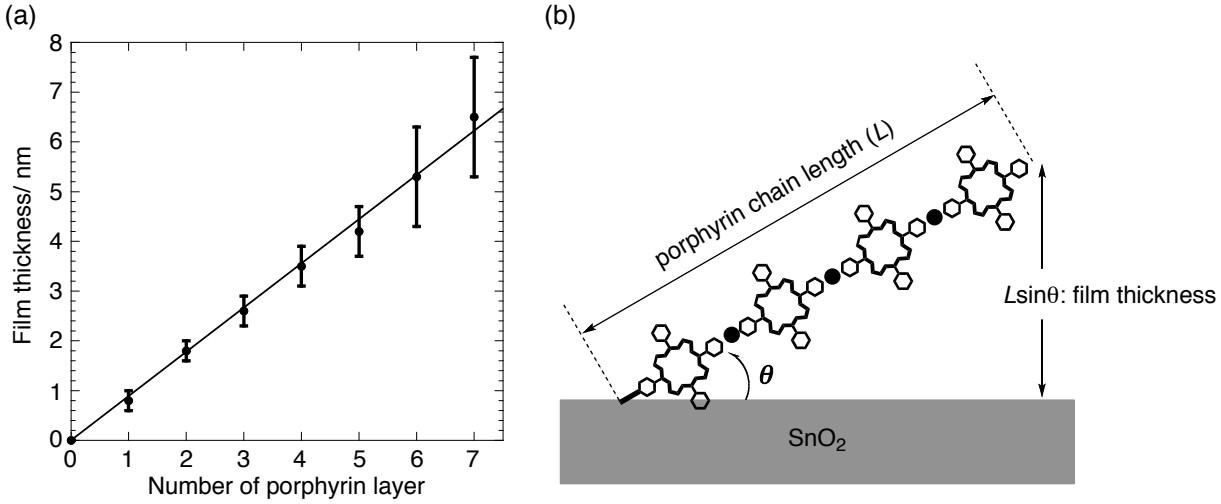

Figure 9. (a) Plot for the film thickness as a function of the number of porphyrin layer, and (b) a schematic structure of the porphyrin chain tilted to the SnO_2 plane.

Table 1. The film thickness and porphyrin chain length.

number of porphyrin layer	experimental film thickness/ nm		calculation	
	$SnO_2/(ZnP)_n$	SnO_2/C_{60}-acid+$(ZnP)_n$+Py-C_{60}	porphyrin chain length, L/ nm[a]	L[sin(28°)]/ nm[a]
1	0.8 ± 0.2	— [b]	1.7	0.8
2	1.8 ± 0.2	1.8 ± 0.3	3.6	1.7
3	2.6 ± 0.3	— [b]	5.5	2.6
4	3.5 ± 0.4	3.3 ± 0.6	7.4	3.5
5	4.2 ± 0.5	— [b]	9.3	4.4
6	5.3 ± 1.0	5.2 ± 1.2	11.2	5.3
7	6.5 ± 1.2	— [b]	13.1	6.2

[a] The sizes of the porphyrins and palladium complexes were calculated by the molecular mechanics calculations. [b] Not measured.

Atomic force microscopy (AFM) measurements were performed for the SnO_2 films modified with ZnP and C_{60} (Figure 10, 11, 12). The images of the $SnO_2/(ZnP)_n$ (Figure 10) and SnO_2/C_{60}-acid+ $(ZnP)_n$+Ph-C_{60} (Figure 12) substrates exhibited domain structures which would result from the aggregation between the porphyrin chains, whereas those of the SnO_2/C_{60}-acid+$(ZnP)_n$+Py-C_{60} (n = 2–5) substrates disclosed the smooth surface morphology (Figure 11). In D-A blend films such as conjugated polymer and fullerene derivative in bulk heterojunction solar cells, an intimate mixing of the components leads to smooth surface morphology of the film which can be confirmed by using AFM.[1] Accordingly, the incorporation of Py-C_{60} molecules into the ZnP arrays suppresses the porphyrin aggregation, yielding the D-A bicontinuous arrays on the SnO_2 electrode.[8]

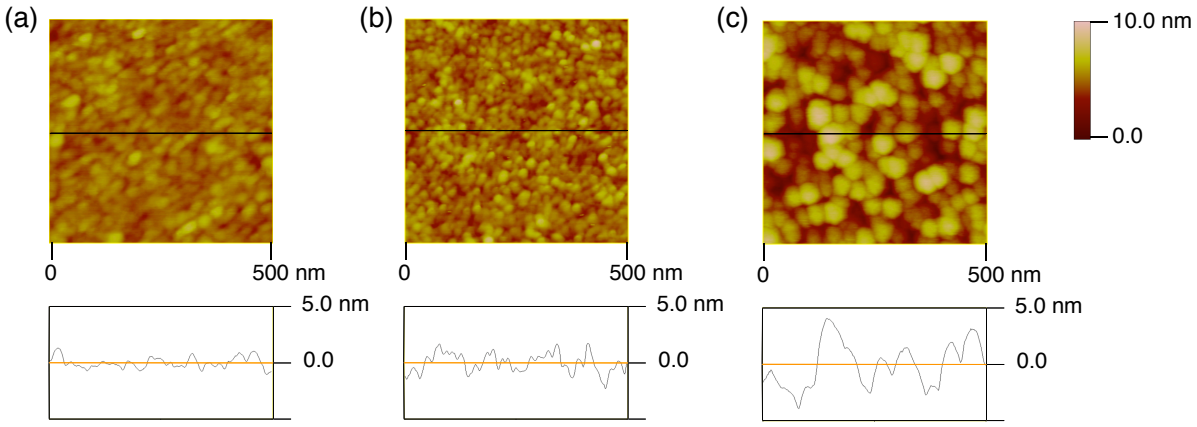

Figure 10. AFM images for surface morphology of (a) $SnO_2/(ZnP)_2$, (b) $SnO_2/(ZnP)_4$, (c) $SnO_2/(ZnP)_6$. The SnO_2 film was prepared on a glass substrate.

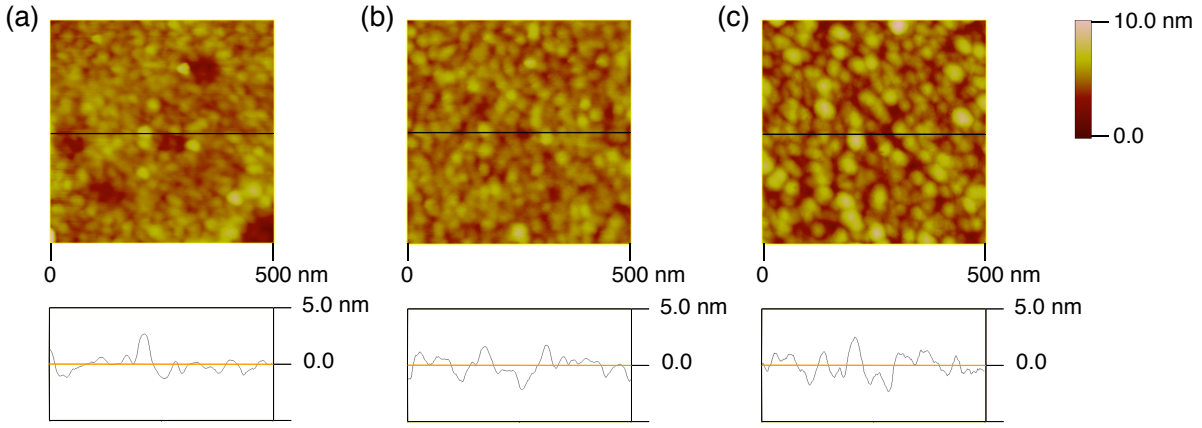

Figure 11. AFM images for surface morphology of (a) SnO_2/C_{60}-acid+$(ZnP)_2$+Ph-C_{60}, (b) SnO_2/C_{60}-acid+$(ZnP)_4$+Ph-C_{60}, (c) SnO_2/C_{60}-acid+$(ZnP)_6$+Ph-C_{60}.

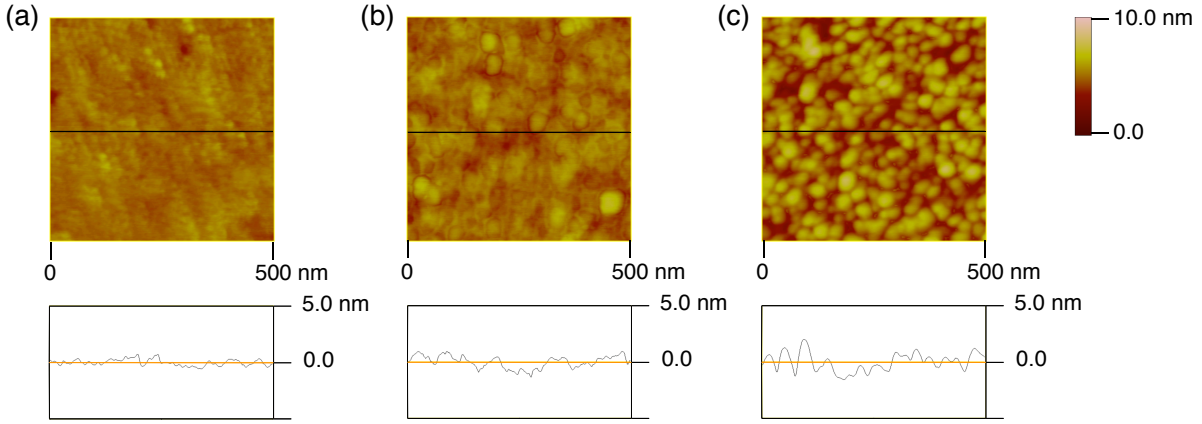

Figure 12. AFM images for surface morphology of (a) SnO_2/C_{60}-acid+$(ZnP)_2$+Py-C_{60}, (b) SnO_2/C_{60}-acid+$(ZnP)_4$+Py-C_{60}, and (c) SnO_2/C_{60}-acid+ $(ZnP)_6$+Py-C_{60}.

Photoelectrochemical Measurements. Figure 13 depicts the photocurrent action spectra for the modified electrodes, which closely resemble the corresponding absorption spectra of the electrodes (Figure 3). IPCE (incident photon-to-current efficiency) and APCE (absorbed photon-to-current efficiency) values of the $SnO_2/(ZnP)_n$ electrodes at 440 nm were plotted as a function of the number of porphyrin layers (n) in Figure 14a and Figure 15a, respectively. With increasing n, the IPCE as well as APCE values increased to reach maxima (n = 3) and then decreased gradually. The energy levels of the porphyrins were determined electrochemically from the first oxidation potential and optically from the band gap (2.00 eV) of Py-ZnP-acid and ZnP-Py_2 in dichloromethane, whereas the others were taken from literatures.[13] As established previously,[1c,2e,8] ^{1}ZnP* (–0.93 V vs NHE) injects electrons into the conduction band (CB) of SnO_2 (0 V vs NHE), followed by ET from I^- (0.50 V vs NHE) to the zinc porphyrin radical cation ($ZnP^{\bullet+}$, 1.07 V vs NHE), generating photocurrent (Scheme 3).

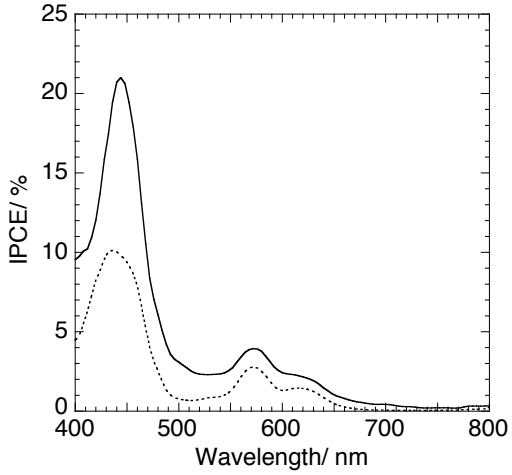

Figure 13. Photocurrent action spectra for $SnO_2/(ZnP)_3$ electrode (dotted line) and SnO_2/C_{60}-acid+$(ZnP)_5$+Py-C_{60} (solid line) electrode; applied potential: 0.05 V vs SCE; 0.5 M LiI and 0.01 M I_2 in acetonitrile.

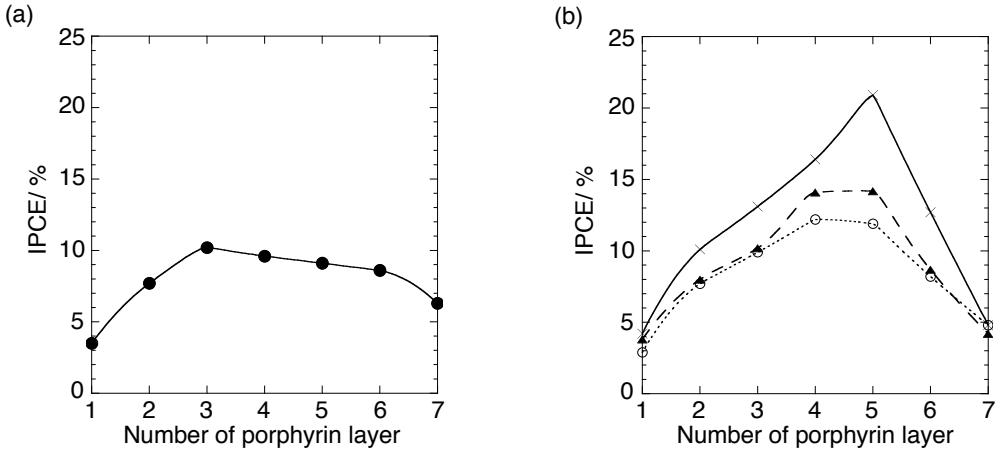

Figure 14. Plots for the IPCE values as a function of the number of porphyrin layers for (a) $SnO_2/(ZnP)_n$ (solid line with filled circles) and (b) SnO_2/C_{60}-acid+$(ZnP)_n$ (dotted line with open circles), SnO_2/C_{60}-acid+$(ZnP)_n$+Ph-C_{60} (dashed line with triangles), and SnO_2/C_{60}-acid+$(ZnP)_n$+Py-C_{60} (solid line with crosses); input power: 63 μW cm^{-2} (λ_{ex} = 440 nm); applied potential: 0.05 V vs SCE; 0.5 M LiI and 0.01 M I_2 in acetonitrile.

The trend is reasonable considering that the exciton diffusion length (~6 nm) of the porphyrin arrays, corresponding to the number of the porphyrins and the total length (n = 3), is comparable to that of copper phthalocyanine (8±3 nm) in bulk heterojunction solar cells.[9] It is noteworthy that, for the SnO_2/C_{60}-acid+$(ZnP)_n$+Py-C_{60} electrodes, the trend on the IPCE and APCE values as a function of n (Figures 14b and 15b) is parallel to that on the infiltrated amount of Py-C_{60} as a function of n. The slight difference in the maxima of the IPCE (n = 5) and the infiltrated amount of Py-C_{60} (n = 6) may result from balance between the porphyrin aggregation and the C_{60} infiltration, as seen in Figure 12. Similar trend is noted for the SnO_2/C_{60}-acid+$(ZnP)_n$+Ph-C_{60} electrodes.

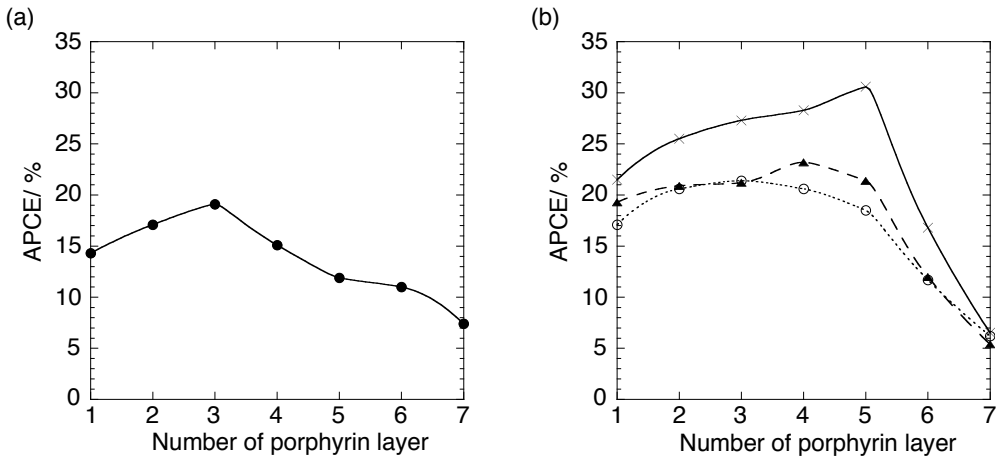

Figure 15. Plots for the APCE (adsorbed photon-to-current efficiency) values as a function of the number of porphyrin layer for (a) $SnO_2/(ZnP)_n$ (solid line with filled circles) and (b) SnO_2/C_{60}-acid+$(ZnP)_n$ (dotted line with open circles), SnO_2/C_{60}-acid+$(ZnP)_n$+Ph-C_{60} (dashed line with triangles), and SnO_2/C_{60}-acid+$(ZnP)_n$+Py-C_{60} (solid line with crosses); input power: 63 μW cm^{-2} (λ_{ex} = 440 nm).

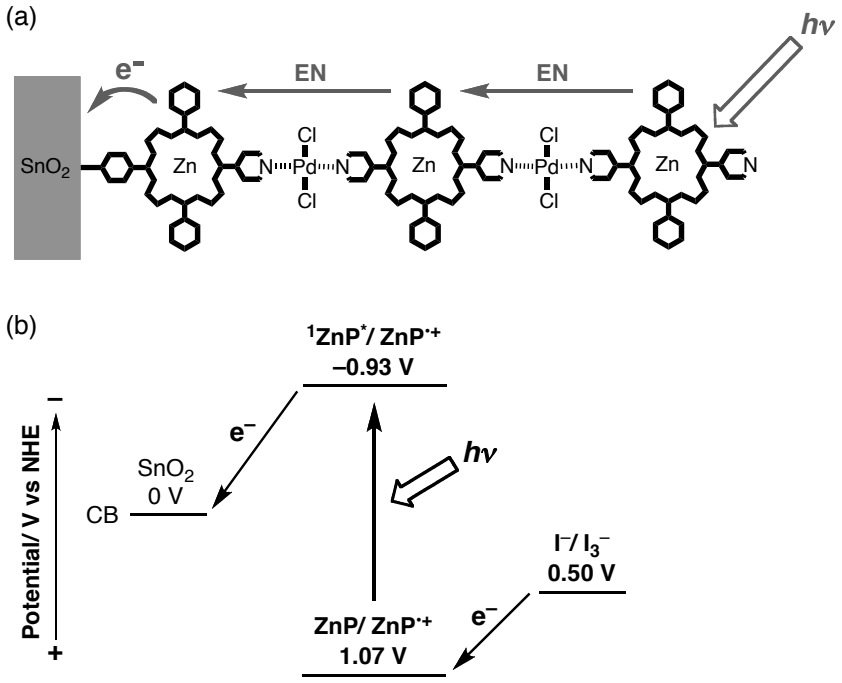

Scheme 3. (a) Schematic illustration for the photocurrent generation in the $SnO_2/(ZnP)_n$ systems revealing photoinduced energy transfer (EN) and electron transfer (ET) and (b) its energy diagram.

The photodynamics of the photoinduced CS processes was studied by femtosecond time-resolved transient absorption measurements (Figure 16). The bleaching at 620 nm arises from ^{1}ZnP*,[10] whereas the broad absorption around 660 nm originates from zinc porphyrin radical cation ($ZnP^{\bullet+}$).[10] Although both ^{1}ZnP* and $ZnP^{\bullet+}$ appear simultaneously, large Δabsorbance of the SnO_2/C_{60}-acid+$(ZnP)_7$+Py-C_{60} relative to the $SnO_2/(ZnP)_7$ around 660 nm exemplifies the additional contribution of the CS between ZnP and C_{60} to the enhancement in the photocurrent generation.

This is consistent with the fact that the APCE value of the SnO_2/C_{60}-acid+$(ZnP)_7$+Py-C_{60} system (7.1% at 560 nm) is larger than that of the $SnO_2/(ZnP)_7$ system (5.0% at 560 nm). That is, the exciton and carrier loss in the porphyrin arrays is suppressed due to the exciton capture and charge dissociation by C_{60}, which can rationalize the facts that the maximum IPCE and APCE values were attained at the higher number of the porphyrin layer for the SnO_2/C_{60}-acid+$(ZnP)_n$+Py-C_{60} systems (n = 5) than the $SnO_2/(ZnP)_n$ systems (n = 3). The decreasing trend of the IPCE and APCE values in the SnO_2/C_{60}-acid+$(ZnP)_7$+Py-C_{60} system (n = 6–8) correlates with the decreasing amount of the incorporated C_{60} molecules between the porphyrin brushes, which arises from the porphyrin aggregation, as seen in the AFM measurements (vide supra). In such a case the CS efficiency between the ^{1}ZnP* and the C_{60} would be decreased with increasing the number of the porphyrin layers, leading to the decrease in the IPCE and APCE values.

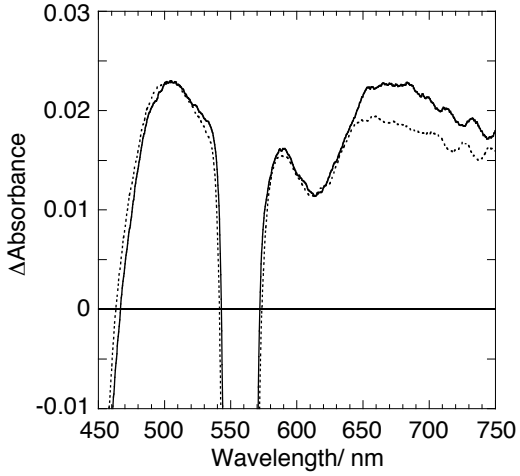

Figure 16. Transient absorption spectra of SnO_2/C_{60}-acid+$(ZnP)_7$ +Py-C_{60} (solid line) and $SnO_2/(ZnP)_7$ (dotted line) electrode at time delay of 1 ps after laser excitation at 560 nm. The spectrum of the $SnO_2/(ZnP)_7$ electrode was normalized to that of the SnO_2/C_{60}-acid+$(ZnP)_7$+Py-C_{60} electrode at 500 nm for comparison.

On the basis of the film structures and the photoelectrochemical properties of the SnO_2/C_{60}-acid+$(ZnP)_n$+Py-C_{60} systems together with the previously established photocurrent generation mechanism in similar porphyrin-fullerene composites on semiconducting electrodes,[1c,2e,8] the author can propose a photocurrent generation diagram as illustrated in Scheme 4. First, CS between ^{1}ZnP* and C_{60} takes place in addition to direct electron injection from ^{1}ZnP* to the CB of the SnO_2. The generated $C_{60}^{\bullet-}$ injects electrons into the CB of the SnO_2 via electron hopping through the C_{60} molecules infiltrated from top to bottom of the porphyrin brushes. Thus, the bicontinuous D-A arrays for the SnO_2/C_{60}-acid+$(ZnP)_n$+Py-C_{60} (n = 2–6) electrodes are responsible for the enhancement of photocurrent generation.

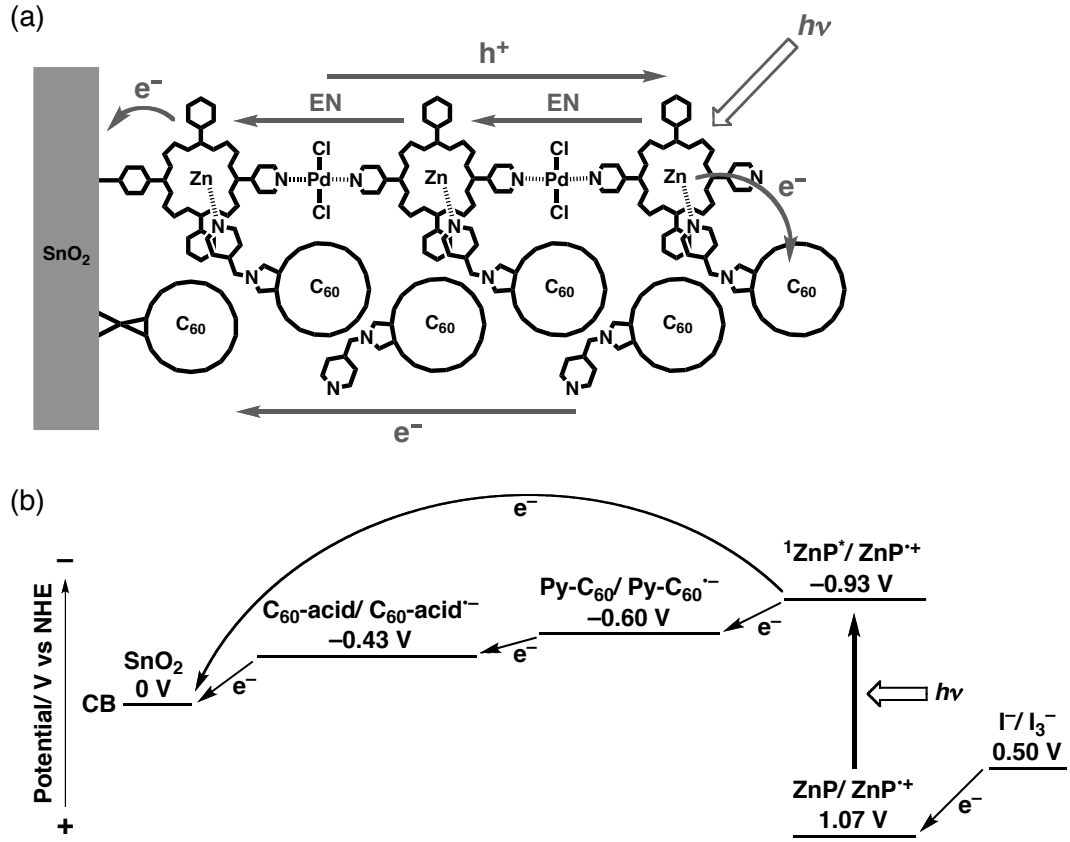

Scheme 4. (a) Schematic illustration for the photocurrent generation in the SnO_2/C_{60}-acid+$(ZnP)_n$+ Py-C_{60} systems and (b) its energy diagram. The levels of C_{60}-acid and Py-C_{60} were determined electrochemically from the first reduction potentials of C_{60}-acid and Py-C_{60} in chloroform.

Conclusion

The author has successfully developed the novel strategy for constructing the vertical arrangement of D-A arrays on a semiconducting electrode by using coordination bonding. The relationship between the film structure and photoelectrochemical properties has been elucidated as a function of the number of donor layers for the first time. UV-visible absorption, steady-state fluorescence, AFM, and TEM measurements disclosed that bicontinuous porphyrin-fullerene arrays were formed on SnO_2 electrodes when the numbers of porphyrin layers are from 2 to 5. The maximum IPCE value (21%) is comparable to the highest value (20%) among vertical arrangement of bicontinuous D-A arrays on electrodes.[3] These results will provide fundamental clue for the molecular design of high-performance organic photovoltaics.

Experimental Section

General. UV-visible absorption spectra were obtained on a Perkin Elmer Lambda 900UV/vis/NIR spectrometer. Steady-state fluorescence spectra were recorded with a SPEX Fluoromax-3 spectrofluorometer (Horiba). AFM measurements were carried out using a Digital Nanoscope III in the tapping mode. TEM micrographs were measured by applying a drop of the sample to a holey polymer support film. Images were recorded using a JEM2000FX-II transmission electron microscope. Transparent conducting glasses (FTO, SnO_2:F, 9.4 Ω/sq) were commercially available from Asahi Glass.

Synthesis. All solvents and chemicals were of reagent grade quality, purchased commercially and used without further purification. Thin-layer chromatography and flash column chromatography were performed with Alt. 5554 DC-Alufolien Kieselgel 60 F_{254} (Merck) and Silica-gel 60N (SiliCycle), respectively. Melting points were recorded on a Yanagimoto micro-melting point apparatus and not corrected. ^{1}H NMR spectra were measured on a JEOL EX-400 and an ECX-400P spectrometer. Matrix-assisted laser desorption/ionization (MALDI) mass spectra (MS) were measured on a Shimadzu Biotech AXIMA-CFR. High-resolution mass spectra (HRMS) were recorded on a JEOL JMS-HX110A spectrometer. Synthesis of C_{60}-acid was carried out according to the previously reported method.[11]

5-(3,5-Dimethoxyphenyl)dipyrromethane (1). A solution of 3,5-dimethoxybenzaldehyde (4.99 g, 30.0 mmol) in pyrrole (83.3 mL, 1.20 mol) was degassed with a stream of argon for 1 h, and then TFA (0.25 mL, 3.3 mmol) was added. The reaction mixture was stirred for 85 min, and CH_2Cl_2 (200 mL) were added. The organic phase was washed with 0.1 M NaOH aqueous solution (500 mL) and water (400 mL) and then dried ($MgSO_4$) and the solvent was removed. Pyrrole was removed with bulb-to-bulb distillation. Column chromatography (silica; CH_2Cl_2/hexane) afforded a colorless solid (5.02 g, 59%): mp 76–77 °C; ^{1}H NMR ($CDCl_3$) δ 7.94 (br s, 2H), 6.69 (dd, J = 2.8 Hz, 4.0 Hz, 2H), 6.39 (d, J = 2.4 Hz, 2H), 6.36 (t, J = 2.4 Hz, 1H), 6.15 (dd, J = 2.8 Hz, 5.8 Hz, 2H), 5.96 (m, 2H), 5.41 (s, 1H), 3.75 (s, 6H); MS (MALDI-TOF, positive mode), found 281 (M^+), $C_{17}H_{18}N_2O_2$ requires 282.

5-(4-Methoxycabonylphenyl)-10,20-bis(3,5-dimethoxyphenyl)-15-(4-pyridyl)-21,23*H*-porphyrin (2). Terephthalaldehydic acid methyl ester (0.207 g, 1.26 mmol) and 4-pyridinecarbaldehyde (0.12 mL, 1.3 mmol) were added to **1** (0.711 g, 2.52 mmol) in propionic acid (22 mL). The mixture was refluxed in a 2-neck flask under nitrogen atmosphere for 1 h, and then the propionic acid was immediately evaporated. The reaction mixture was purified by silica gel column chromatography by using CH_2Cl_2 and EtOAc (CH_2Cl_2/EtOAc = 10:1 and then 5:1) as eluent. Precipitation from CH_2Cl_2/MeOH gave **2** as a purple red solid (35 mg, 0.044 mmol, 3.4%): mp > 300°C; ^{1}H NMR ($CDCl_3$) δ 9.03 (dd, J = 1.5 Hz, 3.9 Hz, 2H, pyridyl-H), 8.97 (m, 4H, β), 8.78

(m, 4H, β), 8.45 (d, J = 7.8 Hz, 2H, 5-Ar-H), 8.30 (d, J = 7.8 Hz, 2H, 5-Ar-H), 8.16 (dd, J = 1.5 Hz, 3.9 Hz, 2H, pyridyl-H), 7.39 (d, J = 2.4 Hz, 4H, 10,20-Ar-H), 6.91 (t, J = 2.4 Hz, 2H, 10,20-Ar-H), 4.12 (s, 3H, CO_2CH_3), 3.96 (s, 12H, methoxy-H), –2.84 (s, 2H, N-H); λ_{abs} ($CHCl_3$) nm (ε, $M^{-1}cm^{-1}$) 420 (4.3×10^5), 514 (1.9×10^4), 549 (5.9×10^3), 588 (5.9×10^3), 643 (2.9×10^3); HRMS (FAB, positive mode) found 793.2904 (M^+), $C_{49}H_{39}N_5O_6$ requires 793.2900.

5-(4-Carboxyphenyl)-10,20-bis(3,5-dimethoxyphenyl)-15-(4-pyridyl)-21,23*H*-porphyrin (3). 2 M KOH aqueous solution (8 mL, 16 mmol) was added to **2** (140 mg, 0.177 mmol) in DMF (100 mL) and the solution was refluxed for 48 h. The solvent was evaporated. The residue was dissolved in CH_2Cl_2/EtOAc, and then washed with 0.1 M HCl aqueous solution and brine. The organic phase was dried over $MgSO_4$ and the solvent was evaporated. Precipitation from THF/water and rinsing with water gave **3** as a purple red solid (112 mg, 0.144 mmol, 81%): mp > 300°C; ^{1}H NMR (DMSO) δ 9.03 (dd, J = 1.5 Hz, 4.4 Hz, 2H, pyridyl-H), 8.96 (m, 4H, β), 8.82 (m, 4H, β), 8.38 (d, J = 8.0 Hz, 2H, 5-Ar-H), 8.33 (d, J = 8.0 Hz, 2H, 5-Ar-H), 8.25 (dd, J = 1.5 Hz, 4.4 Hz, 4.4 Hz, 2H, pyridyl-H), 7.37 (d, J = 2.4 Hz, 4H, 10,20-Ar-H), 6.98 (t, J = 2.4 Hz, 2H, 10,20-Ar-H), 3.92 (s, 12H, methoxy-H), –3.00 (s, 2H, N-H); λ_{abs} (THF) nm (ε, $M^{-1}cm^{-1}$) 417 (3.5×10^5), 511 (1.7×10^4), 547 (6.1×10^3), 587 (5.4×10^3), 645 (2.9×10^3); HRMS (FAB, positive mode) found 779.2726 (M^+), $C_{48}H_{37}N_5O_6$ requires 779.2744.

5-(4-Carboxyphenyl)-10,20-bis(3,5-dimethoxyphenyl)-15-(4-pyridyl)porphyrinatozinc (II) (Py-ZnP-acid). To a solution of **3** (65 mg, 0.083 mmol) in DMF (100 mL) was added a solution of $ZnCl_2$ (500 mg, 3.68 mmol) in MeOH (20 mL). The solution was refluxed for 3 days. The solvent was evaporated and the residue was dispersed in THF/water and centrifuged. Precipitation from THF/water and rinsing with water gave Py-ZnP-acid as a purple red solid (70 mg, 0.083 mmol, 99%): mp > 300°C; ^{1}H NMR (pyridine-d_5) δ 9.37 (m, 4H, β), 9.19 (d, J = 4.4 Hz, 2H, 5-Ar-H), 9.16 (dd, J = 1.5 Hz, 4.4 Hz, 2H, pyridyl-H), 9.10 (d, J = 4.4 Hz, 2H, 5-Ar-H), 8.53 (m, 4H, β), 8.31 (dd, J = 1.5 Hz, 4.4 Hz, 2H, pyridyl-H), 7.75 (d, J = 2.4 Hz, 4H, 10,20-Ar-H), 7.15 (t, J = 2.4 Hz, 2H, 10,20-Ar-H), 3.88 (s, 12H, methoxy-H); λ_{abs} (THF) nm (ε, $M^{-1}cm^{-1}$) 424 (5.3×10^5), 555 (1.9×10^4), 595 (4.1×10^3); HRMS (FAB, positive mode) found 841.1876, $C_{48}H_{35}N_5O_6Zn$ requires 841.1879.

5,15-Bis(3,5-dimethoxyphenyl)-10,20-bis(4-pyridyl)-21,23*H*-porphyrin (4). A solution of 4-pyridinecarbaldehyde (0.24 mL, 2.5 mmol) and **1** (0.711 g, 2.52 mmol) in propionic acid (11 mL) was refluxed in a 2-neck flask under nitrogen atmosphere for 1 h. Then the reaction mixture was allowed to cool to room temperature. Propionic acid was evaporated from the mixture. Column chromatography on silica gel by using CH_2Cl_2 and MeOH (CH_2Cl_2/MeOH=20/1) as eluent and precipitation from CH_2Cl_2/MeOH gave **4** as a purple red solid (74 mg, 0.10 mmol, 8.1%): mp > 300°C; ^{1}H NMR ($CDCl_3$) δ 9.05 (dd, J = 1.8 Hz, 4.3 Hz, 4H, pyridyl-H), 9.00 (d, J = 4.9 Hz, 4H, β), 8.79 (d, J = 4.9 Hz, 4H, β), 8.16 (dd, J = 1.8 Hz, 4.3 Hz, 4H, pyridyl-H), 7.39 (d, J = 2.4 Hz, 4H,

Ar-2,6-H), 6.91 (t, J = 2.4 Hz, 2H, Ar-4-H), 3.97 (s, 12H, methoxy-H), –2.88 (s, 2H, N-H); λ_{abs} ($CHCl_3$) nm (ε, $M^{-1}cm^{-1}$) 419 (4.1×10^5), 513 (1.8×10^4), 547 (4.9×10^3), 587 (5.2×10^3), 643 (2.0×10^3); HRMS (FAB, positive mode) found 736.2796, $C_{46}H_{36}N_6O_4$ requires 736.2798.

5,15-Bis(3,5-dimethoxyphenyl)-10,20-bis(4-pyridyl)porphyrinatozinc (II) (ZnP-Py$_2$). To a solution of **4** (0.040 g, 0.054 mmol) in 50 mL of $CHCl_3$ was added a solution of $Zn(OAc)_2 \bullet 2H_2O$ (240 mg, 1.09 mmol) in MeOH (10 mL). The reaction mixture refluxed overnight and cooled to room temperature. The resulting solution was washed with saturated sodium bicarbonate aqueous solution and water successively and dried over $MgSO_4$, and then the solvent was evaporated. The resulting solid was purified by precipitation from CH_2Cl_2/MeOH to yield ZnP-Py$_2$ as a purple red solid (35 mg, 81%): mp > 300°C; ^{1}H NMR (pyridine-d_5) δ 9.37 (d, J = 4.4 Hz, 4H, β), 9.16 (dd, J = 1.5 Hz, 4.4 Hz, 4H, pyridyl-H), 9.10 (d, J = 4.4 Hz, 4H, β), 8.31 (dd, J = 1.5 Hz, 4.4 Hz, 4H, pyridyl-H), 7.74 (d, J = 2.4 Hz, 4H, Ar-2,6-H), 7.16 (t, J = 2.4 Hz, 2H, Ar-4-H), 3.89 (s, 12H, methoxy-H); λ_{abs} (pyridine) nm (ε, $M^{-1}cm^{-1}$) 430 (7.1×10^5), 561 (3.4×10^4), 602 (1.7×10^4); HRMS (FAB, positive mode) found 798.1940, $C_{46}H_{34}N_6O_4Zn$ requires 798.1933.

***N*-(4-Pyridinylmethyl)glycine ethyl ester (5).** In a two-necked flask was placed NEt_3 (9.7 mL, 70 mmol), 4-aminomethylpyridine (5.0 mL, 50 mmol) and THF (30 mL). The reaction mixture was heated to 50°C, and ethylchloroacetate (5.3 mL, 50 mmol) was added slowly. The reaction mixture was stirred at 50°C for 2 h and at room temperature for 4 days. The reaction mixture was filtered and the filtrate was concentrated by evaporation. Column chromatography on silica gel by using CH_2Cl_2 and MeOH as eluent gave **5** as a white solid (42 g, 43 mmol, 87%): ^{1}H NMR ($CDCl_3$) δ 8.55 (d, J = 4.4 Hz, 2H, pyridyl-H), 7.28 (d, J = 4.4 Hz, 2H, pyridyl-H), 4.20 (q, J = 6.8 Hz, 2H, ethyl-H), 3.84 (pseudo s, 2H, pyridyl-CH_2), 3.40 (pseudo s, 2H, CH_2), 1.96 (pseudo s, 1H, N-H), 1.28 (t, J = 6.8 Hz, 3H, ethyl-H).

***N*-(4-Pyridinylmethyl)glycine (6).** To a solution of **5** (8.3 g, 43 mmol) in 2-propanol (30 mL) was added 6 M KOH aqueous solution (20 mL, 120 mmol). The mixture was heated to reflux for 6h, cooled to room temperature, and then water and CH_2Cl_2 was added. The aqueous phase was neutralized by addition of 35% HCl and the water was evaporated. The residue was washed with MeOH repeatedly to yield **6** as a white solid (3.0 g, 18 mmol, 43%): ^{1}H NMR (D_2O) δ 8.44 (d, J = 6.0 Hz, 2H, pyridyl-H), 7.37 (d, J = 6.0 Hz, 2H, pyridyl-H), 4.06 (pseudo s, 2H, pyridyl-CH_2), 3.41 (pseudo s, 2H, CH_2), 3.21 (pseudo s, 1H, N-H).

***N*-(4-Pyridinylmethyl)-3,4-fulleropyrrolidine (Py-C$_{60}$).** A mixture of C_{60} (186 mg, 0.258 mmol), *N*-(4-pyridinylmethyl)glycine (101 mg, 0.608 mmol) and paraformaldehyde (42.5 mg, 1.42 mmol) was heated at reflux in toluene (200 mL) under argon for 6 h. The reaction mixture was concentrated by evaporation. Column chromatography on silica gel by using toluene and NEt_3 as eluent and precipitation from toluene/MeOH gave pure Py-C_{60} as a brown solid (52 mg, 0.061 mmol,

23%): mp > 300°C; ^{1}H NMR ($CDCl_3$) δ 8.74 (d, J = 4.5 Hz, 2H, pyridyl-H), 7.68 (d, J = 4.5 Hz, 2H, pyridyl-H), 4.46 (s, 4H, pyrrolidine-H), 4.32 (s, 2H, CH_2); λ_{abs} (DMF) nm (ε, $M^{-1}cm^{-1}$) 430 (4.3×10^3); HRMS (FAB, positive mode) found 854.0847, $C_{68}H_{10}N_2$ requires 854.0844.

***N*-Benzyl-3,4-fulleropyrrolidine (Ph-C_{60}).** A mixture of C_{60} (360 mg, 0.500 mmol), *N*-benzylglycine (197 mg, 1.19 mmol) and paraformaldehyde (82.3 mg, 2.75 mmol) was heated at reflux in toluene (350 mL) under argon for 6 h. The reaction mixture was concentrated by evaporation. Column chromatography on silica gel by using toluene and NEt_3 as eluent and precipitation from toluene/MeOH gave Ph-C_{60} as a brown solid (84 mg, 0.098 mmol, 20%): mp > 300°C; ^{1}H NMR ($CDCl_3$) δ 7.72 (d, J = 7.3 Hz, 2H, Ph-H), 7.50 (dd, J = 7.3 Hz, 7.3 Hz, 2H, Ph-H), 7.41 (d, J = 7.3 Hz, 1H, Ph-H), 4.44 (s, 4H, pyrrolidine-H), 4.32 (s, 2H, CH_2); λ_{abs} (DMF) nm (ε, $M^{-1}cm^{-1}$) 430 (4.2×10^3); HRMS (FAB, positive mode) found 853.0912, $C_{69}H_{11}N$ requires 853.0891.

Electrochemical measurements. The redox potentials of porphyrins and fullerenes used in this study were determined by cyclic voltammetric and differential pulse voltammetric measurements, respectively. The electrochemical measurements were performed in chloroform or dichloromethane containing 0.1M *n*-Bu_4NPF_6 as supporting electrolyte using a glassy carbon working electrode, a platinum wire counter electrode, and an Ag/Ag^+ [0.01 M $AgNO_3$, 0.1 M *n*-Bu_4NPF_6 (acetonitrile)] reference electrode on a 660A electrochemical analyzer (ALS/CH Instruments).

Preparation of SnO_2 films on FTO electrodes. Thin and smooth SnO_2 films were prepared by the following procedure described previously by Morazzoni et al.[12] The sol phase was prepared under a nitrogen atmosphere by mixing 1.0 mL of a [$Sn(OBu^t)_4$] solution (0.36 g mL^{-1}) in absolute anhydrous ethanol (0.88 mmol of Sn) with 1.2 mL of ethanol/acetylacetone (5:1, v/v). After a few minutes, 0.20 mL of an ethanol/water solution (4:1, v/v) was added and the sol phase was put into an oil bath at 308 K. SnO_2 films were fabricated by spin coating of 0.1 mL of the solution (spin rate = 4000 rpm, spin time = 30 sec) on a half area of a FTO substrate (1 × 4 cm), then dried at room temperature, followed by annealed at 673 K for 1 h. The roughness factor (1.1) and the thickness (20 nm) of the SnO_2 film on FTO were estimated by AFM measurements.

Preparation of the electrodes modified with porphyrin arrays (Scheme 1). SnO_2 electrodes modified with porphyrin arrays were prepared by following the similar procedure described by Miyake et al.[4b] First, the FTO modified SnO_2 was immersed into the DMF solution containing 0.2 mM Py-ZnP-acid for 4 h, followed by being washed with DMF. After being dipped into methanol for 20 min, the SnO_2 electrode modified with Py-ZnP-acid was immersed into a 3.0 mM K_2PdCl_4 aqueous solution for 20 min, followed by being washed with water and dipped into methanol for 20 min. Then, the substrate was immersed into the 0.20 mM ZnP-Py_2 chloroform/methanol (3:1, v/v) solution for 20 min to form ZnP-Py_2 layer. The electrode modified

with porphyrin arrays was obtained by repetition of the procedures (denoted as $SnO_2/(ZnP)_n$, n = 1–8).

Preparation of the electrodes modified with porphyrin and fullerene arrays (Scheme 2). First, the SnO_2 electrode was immersed into the DMF solution containing Py-ZnP-acid and C_{60}-acid ([Py-ZnP-acid] = 0.20 mM, [C_{60}-acid] = 0.20 mM) for 4 h, followed by being washed with DMF repeatedly. Then, the assembly of ZnP-Py_2 layer was carried out according to the same procedures mentioned in preparation of the $SnO_2/(ZnP)_n$ electrode (vide supra). Finally, the electrode modified with C_{60}-acid and the porphyrin arrays was immersed into the *o*-dichlorobenzene solution containing 1.0 mM Py-C_{60} for 4 h, followed by being washed gently with *o*-dichlorobenzene (denoted as SnO_2/C_{60}-acid+$(ZnP)_n$+Py-C_{60}). The FTO electrodes modified with SnO_2 were employed for the optical, photophysical and photoelectrochemical measurements, whereas glass substrates modified with SnO_2 were used for the AFM measurements.

Preparation of the SnO_2 nanoparticles modified with porphyrin arrays. To a MeOH solution containing Py-ZnP-acid ([Py-ZnP-acid] = 0.20 mM) was added SnO_2 nanoparticles (particle size: 70–110 nm; Wako Pure Chemical Industries, Ltd.). The mixture was stirred overnight at room temperature, then filtered and washed with MeOH and DMF. The resulting powder was dried in a vacuum for a few hours. The SnO_2 powder modified with Py-ZnP-acid was added to 3.0 mM K_2PdCl_4 aqueous solution, and then the reaction mixture was stirred for 1 h at room temperature. The reaction mixture was filtered and washed with water and MeOH. The resulting powder was dried in a vacuum for a few hours. To a $CHCl_3$/MeOH (3:1, v/v) solution containing ZnP-Py_2 ([ZnP-Py_2] = 0.20 mM) was added the SnO_2 powder modified with Py-ZnP-acid and palladium. The mixture was stirred for 1 h at room temperature, then filtered and washed with $CHCl_3$ and MeOH. The resulting powder was dried in a vacuum for a few hours. The assembly of ZnP-Py_2 layer was performed in accordance with the procedures mentioned above.

Determination of amounts of Py-ZnP-acid and C_{60}-acid adsorbed on the SnO_2 electrode. The amounts of Py-ZnP-acid and C_{60}-acid molecules adsorbed on a FTO/SnO_2 electrode were determined by measuring absorbances due to Py-ZnP-acid (at 430 nm, ε (DMF/0.1 M NaOH aqueous solution = 4:1) = 8.1×10^5 M^{-1} cm^{-1}) and C_{60}-acid (at 375 nm, ε (DMF/0.1 M NaOH aqueous solution = 4:1) = 1.2×10^4 M^{-1} cm^{-1}), which were dissolved from the electrode surface into DMF containing 0.1 M NaOH aqueous solution.

Determination of amount of ZnP-Py_2 assembled on the electrode. The amounts of ZnP-Py_2 molecules assembled on the electrodes were determined by measuring absorbance at the Soret band of ZnP-Py_2 (at 430 nm, ε (pyridine) = 7.1×10^5 M^{-1} cm^{-1}), which were dissolved from the electrodes into pyridine.

Photoelectrochemical measurements. Photoelectrochemical measurements were performed

in a one-compartment Pyrex UV cell (5 mL) with an electrolyte solution containing 0.5 M LiI and 0.01 M I_2 in acetonitrile.[13] The samples were excited with monochromatic light using a 500 W Xe arc lamp (Ritsu UXL-500D-0) coupled with a monochromator (Ritsu MC-10N). The illuminated area on the modified surface was 0.20 cm^2. The light intensity was modulated with neutral density filters (HOYA). The film was immersed into the electrolyte solution as a working electrode. The photocurrent was measured in a three-electrode arrangement, the modified SnO_2 working electrode, a platinum wire counter electrode (the distance between the electrodes is 0.3 mm), and an I^-/I_3^- reference electrode using an ALS 630a electrochemical analyzer. The light intensity was monitored by an optical power meter (Anritsu ML9002A) and corrected. The I^-/I_3^- reference electrode was made from platinum wire covered with glass ruggin capillary filled with the acetonitrile solution containing 0.5 M LiI and 0.01 M I_2. The potential measured was converted to the saturated calomel electrode (SCE) scale by adding +0.05 V. The stability of the reference electrode potential was confirmed under the experimental conditions. IPCE values were calculated by normalizing the photocurrent densities for incident light energy and intensity and by use of the expression: IPCE (%) = 100 × 1240 × i/(W_{in} × λ), where i is the photocurrent density (A cm^{-2}), W_{in} is the incident light intensity (W cm^{-2}), and λ is the excitation wavelength (nm). APCE (%) = IPCE/(1–10^{-A}), where A is the absorbance.

Transient absorption measurements. The femtosecond time-resolved transient absorption (TA) spectrometer consisted of a homemade noncollinear optical parametric amplifier (NOPA) pumped by a Ti:sapphire regenerative amplifier system (Quantronix, Integra-C) operating at 1 kHz repetition rate and an optical detection system.[11a] The generated visible NOPA pulses had a pulse width of ~100 fs and an average power of 1 mW in the range 500–700 nm which were used as pump pulses. White light continuum (WLC) probe pulses were generated using a sapphire window (2 mm of thickness) by focusing of small portion of the fundamental 800 nm pulses, which was picked off by a quartz plate before entering to the NOPA. The time delay between pump and probe beams was carefully controlled by making the pump beam travel along a variable optical delay (Newport, ILS250). Intensities of the spectrally dispersed WLC probe pulses are monitored by miniature spectrograph (OceanOptics, USB2000+). To obtain the time-resolved transient absorption difference signal (ΔA) at a specific time, the pump pulses were chopped at 25 Hz and absorption spectra intensities were saved alternately with or without pump pulse. Typically, 6000 pulses excite samples to obtain the TA spectra at a particular delay time. The polarization angle between pump and probe beam was set at the magic angle (54.7°) in order to prevent polarization-dependent signals. Cross-correlation fwhm in pump-probe experiments was less than 200 fs and chirp of WLC probe pulses was measured to be 800 fs in the 400–800 nm region. To minimize chirp, all reflection optics in probe beam path and 2 mm path length of quartz cell were used.

References and Footnotes

(1) (a) Günes, S.; Neugebauer, H.; Sariciftci, N. S. *Chem. Rev.* **2007**, *107*, 1324. (b) Thompson, B. C.; Fréchet, J. M. J. *Angew. Chem., Int. Ed.* **2008**, *47*, 58. (c) Imahori, H. *J. Mater. Chem.* **2007**, *17*, 31. (d) Segura, J. L.; Martín, N.; Guldi, D. M. *Chem. Soc. Rev.* **2005**, *34*, 31.

(2) (a) Schmidt-Mende, L.; Fechtenkötter, A.; Müllen, K.; Moons, E.; Friend, R. H.; MacKenzie, J. D. *Science* **2001**, *293*, 1119. (b) van der Boom, T.; Hayes, R. T.; Zhao, Y.; Bushard, P. J.; Weiss, E. A.; Wasielewski, M. R. *J. Am. Chem. Soc.* **2002**, *124*, 9582. (c) Würthner, F.; Chen, Z.; Hoeben, F. J. M.; Osswald, P.; You, C.-C.; Jonkheijm, P.; Herrikhuyzen, J.; Schenning, A. P. H. J.; van der Schoot, P. P. A. M.; Meijer, E. W.; Beckers, E. H. A.; Meskers, S. C. J.; Janssen, R. A. J. *J. Am. Chem. Soc.* **2004**, *126*, 10611. (d) Sun, S.-S.; Zhang, C.; Ledbetter, A.; Choi, S.; Seo, K.; Bonner, Jr., C. E.; Drees, M.; Sariciftci, N. S. *Appl. Phys. Lett.* **2007**, *90*, 043117. (e) Imahori, H.; et al. *Chem.-Eur. J.* **2007**, *13*, 10182. (f) Li, W.-S.; Yamamoto, Y.; Fukushima, T.; Saeki, A.; Seki, S.; Tagawa, S.; Masunaga, H.; Sasaki, S.; Takata, M.; Aida, T. *J. Am. Chem. Soc.* **2008**, *130*, 8886. (g) Zhou, Z.; Chen, X.; Holdcroft, S. *J. Am. Chem. Soc.* **2008**, *130*, 11711.

(3) (a) Snaith, H. J.; Whiting, G. L.; Sun, B.; Greenham, N. C.; Huck, W. T. S.; Friend, R. H. *Nano Lett.* **2005**, *5*, 1653. (b) Sisson, A. L.; Sakai, N.; Banerji, N.; Fürstenberg, A.; Vauthey, E.; Matile, S. *Angew. Chem., Int. Ed.* **2008**, *47*, 3727.

(4) (a) Drain, C. M.; Nifiatis, F.; Vasenko, A.; Batteas, J. D. *Angew. Chem. Int. Ed.* **1998**, *37*, 2344. (b) Qian, D.-J.; Nakamura, C.; Ishida, T.; Wenk, S.-O.; Wakayama, T.; Takeda, S.; Miyake, J. *Langmuir* **2002**, *18,* 10237.

(5) (a) Troshin, P. A.; Koeppe, R.; Peregudov, A. S.; Peregudova, S. M.; Egginger, M.; Lyubovskaya, R. N.; Sariciftci, N. S. *Chem. Mater.* **2007**, *19*, 5363. (b) D'Souza, F.; Deviprasad, G. R.; Zandler, M. E.; Hoang, V. T.; Klykov, A.; VanStipdonk, M.; Perera, A.; El-Khouly, M. E.; Fujitsuka, M.; Ito, O. *J. Phys. Chem. A* **2002**, *106*, 3243.

(6) Acciarri, M.; Canevali, C.; Mari, C. M.; Mattoni, M.; Ruffo, R.; Scotti, R.; Morazzoni, F.; Barreca, D.; Armelao, L.; Tondello, E.; Bontempi, E.; Depero, L. E. *Chem. Mater.* **2003**, *15*, 2646.

(7) The SnO_2/C_{60}-acid+$(ZnP)_n$+Py-C_{60} electrodes exhibited no characteristic emission around 800 nm due to charge-transfer (CT) interaction between ZnP and Py-C_{60}. This implies that no CT complexes are formed, because the rather long separation distance between ZnP and Py-C_{60} caused by the coordination bonding via the *N*-(4-pyridinylmethyl)pyrrolidine moiety does not allow the porphyrin moiety to make direct contact with the C_{60} molecules.[5b]

(8) (a) Imahori, H.; Liu, J.-C.; Hotta, H.; Kira, A.; Umeyama, T.; Matano, Y.; Li, G.; Ye, S.; Isosomppi, M.; Tkachenko, N. V.; Lemmetyinen, H. *J. Phys. Chem. B* **2005**, *109*, 18465. (b) Kira, A.; Tanaka, M.; Umeyama, T.; Matano, Y.; Yoshimoto, N.; Zhang. Y.; Ye, S.; Lehtivuori,

H.; Tkachenko, N. V.; Lemmetyinen, H.; Imahori, H. *J Phys. Chem. C* **2007**, *111*, 13618.

(9) Peumans, P.; Yakimov, A.; Forrest, S. R. *J. Appl. Phys.* **2003**, *93*, 3693.

(10) (a) Cho, Y.-J.; Ahn, T. K.; Song, H.; Kim, K. S.; Lee, C. Y.; Seo, W. S.; Lee, K.; Kim, S. K.; Kim, D.; Park, J. T. *J. Am. Chem. Soc.* **2005**, *127*, 2380. (b) Imahori, H.; Hagiwara, K.; Aoki, M.; Akiyama, T.; Taniguchi, S.; Okada, T.; Shirakawa, M.; Sakata, Y. *J. Am. Chem. Soc.* **1996**, *118*, 11771. (c) Luo, C.; Guldi, D. M.; Imahori, H.; Tamaki, K.; Sakata, Y. *J. Am. Chem. Soc.* **2000**, *122*, 6535. (d) Imahori, H.; Tamaki, K.; Guldi, D. M.; Luo, C.; Fujitsuka, M.; Ito, O.; Sakata, Y.; Fukuzumi, S. *J. Am. Chem. Soc.* **2001**, *123*, 2607.

(11) (a) Pasimeni, L.; Hirsch, A.; Lamparth, I.; Maggini, M.; Prato, M. *J. Am. Chem. Soc.* **1997**, *119*, 12902. (b) Camps, X.; Hirsch, A. *J. Chem. Soc., Perkin Trans. 1* **1997**, 1595.

(12) (a) Morazzoni, F.; Canevali, C.; Chiodini, N.; Mari, C.; Ruffo, R.; Scotti, R.; Armelao, L.; Tondello, E.; Depero, L. E.; Bontempi, E. *Chem. Mater.* **2001**, *13*, 4355. (b) Acciarri, M.; Canevali, C.; Mari, C.; Mattoni, M.; Ruffo, R.; Scotti, R.; Morazzoni, F.; Barreca, D.; Armelao, L.; Tondello, E.; Bontempi, E.; Depero, L. E. *Chem. Mater.* **2003**, *15*, 2646.

(13) (a) Barazzouk, S.; Hotchandani, S.; Kamat, P. V. *Adv. Mater.* **2001**, *13*, 1614. (b) Kang, S.; Umeyama, T.; Ueda, M.; Matano, Y.; Hotta, H.; Yoshida, K.; Isoda, S.; Shiro, M.; Imahori, H.; *Adv. Mater.* **2006**, *18*, 2549. (c) Kira, A.; Tanaka, M.; Umeyama, T.; Matano, Y.; Yoshimoto, N.; Zhang, Y.; Ye, S.; Lehtivuori, H.; Tkachenko, N. V.; Lemmetyinen, H. Imahori, H. *J. Phys. Chem. C* **2007**, *111*, 13618. (d) Umeyama, T.; Tezuka, N.; Fujita, M.; Hayashi, S.; Kadota, N.; Matano, Y.; Imahori, H. *Chem.-Eur. J.* **2008**, *14*, 4875.

Concluding Remarks

This thesis has described nanostructured hybrid electrodes for organic photovoltaic devices. The author has adopted the two different approaches including development of novel organic photosensitizers for dye-sensitized solar cells and self-assembly of donor-acceptor molecules on semiconducting electrodes. The results and findings in this work are summarized as follows.

Chapter 1

The author has synthesized an oligothiophene bearing 1-oxo-1-hydroxydithieno[2,3-*b*:3',2'-*d*]phosphole (**TP**) as a novel anchoring group for DSSC. Attenuated total reflectance-Fourier transform infrared and X-ray photoelectron spectroscopy measurements disclosed the bidentate binding of the phosphinic acid unit to the TiO_2 surface. TiO_2 cell sensitized with **TP** yielded a maximum incident photon-to-current efficiency (IPCE) of 66% comparable to that of N719 cell, implying that 1-oxo-1-hydroxydithienophosphole is a potential unit as a new type of anchoring groups for DSSC.

Chapter 2

The author has synthesized novel benzo[f]quinoxalino[2,3-β]porphyrin acid (ZnBQA) and quinoxalino[6,7-β]porphyrin acid (ZnQCA) have been synthesized and evaluated as photosensitizers for DSSC. ZnBQA showed the blue-shift of Q bands relative to that of quinoxalino[2,3-β]porphyrin acid (ZnQMA) by introducing the substituents with a benzoquinoxaline, while the Q bands of ZnQCA are red-shifted compared to those of ZnQMA. The ZnBQA-sensitized TiO_2 cell exhibited relatively high η value of 5.1%, while the ZnQCA-sensitized TiO_2 cell yielded low η value of 0.80%. Both η values are smaller than that of ZnQMA-sensitized TiO_2 cell (η = 6.3%). The weak electronic coupling between the LUMO of ZnBQA and the CB of the TiO_2 may result in the lower electron injection efficiency for ZnBQA cell relative to ZnQMA cell, leading to the lower η value of ZnBQA cell than that of ZnQMA one. The ZnQCA cell exhibited the further lower electron injection efficiency due to the short lifetime of the excited state comparable to the time scale of electron injection processes from the excited state of the dyes to the TiO_2 surface. In addition, the V_{OC} value of ZnQCA cell also significantly decreases by the effect of the charge recombination from the injected electrons on the CB of the TiO_2 and the I^-/I_3^- derived from the inhomogeneous adsorption mode of ZnQCA molecules on the TiO_2 surface. Overall, the author has

successfully examined the effects of the π-elongation and the fused position of quinoxaline-fused porphyrins on their photovoltaic properties, which may be useful information to design molecular structures of porphyrins for highly efficient dye-sensitized solar cells.

Chapter 3

The author has successfully prepared clusters of phthalocyanine and phthalocyanine-perylene diimide composite deposited electrophoretically on a nanostructured SnO_2 electrode. The structures of the clusters and their photoelectrochemical properties have been examined in detail. Although the photocurrent generation efficiency of the present phthalocyanine system is rather low compared to similar porphyrin systems, an enhancement of the photocurrent generation efficiency of the composite system is achieved relative to that of the phthalocyanine reference system without the perylene diimide at around 400 nm and 700–800 nm. Such knowledge will provide fundamental information for the design of molecular photoelectrochemical devices that exhibit efficient photocurrent generation.

Chapter 4

The author has examined hydrogen bonding effects on photocurrent generation in the mixed films of porphyrin and/or fullerene with hydrogen bonding on nanostructured SnO_2 electrodes. The nanostructured SnO_2 electrodes modified with the mixed films of porphyrin and fullerene with hydrogen bonding exhibit efficient photocurrent generation (up to IPCE value of 36%) as compared to the reference systems without hydrogen bonding. The evaluation of the film structures, and photoelectrochemical and photodynamical measurements indicate that the hydrogen bonding interaction facilitated the self-assembly of the porphyrin and the C_{60} molecules with a phase-separated, interpenetrating network involving electron and/or hole transporting nanostructures, which leads to efficient photocurrent generation. These results show that hydrogen bonding is a highly promising methodology for the construction of molecular photoelectrochemical devices.

Chapter 5

The author has examined hydrogen bonding effects on photocurrent generation in the mixed films of porphyrin and/or fullerene with hydrogen bonds on nanostructured TiO_2 electrodes for the first time. The nanostructured TiO_2 electrodes modified with the mixed films of porphyrin and fullerene with hydrogen bonds exhibit efficient photocurrent generation as compared to the reference systems without hydrogen bonds. The evaluation of the film

structures, and photoelectrochemical and photodynamical measurements support the significant contribution of hydrogen bonding interaction between the porphyrins or the C_{60} moieties or the both in the films for the improvement of the photocurrent generation efficiency. These results show that hydrogen bonding is a potential methodology for the fabrication of donor and acceptor composites on a nanostructured TiO_2 electrode, which exhibit high open circuit potential relative to that of the corresponding SnO_2 electrode.

Chapter 6

The author has successfully developed the novel strategy for constructing the vertical arrangement of porphyrin-fullerene arrays on a semiconducting electrode with coordination bonding. The relationship between the film structure and photoelectrochemical properties has been elucidated as a function of the number of donor layers for the first time. The maximum IPCE value (21%) is comparable to the highest value among vertical arrangement of bicontinuous D-A arrays on electrodes. These results will provide fundamental clue for the molecular design of high-performance organic photovoltaics.

List of Publications

Chapter 1

Oligothiophene Bearing 1-Oxo-1-hydroxydithieno[2,3-*b*:3',2'-*d*] phosphole as a Novel Anchoring Group for Dye-sensitized Solar Cells

Kira, A.; Shibano, Y.; Kang, S.; Hayashi, H.; Umeyama, T.; Matano, Y.; Imahori, H. *Chem. Lett.* in press.

Chapter 2

Effects of π-Elongation and Fused Position of Quinoxaline-Fused Porphyrins on Optical, Electrochemical, and Photovoltaic Properties

Kira, A.; Matsubara, Y.; Iijima, H.; Umeyama, T.; Matano, Y.; Ito, S.; Niemi, M.; Tkachenko, N. V.; Lemmetyinen, H.; Imahori, H. submitted.

Chapter 3

Structure and Photoelectrochemical Properties of Phthalocyanine and Perylene Diimide Composite Clusters Deposited Electrophoretically on Nanostructured SnO_2 Electrodes

Kira, A.; Umeyama, T.; Matano, Y.; Yoshida, K.; Isoda, S.; Isosomppi, M.; Tkachenko, N. V.; Lemmetyinen, H.; Imahori, H. *Langmuir* **2006**, *22*, 5497–5503.

Chapter 4

Hydrogen Bonding Effects on the Surface Structure and Photoelectrochemical Properties of Nanostructured SnO_2 Electrodes Modified with Porphyrin and Fullerene Composites

Imahori, H.; Liu, J.-C.; Hotta, H.; Kira, A.; Umeyama, T.; Matano, Y.; Li, G.; Ye, S.; Isosomppi, M.; Tkachenko, N. V.; Lemmetyinen, H. *J. Phys. Chem. B* **2005**, *109*, 18465–18474.

Chapter 5

Hydrogen-Bonding Effects on Film Structure and Photoelectrochemical Properties of Porphyrin and Fullerene Composites on Nanostructured TiO_2 Electrodes

Kira, A.; Tanaka, M.; Umeyama, T.; Matano, Y.; Li, Z.; Ye, S.; Lehtivuori, H.; Tkachenko, N. V.; Lemmetyinen, H.; Imahori, H. *J. Phys. Chem. C* **2007**, *111*, 13618–13626.

Chapter 6

Supramolecular Donor-Acceptor Heterojunctions by Vectorial Stepwise Assembly of Porphyrins and Coordination-Bonded Fullerene Arrays for Photocurrent Generation
Kira, A.; Umeyama, T.; Matano, Y.; Yoshida, K.; Isoda, S.; Park, J.-K.; Kim, D.; Imahori, H. *J. Am. Chem. Soc.* **2009**, *131*, 3198–3200.

Other Publications

Gold Nanoparticle Enhanced Charge Transfer in Thin Film Assemblies of Porphyrin-Fullerene Dyads
Kotiaho, A.; Lahtinen, R. M.; Tkachenko, N. V.; Efimov, A.; Kira, A.; Imahori, H.; Lemmetyinen, H. *Langmuir* **2007**, *23*, 13117–13125.

Photoinduced Electron Transfer in Langmuir-Blodgett Monolayers of Double-Linked Phthalocyanine-Fullerene Dyads
Lehtivuori, H.; Kumpulainen, T.; Efimov, A.; Lemmetyinen, H.; Kira, A.; Imahori, H.; Tkachenko, N. V. *J. Phys. Chem. C* **2008**, *112*, 9896–9902.

Photodynamics of Charge Separation and Recombination in Solid Alternating Films of Phthalocyanine or Phthalocyanine-Fullerene Dyad and Perylene Dicarboximide
Lehtivuori, H.; Kumpulainen, T.; Hietala, M.; Efimov, A.; Lemmetyinen, H.; Kira, A.; Imahori, H.; Tkachenko, N. V. *J. Phys. Chem. C* **2009**, *113*, 1984–1992.

Effects of Electrode Structure on Photoelectrochemical Properties of ZnO Electrodes Modified with Porphyrin-Fullerene Composite Layers with an Intervening Fullerene Monolayer
Hayashi, H.; Kira, A.; Umeyama, T.; Matano, Y.; Charoensirithavorn, P.; Sagawa, T.; Yoshikawa, S.; Tkachenko, N. V.; Lemmetyinen, H.; Imahori, H. *J. Phys. Chem. C* **2009**, *113*, 10819–10828.

Electrophoretic Deposition of Donor and Acceptor Molecules for Photovoltaic Devices
Imahori, H.; Kira, A. *Kagaku To Kogyo* **2007**, *81*, 18–24.

Acknowledgment

The studies presented in this thesis have been carried out under the direction of Professor Hiroshi Imahori at the Department of Molecular Engineering, Graduate School of Engineering, Kyoto University.

The author would like to express my gratitude to Professor Hiroshi Imahori for his kind guidance, invaluable suggestions, and encouragement throughout this study. The author is also deeply grateful to Professor Yoshihiro Matano and Assistant Professor Tomokazu Umeyama for their constant advice and helpful discussions during the course of this work.

The author is indebted to Professor Noboru Ono, Assistant Professor Tatsuya Murakami, Dr. Jia-Cheng Liu, Dr. Hiroki Hotta, and Dr. Masanobu Tanaka for their helpful suggestions and technical assistance.

The author would like to thank Professor Nikolai V. Tkachenko (Tampere University of Technology, Finland), Professor Helge Lemmetyinen (Tampere University of Technology, Finland), Professor Seiji Isoda (Kyoto University), Dr. Kaname Yoshida (Kyoto University), Professor Shen Ye (Hokkaido University), Professor Dongho Kim (Yonsei University, Korea), Dr. Naoki Yoshimoto (Hitachi, Ltd. Japan) for their kind guidance and helpful comments.

The author wishes to express her special thanks to Professor Chad A. Mirkin at Department of Chemistry and International Institute for Nanotechnology, Northwesern University for his kind support and valuable suggestions in the author's stay in USA.

Thanks also go to the all members of the laboratory of Photoorganic Chemistry at Department of Molecular Engineering, Graduate School of Engineering, Kyoto University and the people who the author has come to know through my research for their help, valuable suggestions, and heartwarming friendship.

The author acknowledges the Research Fellowship of Japan Society for the Promotion of Science for Young Scientists.

Finally, the author would like to express continuous encouragement and assistant given by her family.

Aiko Kira

Department of Moleuclar Engineering
Graduate School of Engineering
Kyoto University
Kyoto, Japan
2010